Fall 2014

Polyurethane foam infill for fiber reinforced polymer (FRP) bridge deck panels: an evaluation of core alternatives using small scale experimental testing

Matthew Scott Hopkins

Department:

POLYURETHANE FOAM INFILL FOR FIBER REINFORCED POLYMER (FRP) BRIDGE DECK PANELS: AN EVALUATION OF CORE ALTERNATIVES USING SMALL SCALE EXPERIMENTAL TESTING

by

MATTHEW SCOTT HOPKINS

A THESIS

Presented to the Faculty of the Graduate School of the

MISSOURI UNIVERSITY OF SCIENCE AND TECHNOLOGY

In Partial Fulfillment of the Requirements for the Degree

MASTER OF SCIENCE IN CIVIL ENGINEERING

2014

Approved by

Dr. Jeffery S. Volz, Advisor
Dr. K. Chandrashekhara
Dr. Victor Birman

ABSTRACT

Fiber reinforced polymer (FRP) decking is a concept that has been explored in recent decades as one solution to the performance issues of conventional concrete bridge decking. Many sandwich panel designs made of glass reinforced polyester or vinyl ester resin have been well developed, and manufactured using filament winding, hand lay-up, and extrusion methods. The major benefits of these panels was their light weight, corrosion resistance, fatigue performance, and potential for rapid field assembly. However, high initial costs coupled with small state budgets have kept them from main stream adoption. A viable alternative, is a foam/reinforced foam core sandwich panel made of polyurethane materials and glass fibers that is manufactured using the vacuum assisted resin transfer molding (VARTM) process. These type of panels could potentially decrease initial expenses, manufacturing difficulties, and possibly reduce weight further while retaining the benefits provided by previously explored FRP panels. The primary objective of this thesis is to evaluate three potential core alternatives. Type 1 consisted of a rigid polyurethane core, Type 2 consisted of a flexible polyurethane foam core reinforced by a grid work of resin infused glass fibers, and the Type 3 core consisted of trapezoidal blocks of flexible polyurethane foam reinforced with resin infused glass fiber shear layers. Four types of small scale experimental testing were conducted in this research; flatwise compression and tension testing, three point flexural testing, and four point flexural testing. The results showed that both the Type 1 and 2 cores were very weak and flexible making their implementation in bridge deck panels less practical. The Type 3 core was the stiffest and strongest core configuration making in the most practical for implementation in bridge deck panels.

ACKNOWLEDGMENTS

First, I would like to thank my advisor Dr. Jeffery Volz for his guidance and friendship throughout this project. Without his motivation and encouragement this experience would not have been as enjoyable as it was. Additionally, I want to thank my research partner Hesham Tuwair for collaborating with me on this research. His intellectual input and help in the laboratory was essential to our success, and without his friendship this research experience would not have been the same. Furthermore, I would like to thank the members of my thesis committee. Dr. K. Chandrashekhara and his students researched, developed, and constructed the specimens for the core alternatives we evaluated in this research program. We could not have done this without them. Also, I would like to thank Dr. Victor Birman for his insights into composite theory and his willingness to help. I would also like to thank the Missouri Department of Transportation (MoDOT) for funding this project, and the Center for Transportation Infrastructure and Safety-National University Transportation Center (CTIS-NUTC) at Missouri S&T for matching the funding provided by MoDOT. In addition, I would like to thank Gary Abbot and Brian Swift for helping us use the equipment to test our specimens, and for setting up the mobile data acquisition system to do testing in the Interdisciplinary Engineering (IDE) Materials Lab. On the same note, I would like thank Dr. Jeffery Thomas for allowing us to use the machines in the IDE Lab. Next, I would like to thank Jason Cox for his assistance in cutting and preparing test specimens. Also, I would like to thank Scott Parker and Mark Harris for machining the essential pieces for our test fixtures. In closing, I would like to thank my friends and family, especially my wife Melanie and my mother Jackie, for the support and encouragement to pursue my dreams.

TABLE OF CONTENTS

Page

LIST OF FIGURES

LIST OF TABLES

1. INTRODUCTION

1.1. BACKGROUND

The decline of the nation's infrastructure is one of several exigent issues facing the United States in the twenty first century. It is a daily news topic with a broad and complex set of problems impacting politics, economics, and engineering. A small but important piece of this dilemma is the deterioration of our nation's bridges. According to the 2013 Report Card for American Infrastructure, nearly 11% of bridges are structurally deficient in the U.S. and are in need of repair. Add to this the functionally obsolete bridges that need to be replaced and nearly 25% of the nation's bridges are deficient (ASCE, 2013). The primary engineering challenge posed by this problem is to repair and replace these bridges using sustainable design and construction methods. To combat this problem, many civil engineering scholars and transportation agencies have focused their research efforts on the causes of bridge deterioration and ways to mitigate the problem.

The life expectancy of a bridge is effected by many factors but when it comes to deterioration, the most important factor is the durability of the materials it is constructed from. Modern bridges are typically constructed from a combination of structural steel and reinforced concrete. Steel and concrete are considered to be relatively durable, but they are susceptible to a long list of both physical and chemical attacks that can act as mechanisms of bridge deterioration. One well known mechanism is the corrosion of steel rebar in reinforced concrete bridge decks, which is a prevalent issue in Northern and Midwestern states. There are many possible causes of this corrosion, but the most accepted is the use of deicing salts on bridge decks in the winter months. In the last half of the 20^{th} century, deicing salts have been used by many state transportation agencies to clear the roads of

snow and ice in the winter months and provide safer driving conditions. However, the benefits have not come without a cost. Concrete's permeability allows the deicing salt in solution to penetrate to the steel rebar. Then, over time, chloride ions from the salt will reach high enough concentrations to disrupt the chemical balance at the concrete/rebar interface. Along with moisture and oxygen, these conditions result in excessive corrosion of the rebar. In many cases, this corrosion is extreme enough that the bridge deck needs to be prematurely replaced.

There have been many efforts to improve the performance of reinforced concrete bridge decks by improving the durability of its constituent materials, but one solution to this issue is replacing the deck with a material that is not susceptible to chemical attack from deicing salts. Fiber reinforced polymer (FRP) decking is one alternative that has been explored since the early 1980's. Researchers and manufacturers have developed many sandwich panel designs with honeycomb and cellular cores made of E-glass reinforced polyester or vinyl ester resin. These designs have primarily been manufactured using filament winding, hand lay-up, and extrusion methods. The major benefits of these panels was their weight (less than one-third the weight of an equivalent concrete deck), corrosion resistance, good fatigue performance, and potential for rapid field assembly, which could greatly reduce construction costs and interruptions of traffic flow (Zureick et al., 2003). However, these panels were relatively difficult and expensive to manufacture. Even though their low maintenance requirements made life cycle costs reasonable, the high initial cost coupled with small state budgets has kept state transportation departments from using them.

A viable alternative that has not been explored thoroughly, is a foam/reinforced foam core sandwich panel made of polyurethane materials and E-glass that is manufactured

using the vacuum assisted resin transfer molding (VARTM) process. These type of panels could potentially decrease initial expenses, manufacturing difficulties, and possibly reduce weight further while retaining or improving the benefits provided by previously explored FRP panels. Very little research has been done to explore the use of such panels in bridge decks. In order to evaluate the potential of foam core sandwich panels, the Missouri Department of Transportation (MoDOT) has funded the development of a prototype panel for use as bridge decking.

1.2. OBJECTIVES

The development and evaluation of a prototype panel will require five critical tasks. First, a comprehensive literature review must be conducted to understand existing research on FRP bridge decks. Second, a design study must be conducted to determine the materials and sandwich construction that will be used in the final panel. Third, a testing plan to evaluate the final prototype panel must be determined. Fourth, the prototype panels must be constructed and tested. Finally, the results must be used to evaluate the performance and validity of the prototype panel.

The tasks for this project are being spearheaded by a research group of three professors at the Missouri University of Science and Technology. The group consists Dr. Jeffery Volz of the Department of Civil Engineering and Drs. K. Chandrashekhara and Victor Birman of the Department of Mechanical and Aerospace Engineering. This research is part of the second task in the list above. The raw materials that could potentially be used in the prototype panel have been selected based on material properties testing, market availability, and ease of manufacturing. From these materials, small scale beams have been constructed by Dr. Chandrashekhara's group using their composites research lab. The

beams consist of three different configurations and one needs to be chosen to move forward to the design of a full scale panel.

The primary objective of this thesis is to evaluate the structural behavior of three potential core alternatives by testing the small scale specimens that have been manufactured. The results will be used to evaluate the strengths and weaknesses of each configuration and draw comparisons between the three options. From this, the most suitable configuration for the prototype panel will be recommended to move forward in the design process.

1.3. RESEARCH PLAN

Fulfillment of the aforementioned objectives will require a comprehensive research plan that can be broken down into six tasks. The first task is a complimentary literature review that includes general study of the problem and a detailed study of small scale testing methods for sandwich panels. This is essential to understanding of the problem at hand. The second task is to select a set of small scale tests, based on the literature review, to evaluate the three different core alternatives. Then, a test matrix must be developed to summarize the size and number of specimens that will be used for each test, and the development of this matrix will be dependent on the size and quantity of specimens that can be made by Dr. Chandrashekhara's group. The third task will be preparing the specimens for the small scale testing by sectioning them to the appropriate sizes, then applying any instrumentation that might be needed such as strain gauges. The fourth task will be to acquire or manufacture the testing apparatus needed for each test, and adapt the apparatus as necessary to fit within the available testing machines. The fifth task will be testing the specimens and thoroughly recording all of the results for each test. The sixth

and final task will be to analyze the results of each test. Using the results, observations can be made for each core alternative and they can be compared to one another to make a final recommendation.

1.4. OUTLINE

This thesis will consist of seven sections and five appendices. The first section serves as an introduction to the thesis. This includes a brief background of bridge deck corrosion and the use of FRP bridge decking to mitigate this problem, the primary objectives of the project and this thesis, and a description of the research plan for this thesis. The second section is a literature review summarizing the existing research on FRP bridge decks, the theories used to analyze sandwich panels, and the existing standards for small scale testing of sandwich panels. Section three is a description of the three different core alternatives including the raw materials used in each of the sandwich constructions, a summary of the VARTM process used to manufacture small scale beams for each alternative, and the final dimensions of these small scale beams. The fourth section presents the first small scale experiments conducted in this research, which is designated as flatwise testing. The procedure, results, and a discussion of the results in presented for both flatwise compression and tension testing in this section. The fifth section describes the second set of small scale experiments, which was flexural testing. The procedure, results, and a discussion of the results in presented for both the three and four point flexural testing in this section. Section six is an analysis of the flexural testing results in which the flexural stiffness and strength of each core is evaluated. The theoretical principles and equations used in the analysis, the results of the analysis, and a discussion of the results is presented

in this section. The final section completes the thesis with conclusions of the research, recommendations, and a summary of future work on the project.

As for the appendices, the first (Appendix A) details the test results for each individual flatwise compression test specimen. Appendix B details the test results for each individual flatwise tension test specimen. Appendices C and D detail the test results for each individual flexural testing specimen. The three point specimens are detailed in Appendix C, and the four point specimens are detailed in Appendix D. The final appendix (Appendix E) details each iteration of the flexural stiffness calculations.

2. LITERATURE REVIEW

Fiber reinforced polymer (FRP) composites were first created and developed in the first half of the 20th century, and their development continues into the 21st century fueled by engineering problems that require lightweight materials with high strength and durability. They are commonly used in the aerospace, automotive, marine and construction industries for a large variety of applications. The literature and research related to FRP composites is broad and spans across many different disciplines. Therefore, to maintain some brevity, the scope of this discussion must be limited. This literature review will briefly discuss the history of analytical and experimental research on FRP bridge decking. Then, an overview of the different types of theories used to analyze sandwich panels and beams will be presented. Finally, the existing standards for small scale testing on sandwich constructions will be presented.

2.1. SUMMARY OF RESEARCH ON FRP BRIDGE DECKING

The concept of FRP bridge decking was initially researched in the United States in the mid to late 1980's and was funded by the National Science Foundation (NSF) and the Federal Highway Administration (FHWA). The first design concepts consisted of deck panels with truss like cross-sections. These panels were entirely FRP with E-glass fibers and vinyl ester or polyester resin systems. Plecnik and his associates were the first to explore the different panel configurations shown in Figure 2.1. They used finite element analysis to evaluate these different configurations. Their model consisted of truss and plate elements with an average elastic modulus despite the anisotropic nature of the materials that were being modeled. These initial studies showed that the design of these

configurations was always controlled by the deflection limit state, span length divided by 800, rather than the strength limit states. The deflection limit state was based on the serviceability requirements established by the American Association of State Highway and Transportation Officials (AASHTO) in their Standard Specifications for Highway Bridges. They also concluded that the Type II configuration was the most efficient based on the deflection limit state (Henry, 1985; Ahmad and Plecnik, 1989).

After these analytical studies, the most efficient configuration was manufactured out of E-glass and vinyl ester using a combination of filament winding and hand lay-up techniques Figure 2.2 shows one of the manufactured specimens. These specimens were used to experimentally determine the static and fatigue behavior. These initial experiments showed that damage under fatigue loading consisted primarily of delamination and local buckling of delaminated layers (Plecnik and Azar, 1991).

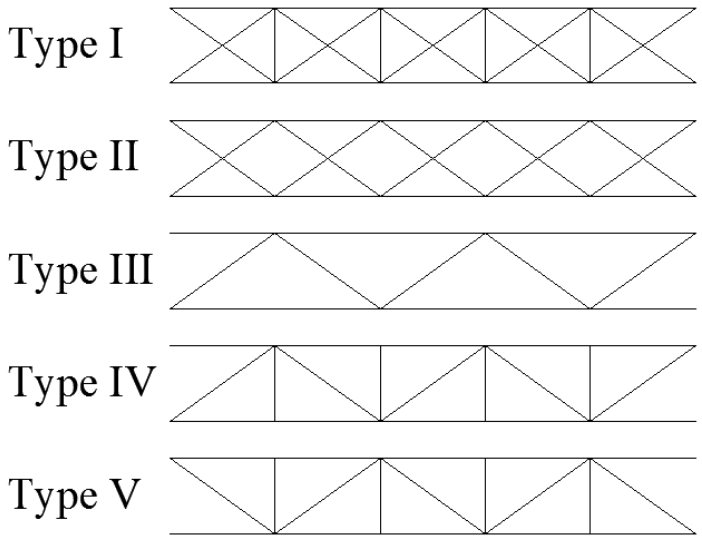

Figure 2.1: Configurations Analyzed by Plecnik and Associates

Separate numerical analysis was also conducted by McGhee and his colleagues using the same configurations presented in Figure 2.1. In this study, they considered the practical application of each configuration, as well as, the behavior predicted by finite element analysis. This investigation considered the practicality of each configuration based on the weight, which effects cost, and ease of manufacturing and assembly. They concluded that the Type III configuration was the best fit for bridge deck applications because it produced the lightest decking system with a weight of 20 lb/ft^3 (McGhee et al., 1991).

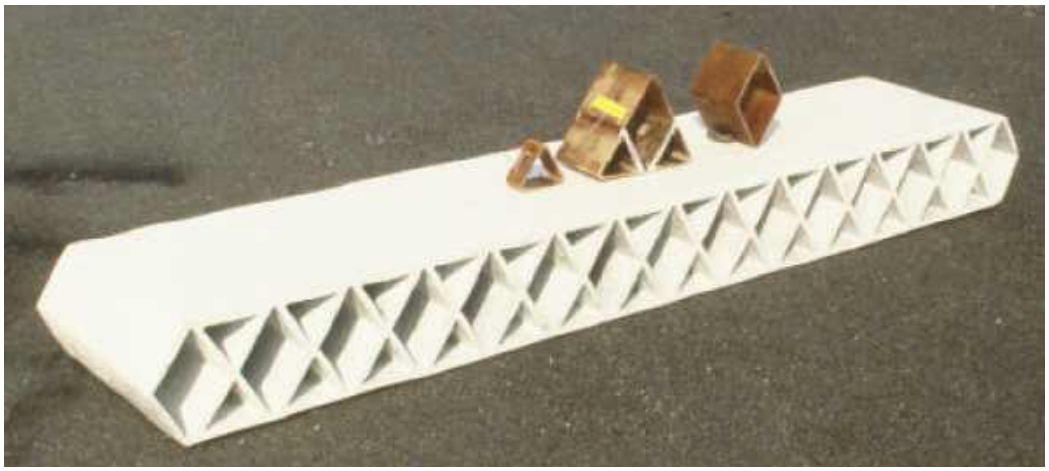

Figure 2.2: Specimen Constructed by Plecnik and Azar (Bank, 2006)

Additionally, Zurieck and his colleagues had begun an experimental and analytical program in the late 1980's to access the viability of the four different configurations shown in Figure 2.3. This resulted in several papers on the design and analysis of FRP bridge decking. In these studies, they conducted several finite element analyses in which they calculated the anisotropic properties of the FRP using laminate theory. From the finite

element analyses, they concluded that the “V” and cross shaped configurations produced the smallest deflections. Zurieck also focused on experimental testing with a focus on material testing of the components and flexural testing of full size panels including static behavior under simply supported three and four point loading and patch loading to simulate tire loading. Panels were constructed using pultruded elements bonded together. A photograph of one the full scale panel tests conducted by Zurieck is shown in Figure 2.4.

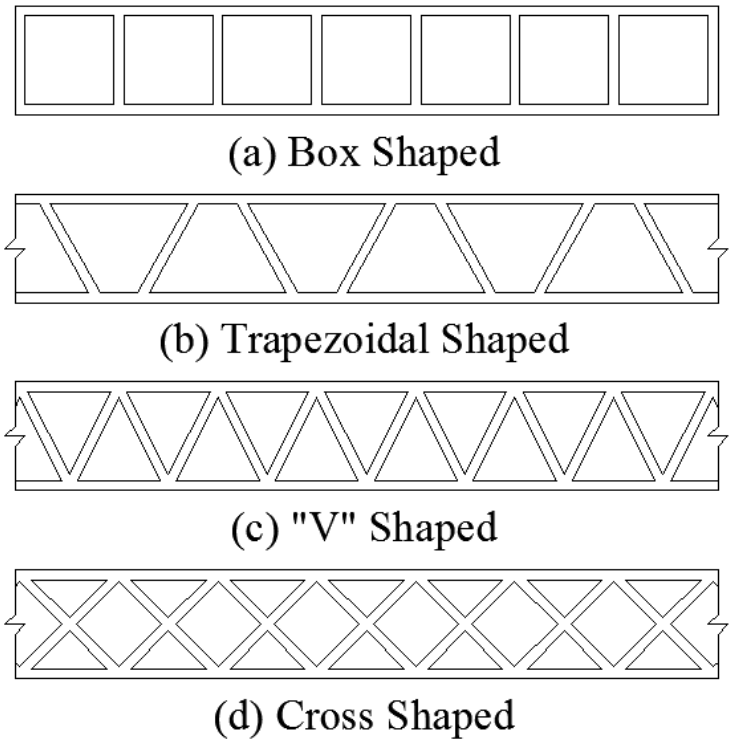

Figure 2.3: Configurations Analyzed by Zurieck

He adopted or modified exiting test standards used in other industries to experimentally measure material properties, and for the design of the panels he adopted and modified existing specifications related the design of highway bridges and marine

structures established by AASHTO, the U.S. Army, and the U.S. Navy. Consequently, two "V" shaped panels (10 ft x 18 ft) were constructed for testing in the field. They were installed on Interstate 81 near Troutville, VA in a pavement excavation adjacent to the "weigh-in-motion" scales. The panels were instrumented with fiber optic strain measurement devices to measure the response to tractor trailer traffic. Using the experimental and in-field tests, they established design guidelines and specifications for decking panels of this type and configuration. This study culminated in a comprehensive report on the design of FRP bridge decking submitted to the FHWA (Zurieck et al., 2003).

Figure 2.4: Full Scale Flexural Test of "V" Shaped Panel Under Patch Load by Zurieck

Concurrently, researchers at West Virginia University – Mongi, GangaRao, and Sotiropoulos – conducted extensive research on FRP decks and stringers. Initially, decks consisting of cellular box sections, "I" sections, "C" sections, and plates connected by bolts

were studied both experimentally and numerically. In these studies, multiple configurations of different sizes and configurations of these members were considered, as well as, different joint types and loading conditions. Two different configurations were constructed for testing. The authors concluded that there was a good correlation between experimental and numerical results, and the best fit decking configuration was made of 2 cellular box sections connected by an "I" beam supported by FRP stringers (Mongi, 1991; GangaRao and Sotiropoulos, 1991). Researchers at West Virginia University continued development of decking fabricated by the pultrusion process in the mid to late 1990's. This led to the development of a panel configuration constructed of hexagonal and trapezoidal tubes shown in Figure 2.5.

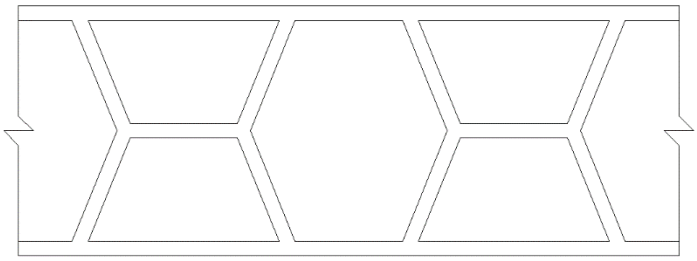

Figure 2.5: Cross-section of FRP Decking Developed by West Virginia University

Three composite deck bridges – the Wick Wire Run Bridge in Taylor County, WV (May 1997); the Laurel Lick Bridge; and the Market Street Bridge in Louis County, WV (September 1997) – were constructed using this decking. The panels for these projects were manufactured by Creative Pultrusions Inc. under the product name Superdeck^{TM}, and a photo of these type of panels being assembled is presented in Figure 2.6. (The details of

this research can be found in GangaRao et al. (1999). Research continued into the 21st century with research and development of second generation deck panels with this cross-section by Shekar (2000).

Figure 2.6: Superdeck Panels used in the West Virginia Bridges (Hastak et al., 2004)

Hybrid concepts using glass fiber reinforced plastic, carbon fiber reinforced composites, and lightweight concrete were explored in the early 1990's by Bakeri and Sunder. They developed a system using these three components which met the deflection limit state previously discussed. However, they assumed a perfect bond between the concrete and FRP (Bakri, 1989; Bakri and Sunder 1990).

Many composite manufacturers began to commercially develop FRP bridge decking by the late 1990's, which led to their implementation in many bridges. The research and development of these commercial panels explored new manufacturing and modelling methods. The following discussion will present some of the commercial panels

available at the turn of the century, as well as, a few of the resulting research programs and construction projects for each panel that have not already been discussed. There were several manufactures of commercial FRP bridge decks, which include but are not limited to Hardcore Composites, Kansas Structural Composites Inc., Infrastructure Composites International, Martin Marietta Composites, Creative Pultrusions Inc., and Strongwell.

Kansas Structural Composites Inc. (KSCI) developed fiber-reinforced polymeric honeycomb (FRPH) sandwich panels constructed using primarily hand lay-up methods. These panels offer a manufacturing cost that is lower than that in aerospace application and competitive with conventional bridge materials (Hastak et al., 2004). No-Name Creek Bridge, near Russell, KS was the first public road bridge to have an all composite deck and was built using these panels in November 1996. The details of this project can be found in a report by Gill and Plunkett (2000). These panels were also implemented in a study by the Missouri Department of Transportation (MoDOT) where the decks of several small span community bridges in St. James, MO were built with these panels. The laboratory and field studies for this project can be found in a report by Nystrom et al. (2002), and a picture of one of the flexural tests conducted in the laboratory is shown in Figure 2.7.

Martin Marietta Composites developed a product called DuraSpan®, which is a pultruded deck with a trapezoidal cross-section made of continuous E-glass fiber reinforcement and polymer resin (Hastak et al., 2004). This FRP decking was used initially in the construction of two bridges in 1997. The first was the INEEL Bridge located near Idaho Falls, ID. The second bridge was the Tech21 Bridge in Butler County, OH. The details of this project were outlined by Zoghi et al. (2002). A photograph of the panels after

installation at the Independence River Bridge located in New York in 2003 is shown in Figure 2.8 (Bank, 2006).

Figure 2.7: Flexural Test of FRPH Panel (Nystrom et al., 2002)

Figure 2.8: DuraSpan® FRP Bridge Deck Panels (Bank, 2006)

Hardcore composites was the leading manufacturer of large-scale FRP components for infrastructure application, but unfortunately no longer exists. They developed a Vacuum Assisted Resin Transfer Molding (VARTM) process to manufacture orthotropic honeycomb core sandwich panels which were used in the construction of five bridges in the New England area between 1998 and 1999 (Hastak et al., 2004; Nystrom et al., 2002). The first was Bennett's Creek Bridge in West Union, NY started in September of 1998. The details of this project have been outlined in a paper by Alampalli et al. (2000). The second was Laurel Run Bridge in Somersat County, PA constructed in October 1998. The details of this construction project were presented by Shekar et al. (2002). The third was Muddy Run Bridge near Newark, DE which was built in November 1998. Details of this project were outlined by Chajes et al. (2000). The fourth was the I-192 Bridge in New Castle County, DE completed in the summer of 1999. The fifth was Bentley Creek Bridge near Elmira, NY built in September 1999. This project was outlined by Wagh (2001).

Strongwell, a manufacturer of purtruded FRP components with many international customers, has supported the use of their technology in infrastructure by developing components for use in pedestrian and vehicular bridges. Specifically, they developed deck panels made of pultruded square tubes bonded together for use in vehicular bridges (Hastak et al., 2004). A photograph of these panels is shown in Figure 2.9. The behavior of these panels has been evaluated by Cousins and Lesko (2004) with in-situ tests at a weighing station in Troutville, VA.

A comparative discussion of the decking systems commercially produced at the turn of the century was conducted by Zhou (2001). Also, a joint bridge project was conducted in September of 1999. Panels provided by Composite Deck Solutions, Creative

Pultrusions Inc., Hardcore Composites, and Infrastructure Composites International were installed on the Salem Avenue Bridge. The goal of the study was to evaluate several deck panels systems in one project. Henderson (2000) and Reising et al. (2001) have presented the details of the project.

Figure 2.9: FRP Bridge Decking Manufactured by Strongwell (Hastak et al., 2004)

Research and development of these commercial FRP bridge deck systems has continued into the 21st century along with experimental and analytical research conducted by scholars. Some other noteworthy studies include the design and construction of a smart composite bridge at the University of Missouri–Rolla detailed by Chandrashekhara et al. (2004), which was constructed using pultruded FRP square box sections. This study included finite element modeling of the structure, material stiffness and strength evaluation of the components, fatigue testing, and in-situ tests of the bridge. They reported a good correlation between experimental and finite element results, and concluded that all-

composite bridge decks of this type were a suitable replacement for conventional short span bridges.

Furthermore, decking consisting of orthotropic square box beams was investigated by Temeles (2001). Temeles conducted experimental research including extensive fatigue testing for which he reported no significant loss in stiffness. Zhou conducted both experimental and analytical research. In this study, he concluded that the method of elastic equivalence based on classical lamination plate theory could predict bending deflections well, but suggested finite element analysis or higher order plate theories to predict deflections under point loads. He also developed methods for failure analysis for FRP decking.

Research was also conducted on 3-D FRP panels by Hassan et al. (2003). These panels utilized sandwich constructions made of FRP facings and foam cores reinforced with three dimensional fiber structures using weaving and injection processes. In this study, they conducted material property tests to establish the behavior of these types of panels, as well as the limitations of ordinary sandwich theory when applied to these types of panels.

In conclusion, this serves as a brief overview of the development of FRP bridge decking in the United States. Research on this topic is two decades in the making now, and the concepts of cellular paneling and honeycomb core panels have been researched and developed thoroughly with established design methods. In the past decade, research has been fairly limited and focused primarily on variations of the designs discussed previously or details in the designs aimed at improving their performance. The diversity of materials has also been limited to primarily E-glass fibers and polyester or vinyl ester resin. Construction of these panels primarily uses filament winding, hand lay-up, and extrusion

methods. Construction methods employing resin transfer molding and vacuum assisted resin transfer molding techniques have been used to a much lesser extent. Reiterating, this is by no means a comprehensive record of research on the topic but serves simply as an indicator of the general direction and scope of the research that has been published and is readily available.

2.2. OVERVIEW OF SANDWICH THEORY

Theoretical analysis of sandwich beams and panels is a well-researched and understood topic. In order to maintain brevity, this discussion will only include some of the milestones in theories related to sandwich constructions. Only the simplified theories used in the analysis of the experimental results will be detailed with governing equations that apply to the behavior of beams, while the remaining extended theories will be discussed in terms of their assumptions and benefits. Sandwich panels with rigid prismatic cross-sections are often analyzed with classical or engineering bending theories in the form of Euler-Bernoulli Beam Theory (EBBT) or Kirchhoff-Love Plate Theory (KLPT). These theories neglect the effects of shear deformations assuming plane sections remain plane and also assume linear elastic material response, homogenous/isotropic material properties, and small deflections. The governing equations of EBBT will be presented here because they are used in the analysis of Section 6. The coordinate system is shown in Figure 2.10, where the x-direction (longitudinal) coincides with the centroidal axis of the beam cross-section and the z-direction (flatwise) and y-direction (transverse) are in the other two orthogonal directions.

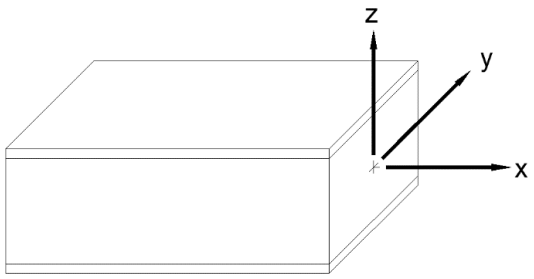

Figure 2.10: Coordinate System Used for EBBT and TBT

Then, the assumed displacement vector of a beam segment under symmetrical loading in the z-direction is described by Equation 2.1.

$$u_x(x,y,z) = 0$$
$$u_y(x,y,z) = 0 \qquad (2.1)$$
$$u_z(x,y,z) = w(x)$$

Where u_x, u_y, and u_z are the components of the displacement vector of the centroidal axis of the beam segment in each or the respective coordinate directions. Therefore, *w(x)* is the displacement of the beam segment in the z-direction at position "x" along the beam. The governing equation relating the deflection to the applied load is then described by Equation 2.2.

$$EI\frac{d^4w}{dx^4} = q(x) \qquad (2.2)$$

Then, using the concepts of static equilibrium and internal bending moments and shear forces. Equation 2.2 can be restated by Equations 2.3 and 2.4.

$$M(x) = -EI\frac{d^2w}{dx^2} \tag{2.3}$$

$$V(x) = \frac{dM}{dx} \tag{2.4}$$

In these equations, *E* is the modulus of elasticity of the beam, *I* is the area moment of inertia of the beam cross-section about the axis of bending. For beams of multiple materials, the term "*EI*" can be calculated as a summation of the contributions of each different material component, or it can be calculated using transformation theory by altering the geometry using the modular ratio between components and transforming the cross-section into one material with the same effective bending stiffness. Then, *q(x)* is the applied load, *M(x)* is the total internal bending moment in the segment, and *V(x)* is the total internal shear force in the segment at position "x" along the beam. The sign convention of positive bending moments and shear forces is presented in Figure 2.11.

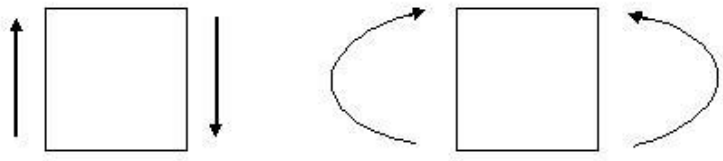

Figure 2.11: Sign Convention for Positive Bending Moments and Shear Forces

For beams consisting of one material, the bending stress under symmetrical loading in the z-direction can then be defined by Equation 2.5. For beams of multiple materials the bending stress can be calculated with this equation by using transformation theory and the modular ratio discussed previously. The average shear stress can be found using Equation 2.6. The shear stress can also be solved for using elasticity theory, and the solution is well known for thin plates and cross-sections of a single material made of thin plates. For symmetrical loading, the exact distribution is generally parabolic and vanishes at the extreme fibers. However, the analytical solutions for shear stress are often difficult to solve for using elasticity theory when the beam geometry is complex or the beam is made of multiple materials. Furthermore, the use of the average shear stress equation is a conservative estimate of the maximum shear stress in the cross-section.

$$\sigma = -\frac{Mz}{I} \tag{2.5}$$

$$\tau_{avg} = \frac{V}{A} \tag{2.6}$$

In Equations 2.5 and 2.6, σ is the axial bending stress and is a function of "x" and "z", τ_{avg} is the average shear stress and is a function of "x", and A is the cross-sectional area. The solutions to classical bending theory are easily calculated, and have been used to estimate the flexural stiffness and strength of sandwich beams with experimental data. On the other hand, the assumptions of this theory are often not technically met when considering FRP composite beams, and several limitations are evident when trying to predict the deflections and stresses in panels with flexible core materials.

Analysis of more modern sandwich constructions using relatively flexible core materials began with work by Plantema (1966) and Allen (1969). They developed a Simplified Sandwich Theory (SST) for the bending behavior of beams and panels with thin facings (the ratio of the core and facing thickness is sufficiently large) and flexible cores. The assumptions of SST are generally the same as the classical bending theory except the contribution of shear stresses is considered using first order shear deformations, however it neglects the transverse flexibility to the cross-section and does not account for changes in the thickness of the cross-section or cross-sectional warping. SST assumes the facings carry the bending stresses while the core carries the shear stresses. The bending stresses in the facings are considered to follow the distribution described by Equation 2.5 where I is the area moment of inertia of the facings, and the shear stress in the core is considered to be constant and essentially equal to the average shear stress in the core found using Equation 2.6 where A is the cross-sectional area of the core. The governing equations relating the deflection to the applied load can be derived using these assumptions and can be found in the previously mentioned texts. Plantema and Allen then continued to simplify the equations by considering the total deflection as a superposition of the bending deflections of the facings and the shear deflections of the core. This leads to a system of governing equations that is equivalent to First Oder Shear Deformation Theory (FOSDT), also known as Mindlin-Reissner Plate Theory for plates and for beams Timoshenko Beam Theory (TBT). The simplified equations used by Plantema and Allen will not be presented here because the specific solutions used in the analysis of this thesis are based on TBT. However, the equations of SST and TBT produce the same solutions when the same assumptions are considered.

If the coordinate system presented in Figure 2.10 is used, then using TBT the displacement of an infinitesimal beam element, under symmetrical loading in the z-direction, is assumed to be described by Equation 2.7. Where u_x, u_y, and u_z are the components of the displacement vector of the centroidal axis of the beam segment in each of the respective coordinate directions. Then, $\varphi(x)$ is the curvature of the beam, and $w(x)$ is the displacement of the centroidal axis in the z-direction at a position "x" along the beam.

$$\begin{aligned} u_x(x,y,z) &= -z\varphi(x) \\ u_y(x,y,z) &= 0 \\ u_z(x,y,z) &= w(x) \end{aligned} \tag{2.7}$$

Then, the governing equations relating the applied load to the deflection can now be defined by Equations 2.8 and 2.9. Then, using the concepts of static equilibrium and bending moments and shear forces, Equations 2.8 and 2.9 can be redefined as Equations 2.10 and 2.11.

$$\frac{d^2}{dx^2}\left(EI\frac{d\varphi}{dx}\right) = q(x) \tag{2.8}$$

$$\frac{dw}{dx} = \varphi(x) - \frac{1}{kAG}\frac{d}{dx}\left(EI\frac{d\varphi}{dx}\right) \tag{2.9}$$

$$M(x) = -EI\frac{d\varphi}{dx} \tag{2.10}$$

$$V(x) = kAG\left(-\varphi + \frac{dw}{dx}\right) \tag{2.11}$$

In these equations, *k* is the shear correction coefficient and *G* is the modulus of rigidity. These equations can easily be applied to beams of a single material, and they can be applied to beams of multiple materials using the transformation theory previously discussed. The application of this theory to sandwich beams with thin facings and flexible cores uses the same assumptions as SST where the facings only contribute to the bending stiffness term "*EI*" and the core only contributes to the shear stiffness term "*kAG*". The details of this theory are presented in a book by Carlsson and Kardomateas (2011). Many of the concepts established by this text and those by Plantema and Allen are used in the analysis of the experimental results in this thesis. The specific solutions and details of these theories utilized can be found in Section 6.

These classical and first order theories provide a good approximation of global deflections and average stresses, which makes them useful in design and measuring effective properties with experimental data. Nonetheless, there are several disadvantages to these theories including over simplification of some of the parameters, as well as, the many limitations of the assumptions. This becomes evident in the analysis of sandwich constructions with relatively flexible cores that experience significant localized effects beneath concentrated loads. These effects are caused by higher order deformations and affect local stress concentrations, which can significantly influence the deflections and failure of sandwich beams and panels. Therefore, several approaches have been developed to predict these localized effects such as higher order theories and extended higher order theories.

High-Order Sandwich Panel Theory (HSAPT) was introduced by Frostig et al. (1992). This theory takes into account the transverse flexibility of the core. The theory assumes that the faces have in-plane and bending rigidities, and the face sheets and core are considered linear elastic. The face sheets include first order shear deformations and undergo large displacements and rotations and moderate strains. The core is considered as a two dimensional linear elastic continuum that undergoes large rigid body displacements (due to its bond to the adjacent face sheets), but with kinematic relations that correspond to those of small deformations, where the core height may change during deformation and its section plane does not remain plane after deformation. The core possesses only shear and vertical normal stiffness, whereas the in-plane (longitudinal) normal stiffness is neglected. Full bond is assumed between the face sheets and the core, and the mechanical loads are applied to the face sheets only. The theory consists of a system of governing equations with five unknowns including two deflection components for the top face, two deflection components for the bottom face, and the shear stress in the core. The HSAPT was later extended to include the in-plane stiffness of the core material in a formulation by Frostig (2010). This Extended High-Order Sandwich Panel Theory (EHSAPT) follows nearly the same assumptions, but accounts for the in-plane stiffness of the core. The theory consists of a system of governing equations with seven unknowns including two deflection components for the top face, two deflection components for the bottom face, two deflection components of the core, and the slope of the core at its centroid.

HSAPT and EHSAPT are two well know examples of higher order theories for sandwich panels, but there are several other variations of these higher order theories that account for different assumptions and use different orders of magnitude for the profile of

the in-plane core deformations. Some examples of other higher order theories can be found in the aforementioned book by Carlsson and Kardomateas (2011). As a whole, the solutions to higher order theories require a numerical approach such as finite differences, and can be evaluated using finite element models. These types of theories have been shown to predict localized deformations and stress concentrations very well, and they are much better than the classical and first order theories at predicting failure of sandwich panels. However, they are complex and difficult to solve, which makes their implementation in design and experimental determination of material properties difficult.

All of the theories mentioned assume linear elastic behavior and isotropic material properties, which is not technically correct for panels or beams made of FRP laminates and/or complex core materials such as honeycomb structures and reinforced foams with anisotropic or orthotropic material behavior. These types of behaviors are often accounted for using effective properties or modifying the theory to account for anisotropic or orthotropic behavior. Effective properties are often measured using experimental testing, discussed in Section 2.3, or calculated using methods of equivalency such as Classical Laminated Plate Theory (CLPT). Carlsson and Kardomateas (2011) discuss the assumptions and CLPT and its application to sandwich composites.

Failure prediction is another very important part of analyzing and designing sandwich beams and panels, and there are several prevalent failure mechanisms which can be found in Figure 2.12. The first four are a function of the facing: (1) is compressive failure of the facing in the form of crushing or yielding, (2) is tension failure in the facing in the form of a fracture or yielding, (3) is localized buckling or wrinkling of the facing in compression, (4) is intra-cellular dimpling, which is localized buckling under compression

with a wavelength proportional to the dimensions of the core cells. The last two are related to the core material: (5) is local indentation characterized by localized crushing or yielding of the core material and wrinkling of the facing in a wave length proportional to the dimensions of the loading pad, and (6) is shear failure of the core in the form a diagonal fracture or yielding of the core material. Another prevalent failure mechanism not presented in the figure is debonding between the facings and the core material or delamination between laminate layers.

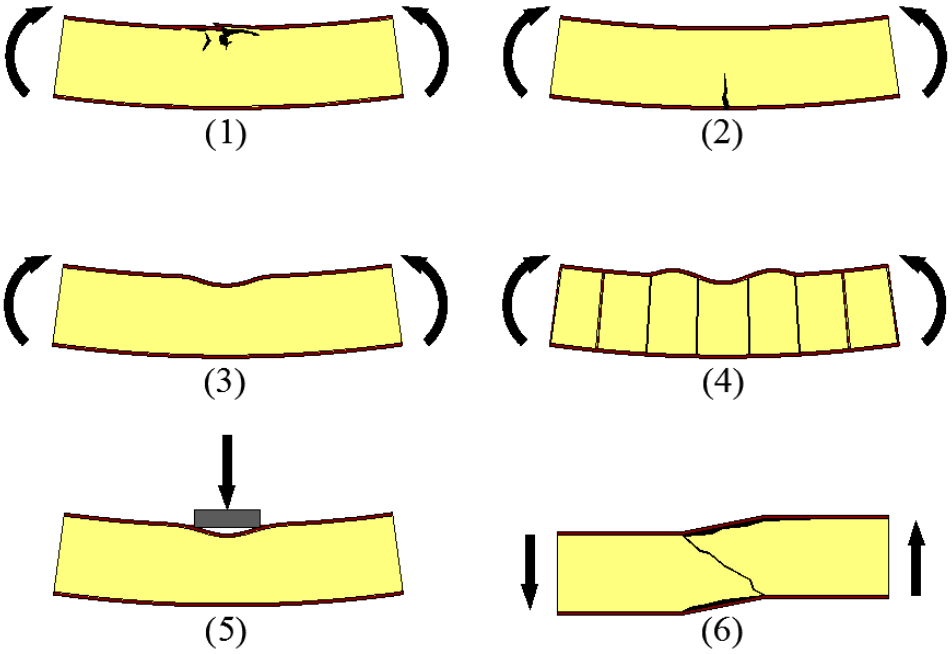

Figure 2.12: Failure Modes of Sandwich Constructions

Failures (1) and (2) are a function of the strength of the facing material and the bending stresses present in the facings. Generally, failure will occur when the bending stress in the facing equals the strength of the material in tension or compression. The

material strength is typically measured using experimental testing, which is discussed in Section 2.3, and the bending stresses are calculated using the theories previously mentioned.

The next two failure modes, (3) and (4), are related to the elastic stability of the facing in compression. This failure mode is typically analyzed by determining the critical compressive load or stress that will initiate localized buckling, then limiting the bending stress to this critical value. Many analytical models have been developed to predict the critical load or stress in the general case of wrinkling and the case of intra-cellular dimpling. A detailed summary of these theories are presented in the previously mentioned book by Carlsson and Kardomateas (2011). Experimental testing is not typically used to directly measure critical local buckling stresses, however it has been used to evaluate the accuracy of these theories and establish specifications aimed at preventing localized buckling. Many of the studies mentioned in the previous Section 2.1 address this issue accordingly.

Local indentation (5) is a function of the out-of-plane (flatwise) compressive strength of the core material and the applied concentrated loads. In design and application, the contact pressure under concentration is typically limited by the flatwise compressive strength of the core material. The flatwise compressive strength of the core can be easily measured experimentally, which will be discussed in Section 2.3, but the contact pressure under the load is often misrepresentative of the out-of-plane stress in the core material especially when taken as an average. The pressure distribution under the load, and consequently the out-of-plane compressive stress in the core, have a nonlinear distribution that is effected by many factors. These factors include the bending stiffness of the facing, the out-of-plane stiffness of the core, and the boundary conditions. This type of failure has

been analyzed by Thomsen (1977), Ashby et al. (2000), and Steeves and Fleck (2004). Again, similar to the treatment with local buckling, experimental testing is typically used to establish specifications that circumvent local indentation failure, and many of the studies mentioned in the previous Section 2.1 address this issue accordingly.

Shear failure in the core is a function of the shear strength of the core material and the shear stresses present in the core. Generally, failure will occur when the shear stress in the core equals the shear strength of the core material. The material strength is typically measured using experimental testing, which is discussed in Section 2.3, and the shear stresses are calculated using the theories previously mentioned. Shear buckling is also a possibility in long slender core components, but typically this is avoided by increasing the thickness of these components in the regions prone to instability.

Debonding between the facings and the core material and delamination between fiber layers are prominent failure mechanisms for sandwich panels. These failure mechanisms are often analyzed using principles of fracture mechanics. The details of fracture mechanics are beyond the scope of this research, however the application of linear elastic fracture mechanics to sandwich composites is thoroughly explained by Carlsson and Kardomateas (2011). This text also details testing methods for analyzing debonding failure, which are not presented in Section 2.3.

In conclusion, this serves as a brief overview of sandwich theory. Analysis of sandwich beams and panels is well developed, and has had several significant advances in the 21st century. For Civil Engineering applications such as FRP bridge decking, analysis and design has primarily consisted of finite element modeling with elements formulated using classical or first order bending theories. Analysis has been expanded to account for

anisotropic or orthotropic material behavior based on CLPT, but very few panel concepts have used core materials or configurations that are flexible enough to require higher order analysis.

2.3. SMALL SCALE TESTING OF SANDWICH CONSTRUCTIONS

There are many standards for small scale testing of sandwich constructions. This discussion will focus primarily on the standards published by the American Society for Testing and Materials (ASTM), as well as, the standards relating specifically to the mechanical properties of FRP facings and sandwich core materials. The mechanical properties of FRP facing materials can be measured directly using coupon testing. ASTM D3039: Standard Test Method for Tensile Properties of Polymer Matrix Composite Materials, details the measurement of FRP mechanical properties in tension. As for mechanical properties in compression, ASTM D3410: Standard Test Method for Compressive Properties of Polymer Matrix Composite Materials with Unsupported Gage Section by Shear Loading, details experimental testing for these properties. These experimental tests can be used to measure the modulus of elasticity, the ultimate strength, and the ultimate strain in the longitudinal and transverse directions, and they can be used to measure the major and minor Poisson's Ratios. These properties can also be measured using long beam flexural testing detailed in ASTM D7249: Standard Test Method for Facing Properties of Sandwich Constructions by Long Beam Flexure. Furthermore, the in-plane shear properties of FRP facings or core components can be measured directly using the methods detailed ASTM D5379: Standard Test Method for Shear Properties of Composite Materials by the V-Notched Beam Method. This test method uses notched short

beam specimens to measure the modulus of rigidity, the ultimate shear strength, and the ultimate shear strain in both the longitudinal and transverse directions.

The mechanical properties of honeycomb and foam/reinforced foam core materials can also be measured directly. For general core materials, the compressive and tensile properties can be measured in the flatwise direction using block segments from larger beams or panels. The compressive properties can be measured using ASTM C365: Standard Test Method for Flatwise Compressive Properties of Sandwich Cores, and the tensile properties can be measured using ASTM C297: Standard Test Method for Flatwise Tensile Strength of Sandwich Constructions. These experiments can be used to measure the modulus of elasticity, the strength, and the strain at strength in the flatwise direction. The compressive and tensile properties can also be measured in the longitudinal and transverse directions in a similar manor using blocks of raw core material. However, due to the diversity of core materials and the numerous ASTM standards written for each material, this discussion will be limited to just the flatwise testing. Moreover, the shear properties of the core can be directly measured using panel segments. This approach is detailed in ASTM C273: Standard Test Method for Shear Properties of Sandwich Core Materials. This experiment can be used to calculate the effective shear properties of the core such as the modulus of rigidity, the shear strength, and the shear strain at strength. These properties can also be measured using short beam flexural testing detailed in ASTM C393: Standard Test Method for Core Shear Properties of Sandwich Constructions by Beam Flexure.

Another important aspect of sandwich constructions is flexural and shear stiffness especially considering that FRP bridge decking is controlled primarily by deflection in

design. ASTM D7250: Standard Practice for Determining Sandwich Beam Flexural and Shear Stiffness, details a method of calculating these values using test results from flexural tests based on ASTMs C393 and D7249. This methodology utilizes the simplified sandwich theory presented in the previous section and can be used to calculate the flexural and shear stiffness of a sandwich construction, as well as, the effective modulus of elasticity of the facings and the effective modulus of rigidity of the core.

In conclusion, there are many ASTM standards that have been developed and used to test FRP composite sandwich constructions and their components. The focus of this study is to evaluate three different core alternatives, for use in bridge deck panels, based on small scale testing. Considering that the specimens provided for these tests are small scale sandwich beams, which are thoroughly detailed in Section 3, the research team has chosen to limit its focus to two sets of experiments. The first set of experiments is flatwise testing to evaluate the material properties of the core materials, and the second is flexural testing to evaluate the flexural response of each sandwich construction. The specific details of these tests are presented in Sections 4 and 5, respectively.

3. CORE ALTERNATIVES

Three different core alternatives were chosen for small scale testing in cooperation with Dr. K. Chandrashekhara of the Department of Mechanical and Aerospace Engineering and his graduate research group. His research group constructed small scale sandwich beams for each alternative using the vacuum assisted resin transfer molding (VARTM) process. In the following section, the constituent materials for each core alternative will be presented, as well as, the materials used for the sandwich facings. Then, the final section will present the details of the manufacturing process along with the final dimensions and density of each sandwich construction.

3.1. CONSTITUENT MATERIALS

Each sandwich construction used the same resin system and facing fibers. The resin system was a two-part thermoset polyurethane made by Bayer Material Science, and the facing fibers consisted of woven bi-directional (+/- 90^o) E-glass fibers manufactured by Owens Corning that were compatible with the resin system. The core alternatives consisted of different polyurethane foam configurations. The Type 1 core consisted of high density closed cell rigid polyurethane foam manufactured by 3M Company. The foam had a density of 6 lb/ft^3 and had no additional reinforcement. A photograph of a raw material block of the Type 1 core is presented in Figure 3.1. The final dimensions of the cross-section for the small scale specimens are presented in the next section.

The Type 2 core was a low density flexible polyurethane foam core (2 lb/ft^3) with a woven bi-directional (+/- 45^o) E-glass fiber mat attached to the top and bottom faces, as well as, fiber glass mat web reinforcement. The web reinforcement is configured in a

rectangular cell pattern with grooves at the edges of the cells to assist resin flow across the web reinforcement. Once the web reinforcement is infused with resin, it becomes rigid and improves the core shear stiffness and strength significantly. The Type 2 core is manufactured by 3M Company. A photograph of a raw material block of the Type 2 core that shows the orientation of the web fiber reinforcement is presented in Figure 3.2. The final dimensions of the cross-section and the web reinforcement for the small scale specimens is presented in the next section.

Figure 3.1: Raw Material Block of the Type 1 Core

The Type 3 core consisted of low density flexible polyurethane foam (2 lb/ft^3) in a trapezoidal shape wrapped in a woven bi-directional (+/- 45^o) E-glass fiber mat. Additionally, woven bi-directional (+/- 45^o) E-glass fiber mats or "shear layers" were inserted between the trapezoidal foam blocks. Once the "shear layers" are infused with resin, they become rigid webs that increase shear strength and stiffness of the core. A photograph of a trapezoidal block of the foam in the Type 3 core is presented in Figure 3.3.

The final dimensions of the cross-section and the configuration of the shear and facing layers for the small scale specimens is presented in the next section.

Figure 3.2: Raw Material Block of the Type 2 Core

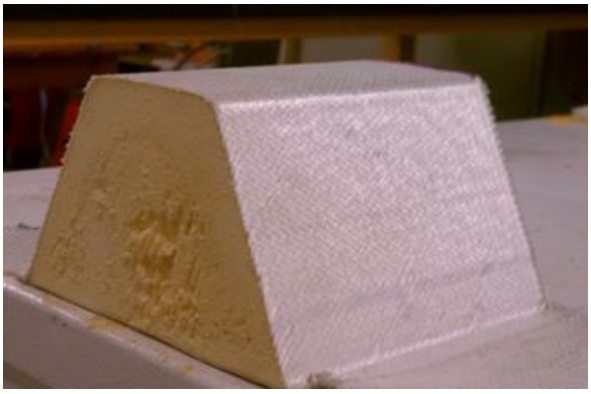

Figure 3.3: Trapezoidal Block of Foam for the Type 3 Core

3.2. MANUFACTURING OF THE SPECIMENS

The small scale specimens were manufactured using the VARTM process. This process utilizes a vacuum to infuse polymer resin into the fiber layers of fiber reinforced

polymer (FRP) composites. In order to achieve this, for the small scale sandwich panels, the core and fiber components of the construction were assembled in the desired configuration inside a vacuum bag with a resin inlet and a vacuum port to remove the air from the bag. The resin is infused through the components using the pressure gradient produced by vacuuming the air from the bag. A photograph of this process is presented in Figure 3.4. After the resin was infused, it hardened in an initial curing period. The specimens were then removed from the vacuum bag and post-cured in a walk in oven. Small scale sandwich beams and panels were constructed for each core type by Dr. Chandrashekhara's research group using this process. The final dimensions of each sandwich construction are presented in the following discussion.

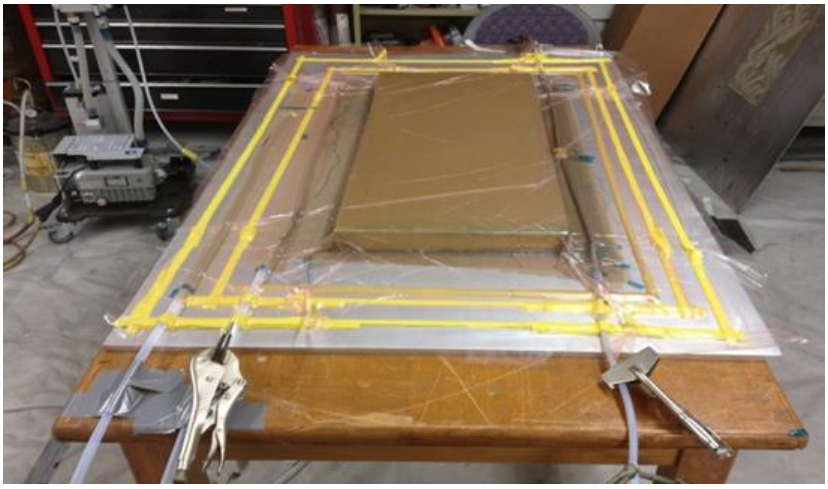

Figure 3.4: VARTM Process for Small Scale Specimens

The facings of the Type 1 specimens consisted of four woven glass fiber layers (+/-90^{o}) infused with polyurethane and had an average thickness of 0.095 in. The core

consisted of the aforementioned rigid high density polyurethane foam and had an average thickness of 1.944 in. As a result, the total thickness of the Type 1 specimens was 2.133 in. on average. Four small scale Type 1 beams were constructed that were approximately 35 in. long and 4 in. wide. Figure 3.5 is a photograph of two of the manufactured beams.

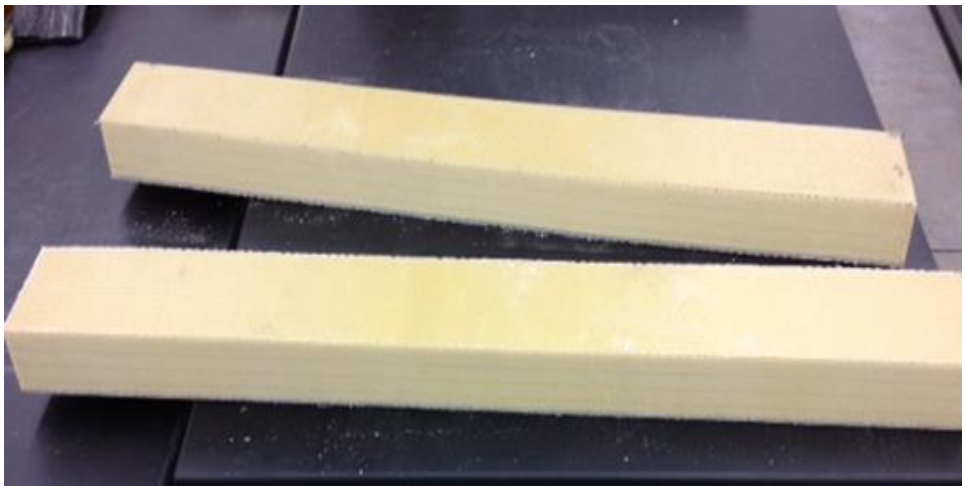

Figure 3.5: Manufactured Type 1 Beams

The facings of the Type 2 specimens consisted of four woven glass fiber layers (+/- 90º) and one woven glass fiber layer (+/- 45º) pre-attached to the core material. Despite the additional layer, the facing of the Type 2 specimens had the same average thickness of 0.095 in. The core of the Type 2 specimens consisted of the previously described flexible low density polyurethane foam with web reinforcement and had an average thickness of 2.143 in. The average total thickness of the Type 2 specimens was 2.333 in. The configuration and dimensions of the infused web reinforcement is presented in Figure 3.6. Four small scale Type 2 beams were constructed that were approximately 35 in. long and

4 in. wide. A photograph of two of the manufactured Type 2 beams is presented in Figure 3.7.

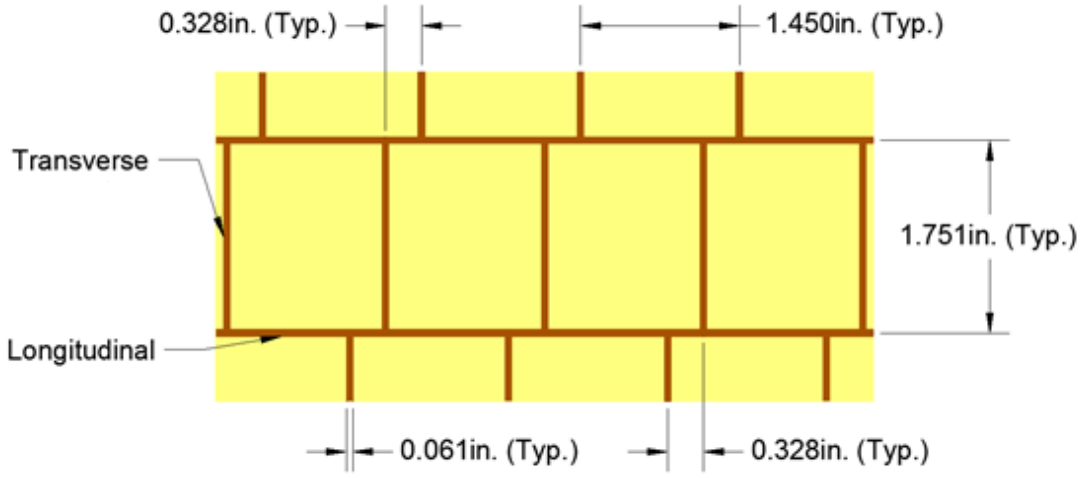

Figure 3.6: Final Dimensions of the Type 2 Web Reinforcement

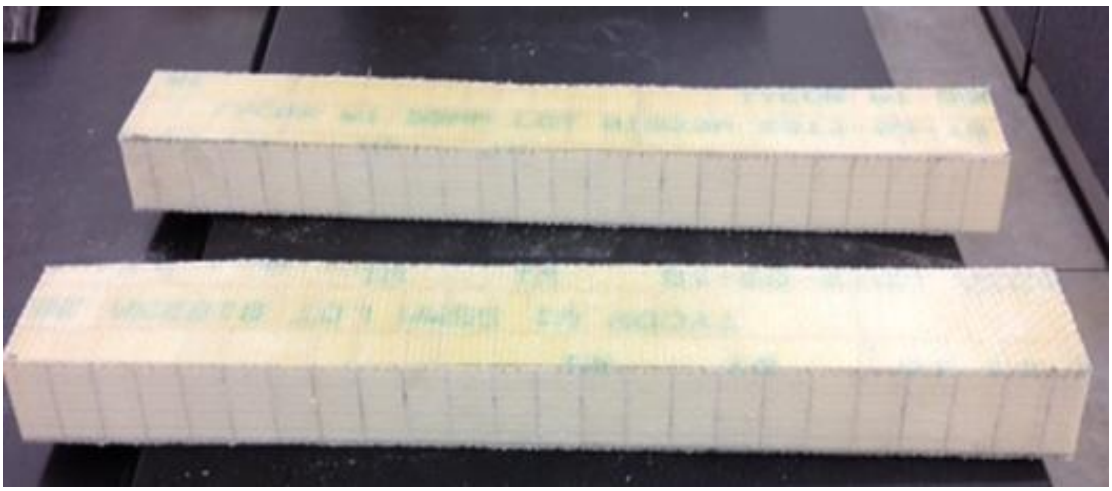

Figure 3.7: Manufactured Type 2 Beams

The fiber layers of the Type 3 specimen consisted of four woven glass fiber layers (+/- 90^{o}) that served as the facings. Then, lapped between the light-weight flexible foam blocks of the core were four woven glass fiber layers (+/- 45^{o}) or "shear layers". Additionally, one woven glass fiber layer (+/- 45^{o}) was pre-attached to the foam blocks. The configuration of the Type 3 construction is depicted in Figure 3.8.

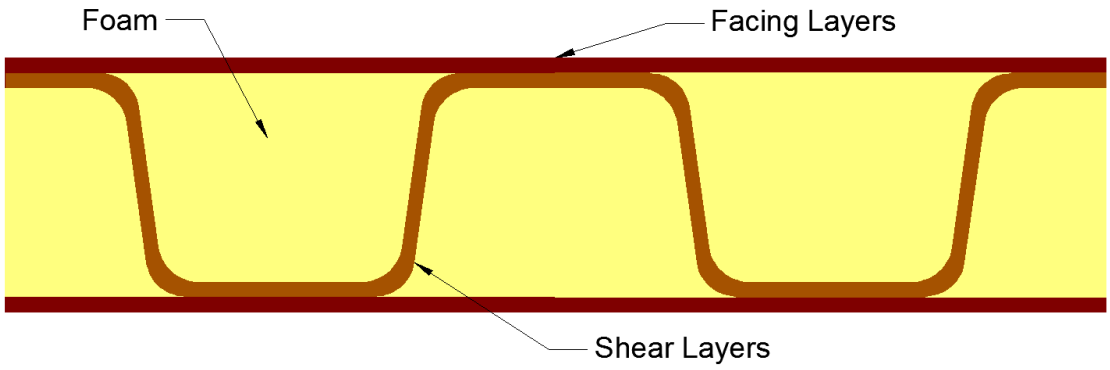

Figure 3.8: Configuration of the Type 3 Sandwich Construction

Unfortunately, the foam blocks needed for the Type 3 small scale specimens were difficult to obtain, therefore only one small scale beam was manufactured which was approximately 36 in. in length. The specimen only contained one prism shaped foam block, and the cross-sectional dimensions are presented in Figure 3.9. There were no photographs taken of the manufactured Type 3 specimen, however there are several photographs of the flexural test specimens that were segmented from the original beam that can be found in Section 5.

All three sandwich constructions had comparable facings but differed significantly in their core materials. Each core material required different amounts of polyurethane resin,

which effects both weight and cost. The bulk density of each construction was calculated by weighing the beams segmented for flexural testing and dividing by their volume, which was calculated using the average dimensions of the beams. The density of the Type 1 construction was 13 lb/ft^3, the density of the Type 2 construction was 13 lb/ft^3, and the Type 3 construction had a density of 37 lb/ft^3. The Type 1 core required the least amount of resin while the Type 2 required more resin to infuse the reinforcing webs, however the foam of the Type 2 construction was one third the density of the foam in the Type 1 construction, which explains why they had the same bulk density. Both the Type 1 and 2 constructions are more than ten times less dense than typical reinforced concrete. The Type 3 core required the most resin to infuse the shear layers, which explains why it had the largest bulk density, but it is still more than four times lighter than typical reinforced concrete.

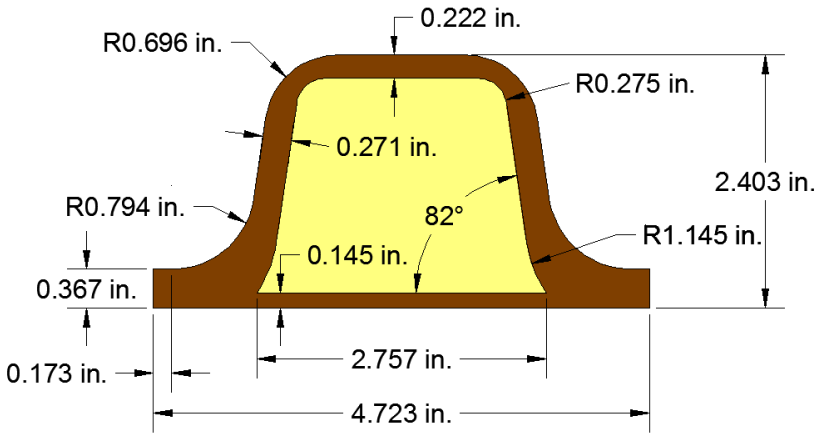

Figure 3.9: Dimensions of the Type 3 Small Scale Beam

4. FLATWISE TESTING

Flatwise testing is a very simple set of small scale experiments for sandwich constructions that has many attractive qualities. The specimens for these tests can easily be produced from a larger panel or beam, the test setups do not require any specialized equipment, and the results can be used to estimate the strength and stiffness of the core material while using very little material. These qualities make flatwise testing ideal for quality control and comparative studies. The only downside to this kind of testing is that the properties are only measured in the flatwise direction, which is perpendicular to the plane of the facings, so it is not completely representative of anisotropic or orthotropic core materials. Also, the specimens need to have relatively constant rectangular or circular cross-section in the direction of the load. As result of these limitations, representative specimens could only be made for the Type 1 and 2 sandwich constructions because the Type 3 construction does not have a consistent flatwise cross-section. Two types of flatwise testing were conducted. The first was compression testing, which is presented in Section 4.1, and the second was tension testing, which is presented in Section 4.2.

4.1. FLATWISE COMPRESSION TESTING

The objective of flatwise compression testing is to measure the compressive strength of the core material, and it can also be used to measure the compressive modulus or stiffness of the core material. Both of these properties are important when evaluating the core material of a sandwich construction in panels or beams because of significant localized effects under concentrated loads that cause high stress concentrations. These concentrations can cause compressive failure in the core and instability in the top facing

just beneath the concentrated load, which leads to premature failure of beams and panels before they reach their full bending capacity. The following sections detail the flatwise compression test methodology, the results, and a discussion of the results.

4.1.1. Test Methodology. There is a standard method for flatwise compression testing that is detailed in ASTM C365: Standard Test Method for Flatwise Compressive Properties of Sandwich Cores. This standard served as a guideline for the tests, however not all the details of the standard were strictly followed. Therefore, a detailed description of the specimen preparation, the test setup, and the test procedure is provided below.

4.1.1.1 Specimen preparation. The specimens for this experiment were produced by cutting small square pieces from a larger beam segment using a fine toothed band saw. The specimens were laid out at random using a ruler and a square. Then, after they were cut, a coarse grit belt sander was used to lightly sand away any imperfections and ensure the sides were adequately straight and orthogonal to the adjacent sides. Initially, three specimens each were cut for Type 1 and Type 2 core configurations, and the specimens for each type of core are shown in Figures 4.1 and 4.2, respectively.

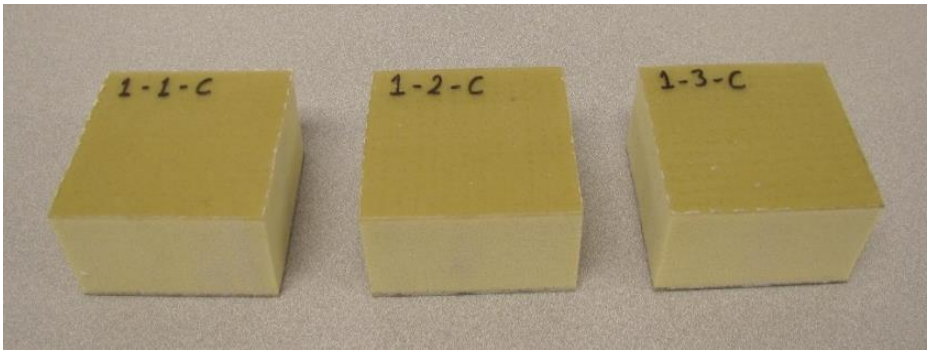

Figure 4.1: Flatwise Compression Testing Specimens for Type 1

These specimens are approximately 3.5 in. x 3.5 in. in the cross section perpendicular to the flatwise direction, and had a depth equal to that of the associated sandwich construction. After testing the initial specimens, one additional specimen for each core type was fabricated to alleviate some issues that occurred in the first tests. These were cut in the same manner and had the same approximate dimensions as the initial specimens.

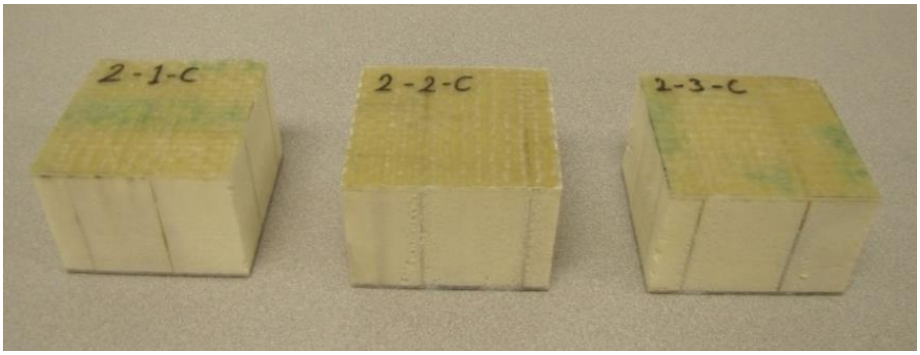

Figure 4.2: Flatwise Compression Testing Specimens for Type 2

4.1.1.2 Test setup. The test setup used for this experiment consists of two compression platens, one fixed and one free to pivot, that impart the load onto the specimen via a displacement controlled drive mechanism. The MTS-880 UTM in the structural engineering lab was use to accomplish the testing. The upper platen consisted of a 4 in. x 4 in. x ½ in. A36 steel plate welded at a right angle to a 2 in. x ½ in. A36 steel strip that was installed into the pneumatic grips of the moveable upper crosshead. The lower platen was a round loading platen with a 12 in. diameter. It consisted of two machined steel pieces that allowed the top to pivot relative to the bottom through a hemispherical interface between the two pieces. This attachment sat on the lower crosshead and, during the test,

was essentially stationary but able to rotate. A picture of the setup is presented in Figure 4.3.

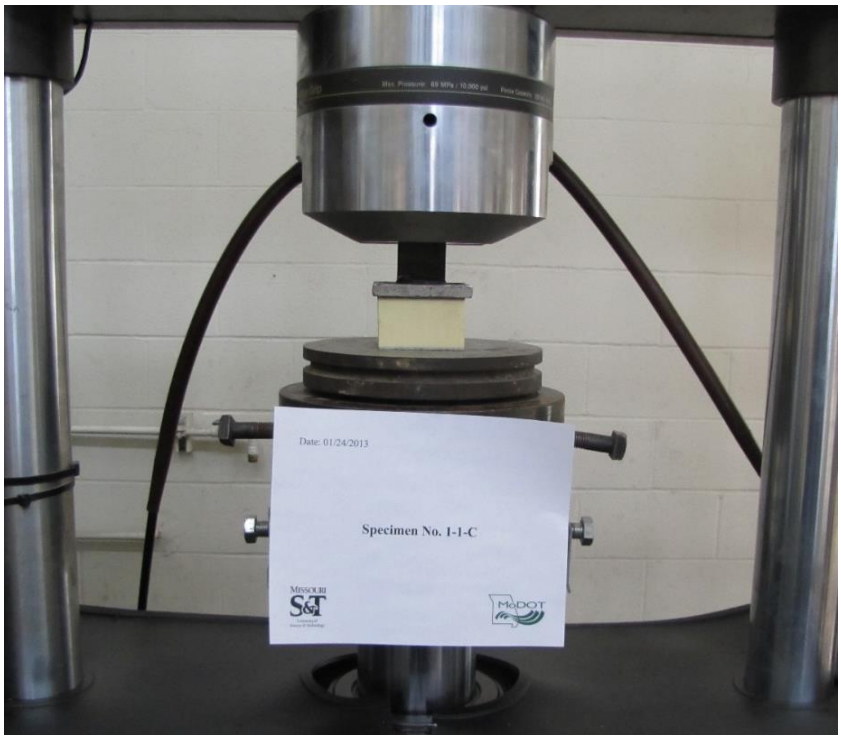

Figure 4.3: Flatwise Compression Testing Setup

4.1.1.3 Test procedure. Specimens were tested on multiple days at about the same time of day under similar temperature and humidity conditions. Before testing, the length and width of each specimen was measured using digital or dial calipers to the nearest 0.001 in a minimum of three measurements were taken for each and the average was recorded. The height and facing thickness of the specimens was measured from the original manufactured beams before the cutting of any specimens. A minimum of 30 measurements were taken for each and the average was reported. The specimen was placed on the lower

platen, and the platens were moved until there was a narrow gap above the specimen. The lower platen was locked into place and adjusted to be parallel with the top platen, and the load was zeroed. The specimen was centered using the concentric rings of the lower platen and the edges of the upper platen as a reference. For specimens with slight wrinkles in the facings, a thin ⅛ in. rubber pad, Shore A hardness of 60, was placed between each platen to avoid any stress concentrations. The upper head was lowered until a small load was registered (10 - 50 lb.), then the displacement was zeroed. The test was displacement-controlled at a rate of 0.1 in/min. Displacement and load were recorded simultaneously at a rate of 5 Hz. The test was stopped once the displacement reached 50 - 80% of the depth of the specimen, which took 10 - 15 minutes, and the specimen was then unloaded.

4.1.2. Test Results. The load and displacement were the primary results for this experiment, and before they could be normalized the data needed to be refined. The load versus displacement plots displayed Hookean (linear elastic) behavior before failure, but there were false nonlinearities and discrepancies in the initial readings. The nonlinearity was caused by small gaps in the system. Also, during testing the displacement was set to zero at a non-zero load. Both of these issues lead to a false offset in the displacement. In order to correct this issue, regression analysis of the linear region of the load versus displacement plot was used to correct this offset. Different ranges of the data were explored, and the range with the best correlation factor was chosen to be representative of the linear region. Then, using the regression equation, the genuine part of the load versus displacement curve was offset by the x-axis intercept of the regression equation. Then, the false data at the beginning of the test was replaced by a projection of the linear region that

intersected the origin. A graphical representation of this procedure is presented in Figure 4.4.

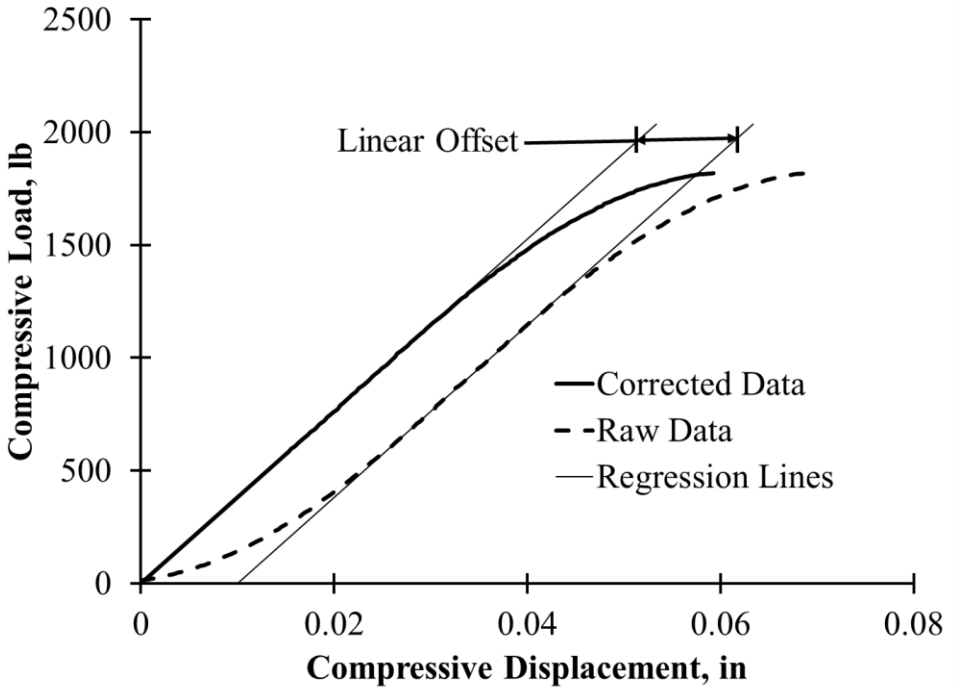

Figure 4.4: Compressive Load vs. Displacement Correction Using Linear Regression

After the data was corrected, the concepts of engineering stress and strain could be used to normalize the load and deflection values for comparison between specimens and core types. The engineering stress and strain in the axial direction can be found using Equations 4.1 and 4.2, respectively.

$$\sigma = \frac{F}{A_o} \tag{4.1}$$

In Equation 4.1, σ is the engineering stress in the axial direction measured in pounds per square inch (psi), F is the applied load in pounds (lb), and A_o is the initial cross-sectional area of the specimen measured perpendicular to the load in inches squared (in^2).

$$\boldsymbol{\varepsilon} = \frac{\boldsymbol{\Delta L}}{\boldsymbol{L_o}} \tag{4.2}$$

In Equation 4.2, ε is the engineering strain in the axial direction measure in inches per inch (in/in), ΔL is the displacement parallel to the load measured in inches (in), and L_o is the initial length of specimen in the direction parallel to the load measured in inches (in). Using the axial stress and strain, one can estimate the axial strength and stiffness of the material in compression.

These concepts can be applied to the core material using the load and displacement results for this experiment by making some observations. The engineering stress and strain are average values over the cross-section, so they are not completely representative of the stresses and strains in individual parts of the core. However, they are a reasonable global approximation that can be representative of the system as a whole. Also, the stress and strain are oriented in the flatwise direction, which is perpendicular the facing, therefore the properties that are estimated in this experiment are not necessarily representative of the properties in the other orthogonal directions.

Special considerations must also be made when using the equations. The height of the core is not the same as the total height of the specimen because the facings contribute to the total height, so the initial length that must be used in Equation 4.2 is equal to the height of the specimen minus twice the thickness of the facings. Next, the displacement

recorded in the test can be considered the same as the displacement in Equation 4.2 as long as the facing material is several orders of magnitude stiffer than the core material. This means the facings compress very little during the test and do not contribute significantly to the measured displacement.

If these assumptions are made, the stress and strain in the core material can be calculated for each test. Then, the stress at failure can be considered the compressive strength of the core because the failure will occur inside the core of the specimen. This will be denoted as the flatwise compressive strength because it is measured in the flatwise direction. Then, linear regression can be performed on the plot of stress versus strain to calculate the axial stiffness of the core in compression. This stiffness is the slope of the line made by a regression of the stress versus strain plot which will be performed over the range or stress and strain that directly corresponds to the range of load and displacement that was formerly used to correct the offset in the load versus displacement plot. This axial stiffness in compression will be denoted as the flatwise compressive modulus.

4.1.2.1 Results for Type 1. Three specimens were originally prepared and tested for the Type 1 core. However, during the testing of the original Specimen 1-1-C, the lower crosshead of the machine was not locked properly and the results were unusable. A fourth specimen was prepared and successfully tested, and the results of this test were used to replace the original 1-1-C data. Once the initial false nonlinearities and discrepancies in the load versus displacement response were corrected, the stress and strain were calculated for each specimen. The plot of stress and strain for each specimen can be seen in Figure 4.5. The stress versus strain response can be divided into three distinct regions, as shown

in Figure 4.6. The Type 1 core is constructed of rigid polyurethane foam that typically displays this type of response, and each region can be explained in physical terms.

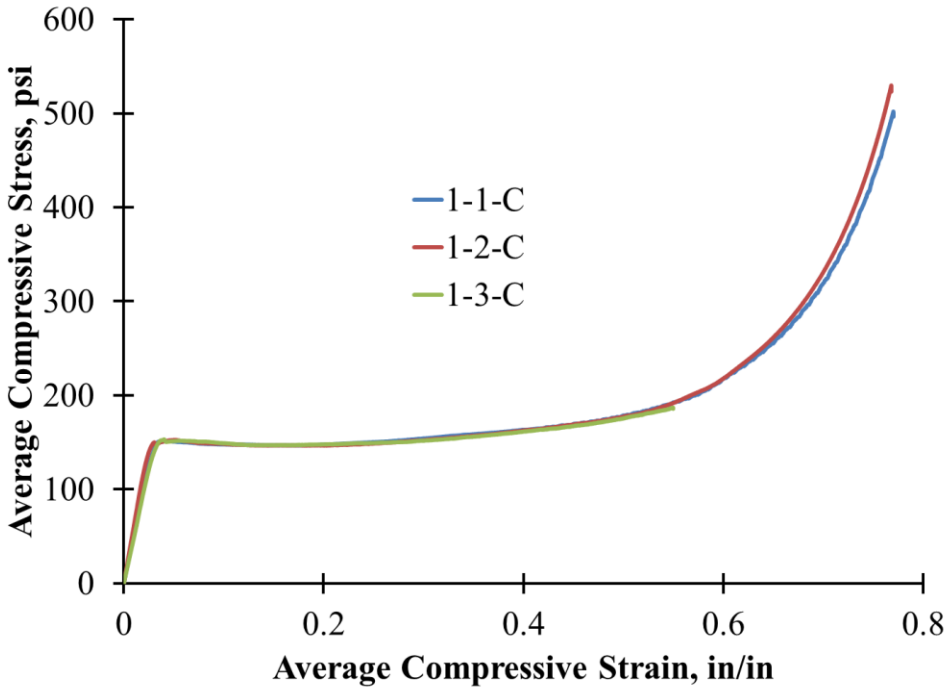

Figure 4.5: Stress vs. Strain Results for Flatwise Compression Testing on Type 1

In the first region, the cells of the foam are compressing uniformly. The cells are distributed relatively evenly in size and location, and the polyurethane plastic that the foam is manufactured from behaves approximately linear elastically to a point. As a result, the foam has a global response that is apparently linear elastic, and the stress versus strain plot in this region is linear. Eventually, some of the cell walls and struts reach their strength or stability limit, and the specimen transitions into the second region.

In the second region, the specimen starts to fail as some of the cells collapse due to excessive buckling, yielding, and/or fracturing of the cell wall and struts. This begins at a critical location which sets off a chain reaction that spreads throughout the cross-section, eventually encompassing the entire cross-section of the specimen. The material has an apparent yield point at the beginning of this region as stress temporarily peaks then fluctuates slightly as it remains nearly constant.

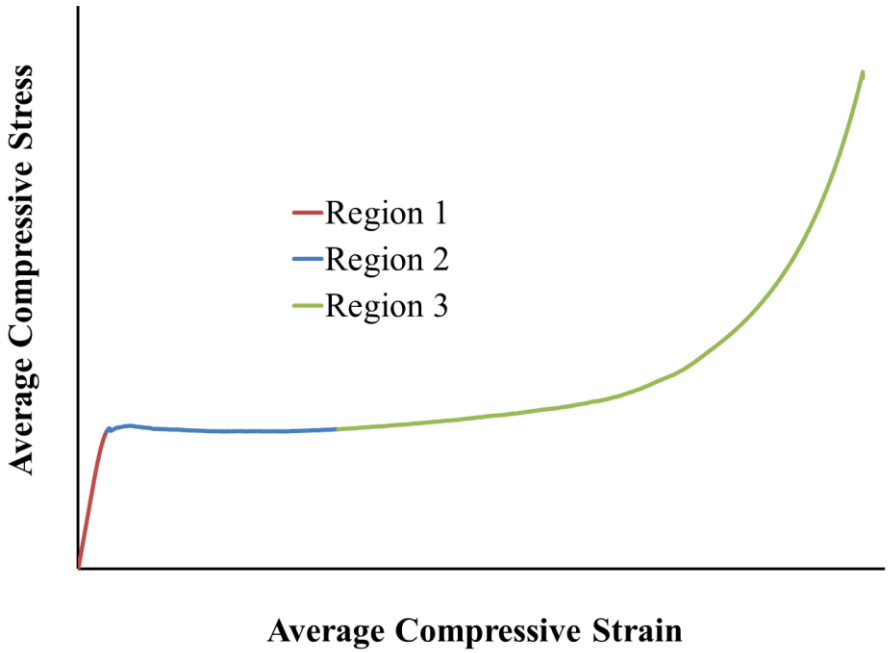

Figure 4.6: Generalized Compressive Stress vs. Strain Response for Type 1

Finally, in the third region, the majority of the cells of the foam have begun to collapse and are permanently damaged. The damaged cell walls and struts deform to the point that their movement is impeded by the cells and struts adjacent to them. Eventually,

through a process commonly called densification, the foam becomes denser and more stable on the cellular scale as the voids close up. This causes the stress to increase in a quasi-exponential manor as the foam becomes apparently stronger.

The plot of stress versus strain was then used to determine the strength and stiffness of the core material. The strength can be considered as the stress at failure, but first a failure point must be established. The failure occurs in the transition between the first two regions described previously and requires closer examination in order to define a failure point. Figure 4.7 shows a close up plot of stress versus strain for the Specimen 1-2-C at the transition.

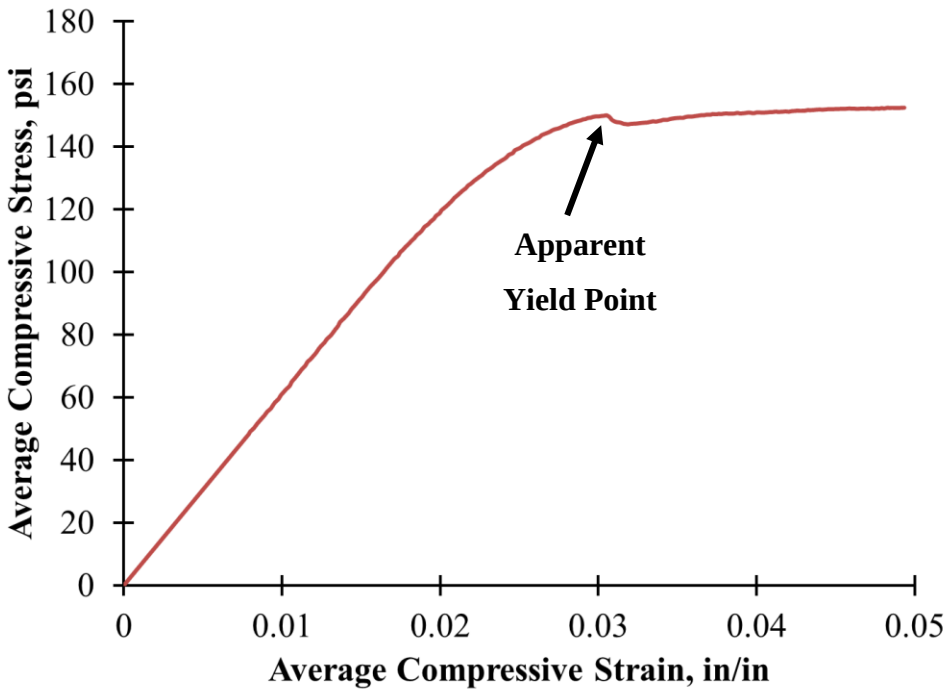

Figure 4.7: Stress vs. Strain at Failure for Flatwise Compression Testing on 1-2-C

In this plot, the transition between the regions is much more gradual, and the point of failure becomes difficult to define and somewhat subjective. However, there is an apparent yielding point that is located at the first small peak in stress where the specimen likely started to fail. Also, this yield point is present on the stress versus strain curves for all three specimens, and it is easy to determine the stress and strain at this point. As a result, the flatwise compressive strength will be considered the stress at this point. A visual representation of what the failure of the specimens actually looked like just after failure and at the end of the test can be seen in Figures 4.8 and 4.9, respectively.

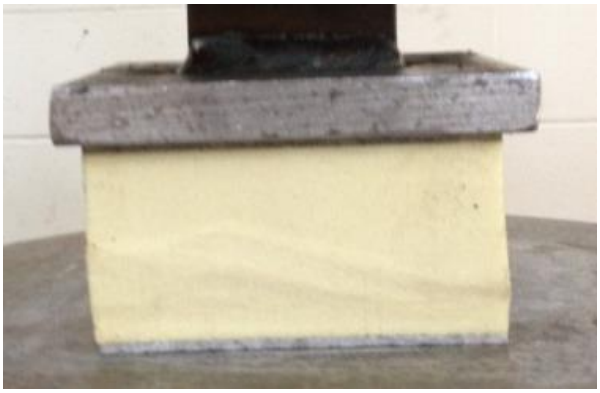

Figure 4.8: Damage at Failure for Flatwise Compression Testing on Type 1

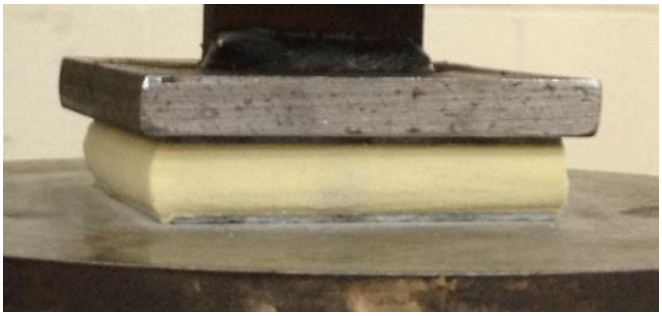

Figure 4.9: Damage at End of Test for Flatwise Compression Testing on Type 1

The axial stiffness is the next item of concern. Linear regression analysis was used to calculate this stiffness by using the range of stress and strain that corresponded to the load and displacement range used to correct the raw data. This range varied between specimens, but on average the regression with the greatest correlation occurred at a strain range of 0.007 to 0.016 in/in and utilized at least 30 data points. The slope of the regression equation was considered the flatwise compressive modulus with units of pounds per square inch (psi). A summary of the results for flatwise compressive strength and modulus for each Type 1 specimen is presented in Table 4.1. A more detailed report of the flatwise compression test results for each Type 1 specimen can be found in Appendix A.

Table 4.1: Flatwise Compression Testing Results for Type 1

Specimen Label	Flatwise Compressive Strength (psi)	Flatwise Compressive Modulus (psi)
1-1-C	151	5,210
1-2-C	150	6,120
1-3-C	153	4,810

4.1.2.2 Results for Type 2. Originally, three specimens were also prepared and tested for the Type 2 core. The results for each of these specimens appeared useable, but the results for the first specimen had a significantly higher strength than the other specimens. A fourth specimen was prepared and tested in an attempt to verify any outliers. The results for the fourth specimen showed a noticeably lower stiffness while the strength was similar to the second and third specimens. There were no immediate mishaps during testing that would indicate poor results for any of the specimens, but after examining the

length of web reinforcement in each specimen, it was found that the first specimen had two complete cells of reinforcement while the other specimens had only one complete cell that hadn't been damaged while sectioning them. Also, it was noted that the fourth specimen was wrinkled on one face and rubber pads were used to distribute the load more evenly. The fourth specimen had also been damaged significantly more along one side while the other three specimens had been damaged relatively uniformly. It was obvious that the Type 2 specimens had a high variability, and the results of the test were highly dependent on the location and quantity of the cells. Nevertheless, no data points were more than two standard deviations from the mean, and the data is sufficient for comparison purposes.

Moving forward with the analysis, the initial false nonlinearities and discrepancies in the load versus displacement response were corrected, and the stress and strain were calculated for each specimen. The plot of stress versus strain is presented in Figure 4.10. The stress versus strain response has two distinct regions that are apparent in the figure, and each region can be explained based on the Type 2 core construction. The Type 2 core is made of low density flexible polyurethane foam with resin infused web reinforcement that formed rectangular cells. This reinforcement played an important role in the stress versus strain response.

In the first region, the stitched reinforcement had an apparent linear elastic behavior because the web reinforcement is made of resin and fibers that display Hookean behavior to a point. The flexible foam contributes almost nothing to the response directly, but it does provide stability for the webs as they are very thin relative to their length. As a result, the global stress versus strain response in this region is linear, but inevitably the webs with less foam to stabilize them began to buckle and the behavior transitioned into the second region.

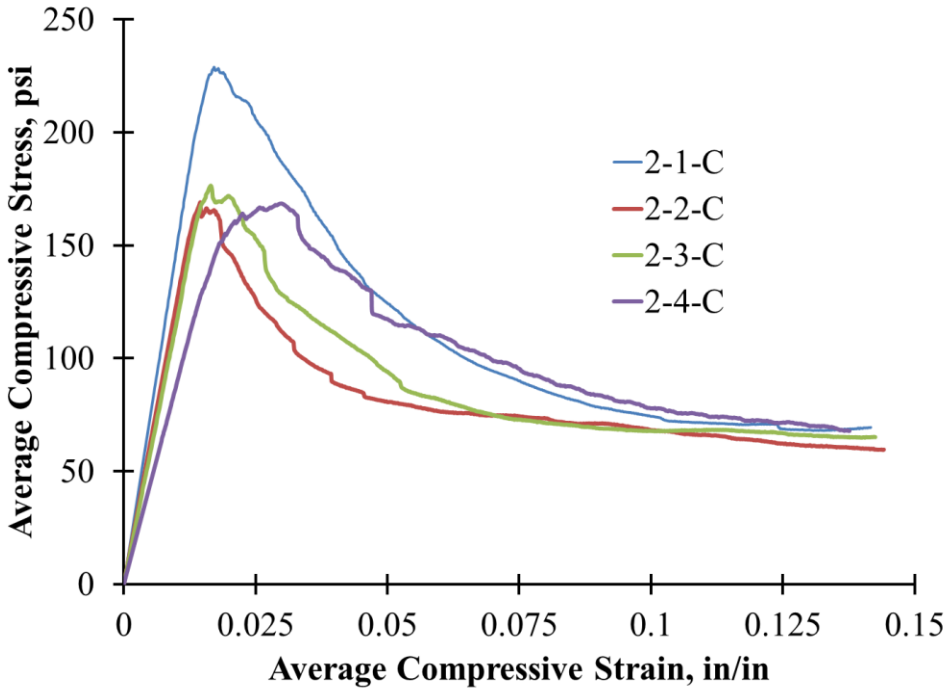

Figure 4.10: Stress vs. Strain Results for Flatwise Compression Testing on Type 2

In the second region, immediately following the linear region, the webs with less support from the foam buckled excessively and began to fracture. The stress redistributed to those webs having more foam support, but they too buckled and fractured as the stress increased. This non-sequential failure of the web reinforcement caused the stress to decrease rapidly and erratically. Due to the very low strength and stiffness of the flexible foam, the stress versus strain plots did not display a yielding failure, and the stress did not noticeably increase at high displacements like the Type 1 specimens.

The compressive strength and stiffness were calculated using the stress versus strain plots. The flatwise compressive strength is more evident for the Type 2 core because failure occurred suddenly and was accompanied by a significant drop in load immediately after the peak load. Therefore, the stress at the maximum load was considered to be the flatwise

compressive strength. What the failure looked like can be seen in Figures 4.11 and 4.12, which show the damage at the onset of failure and the damage at the end of the test, respectively.

Figure 4.11: Damage at Failure for Flatwise Compression Testing on Type 2

Figure 4.12: Damage at End of Test for Flatwise Compression Testing on Type 2

The stiffness is again designated as the flatwise compressive modulus with the same definition and units described in the previous sub-section, and it was found using the same type of linear regression analysis. The regression region once more varied between specimens, but on average the regression with the greatest correlation occurred at a strain

range of 0.006 to 0.012 in/in while using at least 20 data points. A summary of the results for flatwise compression strength and modulus for each specimen is presented in Table 4.2. A detailed report of the flatwise compression test results for each Type 2 specimen can be found in Appendix A.

Table 4.2: Flatwise Compression Testing Results for Type 2

Specimen Label	Flatwise Compressive Strength (psi)	Flatwise Compressive Modulus (psi)
2-1-C	229	14,750
2-2-C	169	12,400
2-3-C	176	11,530
2-4-C	168	8,850

4.1.3. Discussion of the Test Results. The flatwise compressive strength ranged from 150 - 153 psi for the Type 1 specimens, with an average of 151 psi. The flatwise compressive modulus for the Type 1 specimens ranged from 4,810 - 6,120 psi, with an average of 5,380 psi. For the Type 2 specimens, the flatwise compressive strength ranged from 168 - 229 psi, with an average of 186 psi, and the flatwise compressive modulus varied from 8,850 - 14,750 psi, with an average of 11,880 psi. From these results, it can be clearly seen that the Type 2 core is stronger and stiffer in compression than the Type 1 core when measured in the flatwise direction, however both core types have relatively low compressive strength and stiffness in the flatwise direction. So, what does this mean for sandwich beams and panels made with these core types?

Due to the very high transverse flexibility and compressibility of foams, sandwich panels with foam and reinforced foam cores often suffer from significant localized deformations and stress concentrations near and beneath concentrated loads. If the foam has an insufficient compressive strength, the core can fail locally. This promotes localized buckling of the top facing, which occurs immediately under the point load with a wave length proportional to the width of the contact area. The combination of these effects form a failure mode often referred to as local indentation. Local indentation can cause premature failure and prevent sandwich panels and beams from reaching their theoretical moment and shear capacity. Since concentrated loads typically compress the core of beams and panels locally in the flatwise direction, the test results of this experiment can provide insight into how these core types will perform in such a scenario. Both cores have a very low compressive strength in the flatwise direction, which indicates that local indentation under large concentrated loads is a valid concern for panels with these cores. Considering the results presented at the beginning of this subsection, it is also logical to conclude that a panel with the Type 2 core should perform better than a panel with a Type 1 core. Meaning it would experience less localized deformation under a concentrated load, and it would be less likely to fail prematurely. However, the capacity will be dependent on many other factors as the span length increases, and at larger span length to depth ratios, these localized effects could play a negligible role in capacity and deflections. As a final note, these concerns apply to the Type 3 core as well, but unfortunately the geometry of the cross-section and the configuration of the small scale specimen that could be manufactured would not allow for a representative flatwise compression test.

4.2. FLATWISE TENSION TESTING

Flatwise tension testing intends to measure the tensile strength and stiffness of the core in the flatwise direction. These tests are important when evaluating sandwich panels and beams because of significant peeling stresses between the core and facing and significant shear stresses in the core that occur in panels with flexible foam cores. Furthermore, the tensile strength of the core and the strength of the bond between the core and facing can provide insight into failure due to these type of stresses. The following sections detail the flatwise tension test methodology, the results, and a discussion of the results.

4.2.1. Test Methodology. The standard procedure for this experiment is detailed in ASTM C297: Standard Test Method for Flatwise Tensile Strength of Sandwich Constructions. This standard served as a guideline for these tests, but not all the details of the standard were strictly followed. A detailed description of the specimen preparation, the test setup, and the test procedure is provided below to elaborate on any differences.

4.2.1.1 Specimen preparation. As with the flatwise compression specimens, the flatwise tension specimens were prepared from a larger beam segment. The procedure involved using a ruler and square to mark the beam segment and then cutting the specimens with a fine tooth band saw, followed by sanding of any rough edges with a coarse grit belt sander. The final dimensions of the specimens were 3.5 in. x 3.5 in. in plan with a depth corresponding to that of the associated sandwich panel construction. Three specimens were prepared for both the Type 1 and Type 2 core configurations. The respective specimens for each type of core are shown in Figures 4.13 and 4.14.

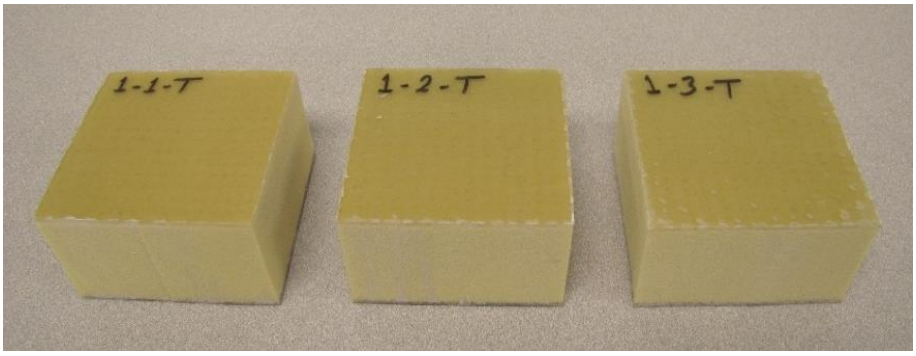

Figure 4.13: Flatwise Tension Testing Specimens for Type 1

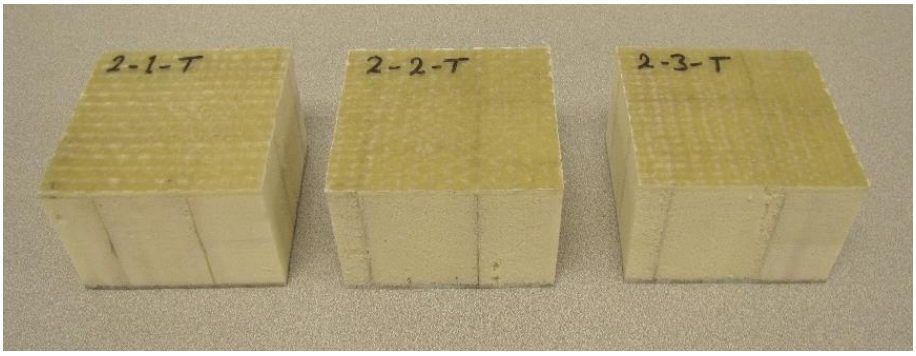

Figure 4.14: Flatwise Tension Testing Specimens for Type 2

After the specimens were prepared, some special measures were required prior to testing. The specimens could not be properly gripped for a tension test, so plates that could be gripped by the testing machine needed to be adhered to the specimens. These plates were manufactured using A36 steel stock and consisted of a 6 in. x 6 in. x ¼ in. plate with a 2 in. x ¼ in. bar welded to the center of the plate at a right angle. These plates are far more rigid than the specimens, and they allow a testing machine to impart tensile stresses on the specimens without significantly influencing the deformation results.

Before the plates were adhered, the length and width of each specimen was measured using digital or dial calipers to the nearest 0.001 in., and three measurements were taken for each. The average was recorded. The height and facing thickness of the specimens was measured from the original beams before the cutting of any specimens. A minimum of 30 measurements were taken and the average was reported. Next, a plate was glued to each facing of the specimen using the following procedure. The first plate was placed into the center of the pneumatic grips of the lower crosshead of the MTS-880 UTM, and using a bubble level the square face of the plate was positioned perpendicular to the applied load. Once the plate was centered and leveled, the grips were fully engaged to hold in place. The lower crosshead was then locked into place to ensure it was stationary. Next, two part epoxy was thoroughly mixed and applied to the flat surface of the plate. The epoxy used was 3M 08101 structural adhesive. Immediately afterwards, the specimen was placed onto the epoxy, and the specimen was centered using the edges of the plate as a reference. Then, additional epoxy was mixed and applied to the top face of the specimen, and the upper plate was placed flat side down onto the specimen. Again the edges of the plate were used to ensure the specimen was centered in the square portion of the plates. The upper pneumatic grips of the test machine were lowered until the bar of the upper plate was sufficiently inside the grips. A bubble level and visual inspection were used to ensure the assembly was properly aligned and centered. The grips were then engaged to lock the upper plate into place, and a small amount of force (10 - 50 lb.) was applied. The procedure up to this point took 5 - 10 minutes to complete. Once pressure was applied the assembly had to cure for one hour before the epoxy had enough usable strength to be moved.

After the initial cure period, the assembly was marked to ensure it would be tested using the same orientation. It was removed and stored at standard room temperature and humidity conditions until testing was completed a few days later. The epoxy required a minimum 8 hour curing period to achieve full strength. Figure 4.15 shows a close up of Specimen 2-1-T after it was adhered to the plates.

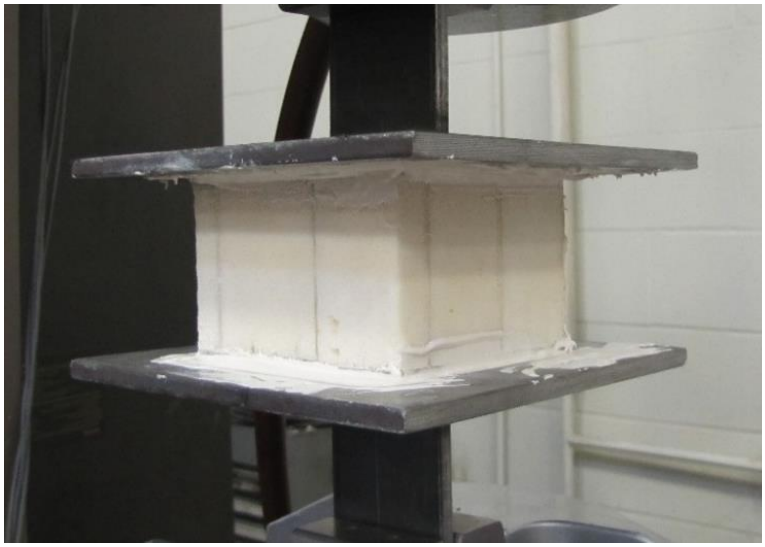

Figure 4.15: Close-Up of the Flatwise Tension Testing Specimen Assembly

4.2.1.2 Test setup. The test setup used for this experiment is relatively simple. After adhering the plates to the specimens and allowing the epoxy to reach full strength, the same pneumatic grip setup on the MTS-880 UTM was used to test the specimens. The assembly was gripped in the same orientation as that used to adhere the plates. The lower crosshead was locked to remain stationary while the upper crosshead served as the moveable head and could be displaced at a specified rate. A picture of the setup is presented in Figure 4.16.

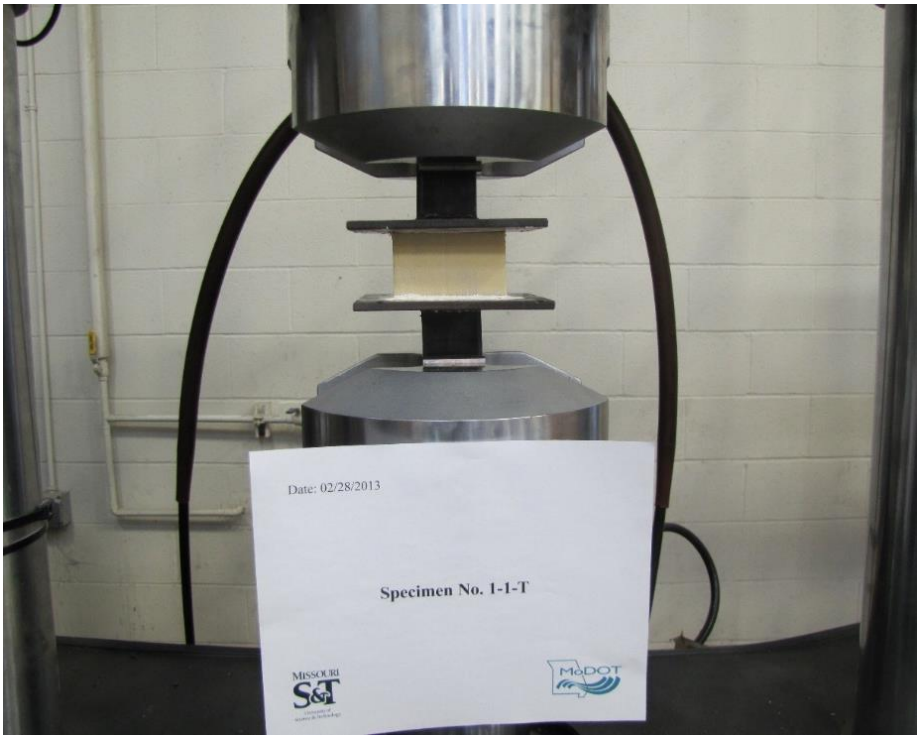

Figure 4.16: Flatwise Tension Testing Setup

4.2.1.3 Test procedure. All specimens were tested at approximately the same time of day in similar temperature and humidity conditions. During testing, the specimen assembly was placed into the pneumatic grips of the lower crosshead in the same position used for adhering the plates, and a bubble level was used to ensure is was aligned perpendicular to the load before the grips were engaged. The lower crosshead was locked into place and the load was zeroed. The upper crosshead was lowered until the top of the assembly was adequately within the grips, and the alignment of the system was visually inspected before the grips were engaged. Once the grips were engaged, the displacement was zeroed and the load was allowed to float. Displacement was then added at a constant rate of 0.01 - 0.02 in/min, and the tensile load was recorded simultaneously. Load and displacement were taken at a rate of 10 Hz. The test was stopped once the displacement

reached 5 - 20% of the sandwich depth, which took 5 - 20 minutes, and then after ensuring the load had decreased to nearly zero, the specimen was pulled apart until it separated into two pieces and was promptly unloaded.

4.2.2. Test Results. Once again, the primary results to be analyzed were the load and displacement, but like the flatwise compression testing, the analysis could not be started until the load versus displacement was corrected. The load versus displacement plots displayed linear elastic behavior before failure, but there were discrepancies in the initial readings caused by setting the displacement to zero at a non-zero load. In order to fix this problem, the same linear regression analysis of the load versus displacement plot was used. Again, different ranges of the data were explored, and the range with the best correlation factor was chosen. Then, using the regression equation, the linear region of the data was offset to make its projection intersect the origin. Graphically this is the same as the method already presented in Figure 4.4 of Section 4.1.2. The only difference is the loads and displacements are in tension, and the nonlinear region caused by slack in the system was not prevalent in the flatwise tension testing. The primary issue was the offset caused by setting the displacement to zero while the load was non-zero.

After the data was corrected, the concepts of engineering stress and strain that were discussed previously in Section 4.1.2 could be used to normalize the load and displacement values for comparison between specimens and core types. The equations used to calculate engineering stress and strain in the axial direction along with an explanation of the variables can be found in the aforementioned section as Equations 4.1 and 4.2, respectively.

Once more assumptions must be made to apply these concepts of stress and strain to the tension specimens. The engineering stress and strain calculated using the

aforementioned equations are average values over the cross-section, and are not completely representative of the stresses and strains in individual parts of the core. They are however an adequate global approximation. The stress and strain are again oriented in the flatwise direction, perpendicular to the facing, and are not representative of material properties in orthogonal directions. Also, the initial length that must be used in Equation 4.2 must again be equal to the height of the specimen minus twice the thickness of the facings, which is the height of the core. Then, since the stiffnesses of the glue and the facing material are much larger than that of the core material, it is reasonable to assume that deformations within the epoxy layer and the facings are negligible, and the recorded displacement can be input directly into Equation 4.2 as the displacement of the core alone.

Using these assumptions, the stress and strain in the core material can be calculated for each test. From these results, the stress at failure can be considered the flatwise tensile strength of the core or the bond between the core and the facings, depending on where the failure initializes. Then, linear regression can once more be performed on the plot of stress versus strain to calculate the axial stiffness of the core in tension. This is done using the same method used in Section 4.1.2 for the flatwise compression tests. The axial stiffness in tension measured in the flatwise direction will be denoted as the flatwise tensile modulus.

4.2.2.1 Results for Type 1. Three specimens were prepared from the larger beam segment for the Type 1 core, and they were prepared and tested using the procedures presented earlier in this section. However, during testing of the first specimen, the upper crosshead of the machine was rotated from its original position, and when the grips clamped down on the assembly, it applied a torsional force to the specimen causing it to

prematurely fail when it was loaded. After the crosshead grips were aligned properly, the other two specimens were successfully tested. Due to a lack of material, no additional specimens could be prepared, so only the results from the two successful tests will be presented.

The initial discrepancies in the load versus displacement response were corrected, and the stress and strain were calculated for each specimen. The plot of stress and strain for each specimen can be seen in Figure 4.17.

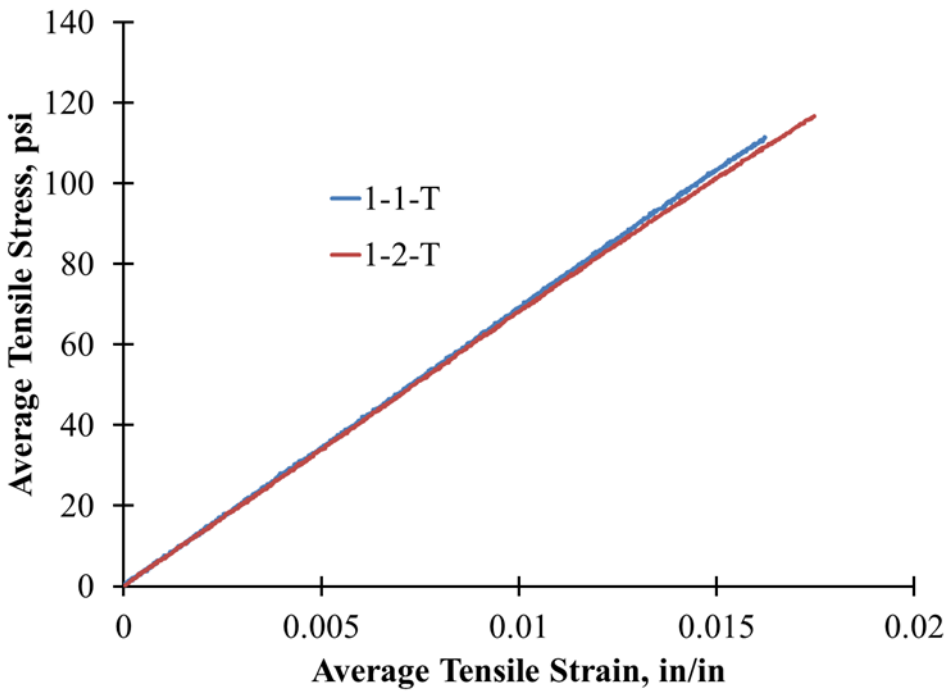

Figure 4.17: Stress vs. Strain Results for Flatwise Tension Testing on Type 1

The stress versus strain response was almost completely linear before failure occurred. Since cells of the foam are uniform in size and distribution, the behavior is similar

to that of the solid polyurethane, which in this case is nearly linear elastic in nature. The plot of stress versus strain was then used to determine the tensile strength and stiffness of the core material. The strength can be considered as the stress at failure which occurred at the maximum stress. The stress at this point will be considered the flatwise tensile strength, and failure occurred in the rigid polyurethane foam for both specimens. Figures 4.18 and 4.19 show the facture of the specimen immediately after peak load and the fracture surface of the specimens at the end of the test, respectively.

Figure 4.18: Damage at Failure for Flatwise Tension Testing on Type 1

Figure 4.19: Fracture at the End of Test for Flatwise Tension Testing on Type 1

Linear regression analysis was used to calculate this stiffness by using the range of stress and strain that corresponded to the load and displacement range used to correct the raw data. The slope of the regression equation was consider the tensile stiffness of the core, and it will be referred to as the flatwise tensile modulus with units of pounds per square inch (psi). The regression region varied between specimens, but on average the regression with the greatest correlation occurred at a strain range of 0.0001 to 0.015 in/in and utilized at least 800 data points. A summary of the results for flatwise tensile strength and modulus for each specimen is presented in Table 4.3. A detailed report of the flatwise tension test results for each Type 1 specimen can be found in Appendix B.

Table 4.3: Flatwise Tension Testing Results for Type 1

Specimen Label	Flatwise Tensile Strength (psi)	Flatwise Tensile Modulus (psi)
1-1-C	112	6,900
1-2-C	117	6,800

4.2.2.2 Results for Type 2. Three specimens were also prepared and tested for the Type 2 core. There were no difficulties while testing the Type 2 specimens. Each specimen had a different configuration of web reinforcement, but only one complete cell was present in each specimen. As a result, there was noticeable variation between specimens, but there was no indication that one of the tests could be a statistical outlier. Following the tests, the initial discrepancies in the load versus displacement response were corrected, and the stress and strain were calculated for each specimen. The plot of stress and strain for each

specimen can be seen in Figure 4.20. The stress versus strain response has two distinct regions visible in the figure that are related to the constituent materials of the Type 2 core.

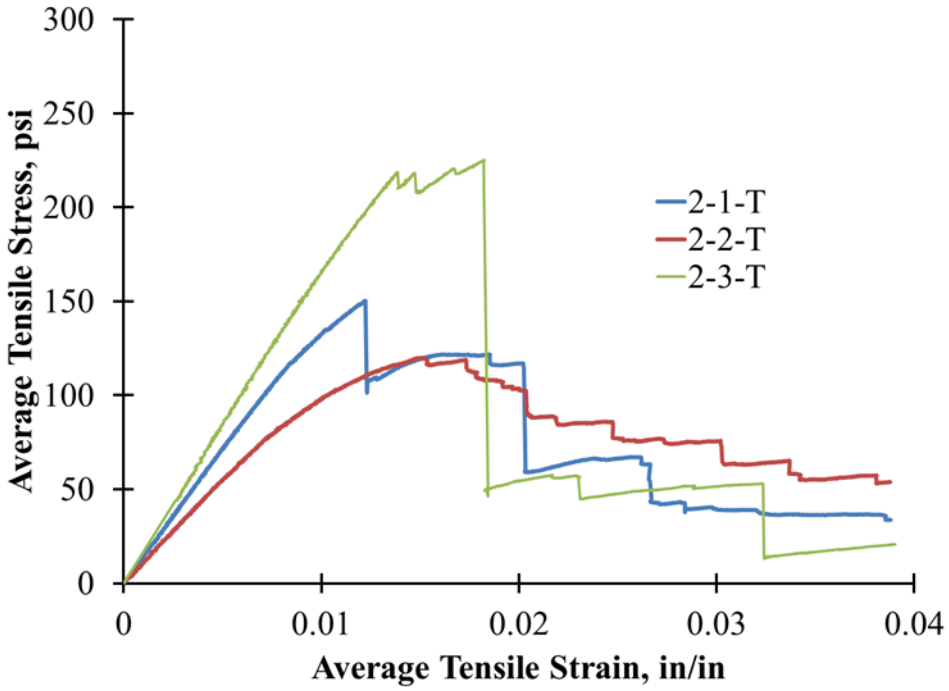

Figure 4.20: Stress vs. Strain Results for Flatwise Tension Testing on Type 2.

The first region has an overall linear stress versus strain response before the first peak in load. In this region, fiber reinforced polyurethane grid work and the flexible polyurethane foam are acting together, but the foam contributes very little to the response. Since the polyurethane and reinforcing fibers are approximately linear elastic in nature, the composite core has a relatively linear stress versus strain response. Then, a transition into the second region occurred due to the very low stiffness and strength of the flexible foam,

the location and distribution of the web reinforcement, and the nature of the bond between the core and facing

The second region began just after the first peak in stress. The stress versus strain behavior became erratic as the stress began to decrease in steps in this region. This was caused by asynchronous failures in different parts of the core. In areas of high stress concentrations, the webs began to break or debond from the facing at their base and the foam started to crack, causing the load to decrease and redistribute to different parts of the core. Failure occurred in the bond between the core and facing for Specimens 2-1-T and 2-3-T, and for Specimen 2-2-T it occurred in the core material alone.

Next, the stress versus strain plot was used to calculate the tensile strength of the core and/or the bond between the core and the facings. The first peak in stress attained by the specimens was considered the failure point and the stress at this point was considered the flatwise tensile strength. The failure can be seen in Figures 4.21 and 4.22. The photographs show the damage during core failure and the damage during bond failure, respectively.

Figure 4.21: Damage During Core Failure for Flatwise Tension Testing on Type 2

Figure 4.22: Damage During Bond Failure for Flatwise Tension Testing on Type 2

The axial stiffness was once again designated as the flatwise tensile modulus with the same definition, units, and regression analysis described previously. The regression region varied between specimens, but on average the regression with the greatest correlation occurred at a strain range of 0.002 to 0.007 in/in while using at least 300 data points. A summary of the results for flatwise tensile strength and modulus for the Type 2 core is presented in Table 4.4. Also, a detailed report of the flatwise tension test results for each Type 2 specimen can be found in Appendix B.

Table 4.4: Flatwise Tension Testing Results for Type 2

Specimen Label	Flatwise Tensile Strength (psi)	Flatwise Tensile Modulus (psi)
2-1-T	150	14,270
2-2-T	120	11,050
2-3-T	219	16,800

4.2.3. Discussion of the Test Results. The flatwise tensile strength ranged from 112 - 117 psi for the Type 1 specimens, with an average of 114 psi. The flatwise tensile modulus for the Type 1 specimens ranged from 6,800 - 6,900 psi, with an average of 6,850 psi. For the Type 2 specimens, the flatwise tensile strength ranged from 120 - 219 psi, with an average of 163 psi, and the flatwise tensile modulus varied from 11,050 - 16,800 psi, with an average of 14,040 psi. From these results, it can be clearly seen that the Type 2 core is stronger and stiffer than the Type 1 core in the flatwise direction when subjected to tensile forces. What does this tell us about sandwich beams and panels made with these core types?

Flatwise tension testing is a good evaluation of the bond between the core and the facing. The results can verify if this bond is stronger or weaker than the core material, which gives insight into how the material behaves. Also, sandwich beams and panels with foam cores typically display significant peeling stresses between the core and facing and shear stresses in the core. When analyzing failures do to these stresses the tensile strength of the core and the bond between the core and facing can provide insight into where and how the failure will occur. From the test results, it can be seen that for the Type 1 core, the bond between the core and the facings was consistently stronger than the core material itself because the failure occurred inside the rigid foam core for both specimens. For the Type 2 core, the failure occurred more often at the bond between the core and the facings, specifically at the locations of the reinforcing webs. This indicates that a failure due to peeling and shear stresses in a beam with a Type 1 core will likely occur inside the rigid foam core, and in a beam with a Type 2 core could likely fail at the interface between the reinforced foam core and the facings due to these types of stresses. Then, when comparing

the two core types, it was noted that the Type 2 core was stronger than the Type 1 core. This suggests a beam with a Type 2 core could withstand higher peeling and shear stresses than a comparable beam with a Type 1 core. Again it should be noted that these concerns apply to the Type 3 core as well, but unfortunately the geometry of the cross-section and the configuration of the small scale specimen that could be manufactured would not allow for a representative flatwise compression test.

5. FLEXURAL TESTING

Flexural testing is another useful experiment that is performed on sandwich constructions. Like the flatwise testing, there were several beneficial aspects of flexural testing. The specimens were small beams that could be easily cut from the beam segments that were manufactured by the Mechanical Engineering Department, and any additional preparation required for the specimens was not extensive. The test set up was more complicated for flexural testing, but the fixtures that were needed could be fabricated or purchased with few difficulties. Furthermore, the results provided insight into the flexural behavior of sandwich constructions using the three different core alternatives, which is an important consideration for their application in bridge deck panels. Deflection is typically the driving factor in the design of sandwich panels as decking, and the deflection is dependent on the flexural stiffness of the panel, which can be estimated using the load versus deflection response measured during these experiments. Also, important strength limit states were identified along with critical factors influencing failure. Another benefit of these experiments is that, unlike the flatwise testing, representative samples could be produced for all three core types.

For these experiments, two different types of flexural tests were performed. The first was a three point bending test with the load at mid-span using a short support span, which was designated three point flexural testing. The second was a four point bending test with loads at the third points using a longer support span, which was designated four point flexural testing. The test procedures, summary of results, and brief discussion of results for each test is presented in Sections 5.1 and 5.2, respectively. Then, the performance of each sandwich construction was analyzed based on stiffness and strength. The theories and

assumptions used in the analysis along with the results of the analysis for each core type and a more comprehensive discussion of the results comparing the different core types is presented in Section 6.

5.1. THREE POINT FLEXUAL TESTING

In this test, relatively short beams were subjected to three-point bending in an effort to increase shear stresses and their impact on deformations while lessening the effects of bending moments and their associated stresses. Initially, the goal was to avoid local failure and cause shear failure in the core by using flat bars and rubber pads at the support and loading points in a an effort to decrease the effect of high pressure concentrations at these locations. However, it became immediately evident that despite this effort the compressive stiffness and strength of the core materials in the flatwise direction was not high enough for shear failure to supersede localized failure under the concentrated load or local indentation. Nevertheless, these tests revealed conditions under which the different core types will fail locally, and they provided the load versus displacement response needed to estimate the flexural stiffness of the core materials. The procedure used for these tests, and the experimental results along with a short discussion of the results for each core type is presented in the following sections.

5.1.1. Test Methodology. The three point tests were based on ASTM C393: Standard Test Method for Core Shear Properties of Sandwich Constructions by Beam Flexure (ASTM C393, 2011). This standard served as a guideline for the tests however not all the details of the standard were strictly followed. Therefore, a detailed description of the specimen preparation, the test setup, and the test procedure is provided in the following sections.

5.1.1.1 Specimen preparation. The specimens for this experiment were produced by cutting small beams from a larger beam segment using a fine toothed band saw. The specimens were partitioned at random using a ruler and a square. After they were cut, a coarse grit belt sander was used to lightly sand away any imperfections and ensure the sides were adequately straight and orthogonal to the adjacent sides. Four specimens were cut for Type 1 and Type 2 core configurations, and one specimen was cut for the Type 3 core configuration. A picture of one specimen for each core type is presented in Figures 5.1, 5.2, and 5.3. These specimens were approximately 3 in. wide by 8 in. long, and had a depth equal to that of the associated sandwich construction.

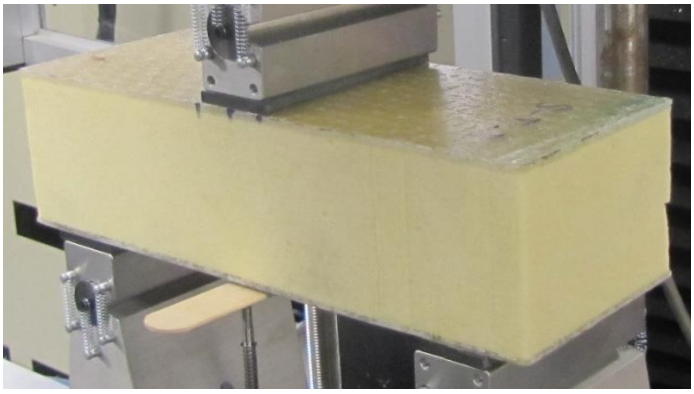

Figure 5.1: Three Point Flexural Test Specimen for Type 1

After the specimens were cut to size, strain gauges were applied to the center of the bottom facing of each specimen. The strain gauges were three-wire, 350 ohm, general purpose strain gauges that had a gauge length of 0.125 in., usable strain range of ± 3%, and were applied using the following procedure. The strain gauges were applied more than 24 hours before testing, and they were applied to the specimens in near standard temperature

and humidity conditions. First, the surface of the facings was insufficiently smooth to allow direct installation. As a result, initial preparation involved lightly sanding the facings at each gauge site. Then, two part epoxy (AE-10) was applied to the site to provide a base for the strain gauge. The epoxy was allowed to cure overnight, then it was sanded to a thin smooth surface. The sanded surface was cleaned using an adhesive catalyst. Once the surface had dried, the location of the gauge was marked using a ruler and a felt tip marker. Then, the gauge was aligned with the markings and affixed to the specimen using clear tape provided by the strain gauge manufacturer. Visual inspection and a ruler were used to ensure the gauge was centered and aligned parallel the sides of the specimen. The tape was then partially removed to expose the bottom side the strain gauge, and the adhesive catalyst was applied to the bottom surface of the strain gauge. Once, the catalyst dried, strain gauge adhesive (M-Bond 200) was applied to the bottom surface of the gauge, and using the tape as a guide, the gauge was pressed onto the specimen. Pressure was applied to the strain gauge by hand for 60 seconds, and the clear tape was removed to ensure the gauge had adhered to the specimen. Next, the gauge wires were protected by securing them to the specimen with tape.

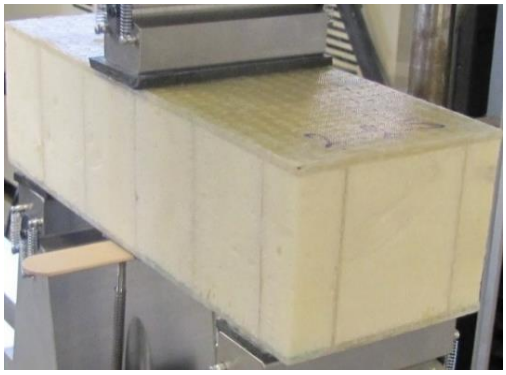

Figure 5.2: Three Point Flexural Test Specimen for Type 2

Figure 5.3: Three Point Flexural Test Specimen for Type 3

5.1.1.2 Test setup. The test setup used for the three point flexural experiment consisted of a test fixture manufactured by Wyoming Test Fixtures that was modified and installed in an Instron 4469 Universal Testing Machine (UTM). The product name of the fixture is the Long Beam Flexure Test Fixture (Model No. CU-LF), and it was constructed of machined aluminum and carbon steel. For the three point loading experiments, the supports were set up for a beam span of 6 in. and a single loading point positioned at mid-span. The loading pads at the supports and loading point were 1 in. wide flat bars that were free to pivot, and they were considered simple supports that impose no concentrated moment on the specimen. Rubber pads with a Shore A hardness of 60 were inserted at the supports and loading point to help reduce and distribute the pressure concentrations under the loads. Linear potentiometers were mounted to the fixture to measure the deflection of the bottom face at mid-span, and since one was position on each side of the specimen, the average of the two was recorded. The linear potentiometers had a metal spring assisted shaft with a 2 in. stroke length. A linear variable differential transducer (LVDT) with a spring assisted metal shaft and a 4 in. stroke length was mounted to the frame of the Instron

4469 UTM, and this LVDT was used to measure the displacement of the crosshead. The load was measured through the 9 pin output of the Instron 4469 UTM. A photograph of the setup just prior to testing is presented in Figure 5.4.

Figure 5.4: Test Setup Used for the Three Point Flexural Test

5.1.1.3 Test procedure. Specimens for the three point flexural tests were tested on multiple days under similar temperature and humidity conditions. Before testing, the width of each specimen was measured using digital or dial calipers to the nearest 0.001 in. A minimum of three measurements were taken and the average was reported. The height and facing thickness of the specimens was measured from the original manufactured beams before partitioning any specimens. A minimum of 10 measurements were taken for each

and the average was reported. The specimens for core Types 1 and 2 were not wide enough to interact with the linear potentiometers that measured the deflection of the bottom face at mid-span, therefore wooden extensions were affixed to the bottom of the specimens using double-sided tape so that the deflection could be measured. The lever arm imposed on the extensions was less than ¼ in. and the force applied to them by the linear potentiometers was very small, therefore the use of the extensions was assumed to have a negligible effect on the deflection measurements. Next, the supports were set to a span length of 6 in. and the loading point was set to mid-span using the markings on the test fixture and a ruler was used to verify the positions. The fixture was leveled, and the LVDT and linear potentiometers were then aligned parallel to the loading direction using a bubble level. The specimen was then placed into the fixture and the rubber pads were inserted at the support and loading points. The specimen was positioned with the strain gage at mid-span using a ruler, and the overhang of the specimen was approximately 1 in. from the center of the support to the end of the specimen. Next, the crosshead was lowered until a small preload of 0-20 lb. was applied to the specimen. The deflection and strain readings were then zeroed. A video camera was used to videotape the tests for further review after the tests were complete, and it was turned on at this point. The method of loading the specimens involved displacement control at a rate of 0.1 in/min. The load, the crosshead displacement, bottom face deflection at mid-span, and the strain in the bottom facing at mid-span were recorded at a rate of 1-2 Hz. Finally, the test was ended once the top face deflection reached 30-70% of the depth of the specimen which took 15-25 min. After failure, the specimen was promptly unloaded.

5.1.2. Test Results. For the three point flexural tests, the specimens displayed linear behavior prior to failure. However, as with the flatwise testing, there were false nonlinearities and discrepancies in the initial readings of the tests. The nonlinearities were caused by small gaps in the system and the compression of the rubber pads. Also, at the beginning of testing, the displacement was set to zero at a non-zero load. Both these discrepancies lead to a false offset in the recorded data. This was corrected using the same methodology presented in Section 4.1.2 in Section 4. Regression analysis was performed on multiple ranges of the data and the range with the highest correlation factor was chosen to be representative of the linear region. The genuine part of each curve was then offset by the x-axis intercept of the regression equation. Then, the false data at the beginning of each curve was replaced by a projection of the linear region that intersected the origin. This is graphically the same approach as shown in Figure 4.4 of Section 4.

In the following sections, the results for the three point flexural testing will be presented for each of the different sandwich constructions and their respective core types. The results and the observations made during the tests provided insights into the behavior of each sandwich construction and the reasons why they failed, and it allows for a qualitative discussion of the results that will presented at the end of this section. A more detailed analysis of the results will be presented in Section 6 along with a comparison of the different core types based on stiffness and strength.

5.1.2.1 Results for Type 1. For the three point flexural tests, four specimens were prepared and successfully tested for the sandwich construction with the Type 1 core. The false nonlinearities and offset were corrected for each of the data curves using the previously mentioned procedures. The bottom face deflection and the strain in the bottom

facing at mid-span were then plotted as the dependent variable versus the load in Figures 5.5 and 5.6, respectively. From these curves, several observations were made about the material behavior, and based on the observations made during the tests, a failure mode for the Type 1 specimens was determined.

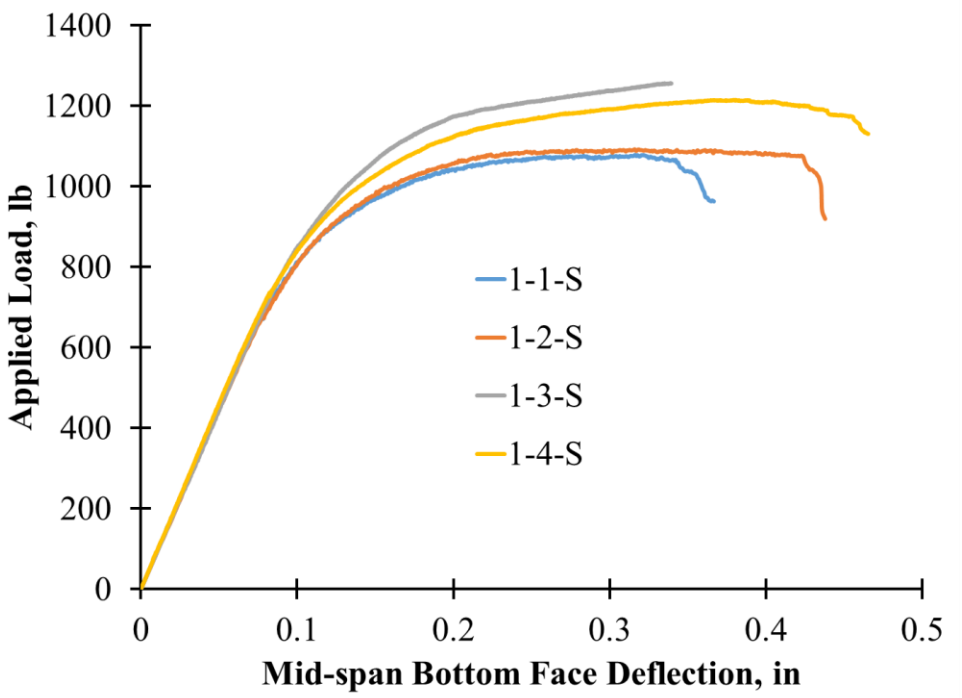

Figure 5.5: Three Point Flexural Test Results of Applied Load vs. Mid-span Bottom Face Deflection for Type 1

All of the curves have a similar shape with two distinct regions. In first the region, the response was very linear and this can be attributed to the constituent materials. The sandwich construction consisted of a Type 1 core made of rigid polyurethane foam and glass fiber reinforced polyurethane facings. The initial response of the rigid polyurethane foam is apparently linear elastic, which is evident in the results of the flatwise compression

and tension tests detailed in the previous section. As for the glass reinforced polyurethane facings, polyurethane is not typically linear elastic but can often be approximated as linear elastic, and coupled with glass fibers which are generally considered linear elastic, the composite has a behavior that is relatively linear elastic. As a result, the initial response in the first region is essentially linear elastic.

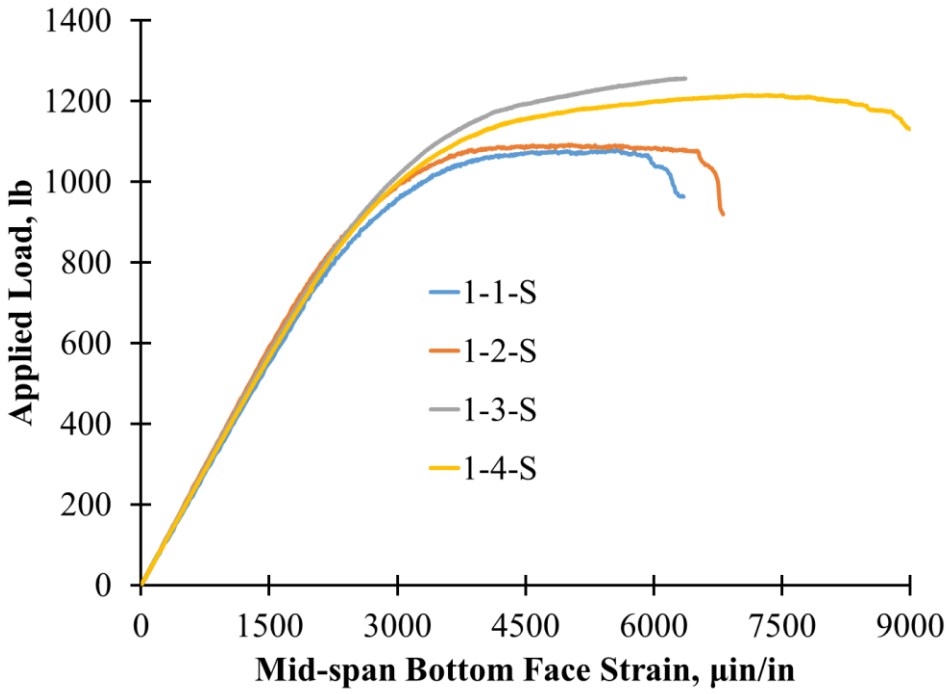

Figure 5.6: Three Point Flexural Test Results of Applied Load vs. Mid-span Bottom Face Strain for Type 1

In the second region, the response became nonlinear, and this is due to the crushable nature of the rigid polyurethane foam core and its relatively low stiffness. In the flatwise compression tests, the rigid polyurethane foam had nonlinear response that was characterized by an apparent yield point at its usable strength, at which point the foam

could not carry any additional stress. During the three point flexural tests, the stress concentrations under the load became larger than the usable compressive strength in the foam, which lead to yielding of the foam under the load. Once the foam began to yield, the top facing had very little support and the lack of stability coupled with the compressive stress in the top facing due to bending moments caused a buckle wave or wrinkle to form under the load. The buckle wave that formed had a wavelength proportional to the width of the loading bar. At this point, the top face began to deflect much more than the bottom face as foam under the load started to crush, which resulted in a permanent indentation in the top of the specimen. This failure mode is often referred to as local indentation. Then, the applied load continued to increase, but the rate at which it increased began to gradually decrease until it peaked, at which point a large portion of the foam under the load had yielded and the top facing had wrinkled excessively under the load. The load then began to decrease, and excessive deflection of the top facing eventually led to high stress concentrations under the edges of the loading bar that caused a facture in the facing and the core material underneath one edge of the loading bar. From this point on, the load began to decrease in an erratic stepped manor.

This type of failure occurred in Specimens 1-1-S, 1-2-S, and 1-4-S. As for Specimen 1-3-S, local indentation caused nonlinearity in the response, but before excessive local indentation could cause ultimate failure, a sudden facture occurred in the foam which resulted in an abrupt drop in the load. The fracture appeared to originate in the foam near the top facing just under the load and propagated diagonally though the core until it reached the bottom facing, where it propagated through the foam along the interface between the core and the bottom facing, at which point a large portion of the core separated from the

bottom facing. However, the failure occurred so quickly that the exact location where the fracture started is uncertain. This type of fracture is indicative of failure in the foam core due to shear stresses, but it is not entirely known why it only occurred in one of the specimens. One possibility could have been irregularities in the facing as the thickness of Specimen 1-3-S was not as uniform as the other specimens. The thickness of the top facing could have been larger under the point load than the average thickness, causing the facing to achieve a higher resistance to excessive local indentation.

In summary, the initial failure mode of all the Type 1 specimens was local indentation. The primary ultimate failure mode was excessive local indentation leading to fracturing of the facing and core due to high stress concentrations at the edges of the loading bar. However, one specimen ultimately failed due to shear stresses in the core. A picture of the initial crushing of the foam where the response became nonlinear is shown in Figure 5.7.

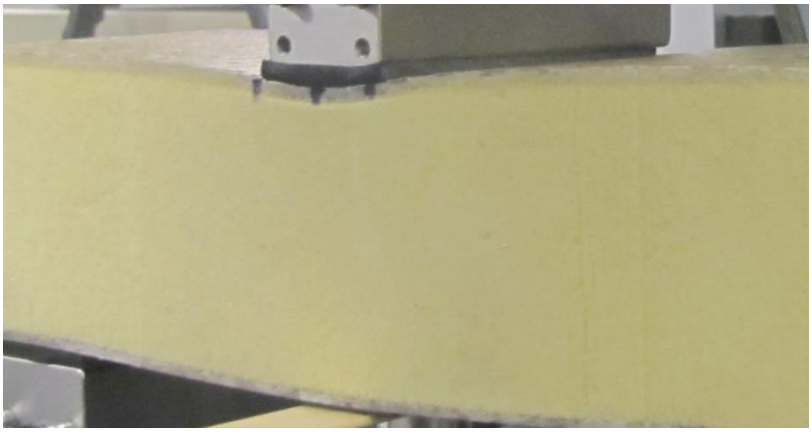

Figure 5.7: Three Point Flexural Testing Initial Failure by Local Indentation for Type 1

Also, pictures of the ultimate failure due excessive wrinkling of the facing, as well as shear failure in the foam, can be found in Figures 5.8 and 5.9, respectively. A detailed report of the three point flexural test results for each Type 1 specimen is presented in Appendix C.

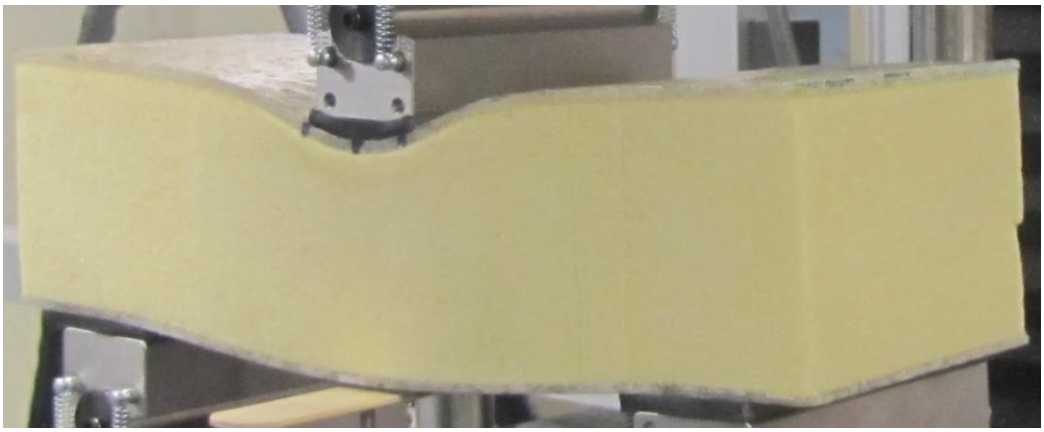

Figure 5.8: Three Point Flexural Testing Ultimate Failure by Excessive Local Indentation for Type 1

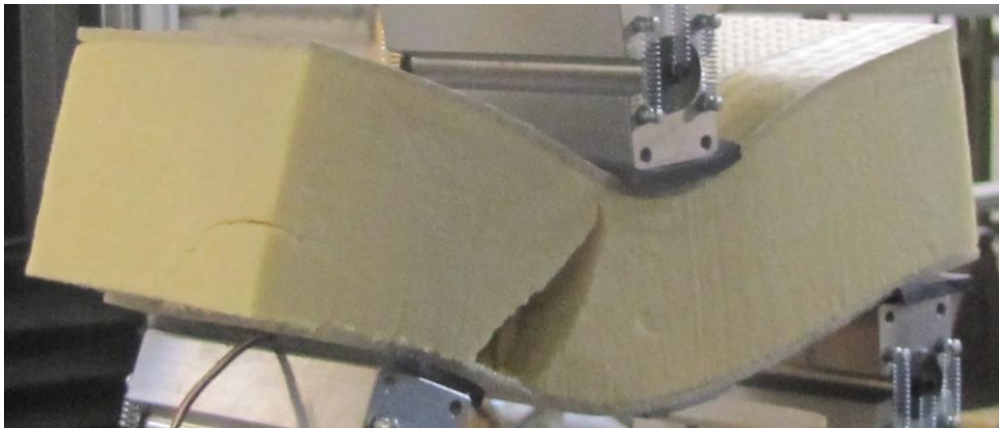

Figure 5.9: Three Point Flexural Testing Ultimate Failure by Shear Fracture in the Core Material for Type 1

5.1.2.2 Results for Type 2. For the three point flexural tests, four specimens were prepared and three were successfully tested for the sandwich construction with the Type 2 core. Unfortunately, during testing, the data for the third specimen was lost due to a programing error, therefore the results for three of the specimens will be presented. Again, the false nonlinearities and offset were corrected for each of the data curves, and the corrected data was plotted. The bottom face deflection and the strain in the bottom facing at mid-span are plotted as the dependent variable versus the load in Figures 5.10 and 5.11, respectively. Using these curves and observations made during the tests, a failure mode for the Type 2 specimens was determined.

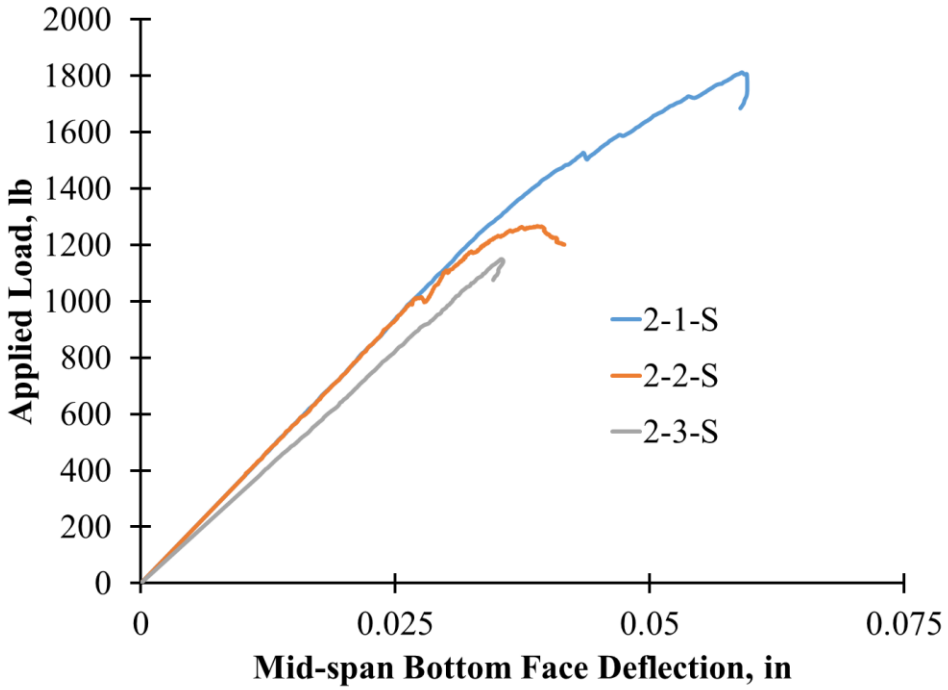

Figure 5.10: Three Point Flexural Test Results of Applied Load vs. Mid-span Bottom Face Deflection for Type 2

Similar to the Type 1 specimens, all of the curves for the Type 2 specimens had a similar shape with two distinct regions. Initially, the response was linear, which can be attributed to the materials used in the construction. The sandwich construction consisted of a Type 2 core made of flexible polyurethane foam with glass fiber web reinforcement that was infused with solid polyurethane, and the facings were made of the same glass fiber reinforced polyurethane used in the Type 1 construction with one additional layer that was pre-attached to the top and bottom of the foam core. The results of the flatwise compression and tension tests presented in the previous section indicate that the Type 2 core can exhibit an apparent linear elastic response. Then, given the facings are nearly the same as the Type 1 construction, it is reasonable that the initial response is apparently linear elastic.

Inevitably, the response became nonlinear for the same reasons that the flatwise compression specimens showed nonlinear behavior. The reinforcing webs of the core carry the majority of the load and the flexible foam provides stability, but the webs are very thin and hence prone to buckling. In the three point flexural specimens, the stress concentrations under the loading point caused the webs under the load to buckle. At which point a wrinkle formed in the top facing under the load due to a lack of support from the core. Just like the Type 1 specimens, the wrinkle wavelength was proportional to the width of the loading bar. Again, this failure mode is typically labeled as local indentation. The load continued to increase, but the rate of increase began to diminish as the top face began to deflect significantly more than the bottom face. At one point, the load peaked when the webs under the load point began to fracture due to excessive buckling, and consequently the top facing began to wrinkle excessively. Eventually, excessive wrinkling of the facing led to buckling and fracturing of the neighboring webs that were not directly under the load, and fractures

also formed in the top facing due to stress concentrations at the edges of the loading bar and at nearby transverse webs. This response caused the load to decrease erratically in a stepped manor as the loading bar crushed the core material beneath it and fractured the facings.

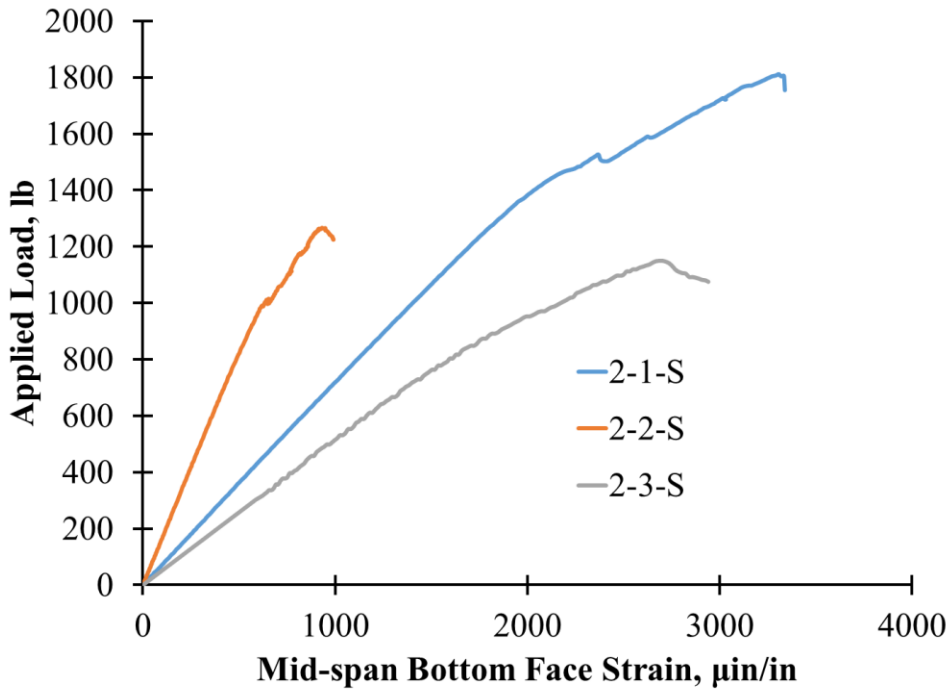

Figure 5.11: Three Point Flexural Test Results of Applied Load vs. Mid-span Bottom Face Strain for Type 2

In conclusion, the initial failure mode for all three specimens was local indentation directly beneath the load initiated by buckling of the reinforcing webs. Then, the ultimate failure mode for each of the specimens was excessive local indentation caused by fracturing of the reinforcing webs. A photograph of the damage to the specimen when the response became nonlinear is presented in Figure 5.12. A photograph of the damage at ultimate

failure when the load reached its peak value is presented in Figure 5.13. A detailed report of the three point flexural test results for each Type 2 specimen is presented in Appendix C.

Figure 5.12: Three Point Flexural Testing Initial Failure by Buckling of the Reinforcing Webs and Local Indentation for Type 2

Figure 5.13: Three Point Flexural Testing Ultimate Failure by Fracturing of the Reinforcing Webs and Excessive Local Indentation for Type 2

5.1.2.3 Results for Type 3. For the three point flexural tests, one specimen was prepared and tested for the sandwich construction with the Type 3 core. Unfortunately, the foam blocks needed to manufacture the Type 3 sandwich construction for the small scale flexural tests were difficult to obtain in the size that was needed, and only one representative small scale beam could be manufactured in the time allowed for this stage of the project. Therefore, very few specimens could be produced from the single beam. After the test, the initial false nonlinearities and offset were corrected for each of the data curves, and the corrected data was plotted. The bottom face deflection and the strain in the bottom facing at mid-span are plotted as the dependent variable versus the load in Figures 5.14 and 5.15, respectively. From the data and the observations made during the test, a failure mode for the Type 3 specimen was determined.

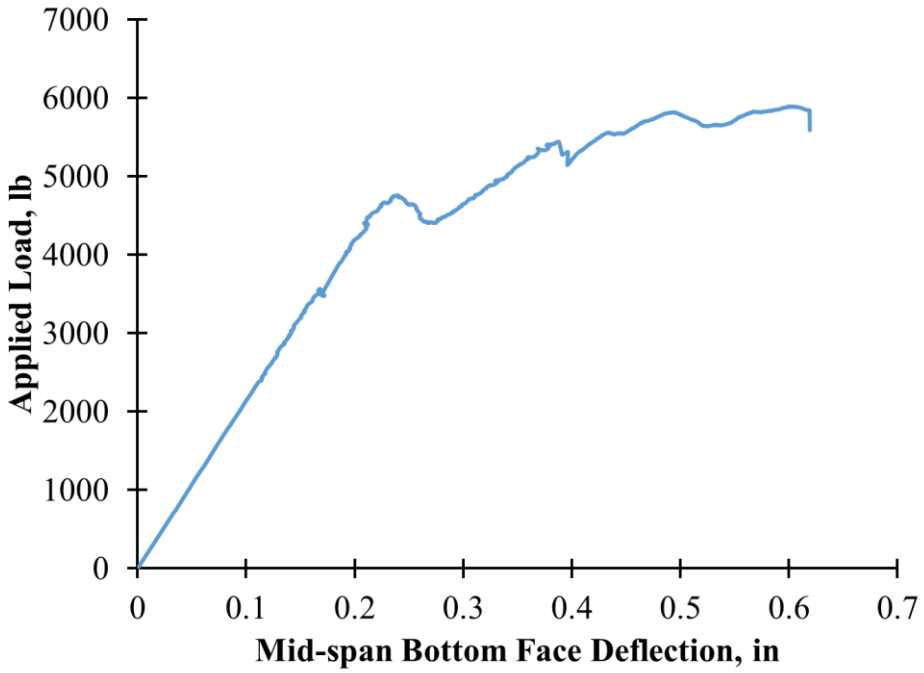

Figure 5.14: Three Point Flexural Test Results of Applied Load vs. Mid-span Bottom Face Deflection for Type 3

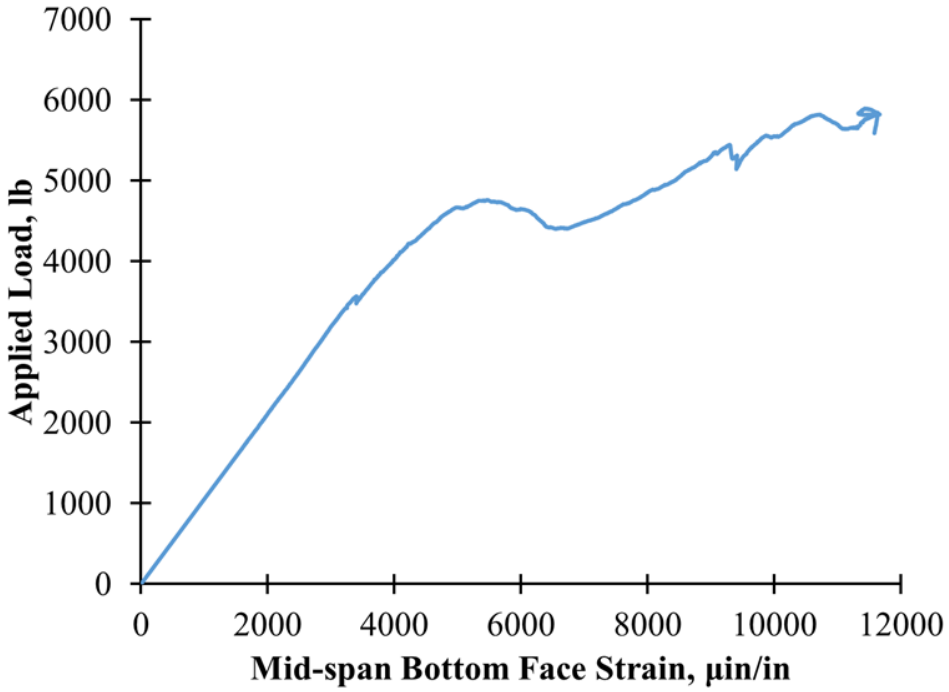

Figure 5.15: Three Point Flexural Test Results of Applied Load vs. Mid-span Bottom Face Strain for Type 3

The curve for the Type 3 specimen had a similar shape to that for the Type 1 and Type 2 specimens, with two distinct regions. The initial response was linear which, as with the other sandwich constructions, can be attributed to the materials used in the construction. The specimen was made with the Type 3 core, which consists of trapezoidal shaped flexible polyurethane foam blocks that are wrapped with a pre-attached glass fiber layer. Then, lapped between the blocks are glass fiber shear layers that are infused with solid polyurethane, and once they are cured they form a corrugated pattern between the foam blocks. Also, there are glass fiber reinforced polyurethane facings attached to the bottom and top of the core that were made from the same materials as the facings on the other two sandwich constructions. The flexible foam contributes very little to the behavior or the sandwich construction in the longitudinal direction, but it does provide extra stability to

the facings and webs. The fiber reinforced polyurethane differs with respect to the orientation of the fibers when comparing the shear layers to the facings layers, but overall the composite behavior should still be generally linear elastic. Therefore, the apparent linear elastic response at the beginning of the test was expected.

The response then became nonlinear as the specimen began to show signs of damage. The first sign of damage was delamination between the shear layers on one corner of the specimen near the bottom facing and just above one of the supports, which caused a small but sudden drop in the load. Then, the load started to increase at nearly the same rate as the initial linear region. Eventually, a wrinkle in the top facing occurred just under the load point due to stress concentrations with a wavelength proportional the width of the loading bar which is indicative of local indentation failure, and the rate of increase in the load began to drop. At this point, the top face of the specimen began to deflect significantly more than the bottom face. The shear layers under the load point eventually began to deform and facture apart as the load peaked and then started to decrease in an erratic stepped manor. After significant damage, the shear layers began to bow outwards, which locally stabilized the specimen temporarily. This led to a slow increase in the load. However, the stress concentrations under the load eventually started to crush the deformed shear layers again, and as the layers gained and lost stability the load continue to increase in general but in a very erratic fashion. At the end of the test, the load was still tending to increase, but the test was stopped as the top face had deflected more than half of the sandwich depth. Meanwhile, as local damage under the load kept intensifying, the initial delamination fracture at the corner of the specimen continued to open and progressively increased in size. By the end the test, the delamination had caused significant

unsymmetrical deformation at the end of the specimen where it occurred. The effects of this deformation are not immediately evident, but it is certain that it significantly affected the response of the specimen by likely causing torsional forces in the specimen.

Summarizing the test, the initial failure mode was delamination between the shear layers just above one of the supports, and the fracture that formed became progressively larger throughout the remainder of the test, which likely had a significant effect on the response of the specimen. The ultimate failure mode was excessive local indentation, which led to crushing of the shear layers under the load point. A photograph of the delamination fracture at the beginning of the test that caused some nonlinearity in the response is presented in Figure 5.16.

Figure 5.16: Three Point Flexural Testing Initial Failure by Delamination Between the Shear Layers for Type 3

Then, the localized damage under the load point that caused erratic jumps in the applied load at the end of the test is presented in Figure 5.17. Also, the severity of the unsymmetrical deformation caused by the delamination fracture by the end of the test is

depicted in Figure 5.18. A detailed report of the three point flexural test results for the Type 3 specimen is presented in Appendix C.

Figure 5.17: Three Point Flexural Testing Ultimate Failure by Excessive Local Indentation and Fracturing of the Shear Layers for Type 3

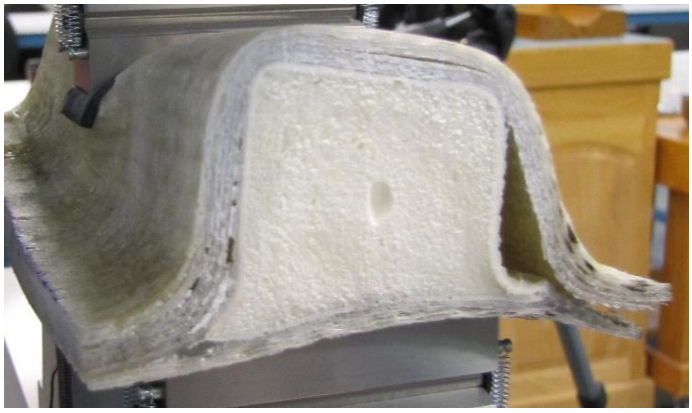

Figure 5.18: Three Point Flexural Testing the Unsymmetrical Deformation Caused by Delamination at the End of the Test for Type 3

5.1.3. Discussion of the Test Results. Using the results of the three point flexural testing, several useful observations can be made about the three different core types and their associated sandwich constructions. All three sandwich constructions displayed some

similar behaviors. The initial response of each of the constructions was apparently linear elastic. All three alternatives also showed nonlinear response before failure due to local strength and stability issues under the concentrated load. It was also apparent during that the test that, based on the displacement of the crosshead, the top face deflected noticeably more than the bottom face even at loads in the linear response range. These observations are consistent with the short span length and the relatively low stiffness and strength of the core materials.

For the Type 1 specimens, the behavior of the rigid polyurethane foam governed the behavior of the specimens. The foam has a low compressive strength and stiffness, which led to local indentation failure. This mechanism was prevalent in all of the specimens, and led to nonlinearity in the response. It also governed the ultimate failure of all but one of the specimens. Specimen 1-3-S failed due to shear stresses in the core at the ultimate load. This shear failure is inconsistent with the majority of Type 1 specimens, but it could have been influenced by inconsistencies in the thickness of the top facing in the specimen. However, overall, the Type 1 specimens showed very little variability with regard to the general deflection and strain response. This consistency in response can be attributed to the consistency in specimen construction, both dimensionally and materially.

As for the Type 2 specimens, the behavior was governed by the reinforcing webs that were very thin relative to their width. Buckling of these webs under the load led to nonlinearity in the response, and eventually led to instability in the top facing, which led to local indention failure. This response was apparent in all of the specimens, and the mechanism eventually led to ultimate failure in all of the specimens do to fracturing of the webs and local indentation. The variation in the results for the Type 2 specimens also

highlights the importance of the distribution of the webs. The width of all the specimens was nearly the same, and the number and location of the longitudinal webs was consistent between the three specimens as well. On the other hand, the distribution of the transverse webs was inconsistent. The results seem to indicate that this distribution effected the deflection and strain response measured in the specimens. This is consistent with the fact that the first sign of failure was buckling in the transverse webs.

The Type 3 specimen failed initially due to delamination between the shear layers at one corner or the specimen. This caused a small but noticeable drop in the load, but afterwards the load continued to increase at a rate comparable to the behavior before the fracture. The ultimate failure of the specimen was caused by local indentation, which eventually led to crushing of the shear layers beneath the load. It was noted that the fiber layers in the specimen were not completely saturated with polyurethane resin, and there were noticeable dislocations between the fibers and the foam at the ends of the specimen. Another troubling result was noticed when correcting the data. The slope of the load versus deflection curve was significantly less than what was expected based on the geometric stiffness of the fiber reinforce polyurethane. This indicates that the specimen most likely performed poorly due to manufacturing defects between the fiber layers that were not present in the specimens for the other two sandwich constructions, and it likely would have performed much better if the resin had fully saturated the fibers.

5.2. FOUR POINT FLEXUAL TESTING

The four point flexural experiments were initially intended to induce flexural failure in the facings by increasing the span length and the effects of bending moments while lessening the effects of shear forces. However, the high strength of the facing materials

proved to be large enough that causing this type of failure would be difficult. Theoretically, the span distances needed to cause tensile or compressive failure in the facings would be too large to construct and test given the constraints of the project. Also, concerns over the stability of the thin facings for the Type 1 and 2 specimens indicated that local buckling in the facings due to compressive bending stresses would likely occur before the strength of the facings was reached. Therefore, the focus of the tests was directed towards the shear strength of the core materials. Using the results of the three point tests, the four point flexural tests were modified to try to induce shear failure in the specimens. The support span was increased, which increased the effects of bending stresses, but the loading bars were increased in width and with an additional loading bar the localized effects near the concentrated loads were significantly reduced. This proved to be somewhat effective, but did not completely produce the desired results. Initial failure of the specimens was again influenced by localized effects under the concentrated load in some of the specimens, then for the other specimens initial failure was influenced by local buckling of the top facing between the two load points. However, the majority of the specimens ultimately failed due to reasons other than localized effects under the load points. Several of the specimens ultimately failed due to shear stresses in the core material, and a couple of specimens had compressive failure in the top facing at the peak load. Nevertheless, several observations were made about the strength and behavior the different core types, and the load versus displacement response needed to estimate the flexural stiffness of the core materials was obtained. The procedure used for these tests, and the experimental results along with a short discussion of the results for each core type is presented in the following sections.

5.2.1. Test Methodology. The four point flexural tests used procedures based on ASTM C393: Standard Test Method for Core Shear Properties of Sandwich Constructions by Beam Flexure (ASTM C393, 2011). This standard served as a guideline for the tests however not all the details of the standard were strictly followed. Therefore, a detailed description of the specimen preparation, the test setup, and the test procedure is provided in the following sections.

5.2.1.1 Specimen preparation. As with the three point tests, the specimens for this experiment were produced by cutting small beams from a larger beam segment using a fine toothed band saw. The specimens were partitioned using the same procedures as with the three point tests, and a coarse grit belt sander was again used to lightly sand away any imperfections and ensure the sides were adequately straight and orthogonal to the adjacent sides. Three specimens were cut for the Type 1 and Type 2 core configurations, and one specimen was cut for the Type 3 core configuration. One specimen for each core type – Type 1, Type 2, and Type 3 – is presented in Figures 5.19, 5.20, and 5.21, respectively. These specimens were approximately 3.5-4.5 in. wide by 26 in. long, and had a depth equal to that of the associated sandwich construction.

Once the specimens were the appropriate size, strain gauges were applied to the center of the top and bottom faces of each specimen. The same strain gages were used, three-wire, 350 ohm, general purpose strain gauges that had a gauge length of 0.125 in. and usable strain range of ± 3%. The gauges were applied using the same procedures as those used for the three point test specimens. The gauges were applied at least 24 hours before testing, and they were applied in nearly standard temperature and humidity conditions. The surface was lightly sanded at the gauge site. Then, two part epoxy (AE-10) was applied to

the site to provide a base for the gauge. The epoxy was allowed to cure overnight, then it was sanded to a thin smooth surface. The surface was cleaned using an adhesive catalyst. Once the surface had dried, the location of the gauge was marked using a ruler and a felt tip marker. The gauge was aligned with the markings and affixed to the specimen using clear tape provided by the strain gauge manufacturer. Visual inspection and a ruler were used to ensure the gauge was centered and aligned parallel to the sides of the specimen. The tape was then partially removed to expose the bottom of the strain gauge, and the adhesive catalyst was applied to the bottom surface of the strain gauge. Once, the catalyst dried, strain gauge adhesive (M-Bond 200) was applied to the bottom surface of the gauge, and using the tape as a guide, the gauge was pressed onto the specimen. Pressure was applied to the strain gauge by hand for 60 seconds, then the clear tape was removed to ensure the gauge had adhered to the specimen. Finally, the gauge wires were protected by securing them to the specimens with tape.

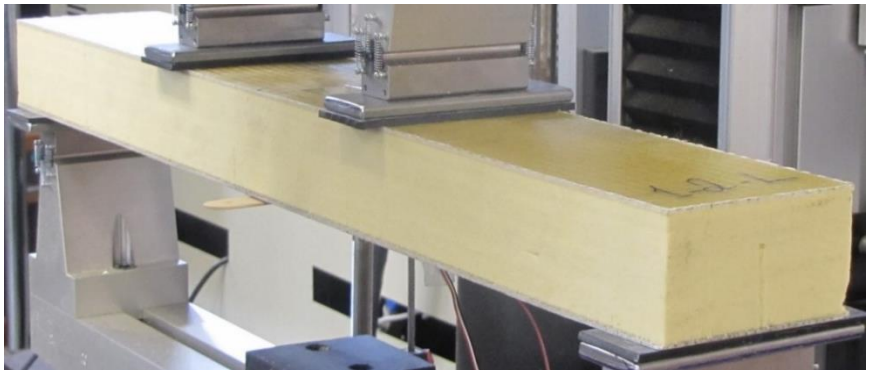

Figure 5.19: Four Point Flexural Test Specimen for Type 1

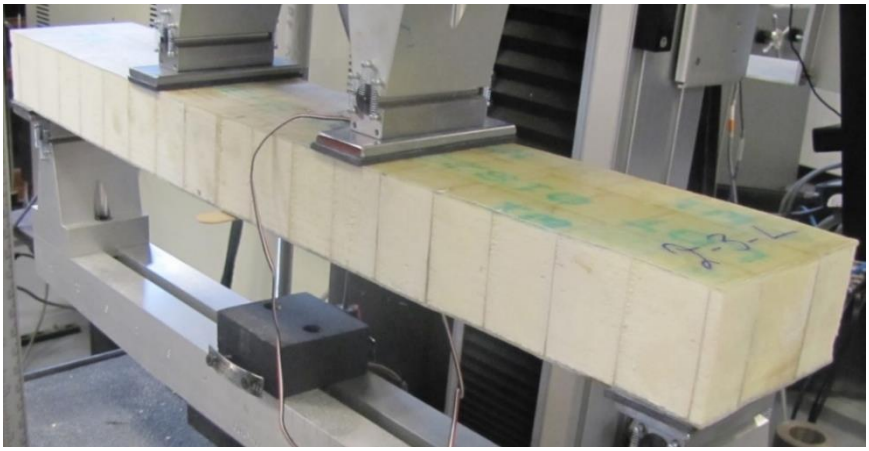

Figure 5.20: Four Point Flexural Test Specimen for Type 2

Figure 5.21: Four Point Flexural Test Specimen for Type 3

5.2.1.2 Test setup. The same fixture manufactured by Wyoming Test Fixtures was installed in the Instron 4469 UTM, and it was reconfigured for the four point flexural testing. The fixture is presented in Figure 5.4 in Section 5.1.1.2. For the four point loading experiments, the supports were set up for a beam span of 24 in. and the two loading points were positioned at the third points of the span. Therefore, the spacing between the load points and the support points was a constant 8 in. The loading pads at the supports and

loading points were increased to 1.5 in. in width by placing ¼ in. thick plates between the stock loading bars and the specimen, and the bars remained free to pivot. Consequently, the supports and load points were again considered to be simple supports that impose no concentrated moment on the specimen. Rubber pads with a Shore A hardness of 60 were again inserted at the supports and loading points to help reduce and distribute the stress concentrations under the concentrated loads. Initially, the same linear potentiometers were mounted to the fixture to measure the deflection of the bottom face at mid-span, and since one was positioned on each side of the specimen the average of the two was recorded. Unfortunately, during the four point flexural tests one of the potentiometers was broken, and only one was recorded for the second and third Type 1 specimens as well as all of the Type 2 specimens. Once again, an LVDT was mounted to the frame of the Instron 4469 UTM, and it was used to measure the displacement of the crosshead. The load was measured through the 9 pin output of the Instron 4469 UTM. A photograph of the set up just prior to testing is presented in Figure 5.22.

5.2.1.3 Test procedure. Specimens for the four point flexural tests were tested on multiple days under similar temperature and humidity conditions, and the same general procedure as the three point flexural tests was used. Before the test was started, the width of each specimen was measured using digital or dial calipers to the nearest 0.001 in. A minimum of three measurements were taken and the average was reported. The cross-sectional dimensions such as the height and facing thickness of the specimens was measured from the original manufactured beams before cutting the specimens. A minimum of 10 measurements were taken for each dimension and the average was reported.

Figure 5.22: Test Setup Used for the Four Point Flexural Test

As in the three point tests, some of specimens were not wide enough to interact with the linear potentiometers that measured the deflection of the bottom face at mid-span, therefore wooden extensions were affixed to the bottom of the specimens using double-sided tape so that the deflection could be measured. This was again assumed to have a negligible effect on the deflection measurements. Next, the supports were set to a span length of 24 in. and the loading points were moved the third points of the span distance using the markings on the test fixture, and a ruler was used to verify the positions. The fixture was leveled, and the LVDT and linear potentiometers were then aligned parallel to the loading direction using a bubble level. The specimen was then placed into the fixture and the rubber pads along with the plates used to widen the loading area were inserted at the support and loading points. The specimen was positioned with the strain gauges at mid-

span using a ruler, and the overhang of the specimen was approximately 1 in. from the center of the support to the end of the specimen. Next, the crosshead was lowered until a small preload of 0-20 lb. was applied to the specimen. The deflection and strain readings were then zeroed. The video camera was turned on to record the results visually. Then, displacement was applied to the specimen at a rate of 0.05-0.1 in/min. The load, the crosshead displacement, the deflection of the bottom face at mid-span, and the strain in the bottom and top facings at mid-span were recorded at a rate of 1-2 Hz. Finally, the test was ended once the crosshead displacement reached 30-60% of the depth of the specimen, which took 10-20 min with the exception of specimen 1-2-L, which was stopped at close to 160% of the specimen depth and took nearly 50 min. Once the test was stopped, the specimen was promptly unloaded.

5.2.2. Test Results. Similar to the three point specimens, the four point specimens displayed linear behavior prior to failure. However, the same false nonlinearities and discrepancies appeared in the initial readings of the four point tests. Again, the nonlinearity was caused by gaps between the loading bars and the specimen as well as the compression of the rubber pads. Also, a false offset was created when the displacements and strains were zeroed at a non-zero load. This was corrected using the same methodology that is presented in Section 4.1.2 in Section 4. Regression analysis of the linear portion of the curve was used to offset the data and replace the false data with a linear projection that intercepted the origin. This has been presented graphically in Figure 4.4 in the aforementioned section of Section 4.

The results for the four point flexural testing will be presented for each of the different sandwich constructions in the following sections. The data recorded and the

observations made during the tests provided insights into the behavior of each sandwich construction and the reasons why they failed. A qualitative discussion of the results based on these insights will be presented at the end of this section. A more detailed analysis of the results will also be presented in Section 6 along with a comparison of the different core types based on stiffness and strength.

5.2.2.1 Results for Type 1. Three specimens with the Type 1 core were prepared and successfully tested under the four point flexural testing protocol. The false nonlinearities and offset were corrected for each of the data curves using the regression analysis previously discussed. The corrected bottom face deflection and the strain in the top and bottom facings at mid-span were then plotted as the dependent variable versus the load and are presented in Figures 5.23, 5.24, and 5.25, respectively, for each specimen. Several observations were made about the material behavior using the data curves, and based on the observations made during the tests a failure mode for the Type 1 specimens was determined.

The behavior of the four point specimens was nearly the same as the behavior of the three point specimens. All of the curves had an initially linear region, and a nonlinear region that occurred just before ultimate failure. The Type 1 sandwich construction displayed an apparent linear elastic behavior for the same reasons that the three point specimens displayed linear elastic behavior. The constituent materials of the sandwich construction, the rigid polyurethane foam core and the glass fiber reinforced polyurethane facings, display linear elastic tendencies. The rigid polyurethane foam core displayed an apparent linear elastic behavior in the initial results of the flatwise tests, and the glass fiber reinforced polyurethane is often considered to have a composite response that is linear

elastic. Therefore, the linear behavior was again expected for the four point flexural specimens.

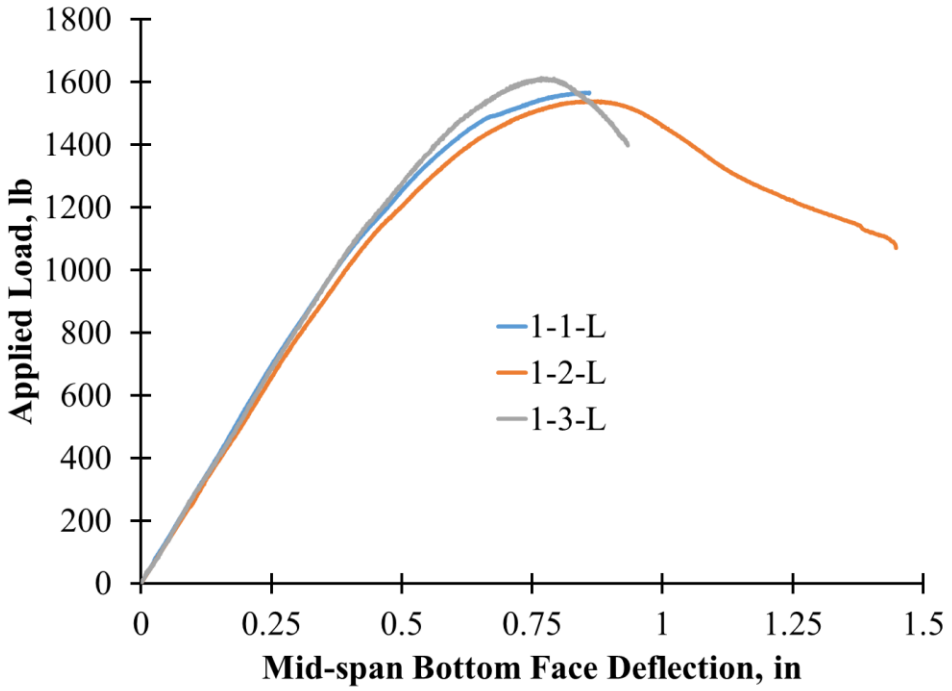

Figure 5.23: Four Point Flexural Test Results of Applied Load vs. Mid-span Bottom Face Deflection for Type 1

As with the three point specimens, the nonlinear behavior was most likely due to the crushable nature of the rigid polyurethane foam core and its relatively low stiffness. The rigid polyurethane foam displayed nonlinear response in the flatwise compressive tests that occurred after the initial linear response, and it was characterized by an apparent yield point at its usable strength, at which point the foam could not support more stress without significant damage and deformation. Amidst the four point flexural tests, the stress concentrations under the loading points became larger than the compressive strength in the

foam which lead to yielding of the foam under the load. Once the foam began to yield, the top facing lost stability and a wrinkle formed under the loading points which had a wavelength proportional the width of the loading bar. Again this failure mode is typically designated as local indentation. At this point, the top face began to deflect much more than the bottom face as foam under the load began to crush, which permanently indented the top of the specimen. The applied load continued to increase but the rate at which it increased began to gradually decrease. For Specimens 1-2-L and 1-3-L, the load peaked once the local indentation became too excessive. After this point, the load began to gradually decrease as the foam under the loading points crushed further. Specimen 1-2-L continued to lose load until excessive deformation led to concentrations of stress at the edges of the loading bars, which fractured the bottom side of the top facing in bending. At which point, the load dropped significantly. From this point on, the load began to decrease in an erratic stepped manor.

As for Specimen 1-3-L, the specimen lost capacity due to excessive local indentation, but before bending fracture occurred in the top facing, the foam core suddenly fractured in a pattern indicative of shear failure in the core. The fracture appeared to start as a diagonal fracture in the core material to the support side of one of the loading points, and it propagated to the interfaces between the core and the top and bottom facings. Once the fracture reached the interface, it propagated through the foam along the interface until it reached the edge of the specimen, and a large piece of the core separated itself from the specimen. The fracture occurred so quickly that the location where the crack began is not certain but it appear to originate within the diagonal crack in the core.

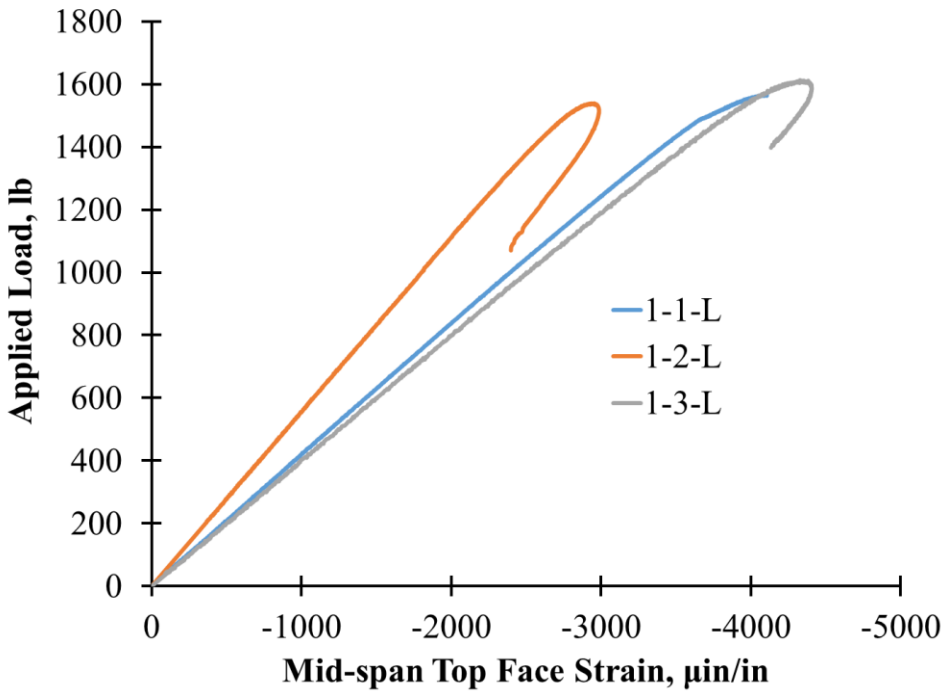

Figure 5.24: Four Point Flexural Test Results of Applied Load vs. Mid-span Top Face Strain for Type 1

Specimen 1-1-L behaved differently, the core yielded and the top facing began to wrinkle, but just before the deformation became excessive enough to cause the load to decrease, the same shear fracture occurred, which is similar to the three point test for Specimen 1-3-S. Both shear fractures in the four point tests occurred suddenly and were more energetic than the shear fracture that occurred in the three point test. The pieces of the foam that separated from the specimens ejected out of the end of the specimens with substantial velocity and the remainder of the specimens ejected from the test fixture in the opposite direction. The reasons why each specimen behaved differently are not fully understood, but the differences are likely related to the different widths of the specimens and possible variations in the thickness of the top facings.

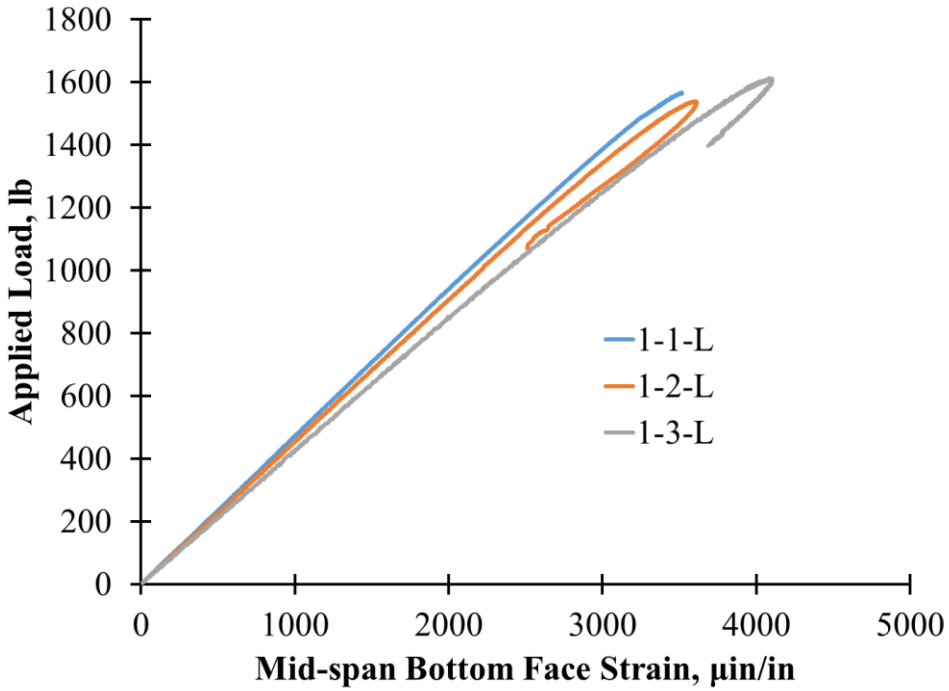

Figure 5.25: Four Point Flexural Testing of Applied Load vs. Mid-span Bottom Face Strain for Type 1

Reviewing the tests, the initial failure mode for all the specimens was local indentation. The primary ultimate failure mode was excessive local indentation, which lead to bending fracture in the top facing or shear failure in the core. One specimen ultimately failed in shear before yielding and wrinkling could cause a loss in load. A photograph of the initial yielding of the foam where the response became nonlinear can be found in Figure 5.26. Photographs of the ultimate failure due to excessive wrinkling of the facing, as well as the fracture caused by shear failure in the foam, can be found in Figures 5.27 and 5.28, respectively. A detailed report of the four point flexural test results for each Type 1 specimen is presented in Appendix D.

Figure 5.26: Four Point Flexural Testing Initial Failure Due to Local Indentation for Type 1

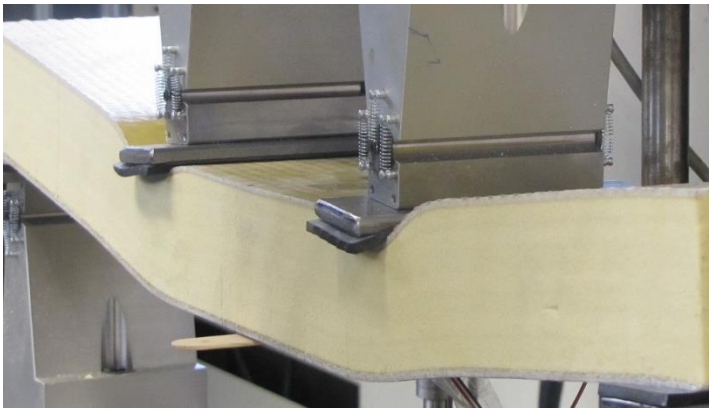

Figure 5.27: Four Point Flexural Testing Ultimate Failure Due to Excessive Local Indentation for Type 1

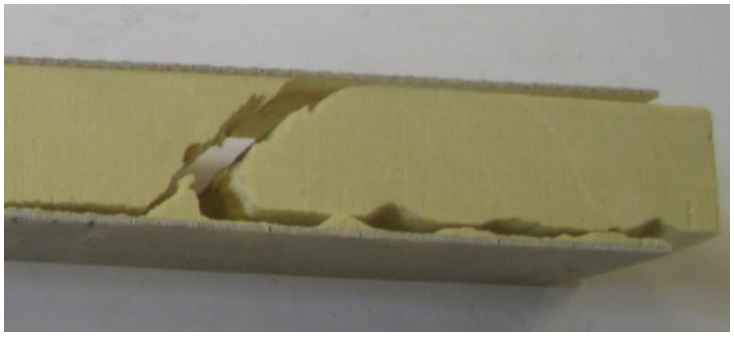

Figure 5.28: Four Point Flexural Testing Ultimate Failure Due to Shear Failure in the Core Material for Type 1

5.2.2.2 Results for Type 2. In the four point flexural tests, three specimens were prepared and successfully tested for the sandwich construction with the Type 2 core. Again, the false nonlinearities and offset were corrected for each of the data curves, and the corrected data was plotted. The corrected bottom face deflection and the strain in the top and bottom facings at mid-span were then plotted as the dependent variable versus the load and are presented in Figures 5.29, 5.30, and 5.31, respectively, for each specimen. Using these curves and observations made during the tests, several observations about the behavior were made and a failure mode for the Type 2 specimens was determined.

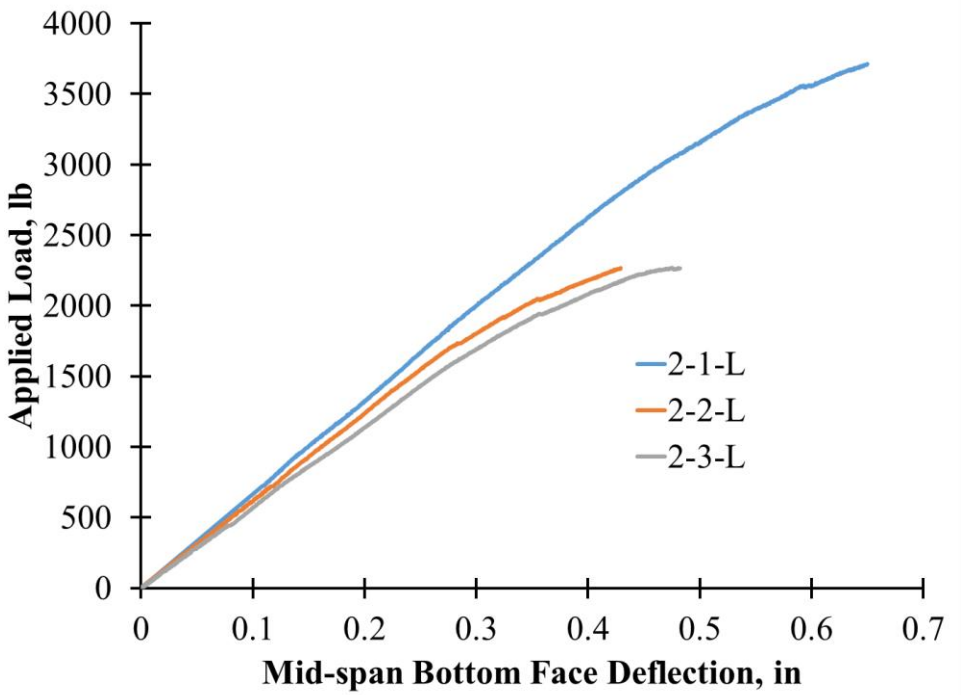

Figure 5.29: Four Point Flexural Test Results of Applied Load vs. Mid-span Bottom Face Deflection for Type 2

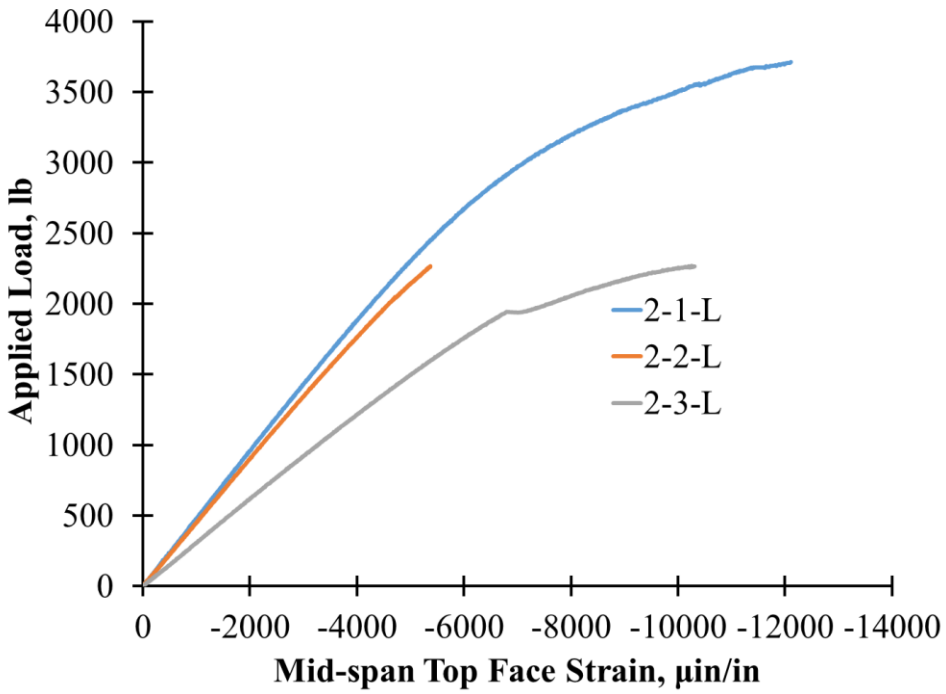

Figure 5.30: Four Point Flexural Test Results of Applied Load vs. Mid-span Top Face Strain for Type 2

The curves are linear initially, and as the load increases they become nonlinear before failure. The initial linear response can be attributed to the materials used in the construction. The stitch reinforced flexible polyurethane foam core and the glass fiber reinforced facings have linear elastic tendencies. The results of the flatwise tests presented in the previous section indicate that the Type 2 core can exhibit an apparent linear elastic response, and fiber reinforced facings are typically considered linear elastic. Therefore, the initial linear elastic response was as expected.

The response became nonlinear for stability reasons that differ from the three point tests. The reinforcing webs of the core are thin and prone to buckling under compression, but no buckling of these webs under the load points was observed. However, the facings of the specimens were very thin relative to their width, and the top facing was prone to

localized buckling between the cellular web reinforcement, also known as intercellular dimpling/buckling. In the four point flexural tests, the compressive stress in the top facing became large enough between the load points that intercellular dimpling occurred. This caused the load to become nonlinear as the stress was limited in buckled sections and was forced to redistribute to more stable regions. The load continued to increase afterwards, but the rate of increase slowly diminished as more of the top face buckled locally between the load points. The load suddenly peaked and immediately dropped at the ultimate failure in all of the specimens but for two distinct reasons. Specimen 2-1-L failed due to sudden compressive failure in the top facing in the form of a fracture under one of the load points.

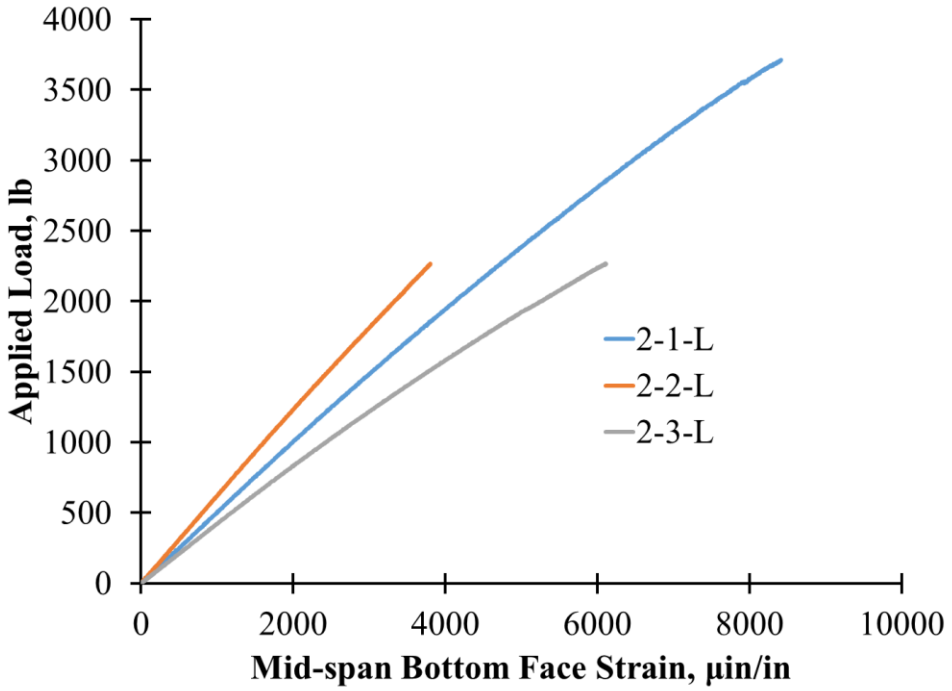

Figure 5.31: Four Point Flexural Test Results of Applied Load vs. Mid-span Bottom Face Strain for Type 2

The other two specimens, 2-2-L and 2-3-L, failed due to a sudden fracture in the core near the supports that was indicative of shear failure. The fracture occurred diagonally through the core between the transverse webs and propagated to the interfaces between the core and the facings. At the interface, the fracture continued to slowly propagate through the core material as load was applied, but no part of the core completely separated from the core. These ultimate failures were energetic, but no quite as catastrophic as the Type 1 shear failures. The initial failure modes of all the specimens was intercellular dimpling but the ultimate failure was different because of the different widths of the specimens and the different number of the longitudinal stiffeners in the specimens. Specimen 2-1-L had three longitudinal stiffeners while the other specimens only had two, which is why the first specimen carried much more load and failed ultimately due to compressive failure in the facings.

In conclusion, the initial failure mode was due to intercellular dimpling in the top facing. The ultimate failure mode was shear failure in the core characterized by a diagonal fracture in the core material for Specimens 2-2-L and 2-3-L. As for 2-1-L, the ultimate failure was cause by compressive failure of the top facing just under the load. A photograph of the initial intercellular dimpling is presented in Figure 5.32. A photograph at ultimate failure due to shear stress is presented in Figure 5.33. Finally, the damage after compressive failure of the top facing in one of the specimens is presented in Figure 5.34. A detailed report of the four point flexural test results for each Type 2 specimen is presented in Appendix D.

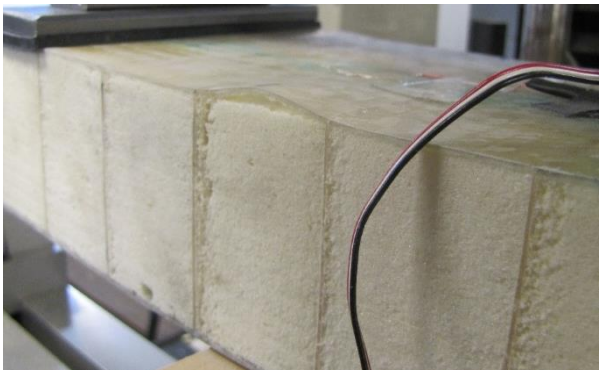

Figure 5.32: Four Point Flexural Testing Initial Failure by Intra-cellular Dimpling of the Top Facing for Type 2

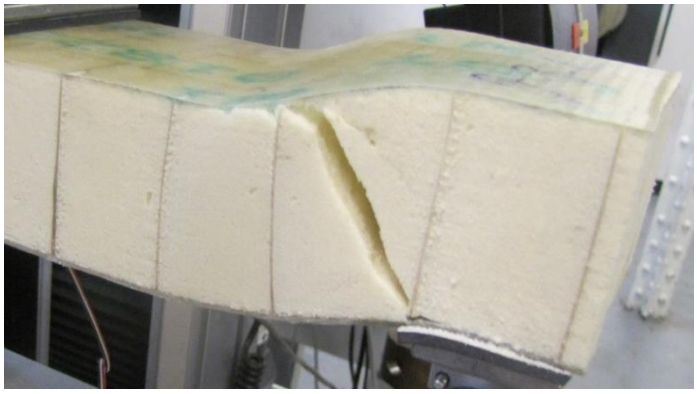

Figure 5.33: Four Point Flexural Testing Ultimate Failure by Shear Fracture in the Core Material for Type 2

Figure 5.34: Four Point Flexural Testing Ultimate Failure by Compressive Failure of the Top Facing for Type 2

5.2.2.3 Results for Type 3. For the four point flexural tests, one specimen was prepared and tested for the sandwich construction with the Type 3 core. Again supply and manufacturing issues due to the small scale of the specimens only allowed for one specimen to be constructed within the time allotted for this stage of the project. Therefore, the number of specimens was severely limited. Once the test was completed, the initial false nonlinearities and offset were corrected for each of the data curves, and the corrected data was plotted. The bottom face deflection and the strain in the top and bottom facings at mid-span are plotted as the dependent variable versus the load in Figures 5.35, 5.36, and 5.37, respectively. Many observations about the behavior of the sandwich construction were deduced from the recorded data, and based on the observations made during the test a failure mode for the Type 3 specimen was determined.

The four point flexural response for the Type 3 specimen has a distinct linear region at the beginning of the test and the response became nonlinear before ultimate failure. The initial linear response is expected considering the behavior of the materials used in the construction. The core of the specimen consisted of a trapezoidal shaped flexible polyurethane foam block that was wrapped with a pre-attached glass fiber layer. Then, lapped over the block are glass fiber shear layers that are infused with solid polyurethane Also, there are glass fiber reinforced polyurethane facings attached to the bottom and top of the core that were made from the same materials as the facings on the other two sandwich constructions. The flexible foam acts as formwork for the shear layers and contributes very little to the behavior or the sandwich construction in the longitudinal direction, but it does provide some extra stability to the facings and webs. The glass fiber shear layers have a different orientation with respect to the direction of the weave when compared to the facing

layers, but overall the composite behavior should still be generally linear elastic. Therefore, the apparent linear elastic response at the beginning of the test was expected.

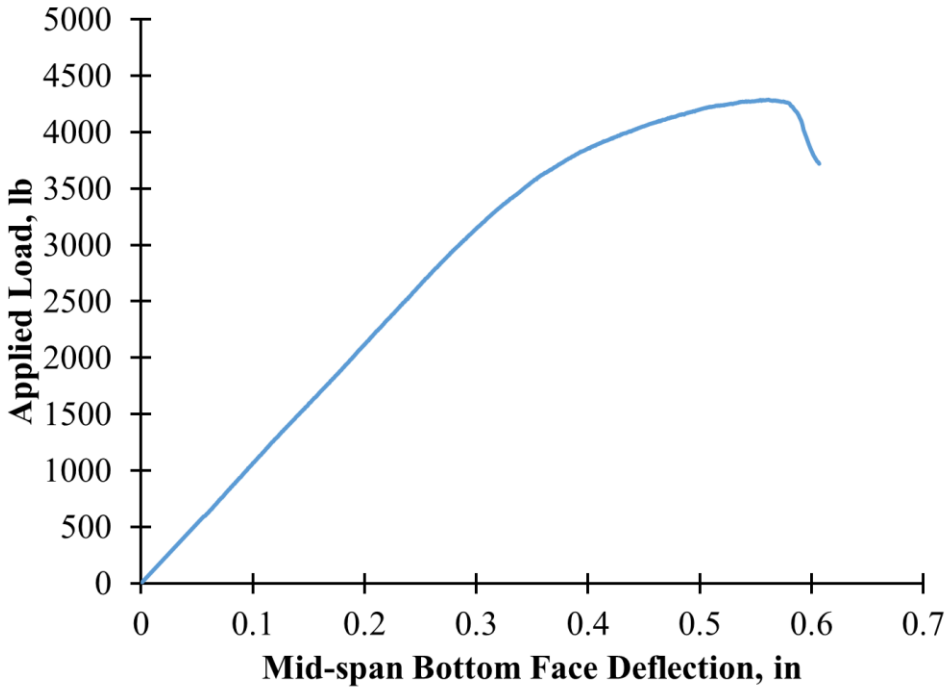

Figure 5.35: Four Point Flexural Test Results of Applied Load vs. Mid-span Bottom Face Deflection for Type 3

The response became nonlinear eventually due to progressive compressive failure in the top facing under the load. The failure began at the outer layers and slowly progressed to the inner layers as the load increased. Due to the geometry of the specimen and the thickness of the top facing, the failure could not occur as one immediate fracture like the failure previously discussed for Specimen 2-1-L. At this point, the load continued to increase, but the rate of increase slowed. As the compressive failure progressed through the top facing and into the webbing, the load peaked as a hinge mechanism formed in the

top facing. Then, as the shear layers in the webbing started to fail in compression, the load dropped significantly and decreased in a stepped manor as the crushing progressed

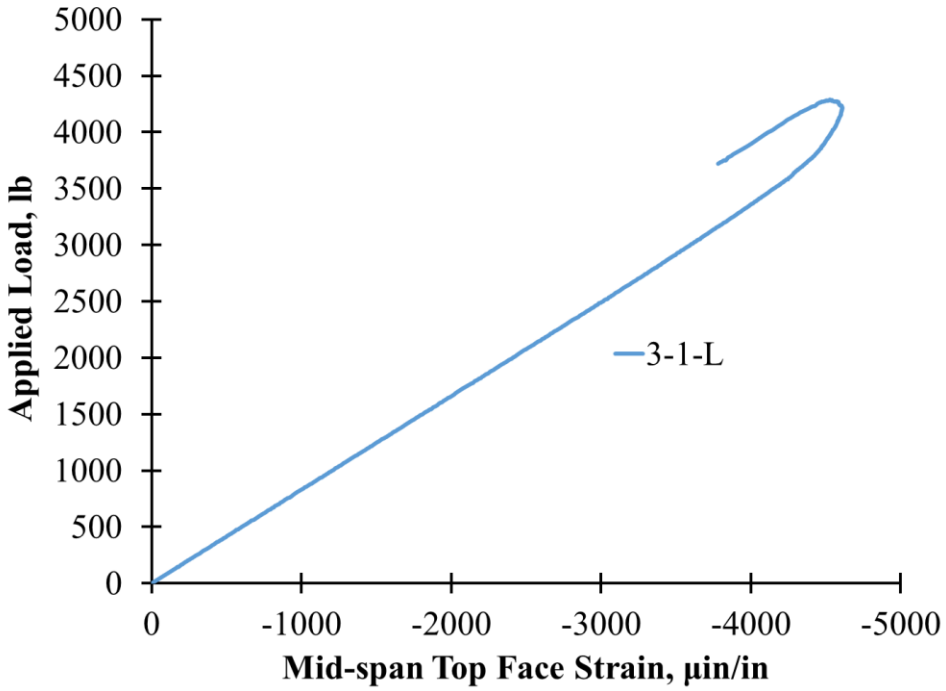

Figure 5.36: Four Point Flexural Test Results of Applied Load vs. Mid-span Top Face Strain for Type 3

Summarizing the test, the failure mode was compressive failure under the load point in the top facing that caused initial nonlinearity. Then, as the compressive failure progressed into the webbing of the specimen, ultimate failure occurred due to the formation of a hinge mechanism in the top facing. Photographs of the compressive failure are presented in Figures 5.38 and 5.39. A detailed report of the four point flexural test results for the Type 3 specimen is presented in Appendix D.

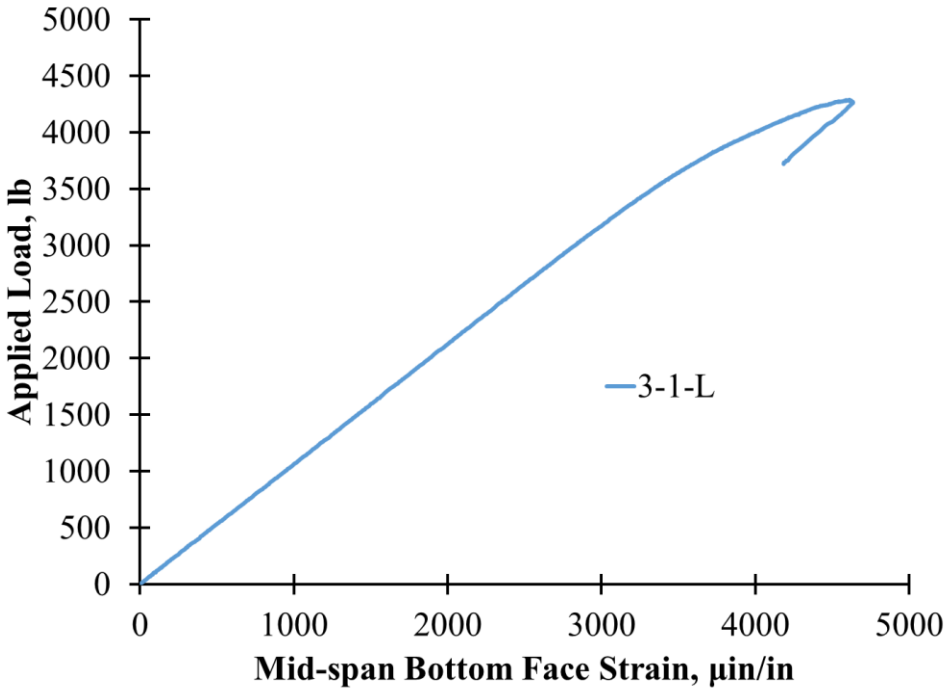

Figure 5.37: Four Point Flexural Testing of Applied Load vs. Mid-span Bottom Face Strain for Type 3

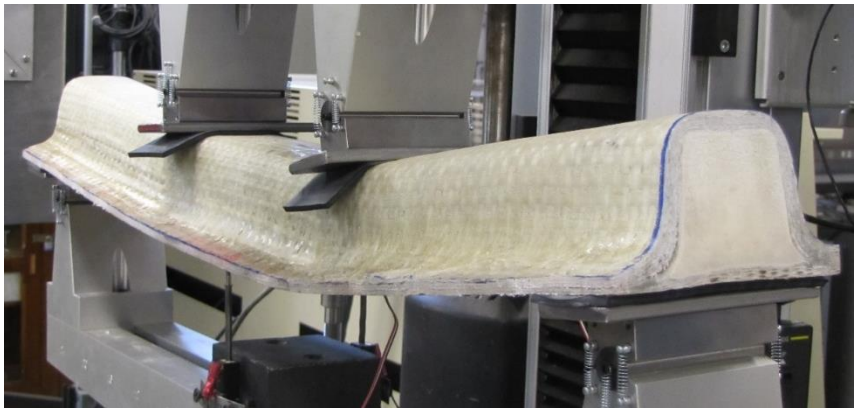

Figure 5.38: Four Point Flexural Testing Ultimate Failure Due to Compression Failure of the Top Facing Under the Load Point for Type 3

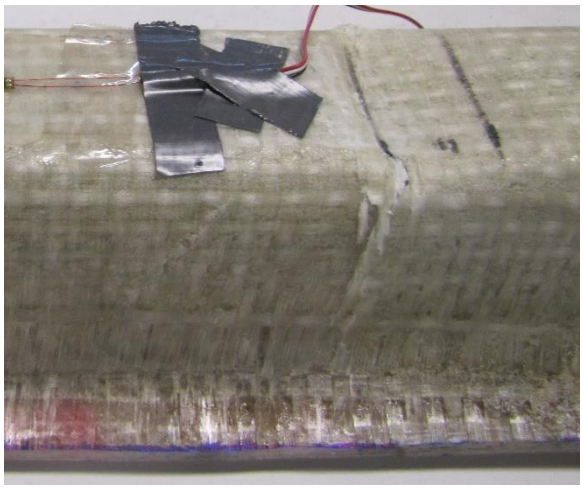

Figure 5.39: Four Point Flexural Testing Fracture Due to Compression Failure of the Top Facing Under the Load Point for Type 3

5.2.3. Discussion of the Test Results. Several useful observations can be made from the four point flexural test results. The initial response of each of the constructions was apparently linear elastic. As far as the nonlinear response is concerned, the observed mechanisms were different for each of the three types. However, this is expected considering the longer support span compared to the three point flexural test and the significant differences between the core types.

For the Type 1 specimens, the behavior of the rigid polyurethane foam continued to govern the behavior of the specimens. The low compressive strength and stiffness of the foam core led to local indentation in the four point specimens. This mechanism was again prevalent in all of the specimens and led to nonlinearity in the response. It also governed the ultimate failure of all but one of the specimens. Specimen 1-1-L failed ultimately due to shear stresses in the core. The variation in ultimate failure was likely due to reasons similar to that of the three point specimens with noticeable variations in the thickness of

the facings. Also, the fact that the specimens had different widths likely contributed to the variations.

For the Type 2 specimens, the behavior was governed by the stability of the top facing. Localized buckling or intercellular dimpling in the top facing between the load points occurred in all three of the specimens. This led to nonlinearity in the response. The ultimate failure in the specimens was caused by two mechanisms. Specimen 2-1-L suffered sudden compressive failure in the top facing just under the load. Specimens 2-2-L and 2-3-L ultimately failed due to shear fracture in the core material adjacent to the support. The variation was due to differences in the width and the number of longitudinal stiffeners in the specimens. The first specimen had three longitudinal stiffeners while the others had two. This allowed compressive failure to dominate in the first specimen while shear failure dominated in the other two specimens.

For the Type 3 specimen, failure occurred due to compressive stresses in the top facing, and as the compressive failure progress into the webbing, a hinge mechanism formed in the top facing that caused ultimate failure. The poor resin saturation and dislocations between the fiber layers were also noticeable in the four point specimens, but no delamination failure occurred during the test. Also, the slope of the load versus deflection curve was of appropriate magnitude when considering the geometric stiffness of the cross-section. Therefore, the effects of the manufacturing defects appeared to be much less prevalent in the four point specimen. Nevertheless, performance would have improved if the defects were not present.

6. ANALYSIS OF FLEXURAL STIFFNESS AND STRENGTH

The flexural behavior of the three different sandwich constructions can be quantitatively analyzed by fitting the experimental results to common theories and models. The low stiffness of the foam materials used in the cores, coupled with the short spans that were used in the tests, described previously, often leads to complex behavior at the load and support points, and to get a truly accurate representation of this behavior detailed models are needed. Higher order shear deformation theories and/or finite element models have often shown very good accuracy for sandwich constructions like the alternatives that were tested, but they take a significant amount of effort to develop and solve. Less exact theories such as Classical/Euler-Bernoulli Beam Theory (EBBT) and Timoshenko Beam Theory (TBT) are not nearly as detailed and are often conservative when estimating material properties, but when applied to beams they can be solved analytically with minimal effort using simple static equilibrium relationships and simplified support conditions. EBBT and TBT cannot predict nonlinear behavior or localized stress concentrations at concentrated loads. However, they can predict global behavior when fitted to linear experimental results, and they can predict global equivalent stresses which can be used as a general comparison tool.

Considering the scope of this study and the goals set forth, the primary goal is to compare the core types based on structural performance using small scale experiments and recommend one to further develop into a bridge deck panel. EBBT and TBT will be sufficient enough to analyze the results and compare the different cores types to one another. The development of sophisticated models will be left to later stages of the project that focus on a single configuration. The assumptions and governing equations for both

EBBT and TBT are presented in the literature review of Section 2. The specific solutions used to estimate the stiffness and strength of each alternative are presented in Sections 6.1 and 6.2, respectively. Finally, a comparison of the of the stiffness and strength limit states is presented in Section 6.3.

6.1. ANALYSIS OF FLEXURAL STIFFNESS

The flexural stiffness of a beam is the combination of certain geometrical and material stiffness properties that relate the applied load to the resulting deflections. The prediction of deflection is a very important tool in designing sandwich panels, especially for their use in bridge decks. The deflection is often limited by certain serviceability criteria that are based on the intended service that the structural member will provide. For bridge decks, the deflection is limited severely to ensure the members do not cause unforeseen complications, and to ensure that people using them are comfortable as they drive over them. Therefore, the stiffness of each sandwich construction is an important comparison, if not the most important, considering this limit state controlled nearly all designs of the fiber reinforced polymer sandwich panels that have been used in bridge decks.

In the following sections, TBT will be used to estimate the flexural stiffness of the Type 1 and 2 sandwich constructions using a procedure similar to that presented in ASTM D7250: Standard Practice for Determining Sandwich Beam Flexural and Shear Stiffness (ASTM D7250, 2012). The procedures in the ASTM were not directly used in this analysis, but they use a similar theory that produces the same analytical solutions. As for the Type 3 construction, EBBT will be used to estimate the flexural stiffness. The governing equations and details of EBBT and TBT are presented in Section 2 Section 2.2, but the specific solutions used in this analysis are presented in the following sections.

6.1.1. Results of the Analysis. If we consider the specific case used in these experiments, the governing equations found in Section 2 can be solved by using static equilibrium and simple boundary conditions. The experimental conditions can be idealized as a simply supported beam with loading points that are equidistant from each support, which is statically determinant and has easily determined shear (*V*) and moment (*M*) distributions based on static equilibrium. The idealization of the experimental conditions is represented in Figure 6.1.

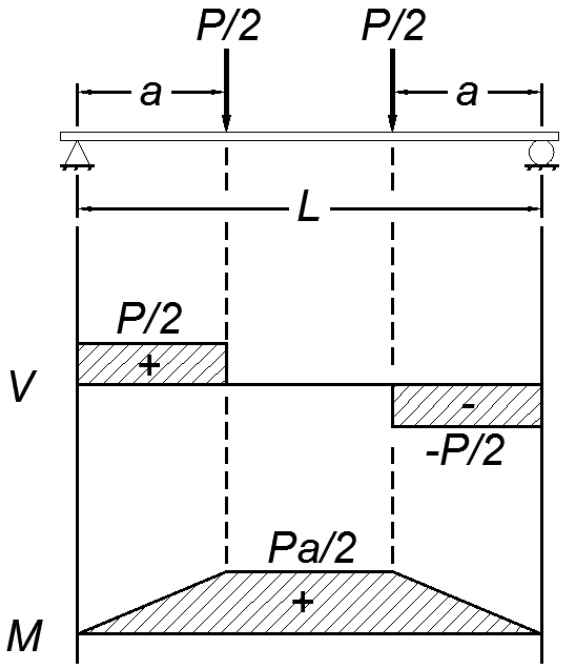

Figure 6.1: Idealization of the General Case

The governing equations for both EBBT and TBT can then be solved using integration, and the integration constants can be solved by using the boundary conditions and the compatibility relationships. The boundary conditions include the curvature is equal

zero at mid-span and the deflection is equal to zero at the supports. Then, compatibility is maintained at $x=a$ where both the curvature and deflection must be equal on the left and right sides. From this, the solution is found in Equation 6.1 for EBBT and Equation 6.2 for TBT, these solutions are symmetric about the mid-span.

$$w(x) = \frac{Px(x^2 + 3a^2 - 3aL)}{12EI}; 0 \leq x \leq a$$
$$w(x) = \frac{Pa(3x^2 - 3Lx + a^2)}{12EI}; a \leq x \leq \frac{L}{2} \quad (6.1)$$

$$w(x) = \frac{Px(x^2 + 3a^2 - 3aL)}{12EI} - \frac{Px}{2kAG}; 0 \leq x \leq a$$
$$w(x) = \frac{Pa(3x^2 - 3Lx + a^2)}{12EI} - \frac{Pa}{2kAG}; a \leq x \leq \frac{L}{2} \quad (6.2)$$

Where the deflection *w(x)* is positive upwards. From these solutions, the deflections at mid-span for the three point loading case ($a = L/2$) and the four point loading case ($a = L/3$) can be determined. Using EBBT, the solution for the three point case is presented in Equation 6.3, and the solution for the four point case is presented in Equation 6.4. As for TBT, the solution for the three point case is presented in Equation 6.5, and the solution for the four point case is presented in Equation 6.6.

$$w_{1,max} = \frac{P_1 L_1^3}{48EI} \quad (6.3)$$

$$w_{2,max} = \frac{23P_2L_2^3}{1296EI} \tag{6.4}$$

$$w_{1,max} = \frac{P_1L_1^3}{48EI} + \frac{P_1L_1}{4kAG} \tag{6.5}$$

$$w_{2,max} = \frac{23P_2L_2^3}{1296EI} + \frac{P_2L_2}{6kAG} \tag{6.6}$$

In these solutions, the sign of the deflection has been reversed so that the deflection *w(x)* is positive downwards, and the subscript "*1*" indicates the three point configuration (*a = L/2*) while "*2*" indicates the four point configuration (*a = L/3*). With these equations, the bending and shear stiffnesses of the sandwich constructions can be calculated based on the load versus deflection curves recorded during the tests. The following sections will show the variations of these equations used for each sandwich construction and the results that the equations produced. Then, the results will be normalized to a "standard" size section of 2 in. tall and 3 in. wide, which was chosen based on the geometric constraints of the specimens. The method of normalization will be applied to each construction while attempting to maintain key geometrical features. These concepts will be presented separately for each sandwich construction, and finally a comparison between the constructions will be presented in Section 6.1.2, which will be based on common deflection limit states for bridge deck members.

6.1.1.1 Results for Type 1. In order to apply the TBT solutions discussed previously to the results for the Type 1 specimens, some observations need to be made along with some algebraic manipulation. For the Type 1 sandwich construction, an

effective *EI* term can be found by summing the contributions of each part of the construction. The total quantity is determined using Equation 6.7.

$$EI = E_f I_f + E_c I_c \tag{6.7}$$

Where the *f* subscript denotes the components from the facings and the *c* subscript denotes the components from the core. This relationship can be expanded using the dimensions of the sandwich construction presented in Figure 6.2. The full expansion is presented in Equation 6.8.

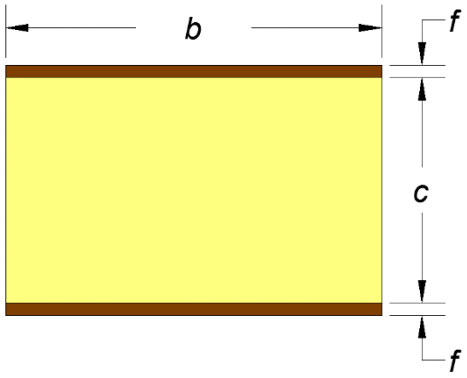

Figure 6.2: Dimensions of the Type 1 Core

$$EI = E_f \left(\frac{bf^3}{6} + \frac{bfd^2}{2}\right) + E_c \frac{bc^3}{12} \tag{6.8}$$

Where *d* is the sum of *c* and *f*, the moment arm between the centroids of the facings. From this expression, some terms can be eliminated because of their small magnitude. The first

term in parentheses is the contribution of the individual facings, and since it is proportional to f^3, it is essentially zero given that the average facing thickness for the Type 1 construction was 0.095 in. Then, the last term, which is the contribution of the core, can be eliminated because the stiffness of the core is several magnitudes smaller than the expected stiffness of the facing. This gives the following expression in Equation 6.9.

$$EI \approx \frac{E_f b f d^2}{2} \tag{6.9}$$

The shear stiffness of the Type 1 core can also be calculated based on the dimensions and material properties of the constituent materials. Typically, for this type of sandwich construction, it is assumed that the shear stresses are completely carried by the foam core. This is due to the small thicknesses of the facings; the first moment of the area of the facings is so small that when the true shear stress predicted by elasticity theory is integrated over the area, the contribution of the facings is found to be negligible. Also, the shear stiffness of the core is low enough that the true shear stress predicted by elasticity theory will vary very little over the depth of the core, and the shear correction factor can be considered to be nearly 1.0 for this type of core. Therefore, the shear stiffness becomes the expression in Equation 6.10.

$$kAG \approx G_c A_c = G_c bc \tag{6.10}$$

From these two expressions for the bending and shear stiffnesses, it is evident that they are both directly proportional to the width. Therefore, dividing these expressions by

the width will provide a per unit width quantity. These quantities are represented in Equation 6.11.

$$D = \frac{EI}{b}$$
$$U = \frac{kAG}{b} \tag{6.11}$$

Where *D* is the bending stiffness per unit width, and *U* is the shear stiffness per unit width. Given these new variables, the TBT solutions presented previously can be rewritten in the forms found in Equations 6.12 and 6.13.

$$w_{1,max} = \frac{P_1 L_1^3}{48 D b_1} + \frac{P_1 L_1}{4 U b_1} \tag{6.12}$$

$$w_{2,max} = \frac{23 P_2 L_2^3}{1296 D b_2} + \frac{P_2 L_2}{6 U b_2} \tag{6.13}$$

Where the subscripts designate which test setup to use for each of the parameters; "*1*" for the three point specimen and "*2*" for the four point specimen. The equations can then be further rearranged to extract *D* and *U* since they are independent of any geometrical expressions in the equations, so that the flexural test data can be used to solve for them as shown in Equations 6.14 and 6.15.

$$D^{-1}\left(\frac{L_1^2}{12}\right) + U^{-1} = \left(\frac{P}{w}\right)_1^{-1}\left(\frac{4 b_1}{L_1}\right) \tag{6.14}$$

$$D^{-1}\left(\frac{23L_2^2}{216}\right) + U^{-1} = \left(\frac{P}{w}\right)_2^{-1}\left(\frac{6b_2}{L_2}\right) \quad (6.15)$$

Where *(P/w)* can be idealized as the slope of the linear region of the load versus mid-span bottom face deflection curve. This is a system of equations that can be readily solved using matrix algebra and the recorded dimensions and load vs. deflection slopes for a three point specimen and a four point specimen. Given that there were four specimens for the three point tests and three specimens for the four point tests, twelve possible iterations could be used to solve the equations. The average, standard deviation, and coefficient of variation for each stiffness calculated using all twelve iterations is presented in Table 6.1. A more detailed summary of the stiffness calculations for each iteration of the Type 1 specimens is presented in Appendix E.

Table 6.1: Flexural Stiffness Results for Type 1

Flexural Stiffness	Average	Standard Deviation	Coefficient of Variation
Bending Stiffness per Unit Width, lb*in	397,600	51,180	12.9%
Shear Stiffness per Unit Width, lb/in	4,653	66	1.4%

The results must now be normalized to "standard" dimensions so a comparison can be made between the core types. The stiffness values need to be altered so that they are representative of a specimen with a gross cross-section of 2 in. by 3 in. that maintains the primary features of the geometry. The primary feature that needs to be maintained is the thickness of the facings. Therefore, the only dimensions that need to change are the depth

of the core and the width of the specimen for the Type 1 construction. This effects the bending stiffness by changing the width of the facings and the moment arm between the facings, and it effects the shear stiffness by change the width and height of the core material. In order make the changes, the bending stiffness per unit with needs to be multiplied by the new width, and then it needs to be multiplied the ratio of the normalized d^2 term to that measured in the specimens. As for the shear stiffness per unit width, it needs to be multiplied by the new width also, then multiplied by the ratio of the normalized core height to the measured core height. A table of the normalized dimensions and the measured dimensions along with the bending and shear correction factors described above is presented in Table 6.2.

Table 6.2: Dimensions and Stiffness Normalization Factors for Type 1

Dimensions	Normalized	Measured
Width, in	3.0	1.0*
Total Depth, in	2.000	2.133
Facing Thickness, in	0.095	0.095
Core Thickness, in	1.811	1.944
Facing Moment Arm, in	1.905	2.039
Normalization Factors		
Bending Stiffness Factor, in	2.621	
Shear Stiffness Factor, in	2.795	
**Note: This is an effective measurement because the stiffness quantities have already been divided by the measured width.*		

Using the correction factors, the total bending stiffness of the normalized cross-section becomes 1,042,000 lb*in^2, and the total shear stiffness of the normalized section is

13,000 lb. Also, the stiffness results can be used to find effective properties of the constituent materials. The bending stiffness can be used to estimate the effective modulus of elasticity of the facing material using Equation 6.9, and the shear stiffness can be used to find the effective modulus of rigidity of the core material using Equation 6.10. The effective modulus of elasticity of the facing was measured to be 2,024,000 psi and the effective modulus of rigidity of the core was measured to be 2,393 psi using the calculated stiffnesses.

6.1.1.2 Results for Type 2. The same concepts and equations used for Type 1 specimens can be applied to the Type 2 specimens to calculate the bending and shear stiffnesses per unit width. The core material has reinforcing webs that could contribute to the bending stiffness of the sandwich construction, but since they are very thin and have a modulus of elasticity that is less than that of the facings, their contribution is negligible. The only significant effect this assumption can have on the calculations is that it could contribute a small amount to the bending stiffness, and eventually lead to a slight over estimation in the effective modulus of elasticity of the facing. Since there were three specimens for the three point tests and three specimens for the four point tests, nine possible iterations could be used to solve Equations 6.14 and 6.15 for the Type 2 specimens. The average, standard deviation, and coefficient of variation for each stiffness calculated using all nine iterations is presented in Table 6.3. A more detailed summary of the stiffness calculations for each iteration of the Type 2 specimens is presented in Appendix E.

The same normalization technique can be used to normalize the results to a “standard” sized specimen with gross cross-sectional dimensions of 2 in. by 3 in. The main features that needed to be maintained were the thickness of the facings and the reinforcing

webs, and by using the same techniques as in the calculations for Type 1, these features are sufficiently preserved. A table of the normalized dimensions and the measured dimensions along with the bending and shear correction factors for the Type 2 sandwich construction is presented in Table 6.4.

Table 6.3: Flexural Stiffness Results for Type 2

Flexural Stiffness	Average	Standard Deviation	Coefficient of Variation
Bending Stiffness per Unit Width, lb*in	528,100	81,790	15.5%
Shear Stiffness per Unit Width, lb/in	20,360	1,304	6.4%

Table 6.4: Dimensions and Stiffness Normalization Factors for Type 2

Dimensions	Normalized	Measured
Width, in	3.0	1.0*
Total Depth, in	2.000	2.333
Facing Thickness, in	0.095	0.095
Core Thickness, in	1.811	2.143
Facing Moment Arm, in	1.905	2.238
Normalization Factors		
Bending Stiffness Factor, in	2.174	
Shear Stiffness Factor, in	2.534	
**Note: This is an effective measurement because the stiffness quantities have already been divided by the measured width.*		

Applying the correction factors, the total bending stiffness of the normalized Type 2 cross-section becomes 1,148,000 lb*in^2, and the total shear stiffness of the normalized

section is 51,590 lb. The stiffness results were then used to find effective properties of the constituent materials. The bending stiffness was used to estimate the effective modulus of elasticity of the facing material using Equation 6.9, and the shear stiffness was used to find the effective modulus of rigidity of the core material using Equation 6.10. The effective modulus of elasticity of the facing was measured to be 2,227,000 psi and the effective modulus of rigidity of the core was measured to be 9,497 psi using the calculated stiffnesses for the Type 2 specimens.

6.1.1.3 Results for Type 3. For the Type 3 specimens, several simplifying assumptions can be made about the behavior of the cross-section. In flexure, the fiber reinforced shear layers and facings will carry the entire load, and the contribution of the foam is negligible. Then, the expression for the bending stiffness becomes Equation 6.16.

$$EI = E_f I_f + E_s I_s \tag{6.16}$$

Where the subscript "*s*" represents the shear layers. The modulus of elasticity of the facings is expected to be the same magnitude as the modulus of elasticity of the shear layers, but since the orientation of the shear layers does not align with the longitudinal direction of the beam, the modulus of elasticity of the shear layers is likely smaller than that of the facings. However, given the variability involved in the construction of these laboratory specimens, combined with the fact that the dimensions of the shear layers cannot be directly measured, the gross properties are that can be considered. Therefore, the gross properties of the combination of facing layers and shear layers were used in the following calculations. With this simplification, Equation 5.16 becomes Equation 5.17.

$$EI = E_g I_g \tag{6.17}$$

Where I_g is the area moment of inertia of all the glass fiber reinforced polyurethane, and E_g is an effective modulus of elasticity of all the glass fiber reinforced polyurethane. As far as shear stiffness is concerned, the same concepts apply when considering the geometry of the Type 3 construction, and it is acceptable to consider the gross properties of the shear and facing layers combined. Therefore, the shear stiffness is represented by Equation 5.18.

$$kAG = k_g A_g G_g \tag{6.18}$$

Where again the terms representative of the shear and facing layers are combined as one gross material. When the geometry of the Type 3 cross-section is examined in detail, the expressions for the area moment of inertia and cross-sectional area are algebraically complicated, and a direct relationship to the width dimensions of the specimen is not possible. In fact, the width varies significantly throughout the cross-section because it is generally trapezoidal in shape, and an effective width of the glass reinforced polyurethane is difficult to define. Therefore, the equations must be used to solve for the total bending stiffness and shear stiffness, which will be represented by the variables in Equation 6.19.

$$\begin{aligned} D_t &= EI \\ U_t &= kAG \end{aligned} \tag{6.19}$$

Where D_t and U_t are the effective bending and shear stiffness for the total cross-section, respectively. Then, Equations 6.14 and 6.15 become Equations 6.20 and 6.21, respectively.

$$D_t{}^{-1}\left(\frac{L_1^2}{12}\right) + U_t{}^{-1} = \left(\frac{P}{w}\right)_1{}^{-1}\left(\frac{4}{L_1}\right) \tag{6.20}$$

$$D_t{}^{-1}\left(\frac{23L_2^2}{216}\right) + U_t{}^{-1} = \left(\frac{P}{w}\right)_2{}^{-1}\left(\frac{6}{L_2}\right) \tag{6.21}$$

If these equations are evaluated using flexural test results for the Type 3 specimens, there is only one iteration and, unfortunately, the solutions for the stiffnesses are illogical. The calculated bending stiffness is negative and the calculated shear stiffness is relatively small in magnitude. The expected result was high bending and shear stiffness based on the geometry of the specimens. This indicates that one or both of the flexural tests for the Type 3 specimens was misrepresentative of the sandwich construction. Based on the observations made during the tests, it is likely that the three point flexural test results were negatively affected by manufacturing defects present in the specimen before testing. These negative effects manifested as premature delamination between the shear layers, and a noticeable lack of stiffness in the specimen's load versus deflection response. The defects were caused by poor resin saturation, and consisted of dislocations between the fiber layers at the interfaces between individual fiber layers and also at the interface between the shear layers and the flexible foam. The defects likely effected the four point test results too, but the effects are far less apparent in the data recorded from the test. Therefore, an attempt to estimate the flexural stiffness using only the four point test result is presented in the following discussion.

In order to solve for any of the stiffness values, the theory must be reduced to one equation and one unknown. Since the magnitude of the shear stiffness of the Type 3 core (the FRP diagonals) is very large compared to that for Types 1 and 2, the shear deformations in the four point specimen are a relatively small percentage of the total deflection, and EBBT can be used to solve for the bending stiffness. Therefore, using Equation 6.4 and applying the bending stiffness definition previously described, the solution for the mid-span deflection in the four point tests becomes Equation 6.22.

$$w_{2,max} = \left(\frac{23P_2L_2^3}{1296D_t}\right) \tag{6.22}$$

From here, the total bending stiffness can be estimated by rearranging Equation 6.22 into Equation 6.23.

$$D_t = \left(\frac{P}{w}\right)_2 \left(\frac{23L_2^3}{1296}\right) \tag{6.23}$$

Using Equation 6.23 and the four point flexural test results, the total bending stiffness of the Type 3 construction was found to be 2,597,000 lb*in^2. Considering the short span to depth ratio (~10) used in the four point experiments, the bending stiffness found in Equation 6.23 will be a conservative estimate because the shear deformations were neglected. However, the deflections that can be predicted using Equation 5.25 and the bending stiffness found using the experimental results will still be sufficient in the linear region of the response. Unfortunately, a sufficient estimate of shear stiffness cannot be

found using the experimental data. A more detailed summary of the stiffness calculations for the Type 3 specimen is presented in Appendix E.

Now the cross-section needs to be normalized to maintain its key features, and fit the gross dimensions of the "standard" specimen, which measures 2 in. by 3 in. In order to accomplish this, the dimensions of the Type 3 cross-section were measured in detail, and a drawing of the specimen's cross-section was done in a CAD software program. From this, the area moment of the inertia of the glass reinforced polyurethane can be readily calculated. Then, the length and height dimensions of the cross-section were reduced without changing any of the facing and web thicknesses or the angular orientation of the webs in order to have a total height of 2 in. and a total cross-sectional area of 6 in^2, which now fits the "standard" specimen definition. From this standard section, the transformed area moment of inertia of the glass reinforced polyurethane was calculated. Then, to normalize the bending stiffness calculated earlier, the value was multiplied by the ratio of the transformed area moment of inertia to measured area moment of inertia of the glass reinforced polyurethane. The dimensions of the measured cross-section and the transformed cross-section are presented in Figures 6.3 and 6.4, respectively.

The area moment of inertia of the fiber reinforced polyurethane was 1.913 in^4 for the actual cross-section, and the normalized cross-section had an area moment of inertia of 1.174 in^4. Therefore, the normalization factor for the bending stiffness was calculated as the ratio of these two values, 0.614. This results in a normalized bending stiffness of 1,594,000 $lb*in^2$, and using Equation 6.19, the effective modulus of elasticity for all the fiber reinforced polyurethane layers combined is estimated to be 1,358,000 psi. Again, this estimation of the modulus of elasticity is conservative for several reasons. The contribution

of shear deformations was not considered in the theory used for the Type 3 specimens. Also, the shear layers were considered to have the same modulus of elasticity as the facing layers when in reality they likely have a slightly lower modulus of elasticity because the shear layers were not oriented in the same direction as the facing layers. Finally, there were several noticeable manufacturing defects in the Type 3 specimens in the form of dislocations between the fiber reinforced layers. All of these factors could lead to the effective modulus of elasticity being lower.

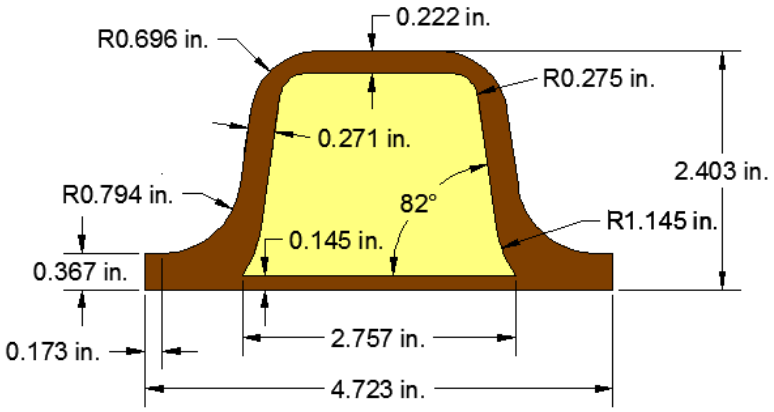

Figure 6.3: Measured Dimensions of the Actual Type 3 Cross-section

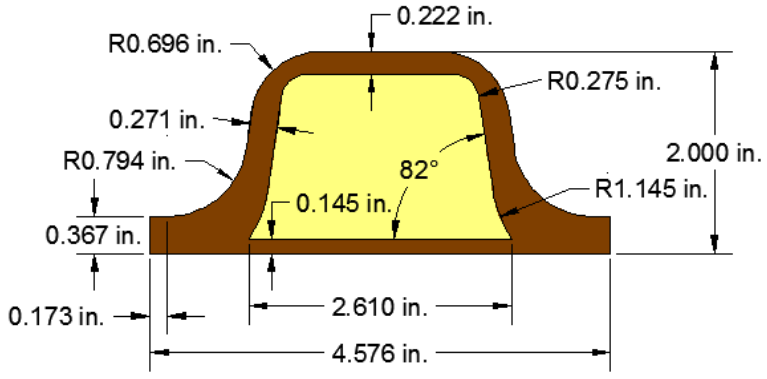

Figure 6.4: Normalized Dimensions of the Transformed Type 3 Cross-section

6.1.2. Discussion of the Results. The analysis of flexural stiffness clearly shows that the Type 3 construction has the highest flexural stiffness despite manufacturing defects due to poor resin saturation. The Type 2 construction had the second best performance, while the Type 1 construction performed the poorest with regard to flexural stiffness. This result is consistent with the geometric stiffness of each construction and the fact that the materials used in each construction were very similar, if not exactly the same in some cases. The Type 3 construction had the largest geometric stiffness, while the Type 2 construction had the second largest, and the Type 1 construction had the lowest geometric stiffness. Table 6.5 summarizes the results for each construction after normalizing each cross-section to a depth of 2 in. and a total cross-sectional area to 6 in^2.

Table 6.5: Summary of Estimated Flexural Stiffnesses for Each Normalized Sandwich Construction

Construction Type	Normalized Total Bending Stiffness ($lb*in^2$)	Normalized Total Shear Stiffness (lb)
1	1,042,000	13,000
2	1,148,000	51,590
3	1,594,000	-

From the stiffness analysis, the material properties for each sandwich construction were also measured. This includes the effective modulus of elasticity of the facing material and the effective shear modulus of the core for the Type 1 and 2 constructions. Also, the effective modulus of elasticity in bending of the Type 3 configuration was estimated, but standard bending theory was used and the facing was a combination of outer facing layers and shear layers. Both of these simplifications coupled with the manufacturing defects

present in the specimen lead to an under estimation of the modulus of elasticity of the facing layers alone, and this is reflected in the results presented in Table 6.6.

Table 6.6: Summary of Estimated Material Properties for Sandwich Construction

Construction Type	Effective Modulus of Elasticity of the Facing (psi)	Effective Shear Modulus of the Core (psi)
1	2,024,000	2,393
2	2,227,000	9,497
3	1,358,000	-

The facings of both Types 1 and 2 were essentially the same material, which is why the effective modulus of elasticity is nearly the same for each. Then, it can be seen from the numbers that the effective modulus of the elasticity for the Type 3 construction is noticeably less but of the same order of magnitude. Again, this is likely due to the simplifications and manufacturing defects discussed previously. However, the geometric stiffness of the Type 3 construction was much larger, which resulted in the largest bending stiffness. As for shear modulus, it can be seen that the Type 1 core is nearly one-fourth of the shear modulus calculated for the Type 2 core; which shows that the reinforcing webs can be more effective than an increase in foam density.

These results are important for evaluating serviceability limit states. All structural elements have deflection limits that are intend to ensure the element functions properly and does not cause discomfort to individuals using the structure. For bridge deck elements, the deflection limits are strict, and typically they are dictated as the span length of the element divided by eight hundred. If this limit state is applied using the normalized stiffness values

for each construction and the four point testing configuration with a 24 in. span, a load limit can be determined, and the results are shown in Table 6.7. For theses load limits, it is evident that the Type 3 construction has a much greater capacity when considering this serviceability limit state. Also, the load limits are quite small, especially when considering the potential strength capacity of these constructions.

Table 6.7: Summary of Load Limits Based on Serviceability for Each Normalized Sandwich Construction

Construction Type	Load Limit Based on Serviceability (lb)
1	55
2	103
3	195

6.2. ANALYSIS OF FLEXURAL STRENGTH

The flexural strength of a sandwich panel is dependent on many factors that are related to the stresses present in each component of the construction. These stresses are used to predict the limiting failure mode and ultimately the capacity of the sandwich construction, which is beneficial to design. Failure can occur in each of the different components with a variety of different mechanisms causing the failure. These mechanisms were discussed in general in Section 2 Section 2.2 and with respect to the specimens in these tests in Sections 5.2.2.1 to 5.2.2.3 of Section 5. The primary failure modes encountered in these tests were local indentation, delamination, shear failure of the core, intra-cellular dimpling, and compressive failure of the facing. Also, failure generally occurred in two phases. The first being initial failure characterized by nonlinearity in the

response and noticeable damage to the specimen, which caused a decrease in the rate of increase in the load but did not cause a loss in load carrying capacity. The second phase was ultimate failure that occurred during the nonlinear response, which was characterized by excessive damage to the specimen and a peak in the load after which the load decreased and never recovered. The ultimate failure load was very easy to define considering that it occurred at the peak load, but the initial failure was difficult to define. It occurred at the transition between linear and nonlinear response, which is difficult to quantify in a precise manor, particularly for complex composite construction such as that used for the sandwich panels. In order to estimate this initial failure load, an offset of the linear response region was used to intercept the data at a point near the transition. Figure 6.5 graphically depicts this methodology.

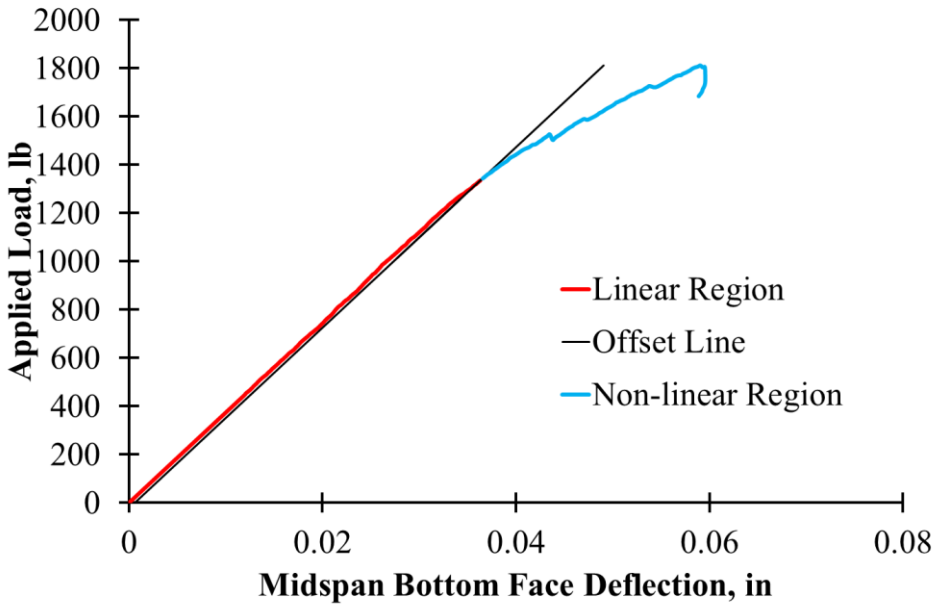

Figure 6.5: Estimation of Initial Failure Load Using the Offset Method for Specimen 2-1-S.

The offset was chosen to minimize the amount of nonlinear behavior before the offset line intercepted the corrected data curve, in effect limiting the overestimation of the initial failure load. The offset also had to be large enough that the noise in the data did not cause the offset to prematurely intercept the corrected data curve, which would cause an underestimation of the initial failure load. Therefore, a 0.01% offset was chosen as a percentage of the span length to meet these criteria. Once the offset was chosen and the initial failure loads were estimated, the global stresses and other useful quantities could be calculated using EBBT and TBT, as well as, other simple physical relationships. These theories are discussed in general in Section 2, but the specific solutions used to calculate these quantities will be presented in the following sections along with the results of an analysis using the experimental results of the flexural tests presented in Section 5. Then, at the end of Section 6.2 a discussion of the analysis results with be used to compare the three different types of sandwich constructions based on strength.

6.2.1. Results of the Analysis. Bending stresses are often the limiting factor for facing failure modes like intra-cellular dimpling and compressive failure of the facing. Shear stresses are the limiting factor for shear failure in the core, and they are related to peeling stresses that cause delamination failures. EBBT and TBT can be adapted to predict bending and shear stresses. The governing equations and details of EBBT and TBT are presented in Section 2 Section 2.2, but the specific solutions used in the analysis are presented below. Considering the specific loading case used in these experiments, Equation 2.5 for bending stress and Equation 2.6 for average shear stress can be solved using static equilibrium. The experimental case can be idealized as the same simply supported beam in

Figure 6.1 of the previous section. The solution for maximum bending stress becomes Equation 6.24 and the equation for maximum average shear stress becomes Equation 6.25.

$$\sigma = \pm \frac{Paz}{2I} \tag{6.24}$$

$$\tau_{avg} = \frac{P}{2A} \tag{6.25}$$

Where σ is the axial bending stress in the "*x*"-direction using the sign convention detailed in Section 2 Section 2.2, with negative signs indicating compressive stress and positive indicating tensile stress. Then, *P* is the total applied load, *a* is the distance from the support to the load, *z* is the distance from the neutral axis to the extreme fibers in the z-direction, *I* is the area moment of inertia about the y-axis, and *A* is the cross-sectional area in shear. From this solution, the stresses can be solved for the three point loading case ($a = L/2$) and the four point loading case ($a = L/3$). The solution for the three point case is present in Equations 6.26 and 6.27, and the solution for the four point case is presented in Equations 6.28 and 6.29.

$$\sigma = \pm \frac{P_1 L_1 z_1}{4I_1} \tag{6.26}$$

$$\tau_{avg} = \frac{P_1}{2A_1} \tag{6.27}$$

$$\sigma = \pm \frac{P_2 L_2 z_2}{6I_2} \tag{6.28}$$

$$\tau_{avg} = \frac{P_2}{2A_2} \tag{6.29}$$

In these solutions, "*1*" indicates the three point configuration ($a = L/2$) while "*2*" indicates the four point configuration ($a = L/3$). Now from these equations, the bending and shear stresses in the sandwich constructions can be calculated based on the dimensions and failure loads recorded for each test.

As for local indentation, there are several factors that effect this failure mode. These include the geometric and material stiffness of the facing and core as well as the strength of the core. Initially, local indentation is dependent on the strength of the core material and the out of plane compressive stress in the core. These out of plane stresses are proportional to the pressure imposed by point loads on the beam, and in design, the pressures are often limited to the compressive strength of the foam. However, in practice, this proves to be conservative in some cases and not conservative in other cases. Nonetheless, the pressure imposed by the point loads is a good indicator of failure due to local indentation. Then, once the initial failure begins, the facing loses stability, allowing bending stresses to wrinkle the facing at the load point, which causes a significant loss in load carrying capacity. The pressure imposed by the point load is estimated using Equation 6.30, since rectangular loading bars were used.

$$p_{pad} = \frac{P}{NA_{pad}} \tag{6.30}$$

Where p_{pad} is the average pressure imposed by the point load, P is the applied load, A_{pad} is contact area between the load point and the specimen, and N is the number of loading

points, N = 1 (3-Point) or N = 2 (4-Point). The following sections will show how these equations for stress and pressure were adapted to each of the sandwich constructions. These concepts will be presented separately for each sandwich construction, and finally a discussion and comparison between the constructions will be presented in Section 6.2.2, also the load at each failure point will be compared to the serviceability load discussed in Section 6.1.2.

6.2.1.1 Results for Type 1. In order to evaluate the stresses present in the Type 1 specimens, it is necessary to examine the sandwich panel construction in order to determine the appropriate values to insert in the equations derived previously. For the Type 1 sandwich construction, bending stresses are carried primarily by the facings, and using the dimensions previously presented in Figure 6.2, the effective moment of inertia can be defined by Equation 6.31.

$$I \approx \frac{bf^3}{6} + \frac{bfd^2}{2} \tag{6.31}$$

From this expression, the first term can be eliminated since it is proportional to f^3 and is essentially zero given that the average facing thickness for the Type 1 construction was 0.095 in. This results in the following expression (Equation 6.32).

$$I \approx \frac{bfd^2}{2} \tag{6.32}$$

Then, the z term needed to find the bending stresses is half the height of the cross-section. This allows Equations 6.26 and 6.28 for the 3-Point and 4-Point test configurations,

respectively, to be re-written as Equations 6.33 and 6.34 for the Type 1 sandwich construction.

$$\sigma = \pm \frac{P_1 L_1 h_1}{4 b_1 f_1 d_1^2} \tag{6.33}$$

$$\sigma = \pm \frac{P_2 L_2 h_2}{6 b_2 f_2 d_2^2} \tag{6.34}$$

Where *h* is the height of the cross-section, and for simplification the magnitude of the stress will be the only thing considered since the bending stresses in the facings will be equal in magnitude and opposite in direction.

Next, the shear stress can be calculated based on the dimensions of the Type 1 core. Typically, for this type of sandwich construction, it is assumed that the shear stresses are completely carried by the foam core. This assumption is due to the small thicknesses of the facings; the first moment of the area of the facings is so small that when the true shear stress predicted by elasticity theory is integrated over the area, the contribution of the facings is found to be negligible. Also, the shear stiffness of the core is low enough that the true shear stress predicted by elasticity theory will vary very little over the depth of the core, causing the average shear stress to be nearly equal to the true shear stress in the core. Therefore, the area of the core can be used in the shear stress Equations 6.27 and 6.29 for the 3-Point and 4-Point test configurations, respectively, resulting in Equations 5.38 and 5.39.

$$\tau_{avg} = \frac{P_1}{2 b_1 c_1} \tag{6.35}$$

$$\tau_{avg} = \frac{P_2}{2b_2c_2} \tag{6.36}$$

The A_{pad} term is simply the width to the loading pad multiplied by the width of the specimen. All of the stress concepts presented previously can now be applied to the initial failure loads of the Type 1. These concepts can also be applied to the ultimate failure load. However, due to localized damage and changes in the cross-sectional geometry that result in the nonlinear portion of the response, the stresses calculated by these equations become much less accurate representation at the ultimate failure conditions. Nevertheless, these stress terms are still valuable tools when comparing the different core types. The values calculated for these quantities at initial are presented in Table 6.8.

Table 6.8: Summary of Failure Analysis for Type 1

	Specimen	Failure Mode	Applied Load (lb)	Avg. Pressure Under the Load (psi)	Max. Bending Stress in the Facings (psi)	Max. Avg. Shear Stress in the Core (psi)
Initial Failure	1-1-S	5	589	198	1611	51
	1-2-S	5	627	210	1713	54
	1-3-S	5	714	237	1931	61
	1-4-S	5	601	199	1621	51
	1-1-L	5	794	67	4392	52
	1-2-L	5	823	72	4718	56
	1-3-L	5	984	75	5524	58
Ultimate Failure	1-1-S	5	1078	362	2948	93
	1-2-S	5	1092	367	2985	94
	1-3-S	6	1257	417	3397	107
	1-4-S	5	1215	403	3278	104
	1-1-L	6	1566	133	8668	103
	1-2-L	5	1539	136	8827	105
	1-3-L	5	1613	123	9054	95
Failure Modes: (1) Compression Failure of the Facing, (2) Tension Failure in the Facing, (3) Localized Buckling/Wrinkling, (4) Intra-cellular Dimpling, (5) Local Indentation, (6) Shear Failure in the Core, and (7) Delamination.						

All of the Type 1 specimens initial failed due to local indentation, and all but two of the specimens (1-3-S and 1-1-L) ultimately failed due to excessive local indentation. In these cases the critical factor is the pressure under the concentrated load. The average pressure under the load point varied considerably from the 3-Point test results to the 4-Point results for both the initial and ultimate failure points. For the 3-Point specimens, failure occurred in a range of average pressure under the load of 198-237 psi at initial failure and 362-403 psi at ultimate failure. For the 4-Point specimens, this occurred in a range of average pressure under the load of 67-75 psi at initial failure and 123-136 psi at ultimate failure. It is clear that the 3-Point specimens failed at significantly higher pressures than the 4-Point specimens. This result is most likely do to the nature of the test setup. The 3-Point setup promotes a symmetrical distribution of pressure beneath the point load, while in the 4-Point setup, an unsymmetrical distribution of pressure beneath the point loads occurs, which could lead to much higher stresses on the outer edges of the loading bars. The loading bars were fabricated to rotate freely during the test in an effort to minimize the effects of this localized stress concentration, but it is not certain that this allowed the pressure to distribute as evenly as expected. Also, the bending stresses in the facings were much larger in the 4-point specimens, which could have contributed to premature local indentation due to stress interaction. It is also interesting to note that when these pressures are compared to the flatwise compression strength values found in Section 4 there is no immediate correlation. If flatwise compressive strength was used to estimate local indentation failure it would be conservative for the 3-Point specimens and an overestimation for the 4-Point specimens.

Two of the specimens, 1-3-S and 1-1-L, had an ultimate failure other than excessive local indentation. These two specimens failed ultimately due to shear fractures in the core. This occurred at average shear stresses of 107 psi and 103 psi for Specimens 1-3-S and 1-1-L, respectively, which is inconsistent with Specimens 1-4-S and 1-2-L, which had average shear stresses of 104 psi and 105 at ultimate failure, respectively, but did not fail due to shear fracture. It is also noteworthy to consider that the average pressure under the load at ultimate failure, when compared to that of the other specimens, was of sufficient magnitude to cause local indentation failure for Specimens 1-3-S and 1-1-L. These inconsistencies are likely due to variations in the thickness of the facing and variations in the material properties of the constituent materials in the Type 1 construction, which are a result of their heterogeneous nature at smaller size scales. Also, at ultimate failure, the core of each specimen had undergone significant damage, which causes inaccuracies in the calculations. In order to better understand the failure mechanisms, more detailed analysis is required; however, higher order and finite element analyses are beyond the scope of this work.

6.2.1.2 Results for Type 2. The same concepts and equations used for the Type 1 specimens can be applied to the Type 2 specimens to calculate the bending and shear stresses as well as the pressures under the load points. The core material has reinforcing webs that could contribute to the bending stiffness of the sandwich construction, but since they are very thin and have a modulus of elasticity that is less than that of the facings, their contribution can be neglected. The only significant effect this assumption may have on the calculations is that it could contribute a small amount to the bending stress, and eventually lead to a slight over estimation in the strength of the facing. These reinforcing webs also

carry the majority of the shear stress, however it is more representative as a comparison tool to consider the average shear stress using the entire area of the core. Tables 6.9 summarizes the failure analysis for each Type 2 specimen.

From these results, it is evident that the initial and ultimate failure mode for all of the Type 2 specimens in the 3-Point test was local indentation. This occurred in a range of average pressure under the load of 336-450 psi at initial failure and 387-606 psi at ultimate failure. From this it is evident that if the flatwise compressive strength estimated in Section 4 was used to predict local indentation failure in these specimens it would have been very conservative. The 4-Point specimens did not fail due to local indentation, but it is evident that the same would hold true for these specimens also.

Table 6.9: Summary of Failure Analysis for Type 2

	Specimen	Failure Mode	Applied Load (lb)	Avg. Pressure Under the Load (psi)	Max. Bending Stress in the Facings (psi)	Max. Avg. Shear Stress in the Core (psi)
Initial Failure	2-1-S	5	1344	450	3316	105
	2-2-S	5	1015	336	2479	78
	2-3-S	5	1150	387	2853	90
	2-1-L	4	2299	176	10405	123
	2-2-L	4	1713	153	9047	107
	2-3-L	4	1666	127	7494	89
Ultimate Failure	2-1-S	5	1812	606	4471	141
	2-2-S	5	1267	420	3095	98
	2-3-S	5	1150	387	2853	90
	2-1-L	1	3712	285	16802	199
	2-2-L	6	2267	203	11972	142
	2-3-L	6	2269	173	10209	121
Failure Modes: (1) Compression Failure of the Facing, (2) Tension Failure in the Facing, (3) Localized Buckling/Wrinkling, (4) Intra-cellular Dimpling, (5) Local Indentation, (6) Shear Failure in the Core, and (7) Delamination.						

The 4-point tests all initially failed due to intra-cellular dimpling, which is caused by stability issues in the top facing of the sandwich panel. The bending stress at which this occurred varied significantly between specimens (7,500-10,400 psi) due to the variation in the distribution of reinforcing webs in the core. It was noted during the tests that for Specimens 2-2-L and 2-3-L, the dimple wave occurred at the free edges of the cells in the top facing because the specimens were cut with two longitudinal rows of webs that were centralized in the width of the specimens, which led to no support from the webs at the edges of the top facing. Specimen 2-1-L had three longitudinal rows of webs, two of which supported the edges of the top facing, and this led to a significant difference in the behavior of this specimen. The inter-cellular dimpling occurred in the interior cells, as a result, the nonlinear response in this specimen was less pronounced, and compression failure in the facing was the ultimate failure mode in Specimen 2-1-L. The bending stress at this point (16,800 psi) is an estimate of the ultimate compressive strength of the facing material, but it should be noted that the intra-cellular dimpling causes a nonlinear distribution of bending stress throughout the width of the top facing, which leads to this value serving as a conservative estimate.

As for the other two specimens, 2-2-L and 2-3-L, the ultimate failure mode was shear failure in the core material, and the average shear stress at these points (142 and 121 psi) is an estimate of the shear strength of the Type 2 core. However, due to the large variation in the distribution of longitudinal webs, this is a conservative estimate because 2-3-L had the same number of longitudinal webs as 2-2-L, but the cross-sectional area was larger, which resulted in a lower average shear stress. Also, 2-1-L withstood a greater amount of shear stress at failure (199 psi) because it had three longitudinal rows of webs,

compared to two rows for Specimens 2-2-L and 2-3-L. This indicates that the average shear stresses in Specimens 2-2-L and 2-3-L are near the lower bound of the true range of shear strength displayed by the Type 2 core.

6.2.1.3 Results for Type 3. Several simplifying assumptions can be made about the behavior of the Type 3 sandwich construction. In flexure about the major axis, the fiber reinforced shear layers and facings will carry the entire load, and the contribution of the foam is negligible. The expressions for the bending stress described in Equations 6.26 and 6.28 then become Equations 5.40 and 5.41.

$$\sigma = \pm \frac{P_1 L_1 z_1}{4 I_{frp}} \tag{6.37}$$

$$\sigma = \pm \frac{P_2 L_2 z_2}{6 I_{frp}} \tag{6.38}$$

Where I_{frp} is the area moment of inertia of the FRP layers and z is measured from the centroidal axis of the FRP layers both of which were calculated using the CAD drawing of the cross-section found in Figure 6.3. These are the same for both the 3-Point and 4-Point specimens. It should be noted the FRP facing layers and shear layers consist of two different glass fiber types and orientations, which means that the any strength values calculated using this equation are effective properties that are conservative when compared the properties of the facing layers alone.

As for the shear stress, it will also be carried entirely by the FRP, but to compare the Type 3 construction to the other two constructions, the shear stress will be averaged across the entire cross-section to calculate the average shear stress in a manner that is more

representative of the one used for the previous two types. This is a very conservative representation of the true shear stresses in the material, but it is a more representative comparison tool, especially considering that similar behavior occurs in the core of the Type 2 sandwich construction. Therefore, in the calculations, Equations 6.27 and 6.29 will be used with the area of the entire cross-section as the shear area.

The calculation for the pressure under the load for the Type 3 construction uses Equation 6.30 were A_{pad} is equal to the width of the loading pad multiplied by the width of the specimen in contact with the load pad, which was determined using the measurements taken of the cross-section taken prior to the tests shown in Figure 6.3. Tables 6.10 summarizes the failure analysis for each Type 3 specimen.

Table 6.10: Summary of Failure Analysis for Type 3

	Specimen	Failure Mode	Applied Load (lb)	Avg. Pressure Under the Load (psi)	Max. Bending Stress in the Facings (psi)	Max. Avg. Shear Stress in the Core (psi)
Initial Failure	3-1-S	7	3479	2885	4084	239
	3-1-L	1	3097	856	9693	212
Ultimate Failure	3-1-S	5	5895	4888	6920	404
	3-1-L	1	4288	1185	13423	294
	Failure Modes: (1) Compression Failure of the Facing, (2) Tension Failure in the Facing, (3) Localized Buckling/Wrinkling, (4) Intra-cellular Dimpling, (5) Local Indentation, (6) Shear Failure in the Core, and (7) Delamination.					

These results indicate the areas of concern for the Type 3 construction. The 3-Point specimen failed initially due to delamination that occurred between the shear layers, and it

ultimately failed due to excessive local indentation. The initial delamination failure was due to dislocations between the shear layers that formed due to poor resin saturation during manufacturing, which severely limited performance of the specimen. However, despite this defect, the effects on strength were fairly small when compared to the effects on stiffness previously discussed. Unfortunately, the 3-Point results do not really allow for accurate estimations of material strength due to the manufacturing defect, but the results do provide some general indications that can be used in comparison to the other two types. The 4-Point specimen failed both initially and ultimately due to compressive failure in the top facing, which allows for a good estimate of the effective compressive strength (9,700 psi at initial failure and 13,400 psi at ultimate failure) of the FRP materials. However, to reiterate, the poor resin saturation likely had a negative effect on the capacity of the specimen. In addition, incorporation of the shear layers into the calculations will lead to a strength in the facing that is expected to be less than the strength of the facings measured in the other two construction types.

6.2.2. Discussion of the Results. The three core types can be compared based on these results. For the Type 1 construction, the primary failure mode was local indentation, which occurred in all of the specimens as the initial failure mode and was the ultimate failure mode for 5 of the 7 specimens (71%). Table 6.11 summarizes the average pressures under the load that caused failure.

From this, the pressure under the load that caused local indentation failure can be analyzed, and it is evident that the beam configuration had a significant effect on the pressure at failure, both the initial and ultimate failure mode. The remaining two specimens failed ultimately due to shear fracture in the core. The ultimate shear strength of the Type

1 core can be estimated based on the average shear stress in the two specimens that ultimately failed due to shear fracture. The estimated average shear strength is 105 psi, which is a conservative estimate considering the circumstances of the tests discussed previously in Section 6.2.1.1. It is also worth noting that, when comparing the results there were several inconsistency which are also discussed in Section 6.2.1.1.

Table 6.11: Summary of Local Indentation Failure Results for Type 1

Test Specimens	Average Pressure Under the Load Point (psi)	
	Initial Failure	Ultimate Failure
3-Point	211	377
4-Point	72	129

As for the Type 2 specimens, local indentation occurred only in the 3-Point specimens at an average pressure under the load of 391 psi at initial failure and 471 psi at ultimate failure. The 4-Point specimens for the Type 2 construction failed initially due to intra-cellular dimpling, which occurred in the top facing at different bending stresses (7,500-10,400 psi) due to the different configurations of reinforcing webs. Then, the specimens failed ultimately due to compressive failure in the facing (one specimen) or shear failure in the core (two specimens). The estimated ultimate compressive strength of the facing was 16,800 psi and the estimated ultimate shear strength of the core was 132 psi, but both of these estimates are conservative for the reasons discussed previously in Section 6.2.1.2.

The Type 3 specimens had a variety of failure modes occur in the flexural tests. For the 3-Point specimen, initially failure occurred due to delamination between the shear layers at an average shear stress of 239 psi. Then, ultimate failure occurred due to excessive local indentation at a pressure under the load of 4,890 psi. As for the 4-Point specimen, both initial and ultimate failure were cause by compression failure in the top facing at an initial bending stress of 9,690 psi and an ultimate bending stress of 13,400 psi. As with the other two sandwich construction types, theses quantities are conservative estimates for reasons discussed previously in Section 6.2.1.3.

From these results, it is apparent that the Type 1 construction performed the lowest. The facing strength is comparable to the other two types, because the facing material is the same for each construction. However, the effectiveness of the facings is directly influenced by the ability of the core to utilize the full capacity of the facing material. In comparison to the other two construction types, the lower stiffness of the Type 1 core reduced the effectiveness of the facings to support the load. The core material was relatively weak compared to Types 2 and 3, which led to reductions in capacity caused by local indentation and shear failure in the core. This is validated by the fact that the Type 1 specimens supported the lowest pressures under the load point, and they also failed in shear at the lowest estimated shear strength.

The Type 2 core was second best in terms of strength performance. With regard to the strength of the facings, the Type 2 had the second best utilization of flexural modulus through the use of reinforcing webs in a flexible foam, which improved the effective moment of inertia while remaining very light in weight. Unfortunately, this construction also had stability issues in the facing that limited the capacity due to intra-cellular dimpling.

The Type 2 construction was also second highest in terms of the ability of the core material to withstand pressures under the concentrated load. Finally, the estimated shear strength for the Type 2 construction was also significantly greater than that for the Type 1 core but not as large as the shear stresses withstood by the Type 3 core.

The Type 3 core had the best performance with regard to strength. The addition of the diagonal shear layers between the flexible foam blocks proved to be the most effective utilization of the cross section by utilizing the full capacity of the facings in the 4-Point specimen. However, this modification also significantly increased the weight and complexity, which lead to several manufacturing issues that limited the quantity and performance of small scale specimens. Despite the small number of specimens and the poor performance of the 3-Point specimen, the Type 3 core displayed the highest potential material strength by withstanding far greater pressures under the loading point than the other two cores, as well as withstanding the largest calculated average shear stresses.

6.3. COMPARSION OF STIFFNESS AND STRENGTH LIMIT STATES

These results can also provide insight into which limit state governs the failure of these sandwich constructions. For bridge deck elements, there are serviceability limit states, related to the deflection of the element and its flexural stiffness; and there are strength limit states discussed in the previous sections. The serviceability or deflection limit state, previously discussed in Section 6.1.2, of span length divided by eight hundred, can be imposed on our small scale specimens by using the slope of the load vs. bottom face deflection plot to find the load that causes the limiting deflection in the bottom facing. Then, this serviceability load can be compared to the load at initial and ultimate failure.

Table 6.12 summarizes the comparison of the strength limit states to the serviceability limit state.

This comparison of the strength limits to the serviceability limits shows definitively that serviceability was the controlling limit state for all of the flexural specimens in these experiments. This result indicates that the design of these panels will likely always be controlled by flexural stiffness and serviceability rather than strength. This result is also expected, considering that the fiber reinforced polymer panels that were explored in previous research were almost always controlled by serviceability in experiments and design.

Table 6.12: Comparison of Strength Load Limits to Serviceability Load Limits

Specimen	Initial Failure Load	Ultimate Failure Load	Serviceability Load	Ratio of Initial Failure to Serviceability	Ratio of Ultimate Failure to Serviceability
	lb	lb	lb		
1-1-S	589	1078	68	8.70	15.9
1-2-S	627	1092	67	9.41	16.4
1-3-S	714	1257	67	10.7	18.9
1-4-S	601	1215	69	8.70	17.6
1-1-L	794	1566	83	9.53	18.8
1-2-L	823	1539	79	10.5	19.6
1-3-L	984	1613	82	12.1	19.8
2-1-S	1344	1812	280	4.79	6.46
2-2-S	1015	1267	280	3.62	4.52
2-3-S	1150	1150	246	4.68	4.68
2-1-L	2299	3712	200	11.5	18.6
2-2-L	1713	2267	186	9.23	12.2
2-3-L	1666	2269	171	9.73	13.3
3-1-S	3479	5895	160	21.7	36.7
3-1-L	3097	4288	318	9.75	13.5

7. FINDINGS, CONCLUSIONS, AND RECOMMENDATIONS

The small scale tests performed in this research have provided several insights into the behavior of the three different core alternatives and their respective sandwich constructions. In this section, the findings of this research will be presented in the first section. Then, the conclusions deduced from these findings will be discussed in the second section. Finally, these conclusions and practical considerations will be used to establish the advantages and disadvantages of each core alternative, and the alternative that is most fit for developing a prototype panel will be recommended.

7.1. FINDINGS

The major findings of this research will be discussed briefly in this section. The discussion will begin with the flatwise testing, followed by the flexural testing, and then conclude with the stiffness and strength analysis.

7.1.1. Flatwise Testing. The flatwise tests consisted of two types of testing, flatwise compression testing and flatwise tension testing. These tests were performed on specimens for the Type 1 and 2 sandwich constructions, between two and four for each test. Unfortunately, representative specimens could not be manufactured for the Type 3 construction. The findings for these tests will be presented separately in the following sections.

7.1.1.1 Flatwise compression testing. All of the specimens displayed initially linear elastic stress versus strain response, which was used to measure the flatwise compressive modulus. The Type 1 specimens failed due to crushing of the foam core and displayed nonlinear stress versus strain response prior to failure that is typical of

compressible foams. From this behavior, the useable flatwise compressive strength was measured. The Type 2 specimens failed due to crushing of the foam and displayed nonlinear stress versus strain response prior to failure that was governed by the stability of the web reinforcement. From this behavior, the useable flatwise compressive strength was measured. The flatwise compressive modulus and flatwise compressive strength were both larger for the Type 2 specimens compared to the Type 1 specimens, and the Type 2 results had noticeably more variability than the Type 1 specimens.

7.1.1.2 Flatwise tension testing. All of the specimens displayed initially linear elastic stress versus strain response, which was used to measure the flatwise tensile modulus. The Type 1 specimens failed as a result of fracture in the foam and displayed no nonlinear stress versus strain response before failure. Failure resulted in a complete loss of load carrying capacity, therefore the peak stress was considered the flatwise tensile strength. The Type 2 specimens failed primarily from a fracture at the interface between the core and the facings (2 of 3 specimens). The remaining specimen failed in the core material. All three specimens displayed nonlinear stress versus strain response before initial failure. The source of this nonlinearity is uncertain. However, the nonlinear response after initial failure was a result of asynchronous failures of the web reinforcement. The first peak in the stress was considered the flatwise tensile strength. The flatwise tensile modulus and flatwise tensile strength were both larger for the Type 2 specimens compared to the Type 1 specimens, and the Type 2 results had noticeably more variability than the Type 1 specimens.

7.1.2. Flexural Testing. The flexural tests consisted of two types of testing, three point and four point flexural testing. These tests were performed on specimens for all three

core types. There were between three and four specimens per test for the Type 1 and 2 constructions. However, manufacturing difficulties limited the number of Type 3 specimens to one specimen per test. The findings for these tests will be presented separately in the following sections.

7.1.2.1 Three point flexural testing. The load response was initially linear elastic for all three sandwich constructions. The Type 1 specimens failed initially due to local indentation, which caused nonlinear response and was a result of the low compressive strength and stiffness of the core material. Excessive local indentation eventually caused ultimate failure at the peak load capacity in the majority of the specimens (3 of 4 specimens). The remaining specimen experienced shear failure in the core at the peak load capacity. The Type 2 specimens failed initially and ultimately due to local indentation. Initial failure was caused by buckling of the web reinforcement under the load point and resulted in nonlinear response. Ultimate failure was caused by excessive buckling and crushing of the web reinforcement under the load point and resulted in the peak load capacity. The Type 3 specimen failed initially due to delamination between the shear layers of the core. This caused a spike in the load, but afterwards the load continued to climb at nearly the same rate as before the delamination with little noticeable nonlinearity. Eventually, a wrinkle formed under the point load and the shear layers under the point load began to deform and fracture. Designated as local indentation, it caused a jagged nonlinear response which eventually caused a peak in the load capacity. There were noticeable dislocations and manufacturing flaws in the Type 3 specimen caused by poor resin saturation. It was noted that the delamination was likely caused by these dislocations

between the shear layers, and the slope of the load versus bottom face deflection curve was significantly lower than expected because of these dislocations.

7.1.2.2 Four point flexural testing. The load response was initially linear elastic for all three sandwich constructions. The Type 1 specimens failed initially due to local indentation, which caused nonlinear response and was a result of the low compressive strength and stiffness of the core material. Excessive local indentation eventually caused ultimate failure at the peak load capacity in the majority of the specimens (2 of 3 specimens). The remaining specimen experienced shear failure in the core at the peak load capacity. The Type 2 specimens failed initially due to intra-cellular dimpling of the top facing between the loading points which resulted in nonlinear response. Then, one of the specimens experienced compression failure in the top facing while the remaining two specimens experienced shear failure in the core at the peak load. The Type 3 specimen experienced compression failure in the top facing at initial failure which caused a nonlinear response. Crushing of the fiber reinforced layers progressed through the top facing until a hinge mechanism formed at the peak load. There were again noticeable dislocations and manufacturing flaws in the Type 3 specimen caused by poor resin saturation, but the effects of these dislocations was less noticeable in the four point specimen, however, it is still certain that they negatively affected the performance of the four point specimen.

7.1.3. Analysis of Flexural Stiffness and Strength. Classical Euler-Bernoulli Beam Theory (EBBT) and Timoshenko Beam Theory (TBT) were used to analyze the results of the three and four point flexural tests. The goal of this analysis was to normalize the results of the flexural tests and to provide a comparison of the three different core alternatives based on the flexural stiffness and strength of their respective sandwich

constructions. TBT was used to estimate the bending and shear stiffness of the Type 1 and 2 constructions, while EBBT was used to estimate the bending stiffness of the Type 3 construction due to the poor results of the three point specimen. The flexural stiffness terms were then used to estimate the effective material properties for each of the constituent materials, and the standard serviceability limit state for bridge deck elements was evaluated. As for the strength analysis, three different strength terms were considered in the analysis of flexural strength. The bending stress was calculated at the extreme fibers using the classical equations for bending stress, the average shear stress over the cross-section was calculated, and the average pressure under the load point was calculated. Finally, the serviceability limit state for bridge deck elements was applied to the small scale specimens and the limiting load was compared to the initial and ultimate failure modes. The findings of this analysis will be presented in the following sections.

7.1.3.1 Analysis of flexural stiffness. The Type 3 construction had the largest calculated bending stiffness, followed by the Type 2 construction, while the Type 1 construction had the lowest. These results coincided with the geometric stiffness of the FRP layers. The shear stiffness of the Type 2 construction was significantly larger than the Type 1 construction. The shear stiffness of the Type 3 construction could not be estimated. It was also noted that the Type 2 specimens had a larger variation in the results than the Type 1 specimens, while the variability of the Type 3 specimens could not be established because of the small number of specimens. The estimated modulus of elasticity of the FRP layers was of the same magnitude for all three constructions. However, the Type 3 modulus of elasticity was significantly lower than the other two constructions. This was a result of the conservative nature of the calculations and the manufacturing defects in the specimen.

The estimated modulus of rigidity of the core material was larger for the Type 2 core than the Type 1 core. The effective modulus of rigidity could not be calculated for the Type 3 construction. Then, evaluation of the standard serviceability limit state for bridge deck elements showed that when considering the normalized cross-section, the Type 3 construction had the largest capacity while the Type 1 construction had the lowest capacity.

7.1.3.2 Analysis of flexural strength. The bending stresses in all three constructions were relatively comparable. The Type 1 specimens did not develop enough bending stress to cause failure in the facings due to premature failure of the core. However, one Type 2 four point specimen did develop enough bending stress to cause compression failure in the top facing. It should be noted though that this failure was influenced significantly by intra-cellular dimpling, which causes higher stress concentrations in unbuckled regions of the facing. The Type 3 four point specimen also failed due to compressive bending stress in the facing, but there were likely stress concentrations caused by dislocations between the fiber layers that cause premature failure. The average shear stresses in the core provided an indication of the shear strength of each core material. The Type 1 specimens the lowest estimated shear strength, the Type 2 specimens had a larger estimated shear strength, but the Type 3 specimens supported the largest average shear stresses. Next, the average pressure under the load provided an indication of the sandwich construction's ability to resist local indentation failure. The Type 1 specimens supported the lowest pressures under the load, the Type 2 specimens supported larger pressures, and the Type 3 specimens supported the largest pressures under the load. Finally, there were several inconsistencies in the strength analysis that made it evident that more sophisticated

models are needed to better predict failure, however these inconsistencies did not detract from the general findings of the analysis.

7.1.3.3 Comparison of stiffness and strength limit states. The serviceability limit state for bridge deck elements was applied to each small scale specimen using the slope of the load versus bottom face deflection response. Then, this serviceability load was compared to the initial and ultimate failure loads. The serviceability limit state controlled for every flexural test specimen.

7.2. CONCLUSIONS

The conclusions of this research will be discussed in this section. The conclusions of the flatwise testing, flexural testing, and stiffness and strength analysis will each be discussed separately.

7.2.1. Flatwise Testing. The flatwise testing results indicated that the Type 1 and 2 constructions were susceptible to certain types of failure in the core material. Their low flatwise compressive modulus and strength indicated that local indentation failure is a concern for beams with these core types. Also, their low flatwise tensile modulus and strength indicated that failures causing fractures in the core material or at the facing/core interface due to shearing or peeling stresses are a concern for beams with these core types. Since the Type 2 specimens performed better than the Type 1 specimens in these tests, it stands to reason that beams with the Type 2 core could resist these types of failures better than beams with the Type 1 core. Also, the higher variation of the Type 2 specimens can be attributed to inconsistencies in the distribution of the web reinforcement. These concerns are also valid for the Type 3 core, but no representative specimens could be manufactured for the Type 3 core.

7.2.2. Flexural Testing. The flexural tests confirmed the concerns that were raised by the flatwise tests. The behavior and failure of nearly all the specimens was governed by the strength and stiffness of the core material, which is validated by the prominence of core related failure modes. The failure modes observed in these tests included local indentation, shear failure in the core, intra-cellular dimpling, delamination, and compression failure of the top facing. All of the three point specimens failed due to inadequacy of the core material (local indentation, shear failure in the core, and/or delamination). As for the four point specimens, only two of seven developed sufficient bending stress to cause failure in the facing material, and these failures where influenced by intra-cellular dimpling in the Type 2 specimen and dislocations between the fiber reinforced layers in the Type 3 specimen. The remaining specimens failed due to local indentation, intra-cellular dimpling, and/or shear failure in the core material, which are all related to the strength or stiffness of the core material.

7.2.3. Analysis of Flexural Stiffness and Strength. The stiffness and strength analysis showed that despite the manufacturing flaws caused by poor resin saturation, the Type 3 construction had superior flexural stiffness, resistance to local indentation, and shear strength. The Type 2 construction had the second best performance considering these criteria, and the Type 1 construction had the worst performance. It is also evident from the results that the serviceability limit state will likely govern the design of these types of panels rather than the strength limit states. Finally, classical or first order analysis was adequate for drawing general comparisons between the core alternatives, however, it is evident that this type of analysis cannot adequately describe the complex behavior under the concentrated loads.

7.3. RECOMMENDATIONS

There are several advantages and disadvantages of each sandwich construction, and these will be discussed in this section, with the most adequate sandwich construction recommended for the prototyping process. The Type 1 construction has several advantages. The simple configuration is relatively easy to manufacture, promotes low bulk density, promotes lower resin volumes, and promotes consistent structural behavior. However, it evident from the small scale tests that the rigid polyurethane core material is very weak and flexible, which promotes low flexural stiffness and high deflections, as well as premature failure of the core material resulting in inefficient utilization of the facings. In context, this means bridge deck panels using this configuration and these materials will require relatively thick and inefficient facings and a core depth that is very large and impractical.

The Type 2 construction also has several advantages and disadvantages. The configuration is still relatively simple and easy to manufacture. The web reinforcement increases bulk density, but this is counteracted by the lower density foam, and for the small scale specimens, this resulted in a bulk density that was the same as the Type 1 specimens. The web reinforcement does require more resin, and the distribution of the web reinforcement promotes higher variations in the structural behavior. On the other hand, the small scale tests showed the web reinforcement significantly improved the strength and stiffness of the sandwich construction. This resulted in higher flexural stiffness and lower deflections, and the effects of premature failure in the core material were improved, resulting in great efficiency of the facings. Bridge decking utilizing this sandwich construction type would be more practical than using the Type 1 construction, however,

the panels would still require relatively thicker facings, thicker web reinforcement, and a relatively large core depth.

There are also several advantages and disadvantages for Type 3 construction. The configuration is relatively complex and proved to be more difficult to manufacture. This was evident in the manufacturing defects of the small scale Type 3 specimens. The polyurethane infused shear layers significantly increased the bulk density, required much more resin, and the configuration of the shear layers significantly effects the structural behavior. Nevertheless, the small scale tests showed the shear layers significantly improved the strength and stiffness of the sandwich construction. This resulted in the highest flexural stiffness and lowest deflections, and the effects of premature failure in the core material were improved even further despite manufacturing defects that negatively affected the performance. Considering that the manufacturing process can be improved, this construction type is likely the most practical for implementation in bridge decking. Meeting the serviceability requirements of bridge decking will require a larger cross-section, but it will be achievable with reasonable facing and shear layer thicknesses, as well as a smaller and more practical panel depth than the other two construction types. In conclusion, the Type 3 sandwich construction is recommend to move forward with the prototyping process.

APPENDIX A:

FLATWISE COMPRESSION TESING RESULTS

Table A.1: Summary of Flatwise Compression Test for Specimen 1-1-C

General Information		
Specimen Label	1-1-C	
Displacement Controlled Loading Rate	0.1	in/min
Data Recording Rate for Load and Displacment	5	Hz
Total Time Elapsed During Testing	15	min
Dimensions		
Total Height of the Specimen, h	2.133	in
Thickness of the Facings, f	0.095	in
Thickness of the Core, c	1.944	in
Width of the Specimen, w	3.528	in
Length of the Specimen, l	3.490	in
Cross-Sectional Area in the Flatwise Direction, A_{fw}	12.31	in^2
Regression Analysis for Correcting the Load vs. Displacement		

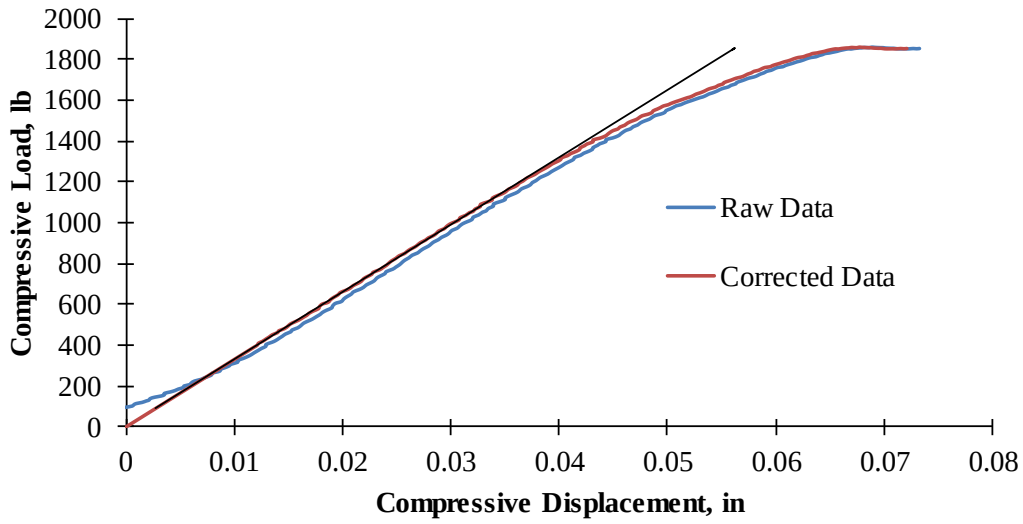

Slope of the Regression Line	32,990	lb/in
Offset Correction in Compressive Displacement	0.001	in
Coefficient of Determination	0.9998	
Number of Data Points	70	
Range of Corrected Displacement	0.012 - 0.035	in
Corresponding Strain Range	0.006 - 0.018	in/in

Table A.1: Summary of Flatwise Compression Test for Specimen 1-1-C (Continued)

Corrected Load vs. Displacement

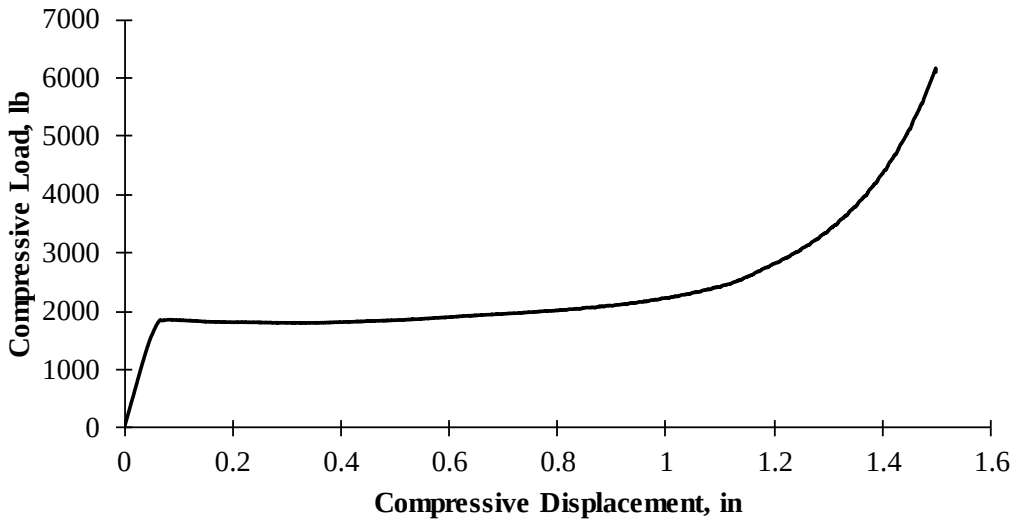

Stress vs. Strain in the Core Material

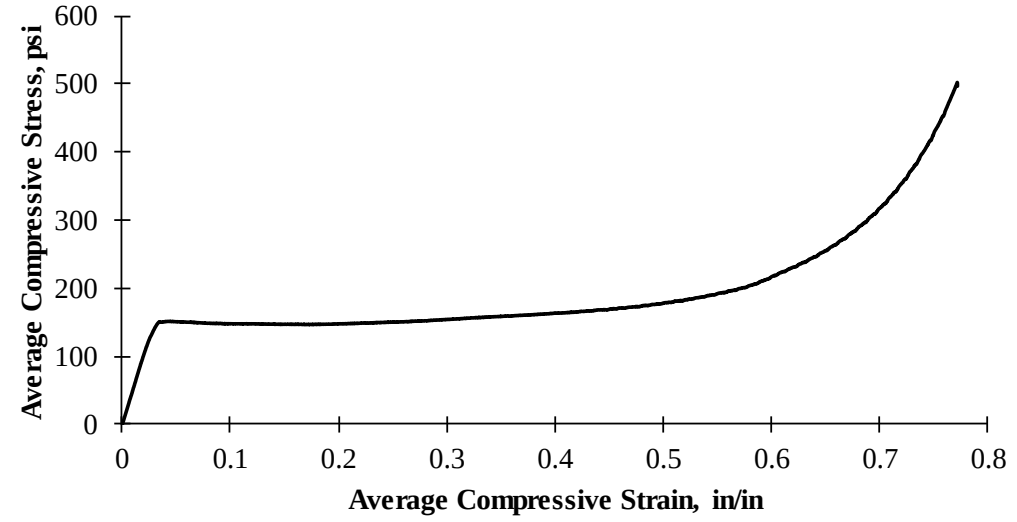

Strength and Stiffness Analysis

Flatwise Compressive Strength	151	psi
Stain at Flatwise Compressive Strength	0.035	in/in
Flatwise Comrpessive Modulus	5,210	psi

Note: Rubber pads that were 1/8 in. thick with Durometer A hardness 60 were used.

Table A.2: Summary of Flatwise Compression Test for Specimen 1-2-C

General Information		
Specimen Label	1-2-C	
Displacement Controlled Loading Rate	0.1	in/min
Data Recording Rate for Load and Displacment	5	Hz
Total Time Elapsed During Testing	15	min
Dimensions		
Total Height of the Specimen, h	2.133	in
Thickness of the Facings, f	0.095	in
Thickness of the Core, c	1.944	in
Width of the Specimen, w	3.483	in
Length of the Specimen, l	3.480	in
Cross-Sectional Area in the Flatwise Direction, A_{fw}	12.12	in^2
Regression Analysis for Correcting the Load vs. Displacement		

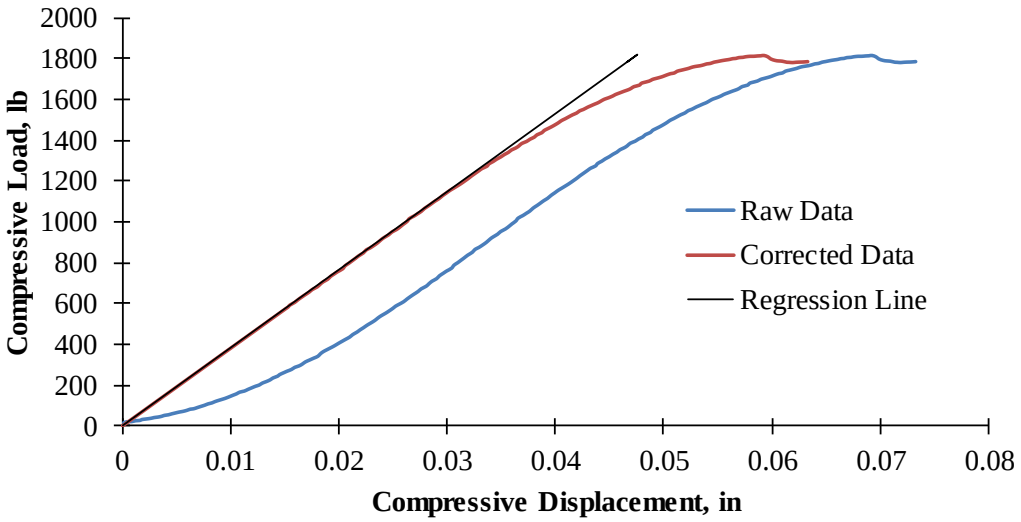

Slope of the Regression Line	38,140			lb/in
Offset Correction in Compressive Displacement	0.010			in
Coefficient of Determination	0.9998			
Number of Data Points	50			
Range of Corrected Displacement	0.016	-	0.032	in
Corresponding Strain Range	0.008	-	0.016	in/in

Table A.2: Summary of Flatwise Compression Test for Specimen 1-2-C (Continued).

Corrected Load vs. Displacement

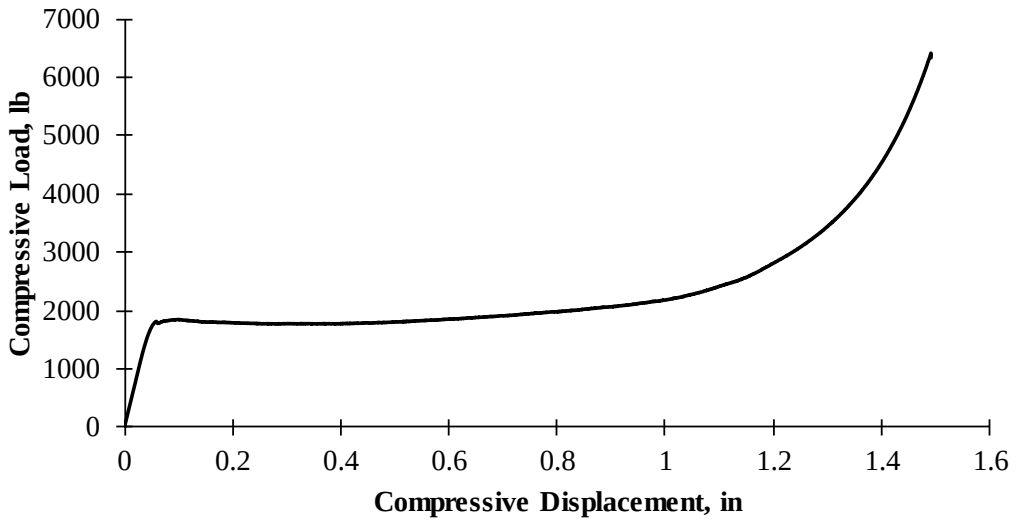

Stress vs. Strain in the Core Material

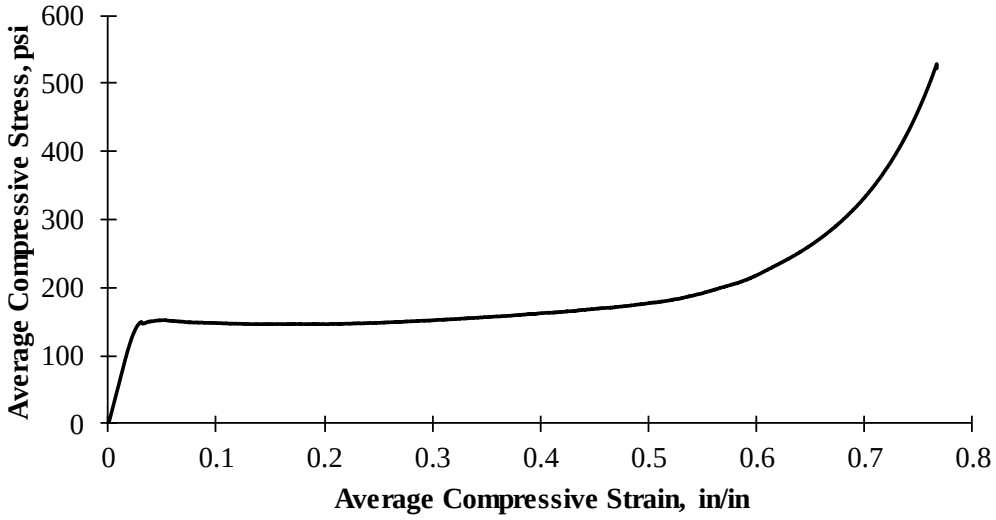

Strength and Stiffness Analysis

Flatwise Compressive Strength	150	psi
Stain at Flatwise Compressive Strength	0.030	in/in
Flatwise Compressive Modulus	6,120	psi

Table A.3: Summary of Flatwise Compression Test for Specimen 1-3-C

General Information		
Specimen Label	1-3-C	
Displacement Controlled Loading Rate	0.1	in/min
Data Recording Rate for Load and Displacment	5	Hz
Total Time Elapsed During Testing	11	min
Dimensions		
Total Height of the Specimen, h	2.133	in
Thickness of the Facings, f	0.095	in
Thickness of the Core, c	1.944	in
Width of the Specimen, w	3.481	in
Length of the Specimen, l	3.481	in
Cross-Sectional Area in the Flatwise Direction, A_{fw}	12.12	in^2
Regression Analysis for Correcting the Load vs. Displacement		

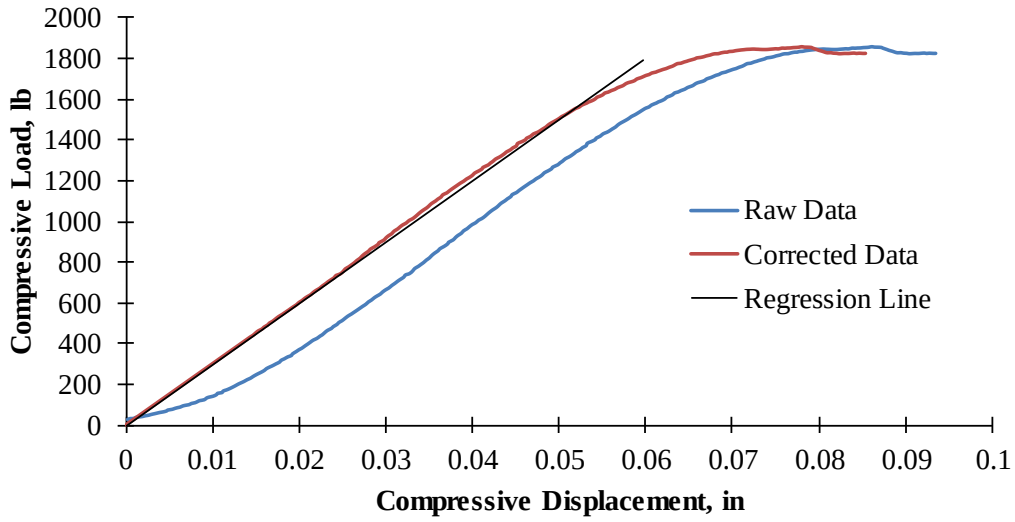

Slope of the Regression Line	29,990	lb/in
Offset Correction in Compressive Displacement	0.008	in
Coefficient of Determination	0.9998	
Number of Data Points	30	
Range of Corrected Displacement	0.014 - 0.024	in
Corresponding Strain Range	0.007 - 0.012	in/in

Table A.3: Summary of Flatwise Compression Test for Specimen 1-3-C (Continued)

Corrected Load vs. Displacement

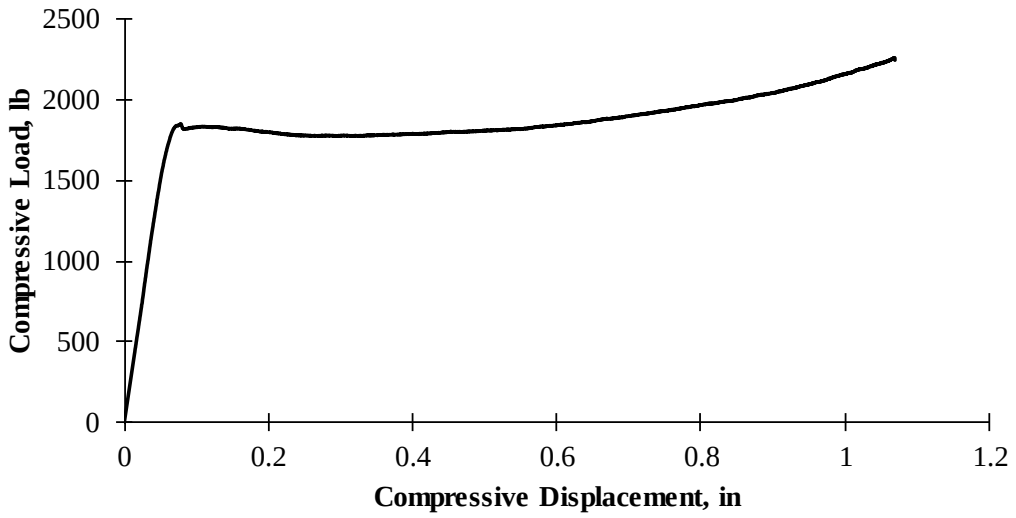

Stress vs. Strain in the Core Material

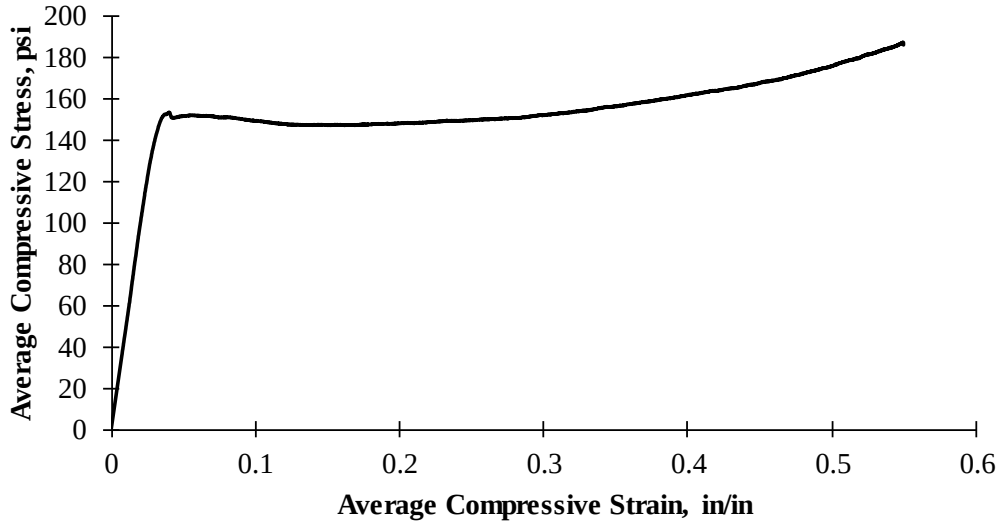

Strength and Stiffness Analysis		
Flatwise Compressive Strength	153	psi
Stain at Flatwise Compressive Strength	0.040	in/in
Flatwise Compressive Modulus	4,810	psi

Table A.4: Summary of Flatwise Compression Test for Specimen 2-1-C

General Information		
Specimen Label	2-1-C	
Displacement Controlled Loading Rate	0.1	in/min
Data Recording Rate for Load and Displacment	5	Hz
Total Time Elapsed During Testing	12	min
Dimensions		
Total Height of the Specimen, h	2.333	in
Thickness of the Facings, f	0.095	in
Thickness of the Core, c	2.143	in
Width of the Specimen, w	3.479	in
Length of the Specimen, l	3.538	in
Cross-Sectional Area in the Flatwise Direction, A_{fw}	12.31	in^2
Regression Analysis for Correcting the Load vs. Displacement		

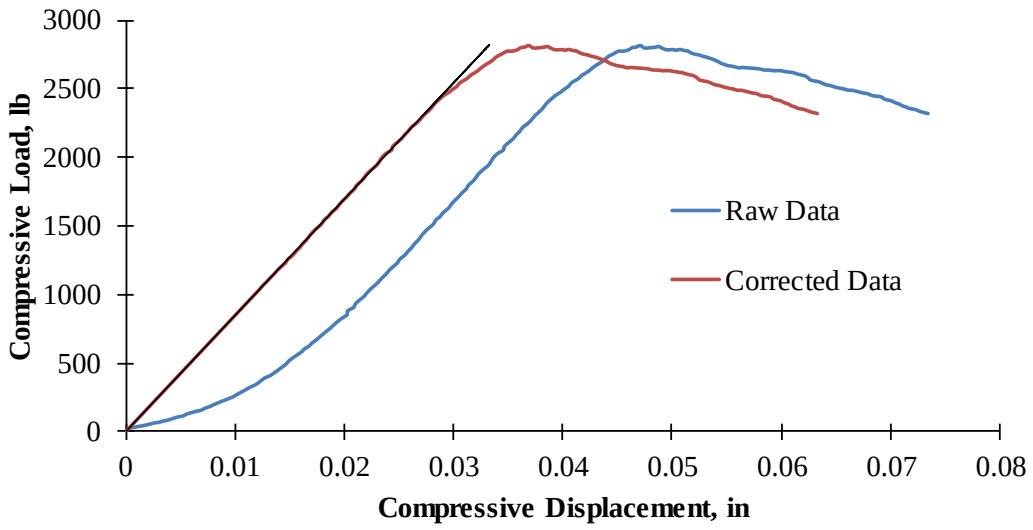

Slope of the Regression Line	84,700			lb/in
Offset Correction in Compressive Displacement	0.010			in
Coefficient of Determination	0.9998			
Number of Data Points	50			
Range of Corrected Displacement	0.013	-	0.029	in
Corresponding Strain Range	0.006	-	0.013	in/in

Table A.4: Summary of Flatwise Compression Test for Specimen 2-1-C (Continued)

Corrected Load vs. Displacement

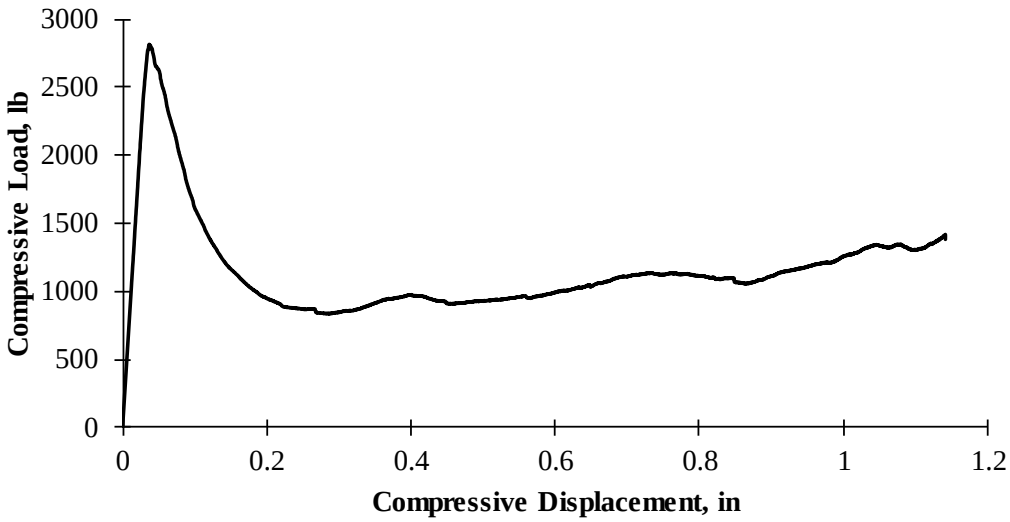

Stress vs. Strain in the Core Material

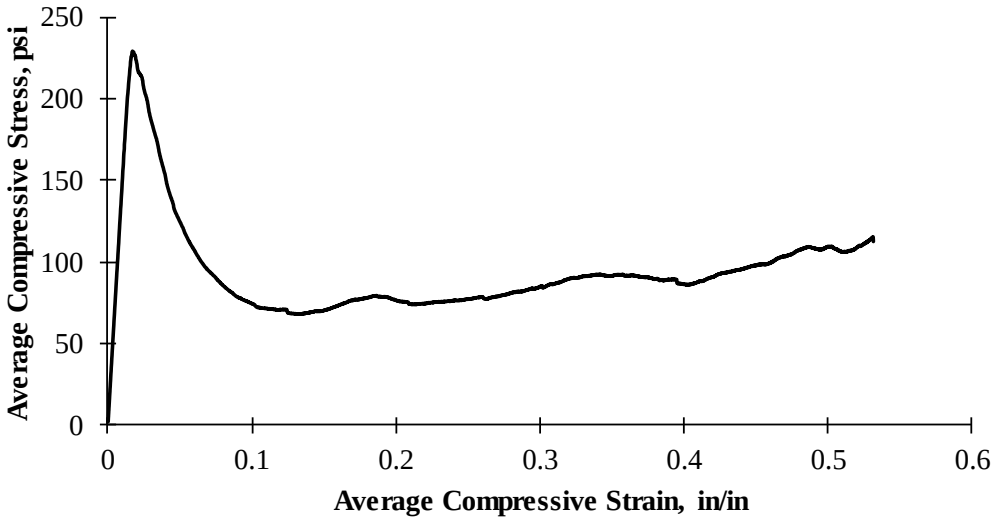

Strength and Stiffness Analysis		
Flatwise Compressive Strength	229	psi
Stain at Flatwise Compressive Strength	0.017	in/in
Flatwise Comressive Modulus	14,750	psi

Table A.5: Summary of Flatwise Compression Test for Specimen 2-2-C

General Information		
Specimen Label	2-2-C	
Displacement Controlled Loading Rate	0.1	in/min
Data Recording Rate for Load and Displacment	5	Hz
Total Time Elapsed During Testing	12	min
Dimensions		
Total Height of the Specimen, h	2.333	in
Thickness of the Facings, f	0.095	in
Thickness of the Core, c	2.143	in
Width of the Specimen, w	3.556	in
Length of the Specimen, l	3.492	in
Cross-Sectional Area in the Flatwise Direction, A_{fw}	12.42	in^2
Regression Analysis for Correcting the Load vs. Displacement		
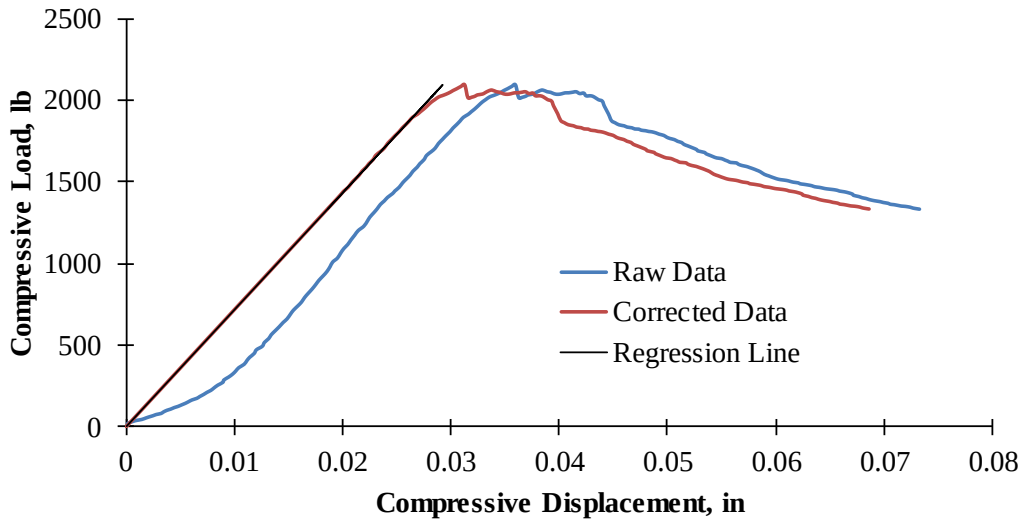		
Slope of the Regression Line	71,850	lb/in
Offset Correction in Compressive Displacement	0.005	in
Coefficient of Determination	0.9996	
Number of Data Points	20	
Range of Corrected Displacement	0.020 - 0.026	in
Corresponding Strain Range	0.009 - 0.012	in/in

Table A.5: Summary of Flatwise Compression Test for Specimen 2-2-C (Continued)

Corrected Load vs. Displacement

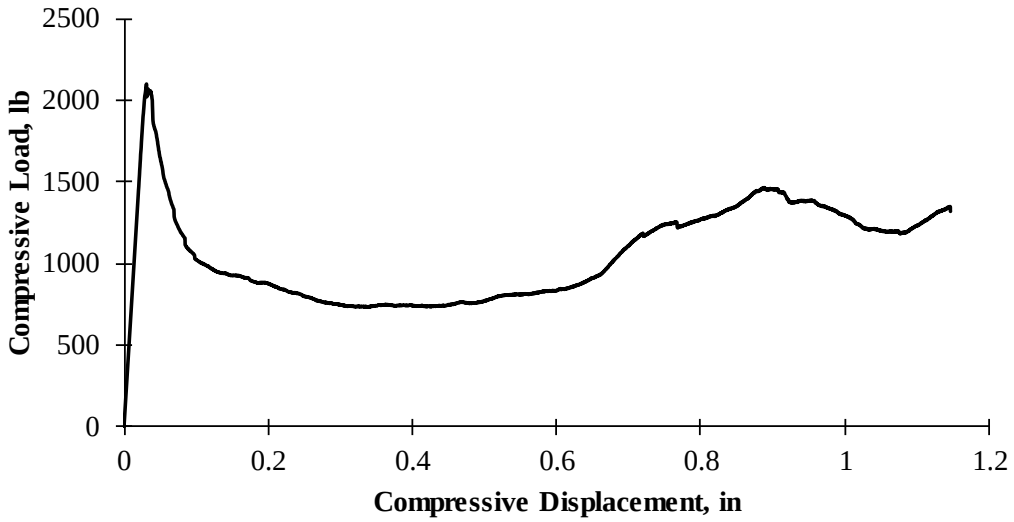

Stress vs. Strain in the Core Material

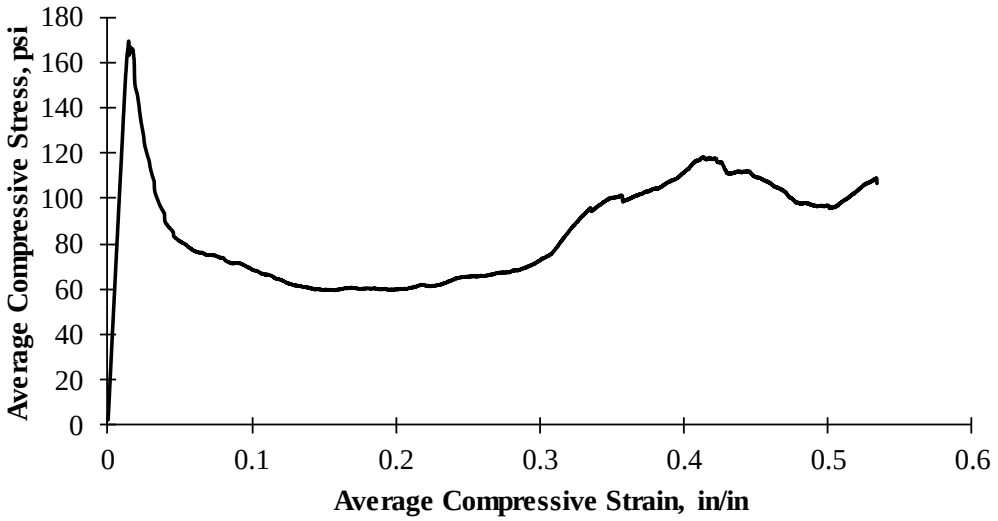

Strength and Stiffness Analysis

Flatwise Compressive Strength	169	psi
Stain at Flatwise Compressive Strength	0.015	in/in
Flatwise Comressive Modulus	12,400	psi

Table A.6: Summary of Flatwise Compression Test for Specimen 2-3-C

General Information		
Specimen Label	2-3-C	
Displacement Controlled Loading Rate	0.1	in/min
Data Recording Rate for Load and Displacment	5	Hz
Total Time Elapsed During Testing	12	min
Dimensions		
Total Height of the Specimen, h	2.333	in
Thickness of the Facings, f	0.095	in
Thickness of the Core, c	2.143	in
Width of the Specimen, w	3.542	in
Length of the Specimen, l	3.491	in
Cross-Sectional Area in the Flatwise Direction, A_{fw}	12.36	in^2
Regression Analysis for Correcting the Load vs. Displacement		

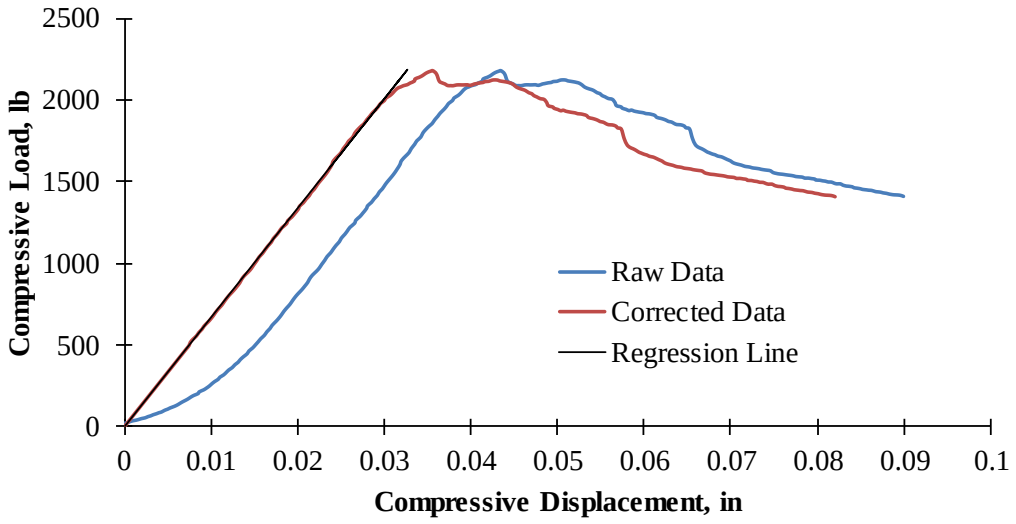

Slope of the Regression Line	66,530			lb/in
Offset Correction in Compressive Displacement	0.008			in
Coefficient of Determination	0.9998			
Number of Data Points	50			
Range of Corrected Displacement	0.008	-	0.024	in
Corresponding Strain Range	0.004	-	0.011	in/in

Table A.6: Summary of Flatwise Compression Test for Specimen 2-3-C (Continued)

Corrected Load vs. Displacement

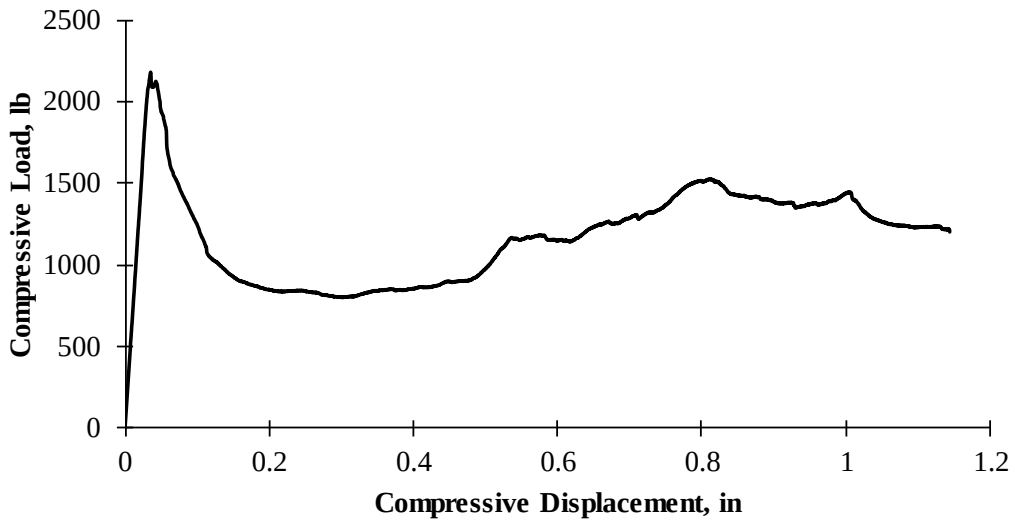

Stress vs. Strain in the Core Material

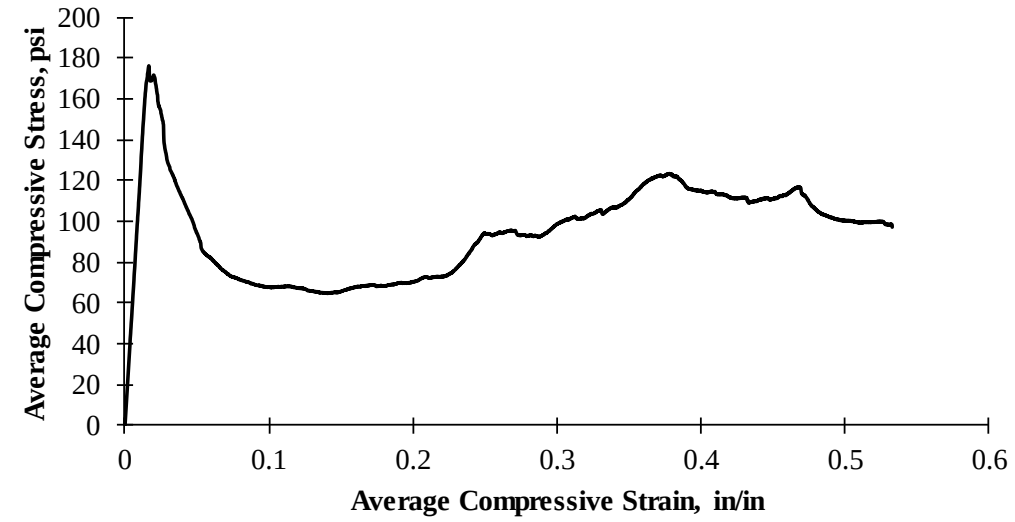

Strength and Stiffness Analysis		
Flatwise Compressive Strength	176	psi
Stain at Flatwise Compressive Strength	0.017	in/in
Flatwise Comressive Modulus	11,530	psi

Table A.7: Summary of Flatwise Compression Test for Specimen 2-4-C

General Information		
Specimen Label	2-4-C	
Displacement Controlled Loading Rate	0.1	in/min
Data Recording Rate for Load and Displacment	5	Hz
Total Time Elapsed During Testing	15	min
Dimensions		
Total Height of the Specimen, h	2.333	in
Thickness of the Facings, f	0.095	in
Thickness of the Core, c	2.143	in
Width of the Specimen, w	3.526	in
Length of the Specimen, l	3.563	in
Cross-Sectional Area in the Flatwise Direction, A_{fw}	12.56	in^2
Regression Analysis for Correcting the Load vs. Displacement		

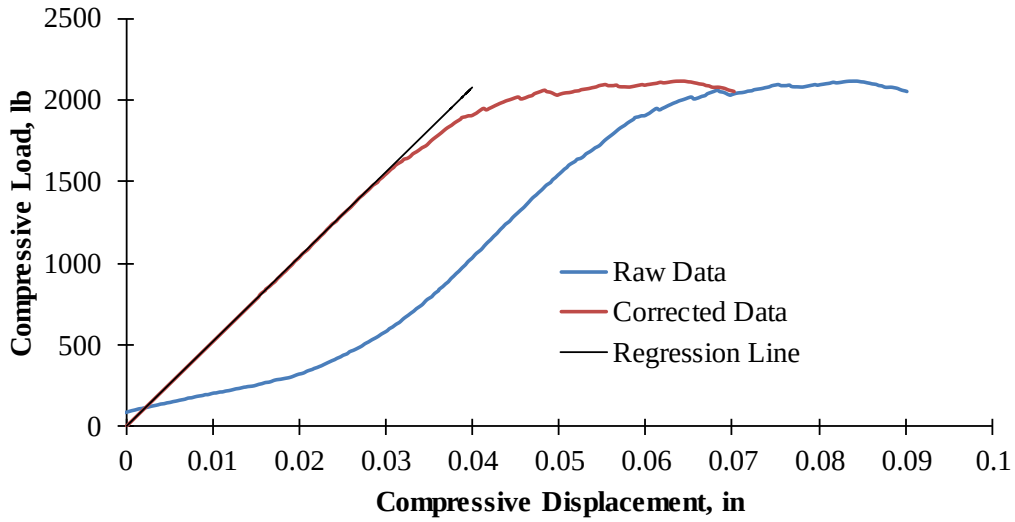

Slope of the Regression Line	51,890			lb/in
Offset Correction in Compressive Displacement	0.020			in
Coefficient of Determination	0.9999			
Number of Data Points	40			
Range of Corrected Displacement	0.015	-	0.029	in
Corresponding Strain Range	0.007	-	0.013	in/in

Table A.7: Summary of Flatwise Compression Test for Specimen 2-4-C (Continued)

Corrected Load vs. Displacement

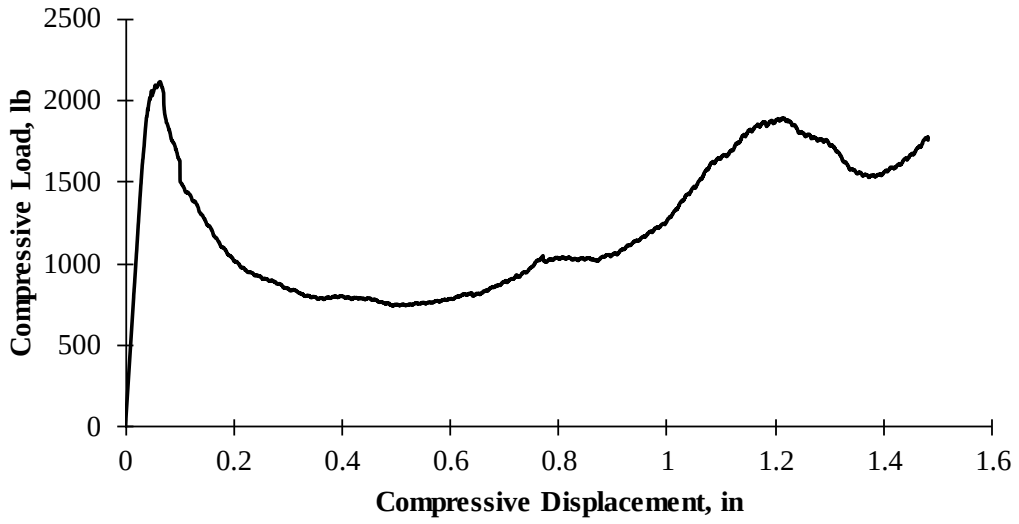

Stress vs. Strain in the Core Material

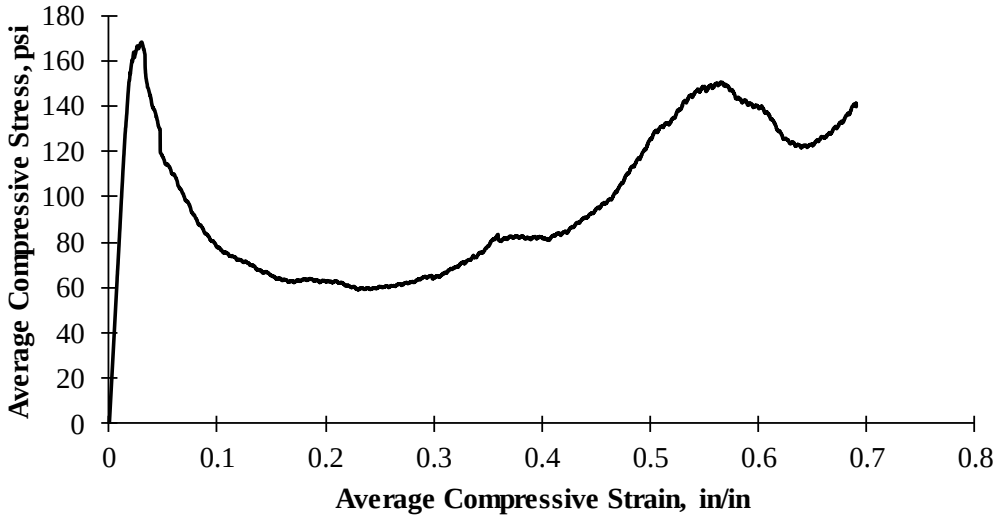

Strength and Stiffness Analysis

Flatwise Compressive Strength	168	psi
Stain at Flatwise Compressive Strength	0.030	in/in
Flatwise Comressive Modulus	8,850	psi

Note: Rubber pads that were 1/8 in. thick with Durometer A hardness 60 were used.

APPENDIX B:

FLATWISE TENSION TESING RESULTS

Table B.1: Summary of Flatwise Tension Test for Specimen 1-1-T

General Information		
Specimen Label	1-1-T	
Displacement Controlled Loading Rate	0.01	in/min
Data Recording Rate for Load and Displacment	10	Hz
Total Time Elapsed During Testing	9	min
Dimensions		
Total Height of the Specimen, h	2.133	in
Thickness of the Facings, f	0.095	in
Thickness of the Core, c	1.944	in
Width of the Specimen, w	3.530	in
Length of the Specimen, l	3.502	in
Cross-Sectional Area in the Flatwise Direction, A_{fw}	12.36	in^2
Regression Analysis for Correcting the Load vs. Displacement		

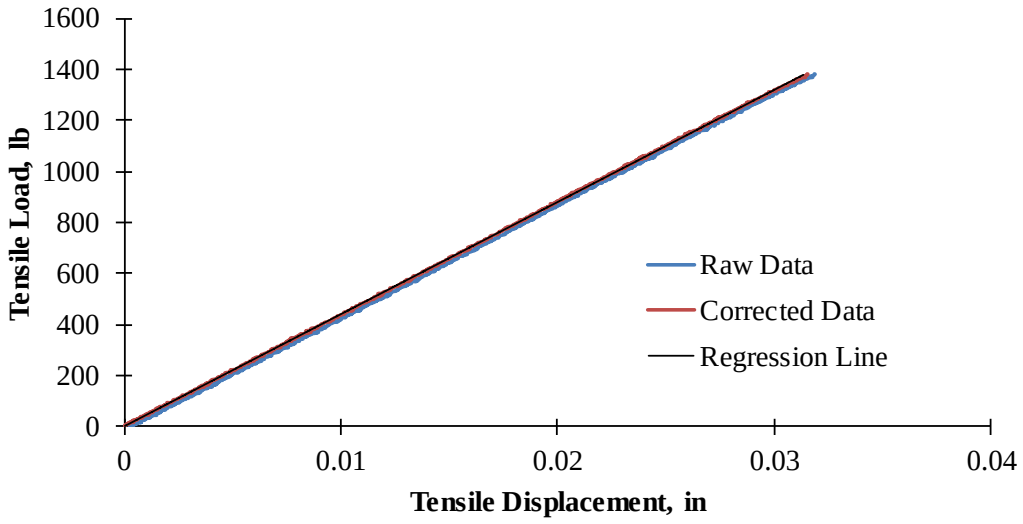

Slope of the Regression Line	43,910			lb/in
Offset Correction in Compressive Displacement	0.0004			in
Coefficient of Determination	0.9999			
Number of Data Points	900			
Range of Corrected Displacement	0.0000	-	0.030	in
Corresponding Strain Range	0.0000	-	0.015	in/in

Table B.1: Summary of Flatwise Tension Test for Specimen 1-1-T (Continued)

Corrected Load vs. Displacement

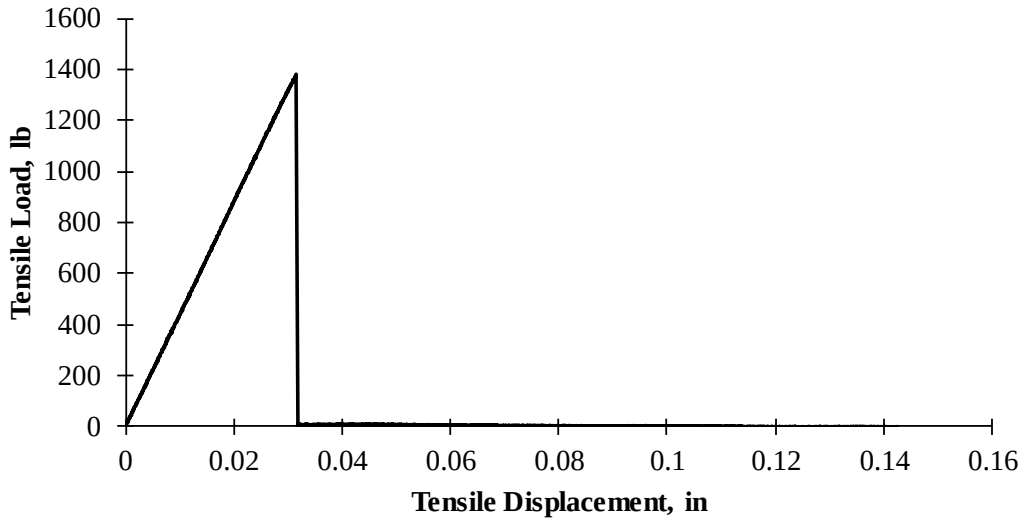

Stress vs. Strain in the Core Material

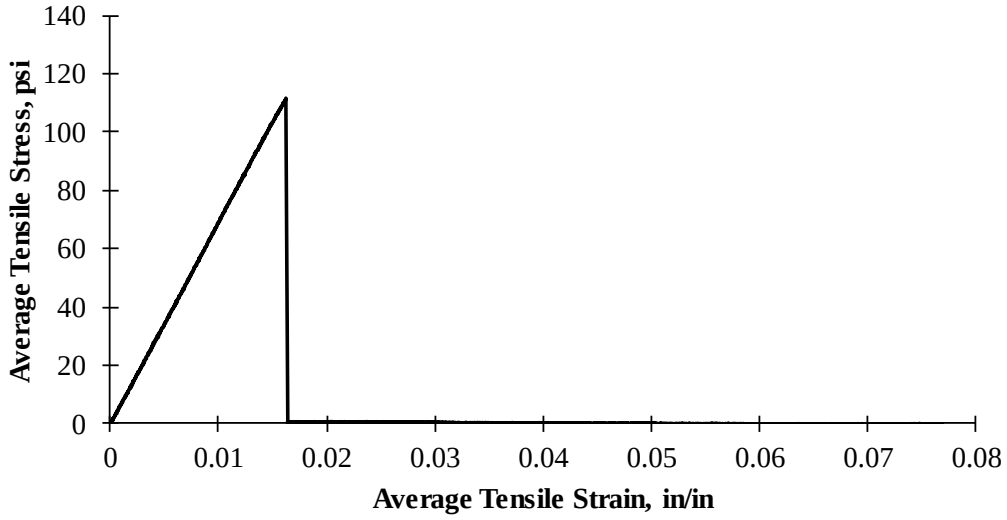

Strength and Stiffness Analysis		
Flatwise Tensile Strength	112	psi
Stain at Flatwise Tensile Strength	0.016	in/in
Flatwise Tensile Modulus	6,900	psi

Table B.2: Summary of Flatwise Tension Test for Specimen 1-2-T

General Information		
Specimen Label	1-2-T	
Displacement Controlled Loading Rate	0.02	in/min
Data Recording Rate for Load and Displacment	10	Hz
Total Time Elapsed During Testing	6	min
Dimensions		
Total Height of the Specimen, h	2.133	in
Thickness of the Facings, f	0.095	in
Thickness of the Core, c	1.944	in
Width of the Specimen, w	3.482	in
Length of the Specimen, l	3.490	in
Cross-Sectional Area in the Flatwise Direction, A_{fw}	12.15	in^2
Regression Analysis for Correcting the Load vs. Displacement		
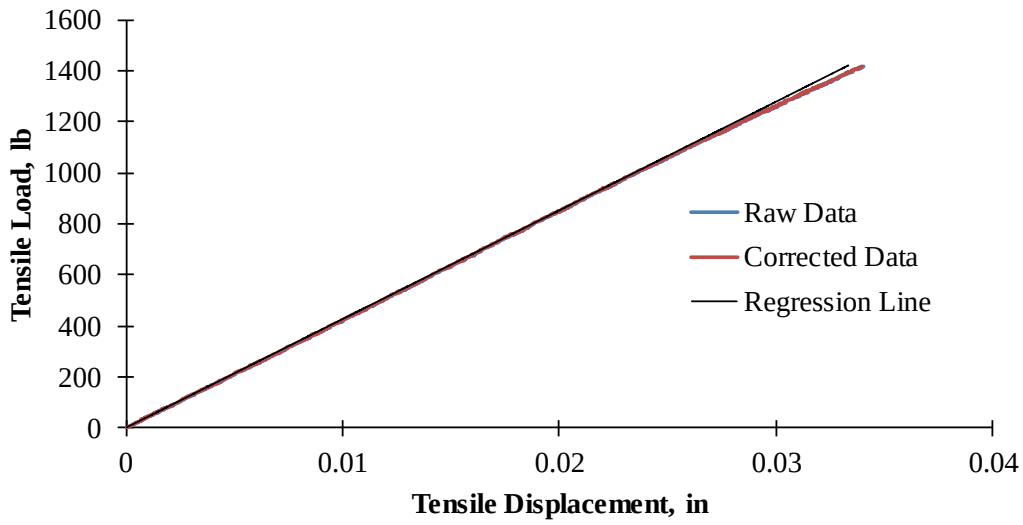		
Slope of the Regression Line	42,530	lb/in
Offset Correction in Compressive Displacement	0.0001	in
Coefficient of Determination	1.0000	
Number of Data Points	800	
Range of Corrected Displacement	0.0002 - 0.027	in
Corresponding Strain Range	0.0001 - 0.014	in/in

Table B.2: Summary of Flatwise Tension Test for Specimen 1-2-T (Continued)

Corrected Load vs. Displacement

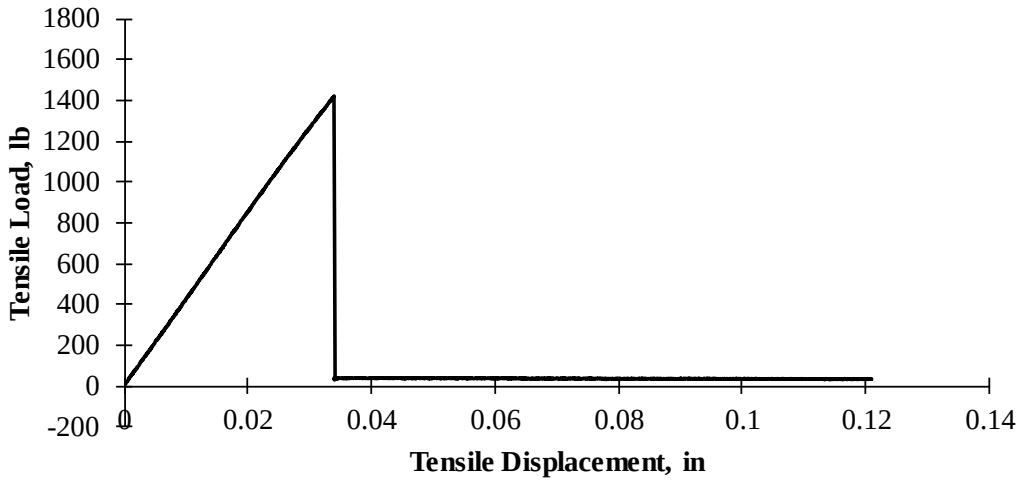

Stress vs. Strain in the Core Material

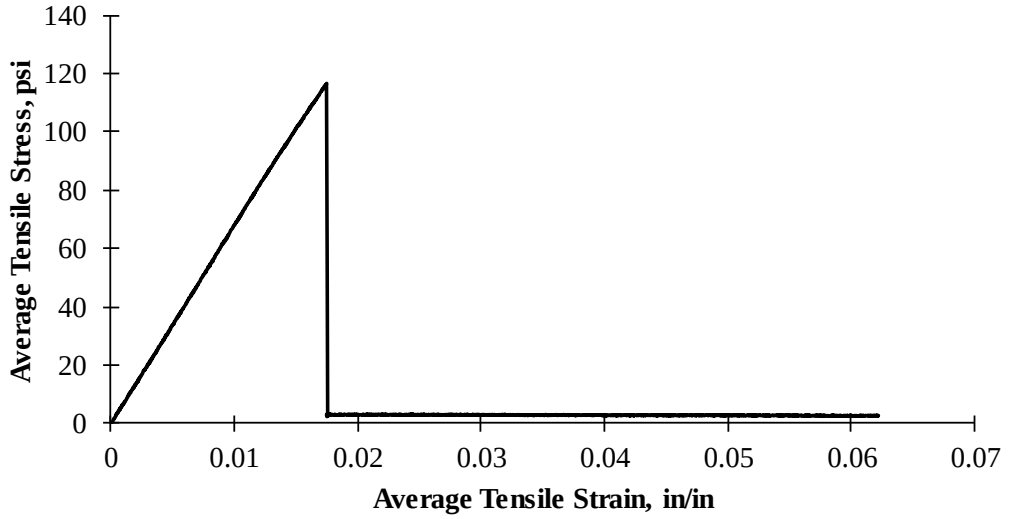

Strength and Stiffness Analysis		
Flatwise Tensile Strength	117	psi
Stain at Flatwise Tensile Strength	0.017	in/in
Flatwise Tensile Modulus	6,800	psi

Table B.3: Summary of Flatwise Tension Test for Specimen 2-1-T

General Information		
Specimen Label	2-1-T	
Displacement Controlled Loading Rate	0.01	in/min
Data Recording Rate for Load and Displacment	10	Hz
Total Time Elapsed During Testing	20	min
Dimensions		
Total Height of the Specimen, h	2.333	in
Thickness of the Facings, f	0.095	in
Thickness of the Core, c	2.143	in
Width of the Specimen, w	3.578	in
Length of the Specimen, l	3.482	in
Cross-Sectional Area in the Flatwise Direction, A_{fw}	12.46	in^2
Regression Analysis for Correcting the Load vs. Displacement		

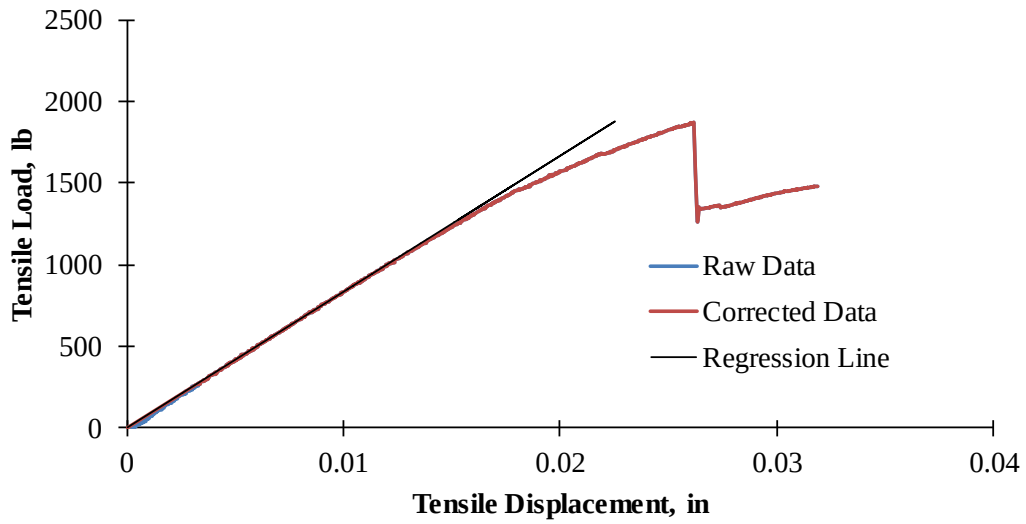

Slope of the Regression Line	82,940			lb/in
Offset Correction in Compressive Displacement	-0.0001			in
Coefficient of Determination	0.9996			
Number of Data Points	300			
Range of Corrected Displacement	0.003	-	0.013	in
Corresponding Strain Range	0.001	-	0.006	in/in

Table B.3: Summary of Flatwise Tension Test for Specimen 2-1-T (Continued)

Corrected Load vs. Displacement

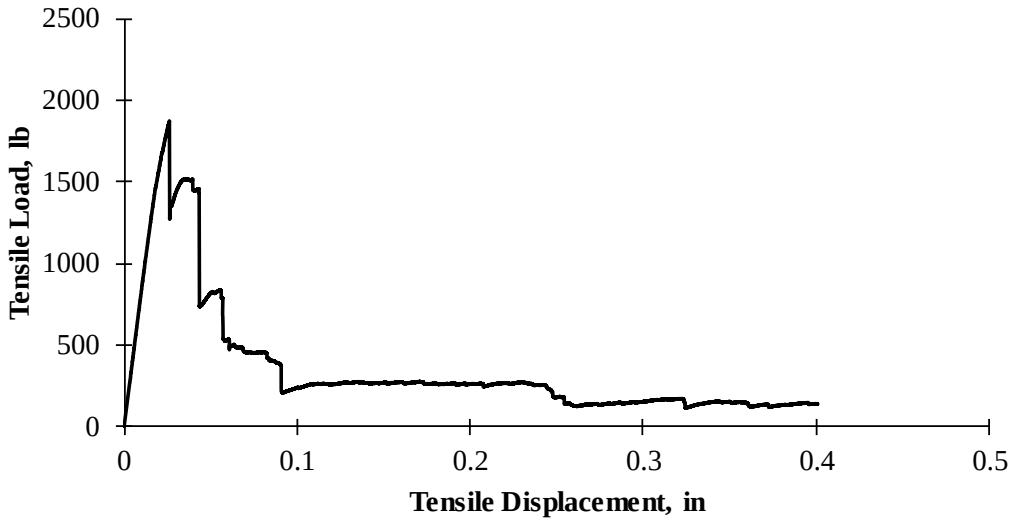

Stress vs. Strain in the Core Material

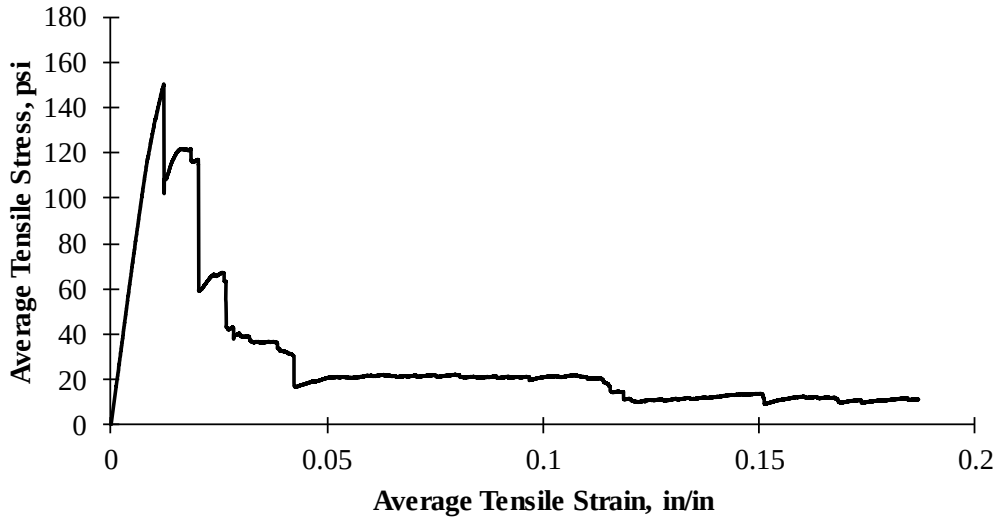

Strength and Stiffness Analysis		
Flatwise Tensile Strength	150	psi
Stain at Flatwise Tensile Strength	0.012	in/in
Flatwise Tensile Modulus	14,270	psi

Table B.4: Summary of Flatwise Tension Test for Specimen 2-2-T

General Information		
Specimen Label	2-2-T	
Displacement Controlled Loading Rate	0.01	in/min
Data Recording Rate for Load and Displacment	10	Hz
Total Time Elapsed During Testing	12	min
Dimensions		
Total Height of the Specimen, h	2.333	in
Thickness of the Facings, f	0.095	in
Thickness of the Core, c	2.143	in
Width of the Specimen, w	3.527	in
Length of the Specimen, l	3.487	in
Cross-Sectional Area in the Flatwise Direction, A_{fw}	12.30	in^2
Regression Analysis for Correcting the Load vs. Displacement		
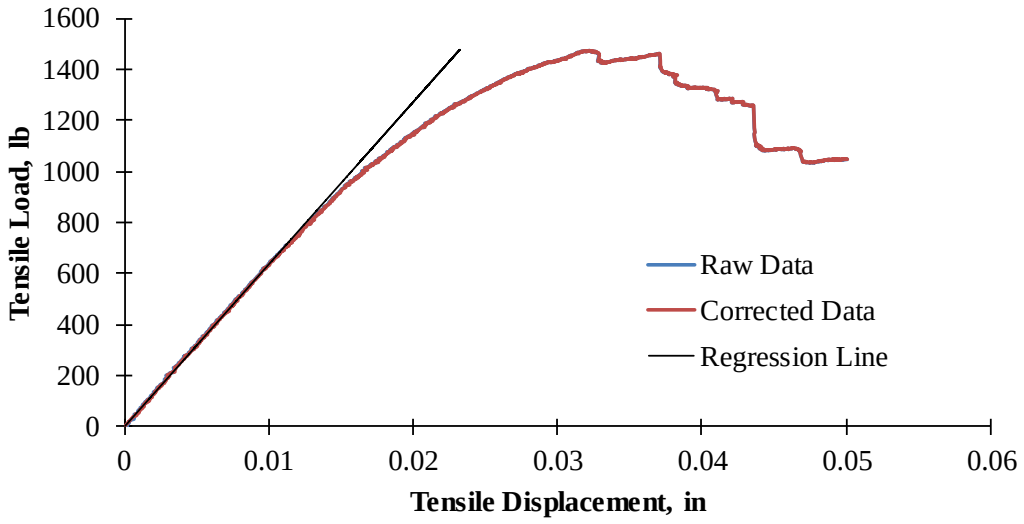		
Slope of the Regression Line	63,440	lb/in
Offset Correction in Compressive Displacement	-0.0001	in
Coefficient of Determination	0.9995	
Number of Data Points	300	
Range of Corrected Displacement	0.001 - 0.011	in
Corresponding Strain Range	0.000 - 0.005	in/in

Table B.4: Summary of Flatwise Tension Test for Specimen 2-2-T (Continued)

Corrected Load vs. Displacement

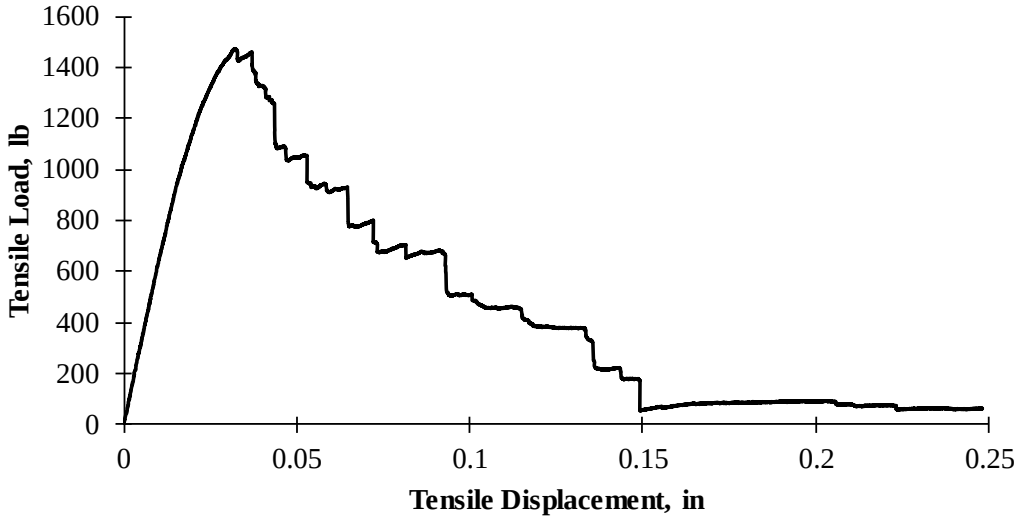

Stress vs. Strain in the Core Material

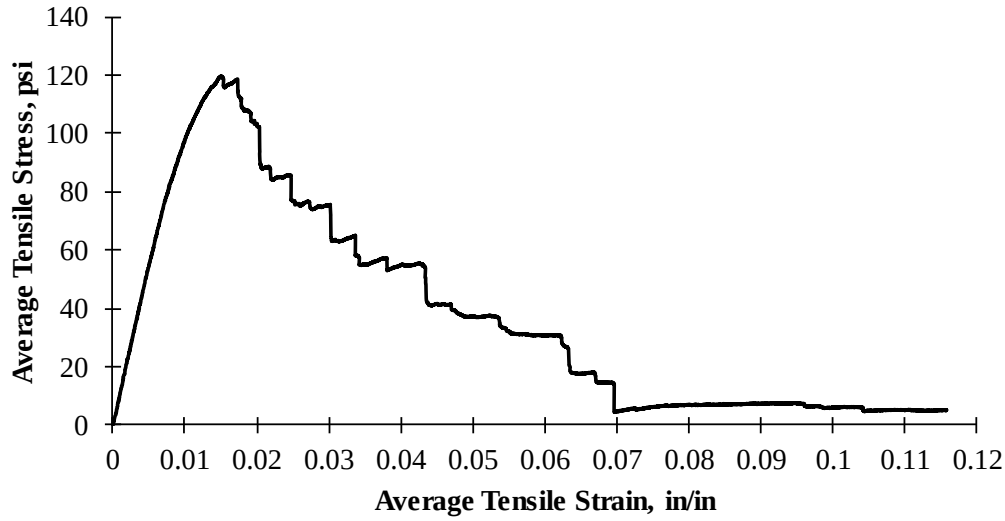

Strength and Stiffness Analysis

Flatwise Tensile Strength	120	psi
Stain at Flatwise Tensile Strength	0.015	in/in
Flatwise Tensile Modulus	11,050	psi

Table B.5: Summary of Flatwise Tension Test for Specimen 2-3-T

General Information		
Specimen Label	2-3-T	
Displacement Controlled Loading Rate	0.01	in/min
Data Recording Rate for Load and Displacment	10	Hz
Total Time Elapsed During Testing	19	min
Dimensions		
Total Height of the Specimen, h	2.333	in
Thickness of the Facings, f	0.095	in
Thickness of the Core, c	2.143	in
Width of the Specimen, w	3.544	in
Length of the Specimen, l	3.469	in
Cross-Sectional Area in the Flatwise Direction, A_{fw}	12.29	in^2
Regression Analysis for Correcting the Load vs. Displacement		

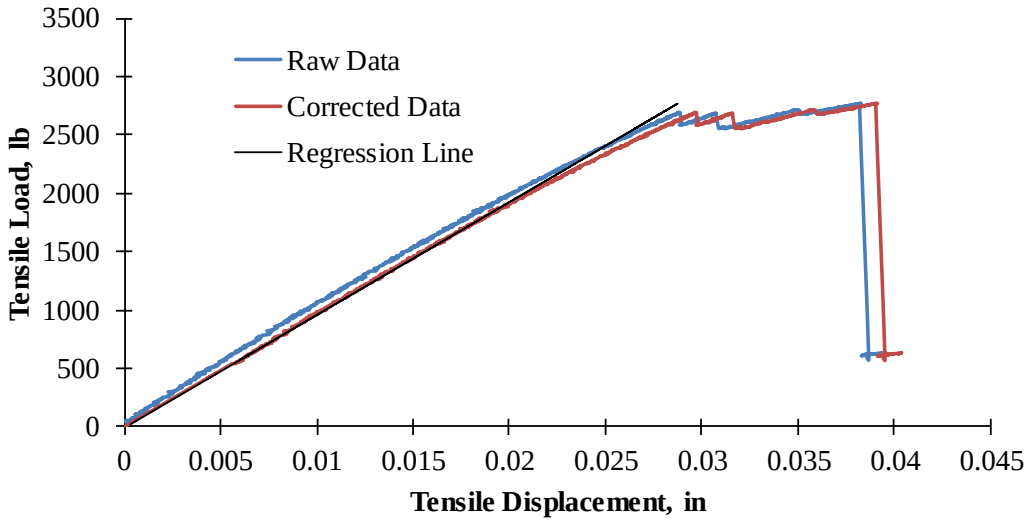

Slope of the Regression Line	96,360			lb/in
Offset Correction in Compressive Displacement	-0.001			in
Coefficient of Determination	0.9992			
Number of Data Points	400			
Range of Corrected Displacement	0.006	-	0.019	in
Corresponding Strain Range	0.003	-	0.009	in/in

Table B.5: Summary of Flatwise Tension Test for Specimen 2-3-T (Continued)

Corrected Load vs. Displacement

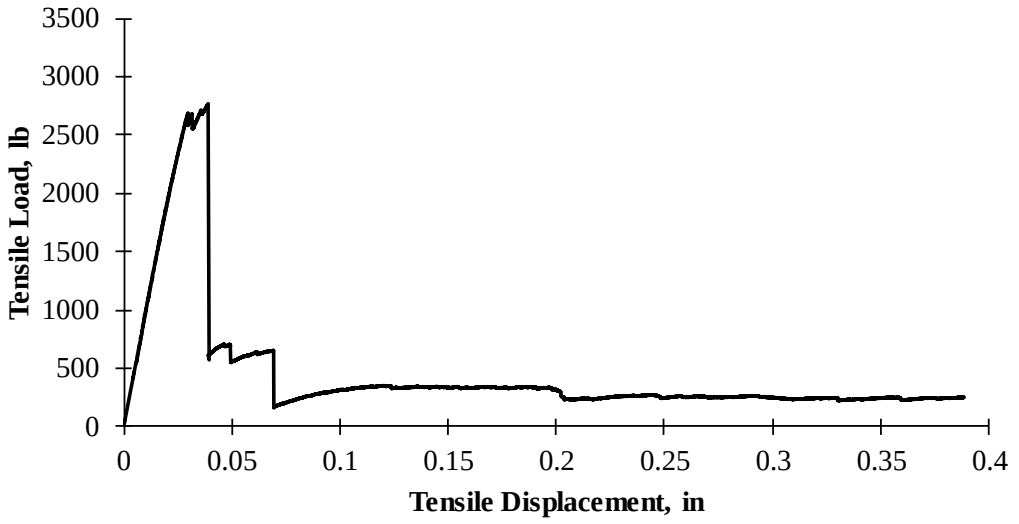

Stress vs. Strain in the Core Material

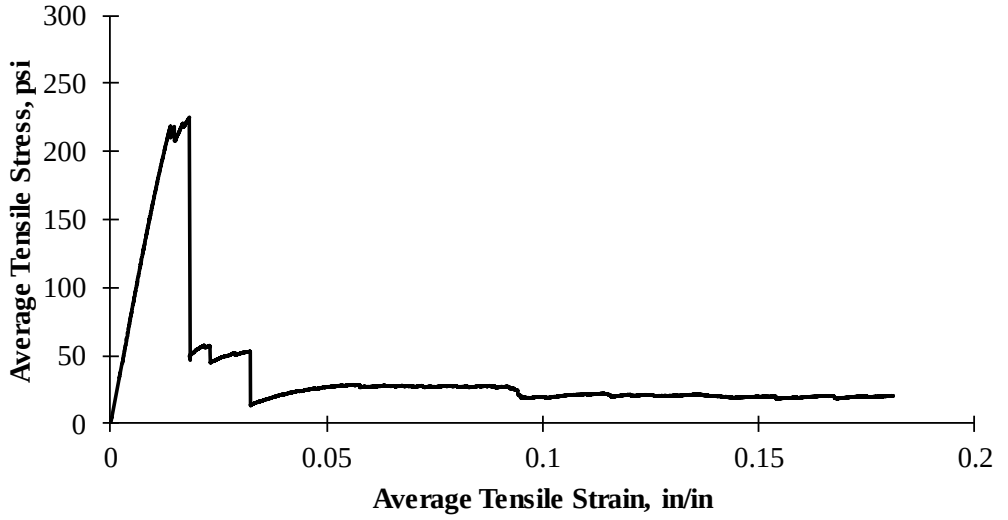

Strength and Stiffness Analysis		
Flatwise Tensile Strength	219	psi
Stain at Flatwise Tensile Strength	0.014	in/in
Flatwise Tensile Modulus	16,800	psi

APPENDIX C:

THREE POINT FLEXURAL TESING RESULTS

Table C.1: Summary of Three Point Flexural Test for Specimen 1-1-S

General Information		
Specimen Label	1-1-S	
Displacement Controlled Loading Rate	0.1	in/min
Data Recording Rate for Load and Displacment	1	Hz
Total Time Elapsed During Testing	15	min
Specimen Dimensions		
Total Height of the Specimen, h	2.133	in
Thickness of the Facings, f	0.095	in
Thickness of the Core, c	1.944	in
Width of the Specimen, b	2.977	in
Ratio of the Core Thickness to Facing Thickness, c/f	20.56	
Moment Arm Between the Facings, d	2.039	in
Length of the Specimen, l	8.0	in
Moment of Inertia of the Facings, I_f	0.585	in^4
Area of the Core, A_c	5.788	in^2
Configuration and Dimension of the Flexural Setup		
Span Between the Supports, L	6.00	in
Width of the Load and Support Bars, l_{pad}	1.00	in
Loading Configuration	3-Point Midspan Loading	
Regression Analysis for Correcting the Load vs. Bottom Face Deflection		
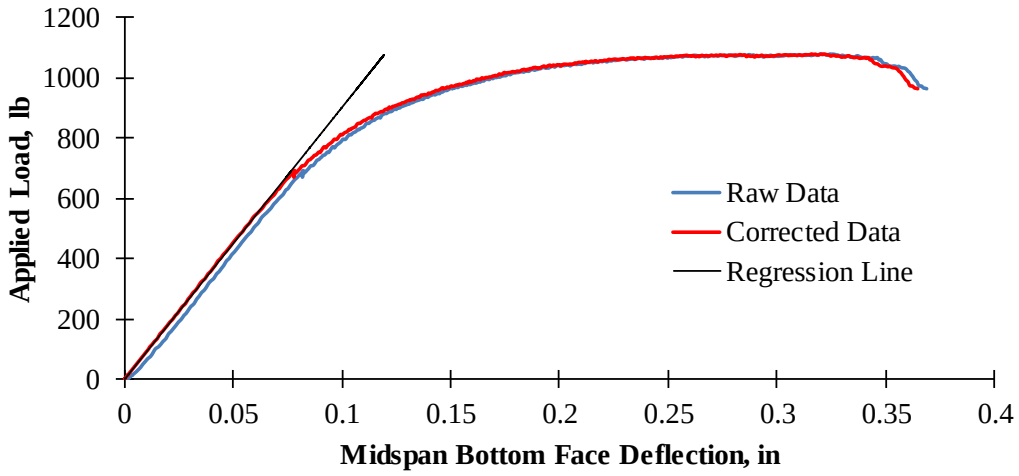		
Slope of the Regression Line	9,032	lb/in
Offset Correction in Bottrom Face Deflection	0.004	in
Coefficient of Determination	0.9998	
Number of Data Points	40	
Range of Corrected Deflection Used	0.012 - 0.057	in

Table C.1: Summary of Three Point Flexural Test for Specimen 1-1-S (Continued)

Regression Analysis for Correcting the Load vs. Crosshead Displacement		
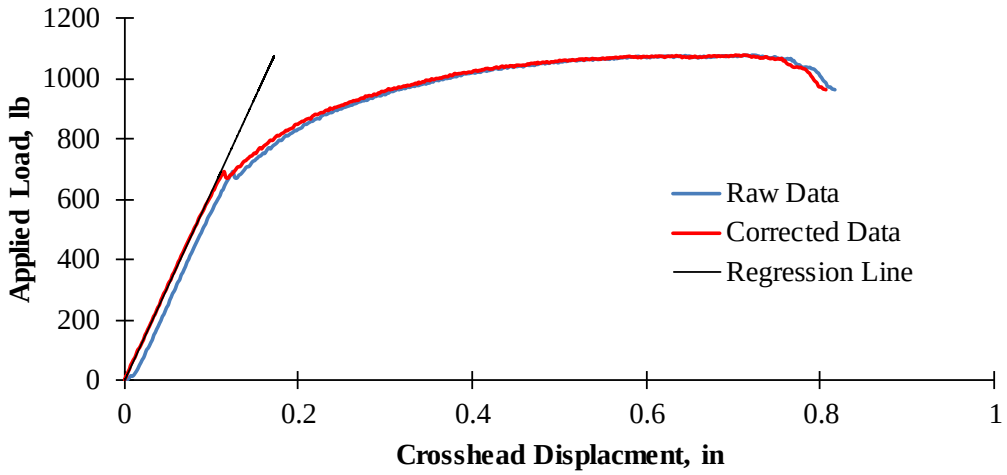		
Slope of the Regression Line	6,243	lb/in
Offset Correction in Crosshead Displacement	0.010	in
Coefficient of Determination	0.9998	
Number of Data Points	50	
Range of Corrected Displacement Used	0.008 - 0.089	in
Regression Analysis for Correcting the Load vs.Bottom Face Strain		
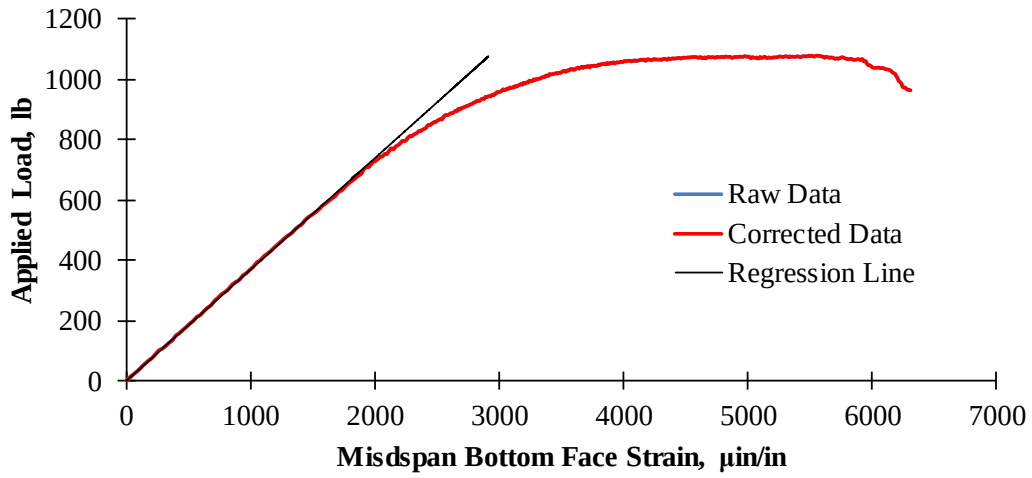		
Slope of the Regression Line	0.369	lb/µin/in
Offset Correction in Bottom Face Strain	-5.024	µin/in
Coefficient of Determination	0.9999	
Number of Data Points	60	
Range of Corrected Strain Used	5 - 1474	µin/in

Table C.1: Summary of Three Point Flexural Test for Specimen 1-1-S (Continued)

Corrected Load vs.Bottom Face Deflection

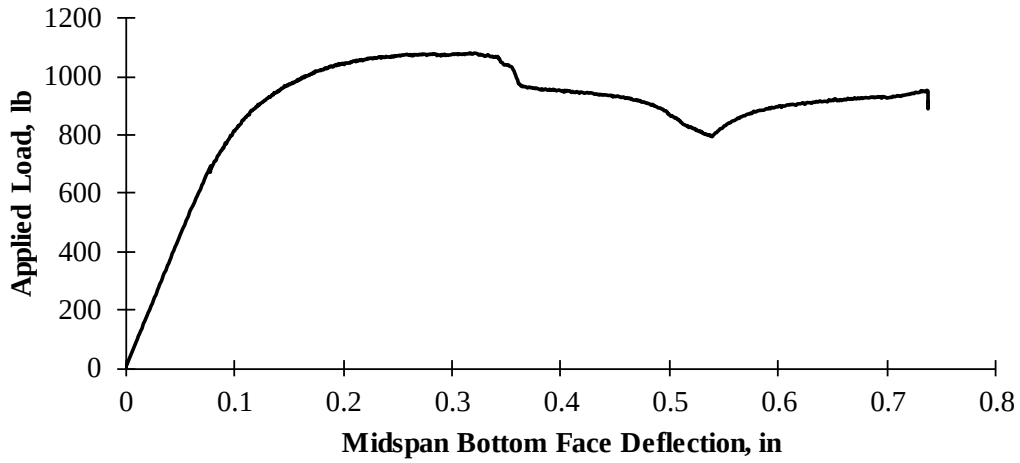

Corrected Load vs.Crosshead Displacement

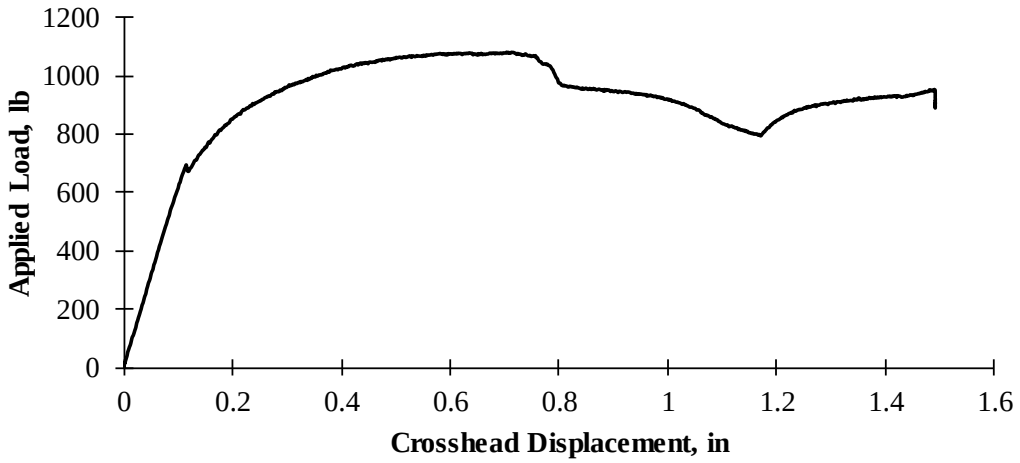

Corrected Load vs.Bottom Face Strain

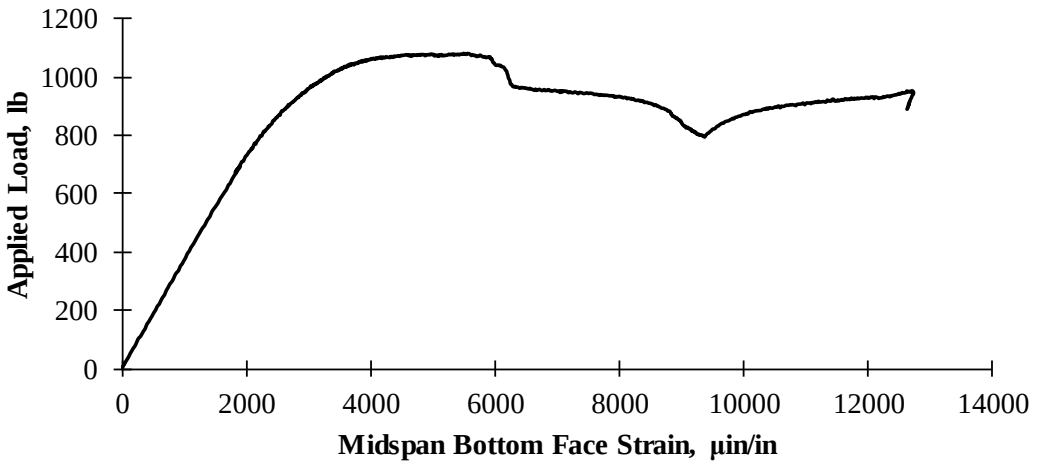

Table C.1: Summary of Three Point Flexural Test for Specimen 1-1-S (Continued)

Strength Analysis		
Initial Failure Mode	Localized Crushing of the Core Coupled with Wrinkling of the Top Facing Immediately Under the Load (Local Indenation)	
Estimation of the Intial Failure Load Using the Offset Method		
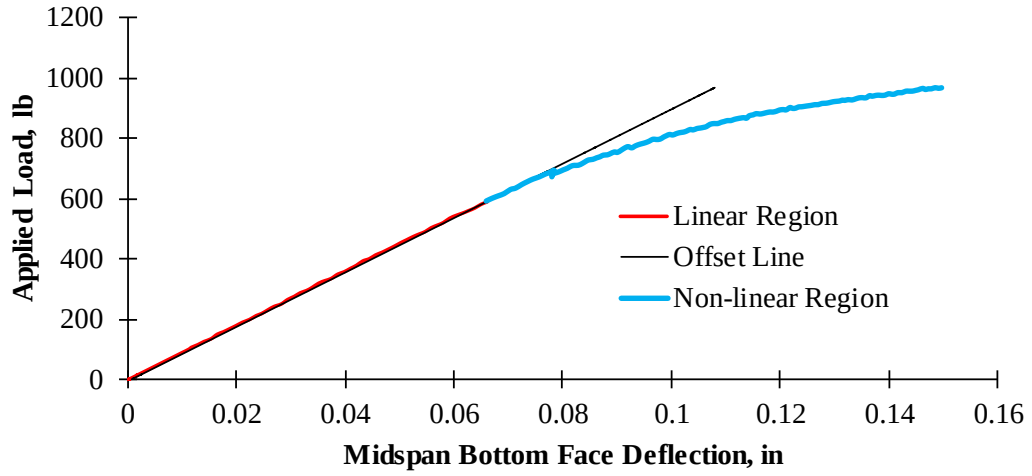		
Offset of Linear Region as a Pecent of Span Length	0.01%	
Load at Initial Failure	589	lb
Max. Internal Bending Moment at Initial Failure	884	lb*in
Max. Internal Shear Force at Initial Failure	295	lb
Average Pressure Under the Load at Initial Failure	198	psi
Max. Bending Stress in the Facings	1611	psi
Max. Average Shear Stress in the Core	51	psi
Ultimate Failure Mode	Excessive Crushing of the Core Coupled with Excessive Wrinkling of the Top Facing Immediately Under the Load (Local Indentation)	
Load at Ultimate Failure	1078	lb
Max. Internal Bending Moment at Ultimate Failure	1617	lb*in
Max. Internal Shear Force at Ultimate Failure	539	lb
Average Pressure Under Load at Ultimate Failure	362	psi
Max. Bending Stress in the Facing	2948	psi
Max. Average Shear Stress in the Core	93	psi
Serviceability Analysis		
Limiting Deflection (L/800)	0.0075	in
Load at Limiting Deflection	68	lb
Comparison of Serviceability to Strength		
Ratio of Initial Failure to Serviceability Load	8.70	
Ratio of Ultimate Failure to Serviceability Load	15.9	

Table C.2: Summary of Three Point Flexural Test for Specimen 1-2-S

General Information		
Specimen Label	1-2-S	
Displacement Controlled Loading Rate	0.1	in/min
Data Recording Rate for Load and Displacment	1	Hz
Total Time Elapsed During Testing	15	min
Specimen Dimensions		
Total Height of the Specimen, h	2.133	in
Thickness of the Facings, f	0.095	in
Thickness of the Core, c	1.944	in
Width of the Specimen, b	2.979	in
Ratio of the Core Thickness to Facing Thickness, c/f	20.56	
Moment Arm Between the Facings, d	2.039	in
Length of the Specimen, l	8.0	in
Moment of Inertia of the Facings, I_f	0.585	in^4
Area of the Core, A_c	5.791	in^2
Configuration and Dimension of the Flexural Setup		
Span Between the Supports, L	6.0	in
Width of the Load and Support Bars, l_{pad}	1.0	in
Loading Configuration	3-Point Midspan Loading	
Regression Analysis for Correcting the Load vs. Bottom Face Deflection		
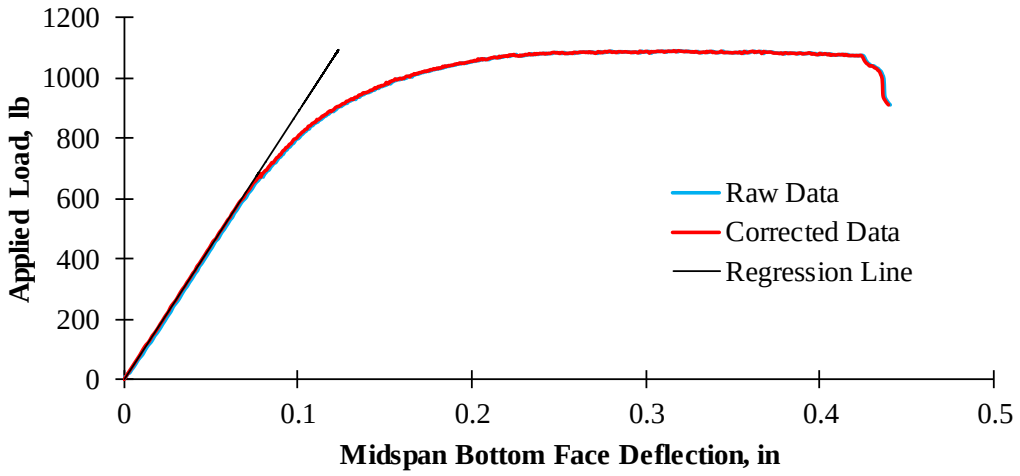		
Slope of the Regression Line	8,875	lb/in
Offset Correction in Bottrom Face Deflection	0.001	in
Coefficient of Determination	0.9999	
Number of Data Points	50	
Range of Corrected Deflection Used	0.009 - 0.067	in

Table C.2: Summary of Three Point Flexural Test for Specimen 1-2-S (Continued)

Regression Analysis for Correcting the Load vs. Crosshead Displacement		
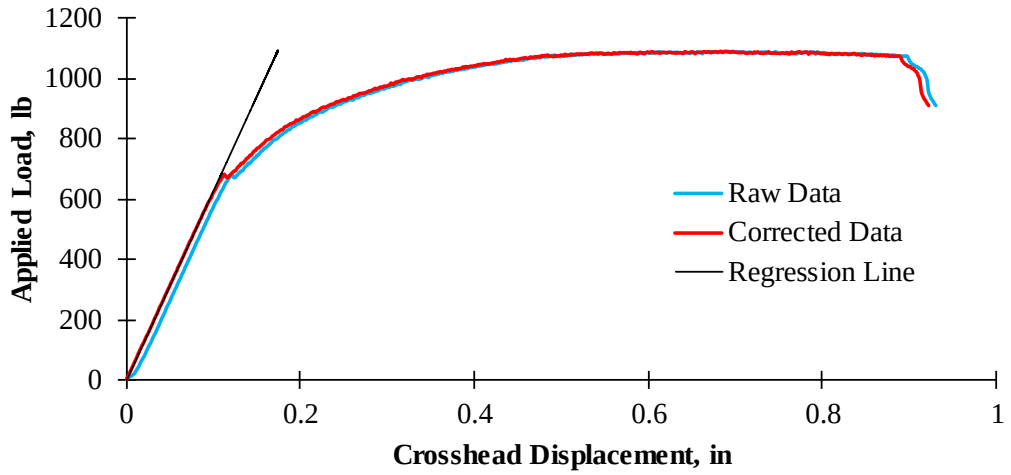		
Slope of the Regression Line	6,261	lb/in
Offset Correction in Crosshead Displacement	0.008	in
Coefficient of Determination	0.9999	
Number of Data Points	50	
Range of Corrected Displacement Used	0.013 - 0.095	in
Regression Analysis for Correcting the Load vs.Bottom Face Strain		
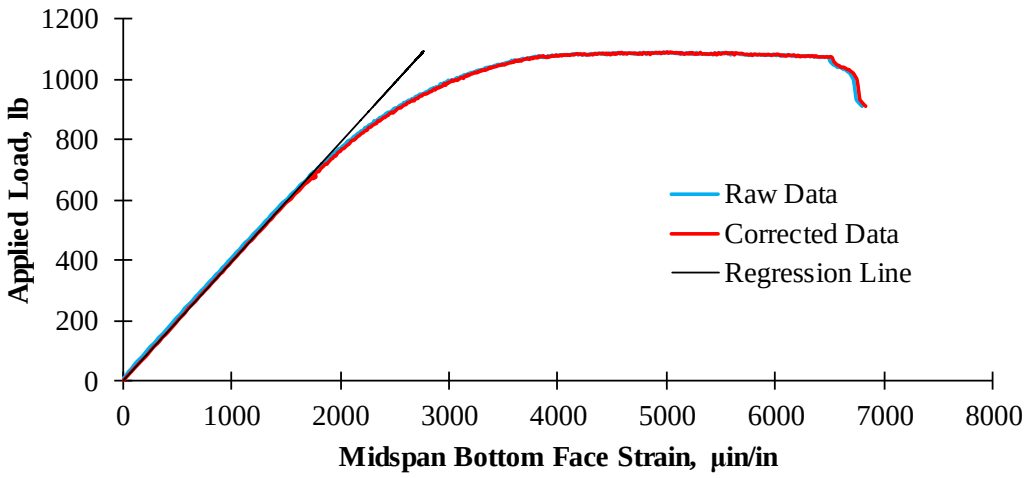		
Slope of the Regression Line	0.395	lb/µin/in
Offset Correction in Bottom Face Strain	-35.883	µin/in
Coefficient of Determination	0.9999	
Number of Data Points	50	
Range of Corrected Strain Used	151 - 1424	µin/in

Table C.2: Summary of Three Point Flexural Test for Specimen 1-2-S (Continued)

Corrected Load vs.Bottom Face Deflection

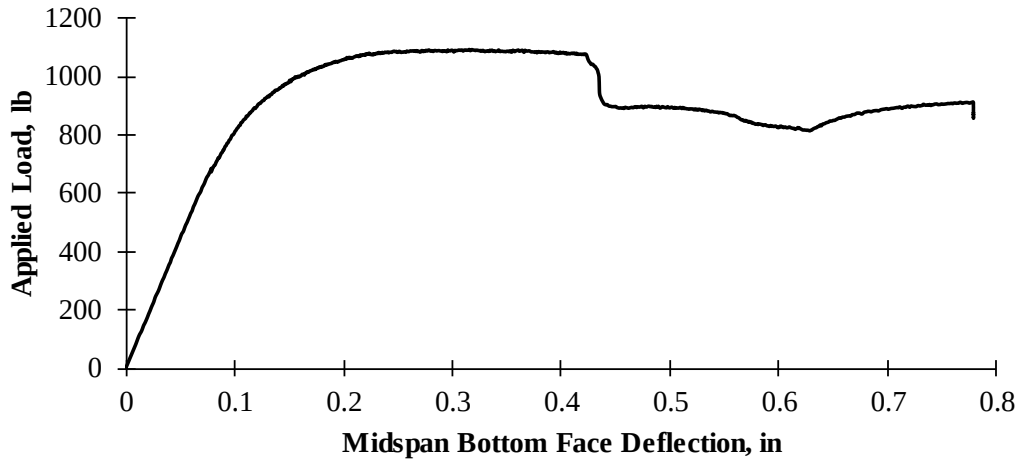

Corrected Load vs. Crosshead Displacement

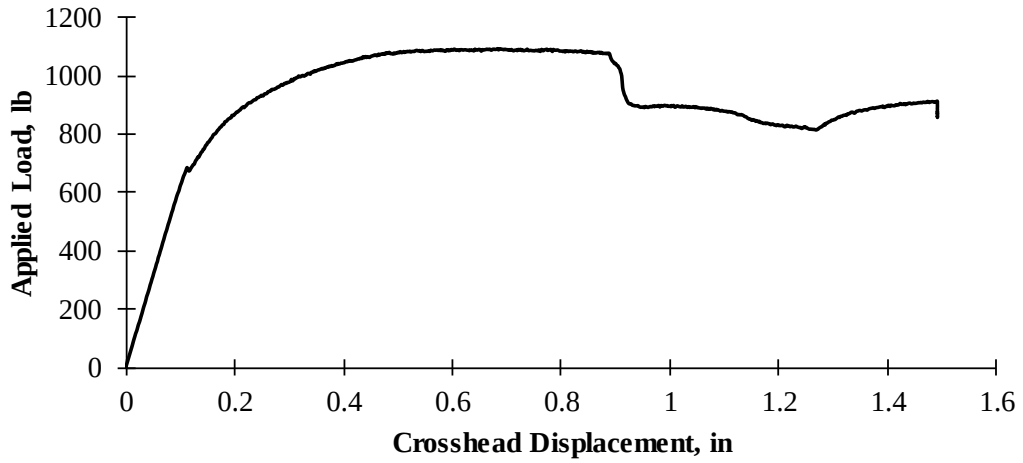

Corrected Load vs.Bottom Face Strain

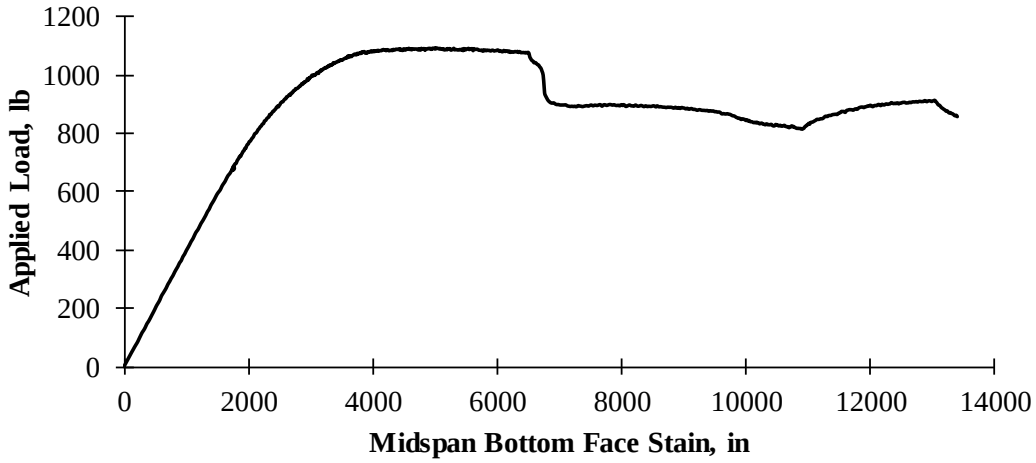

Table C.2: Summary of Three Point Flexural Test for Specimen 1-2-S (Continued)

Strength Analysis		
Initial Failure Mode	Localized Crushing of the Core Coupled with Wrinkling of the Facing Immediately Under the Load (Local Indentation)	
Estimation of the Intial Failure Load Using the Offset Method		
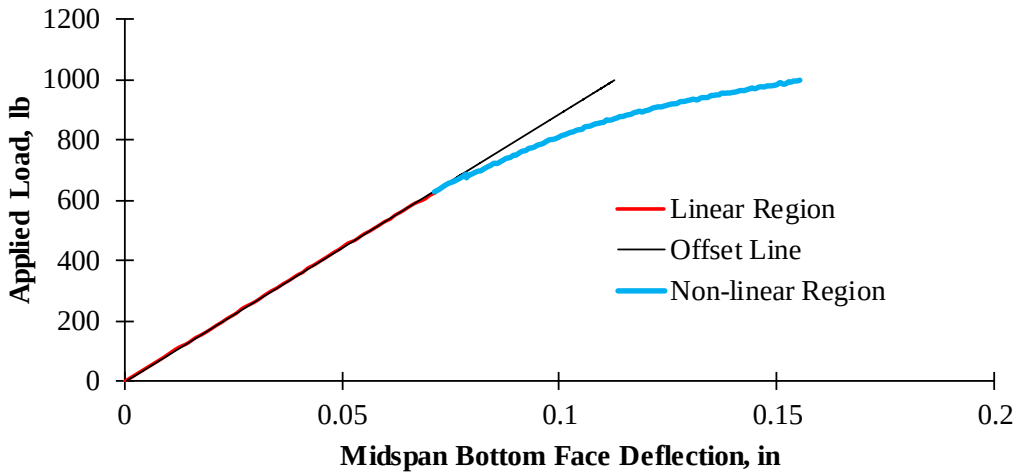		
Offset of Linear Region as a Pecent of Span Length	0.01%	
Load at Initial Failure	627	lb
Max. Internal Bending Moment at Initial Failure	940	lb*in
Max. Internal Shear Force at Initial Failure	313	lb
Average Pressure Under the Load at Initial Failure	210	psi
Max. Average Bending Stress in the Facing	1713	psi
Max. Average Shear Stress in the Core	54	psi
Ultimate Failure Mode	Excessive Crushing of the Core Coupled with Excessive Wrinkling of the Facing Immediately Under the Load (Local Indentation)	
Load at Ultimate Failure	1092	lb
Max. Internal Bending Moment at Ultimate Failure	1638	lb*in
Max. Internal Shear Force at Ultimate Failure	546	lb
Average Pressure Under Load at Ultimate Failure	367	psi
Max. Average Bending Stress in the Facing	2985	psi
Max. Average Shear Stress in the Core	94	psi
Serviceability Analysis		
Limiting Deflection (L/800)	0.0075	in
Load at Limiting Deflection	67	lb
Comparison of Serviceability to Strength		
Ratio of Initial Failure to Serviceability Load	9.4	
Ratio of Ultimate Failure to Serviceability Load	16.4	

Table C.3: Summary of Three Point Flexural Test for Specimen 1-3-S

General Information		
Specimen Label	1-3-S	
Displacement Controlled Loading Rate	0.05	in/min
Data Recording Rate for Load and Displacment	2	Hz
Total Time Elapsed During Testing	14	min
Specimen Dimensions		
Total Height of the Specimen, h	2.133	in
Thickness of the Facings, f	0.095	in
Thickness of the Core, c	1.944	in
Width of the Specimen, b	3.012	in
Ratio of the Core Thickness to Facing Thickness, c/f	20.56	
Moment Arm Between the Facings, d	2.039	in
Length of the Specimen, l	8.0	in
Moment of Inertia of the Facings, I_f	0.592	in^4
Area of the Core, A_c	5.855	in^2
Configuration and Dimension of the Flexural Setup		
Span Between the Supports, L	6.0	in
Width of the Load and Support Bars, l_{pad}	1.0	in
Loading Configuration	3-Point Midspan Loading	
Regression Analysis for Correcting the Load vs. Bottom Face Deflection		
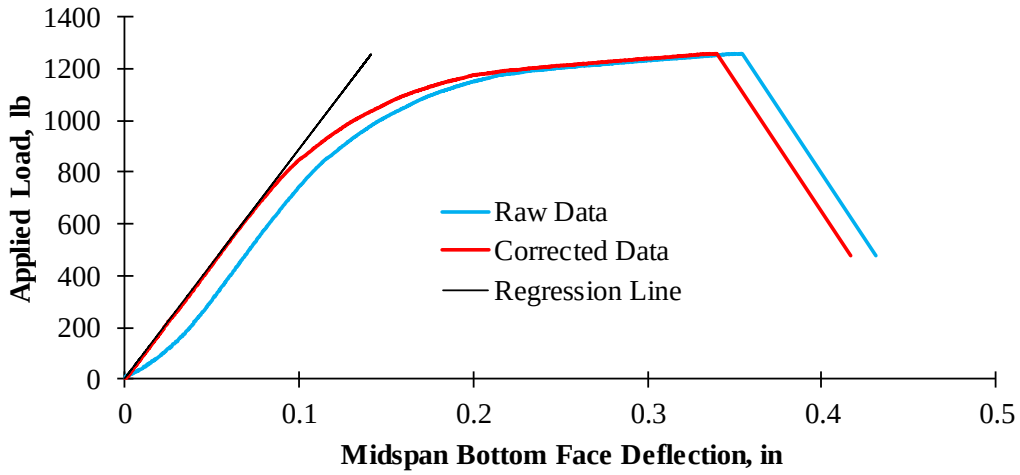		
Slope of the Regression Line	8,867	lb/in
Offset Correction in Bottrom Face Deflection	0.015	in
Coefficient of Determination	0.9998	
Number of Data Points	200	
Range of Corrected Deflection Used	0.022 - 0.078	in

Table C.3: Summary of Three Point Flexural Test for Specimen 1-3-S (Continued)

Regression Analysis for Correcting the Load vs. Crosshead Displacement			
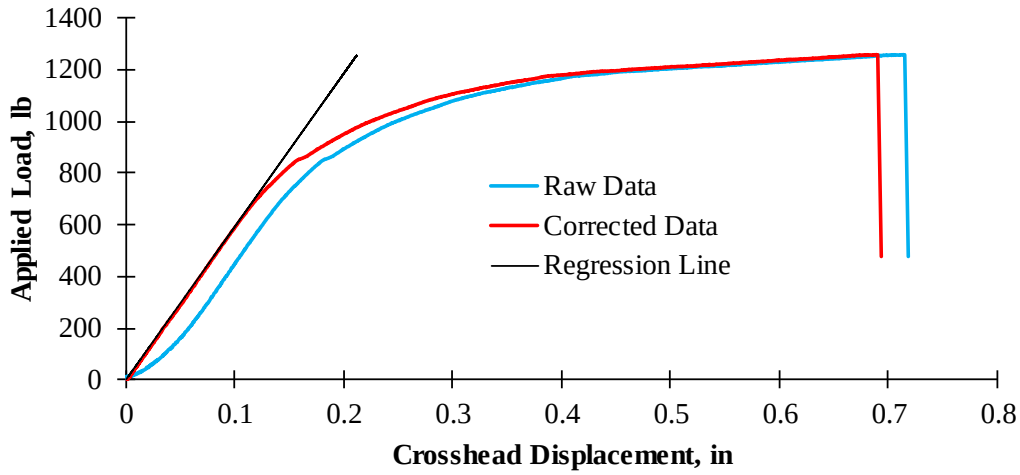			
Slope of the Regression Line	5,929		lb/in
Offset Correction in Crosshead Displacement	0.025		in
Coefficient of Determination	0.9998		
Number of Data Points	200		
Range of Corrected Displacement Used	0.031	- 0.115	in
Regression Analysis for Correcting the Load vs.Bottom Face Strain			
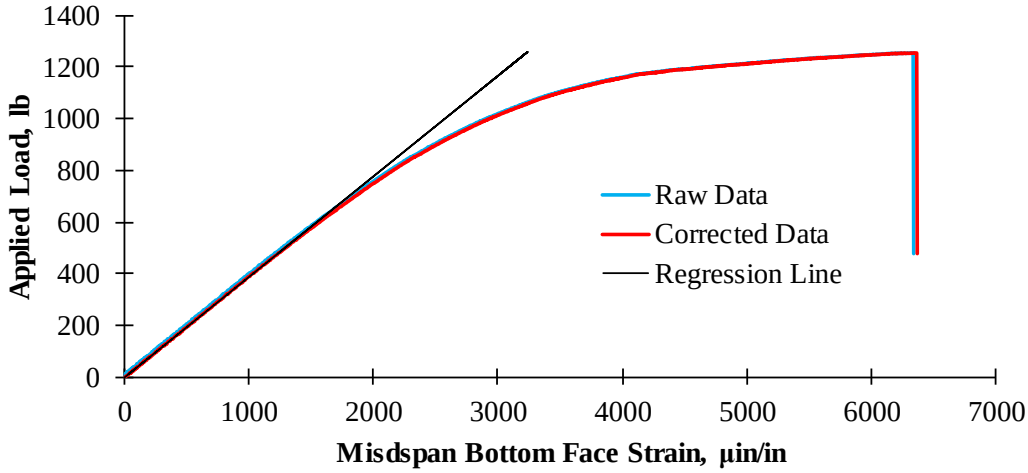			
Slope of the Regression Line	0.388		lb/µin/in
Offset Correction in Bottom Face Strain	-29.710		µin/in
Coefficient of Determination	0.9999		
Number of Data Points	300		
Range of Corrected Strain Used	30	- 1537	µin/in

Table C.3: Summary of Three Point Flexural Test for Specimen 1-3-S (Continued)

Corrected Load vs.Bottom Face Deflection

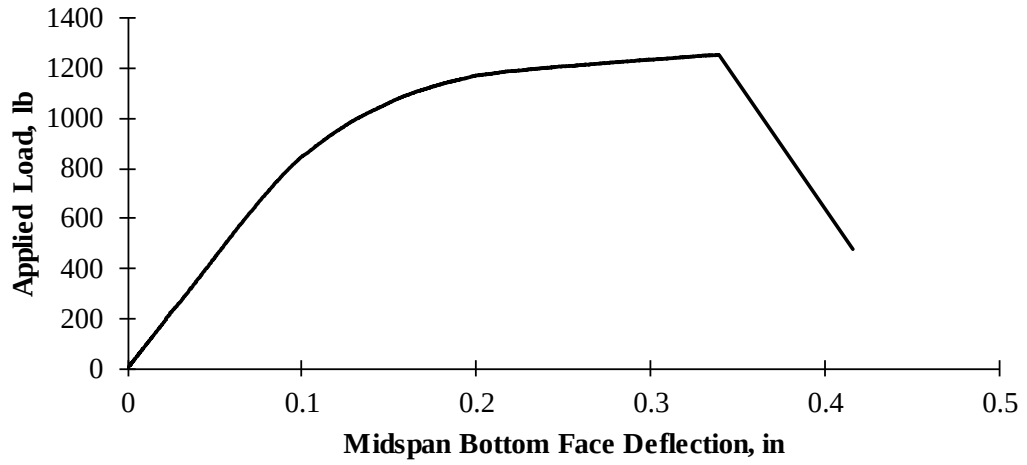

Corrected Load vs.Crosshead Displacement

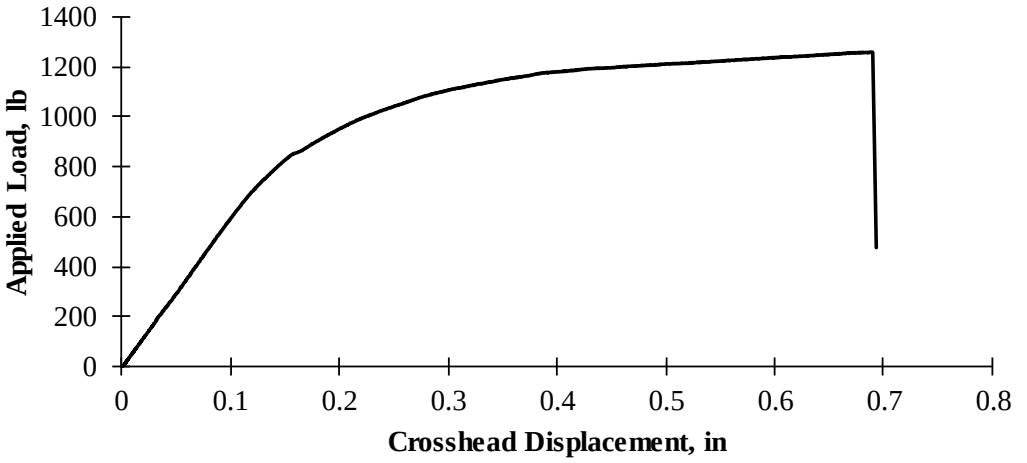

Corrected Load vs.Bottom Face Strain

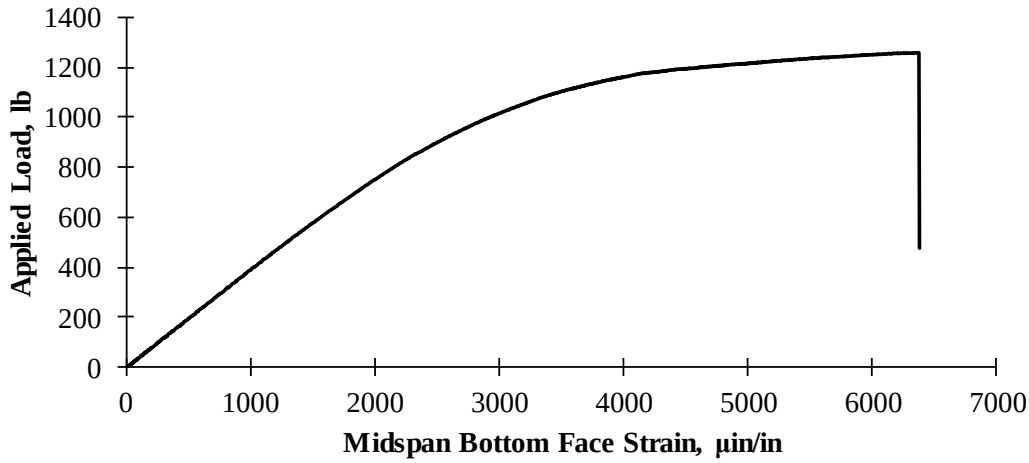

Table C.3: Summary of Three Point Flexural Test for Specimen 1-3-S (Continued)

Strength Analysis		
Initial Failure Mode	Localized Crushing of the Core Coupled with Wrinkling of the Facing Immediately Under the Load (Local Indentation)	
Estimation of the Intial Failure Load Using the Offset Method		
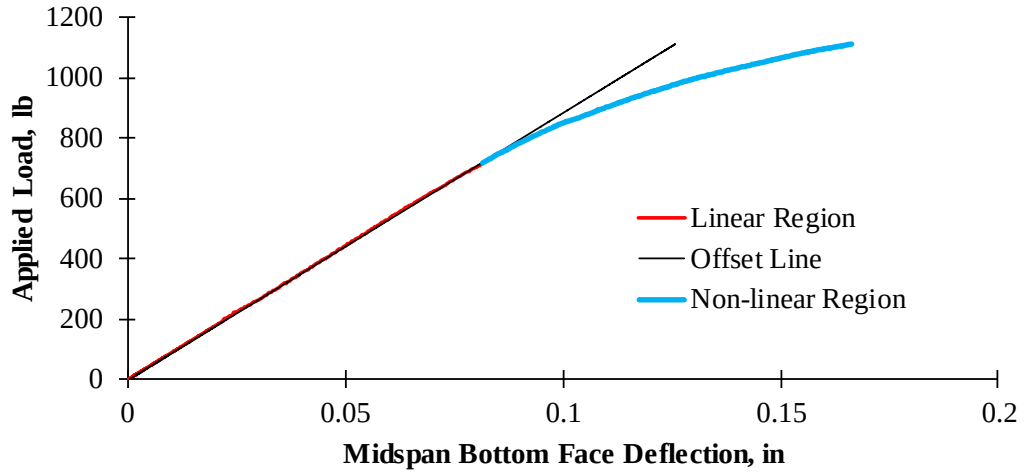		
Offset of Linear Region as a Pecent of Span Length	0.01%	
Load at Initial Failure	714	lb
Max. Internal Bending Moment at Initial Failure	1072	lb*in
Max. Internal Shear Force at Initial Failure	357	lb
Average Pressure Under the Load at Initial Failure	237	psi
Max. Average Bending Stress in the Facing	1931	psi
Max. Average Shear Stress in the Core	61	psi
Ultimate Failure Mode	Shear Failure in the Core Material Characterized by a Sudden Diagonal Fracture	
Load at Ultimate Failure	1257	lb
Max. Internal Bending Moment at Ultimate Failure	1885	lb*in
Max. Internal Shear Force at Ultimate Failure	628	lb
Average Pressure Under Load at Ultimate Failure	417	psi
Max. Average Bending Stress in the Facing	3397	psi
Max. Average Shear Stress in the Core	107	psi
Serviceability Analysis		
Limiting Deflection (L/800)	0.0075	in
Load at Limiting Deflection	67	lb
Comparison of Serviceability to Strength		
Ratio of Initial Failure to Serviceability Load	10.7	
Ratio of Ultimate Failure to Serviceability Load	18.9	

Table C.4: Summary of Three Point Flexural Test for Specimen 1-4-S

General Information		
Specimen Label	1-4-S	
Displacement Controlled Loading Rate	0.05	in/min
Data Recording Rate for Load and Displacment	2	Hz
Total Time Elapsed During Testing	26	min
Specimen Dimensions		
Total Height of the Specimen, h	2.133	in
Thickness of the Facings, f	0.095	in
Thickness of the Core, c	1.944	in
Width of the Specimen, b	3.018	in
Ratio of the Core Thickness to Facing Thickness, c/f	20.56	
Moment Arm Between the Facings, d	2.039	in
Length of the Specimen, l	8.0	in
Moment of Inertia of the Facings, I_f	0.593	in^4
Area of the Core, A_c	5.867	in^2
Configuration and Dimension of the Flexural Setup		
Span Between the Supports, L	6.0	in
Width of the Load and Support Bars, l_{pad}	1.0	in
Loading Configuration	3-Point Midspan Loading	
Regression Analysis for Correcting the Load vs. Bottom Face Deflection		
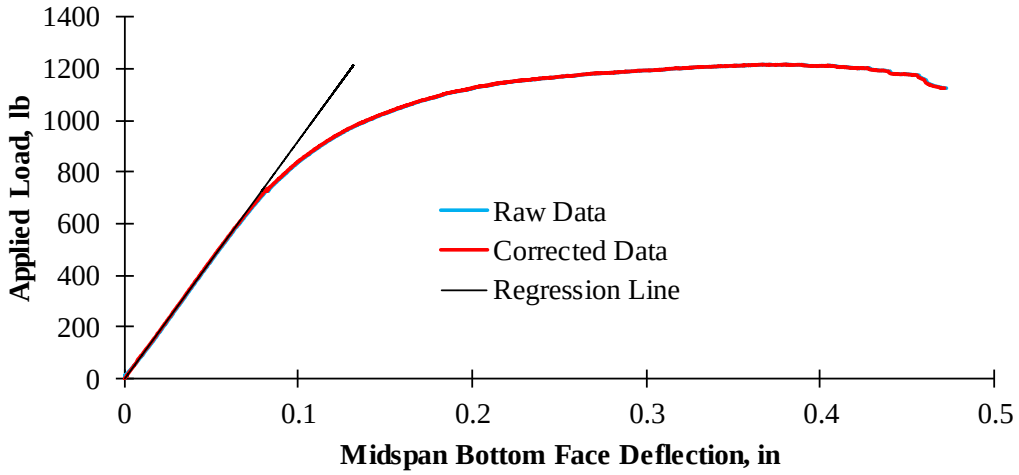		
Slope of the Regression Line	9,207	lb/in
Offset Correction in Bottrom Face Deflection	0.001	in
Coefficient of Determination	0.9999	
Number of Data Points	200	
Range of Corrected Deflection Used	0.008 - 0.064	in

Table C.4: Summary of Three Point Flexural Test for Specimen 1-4-S (Continued)

Regression Analysis for Correcting the Load vs. Crosshead Displacement		
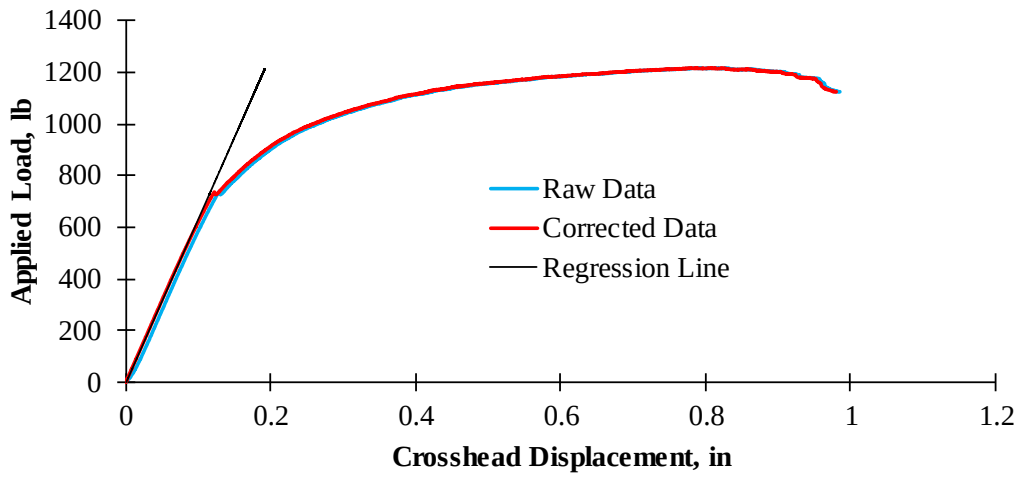		
Slope of the Regression Line	6,337	lb/in
Offset Correction in Crosshead Displacement	0.006	in
Coefficient of Determination	0.9999	
Number of Data Points	100	
Range of Corrected Displacement Used	0.027 - 0.069	in
Regression Analysis for Correcting the Load vs.Bottom Face Strain		
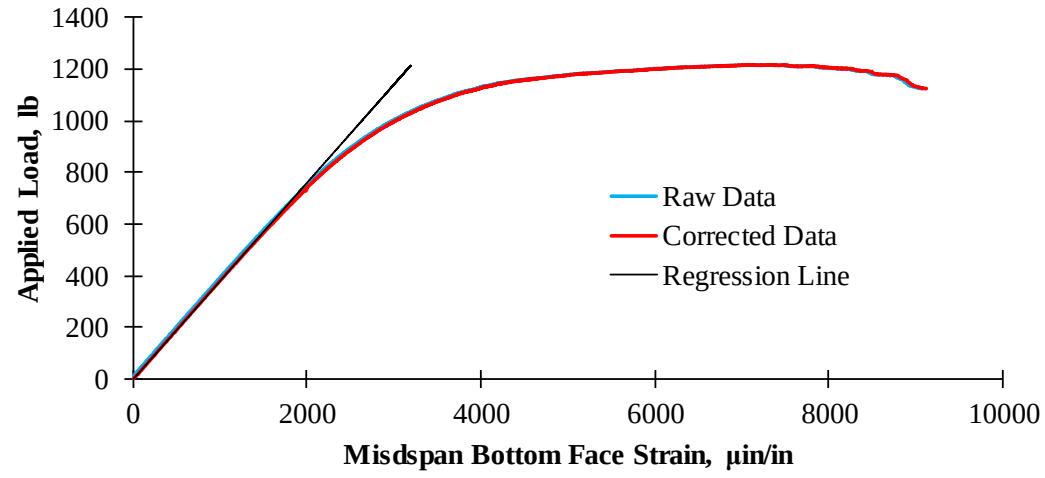		
Slope of the Regression Line	0.380	lb/µin/in
Offset Correction in Bottom Face Strain	-33.648	µin/in
Coefficient of Determination	0.9999	
Number of Data Points	200	
Range of Corrected Strain Used	62 - 1392	µin/in

Table C.4: Summary of Three Point Flexural Test for Specimen 1-4-S (Continued)

Corrected Load vs.Bottom Face Deflection

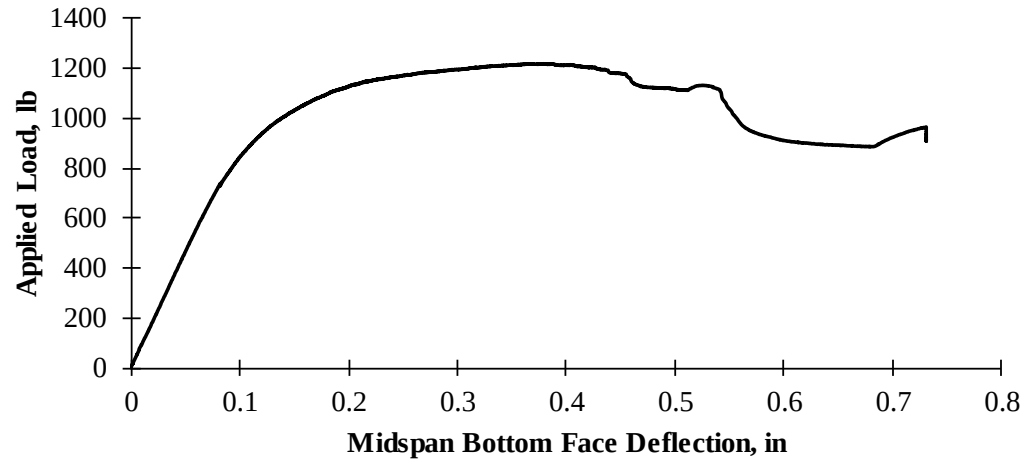

Corrected Load vs.Crosshead Displacement

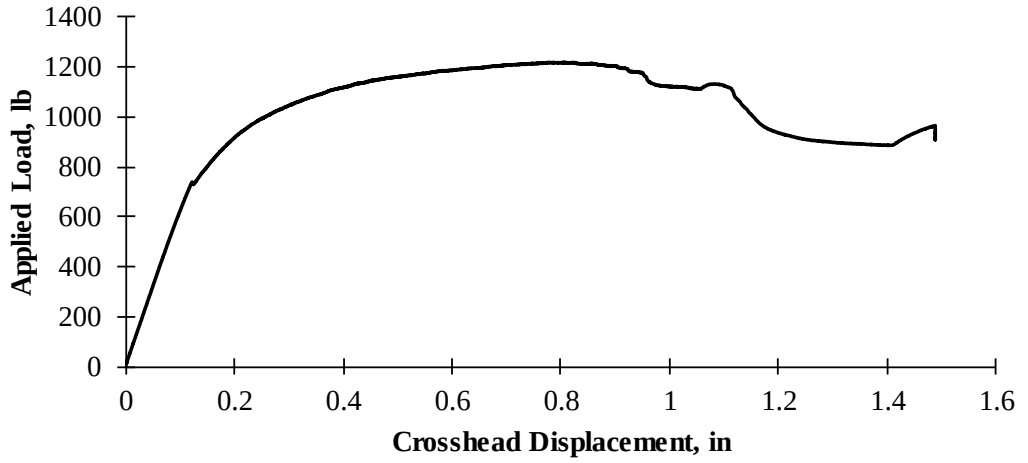

Corrected Load vs.Bottom Face Strain

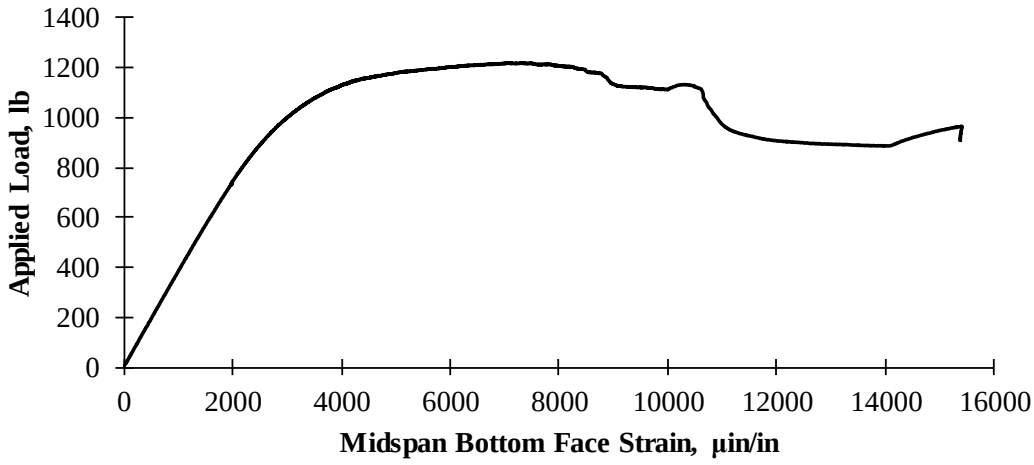

Table C.4: Summary of Three Point Flexural Test for Specimen 1-4-S (Continued)

Strength Analysis		
Initial Failure Mode	Localized Crushing of the Core Coupled with Wrinkling of the Facing Immediately Under the Load (Local Indentation)	
Estimation of the Intial Failure Load Using the Offset Method		
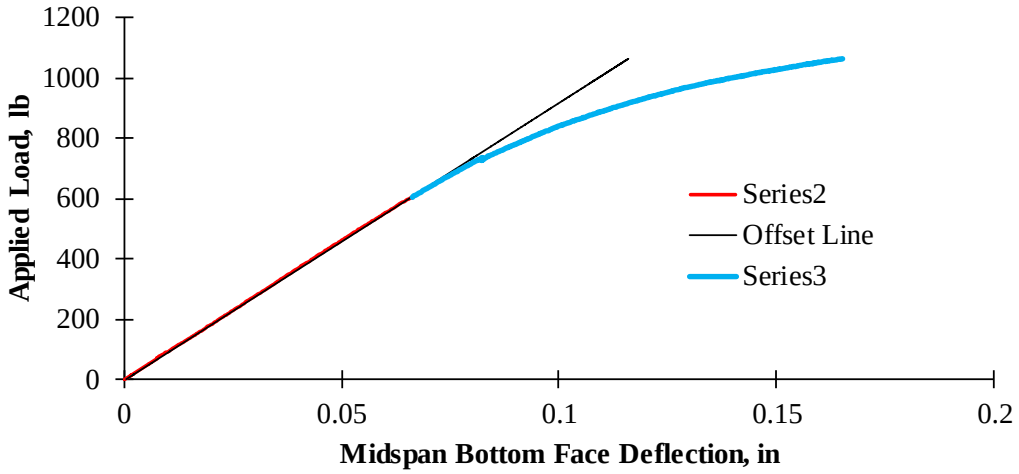		
Offset of Linear Region as a Pecent of Span Length	0.01%	
Load at Initial Failure	601	lb
Max. Internal Bending Moment at Initial Failure	901	lb*in
Max. Internal Shear Force at Initial Failure	300	lb
Average Pressure Under Load at Initial Failure	199	psi
Max. Average Bending Stress in the Facing	1621	psi
Max. Average Shear Stress in the Core	51	psi
Ultimate Failure Mode	Excessive Crushing of the Core Coupled with Excessive Wrinkling of the Facing Immediately Under the Load (Local Indentation)	
Load at Ultimate Failure	1215	lb
Max. Internal Bending Moment at Ultimate Failure	1822	lb*in
Max. Internal Shear Force at Ultimate Failure	607	lb
Average Pressure Under Load at Ultimate Failure	403	psi
Max. Average Bending Stress in the Facing	3278	psi
Max. Average Shear Stress in the Core	104	psi
Serviceability Analysis		
Limiting Deflection (L/800)	0.0075	in
Load at Limiting Deflection	69	lb
Comparison of Serviceability to Strength		
Ratio of Initial Failure to Serviceability Load	8.70	
Ratio of Ultimate Failure to Serviceability Load	17.6	

Table C.5: Summary of Three Point Flexural Test for Specimen 2-1-S

General Information		
Specimen Label	2-1-S	
Displacement Controlled Loading Rate	0.05	in/min
Data Recording Rate for Load and Displacment	2	Hz
Total Time Elapsed During Testing	25	min
Specimen Dimensions		
Total Height of the Specimen, h	2.333	in
Thickness of the Facings, f	0.095	in
Thickness of the Core, c	2.143	in
Width of the Specimen, b	2.989	in
Ratio of the Core Thickness to Facing Thickness, c/f	22.63	
Moment Arm Between the Facings, d	2.238	in
Length of the Specimen, l	8.0	in
Moment of Inertia of the Facings, I_f	0.709	in^4
Area of the Core, A_s	6.407	in^2
Configuration and Dimension of the Flexural Setup		
Span Between the Supports, L	6.0	in
Width of the Load and Support Bars, l_{pad}	1.0	in
Loading Configuration	3-Point Midspan Loading	
Regression Analysis for Correcting the Load vs. Bottom Face Deflection		
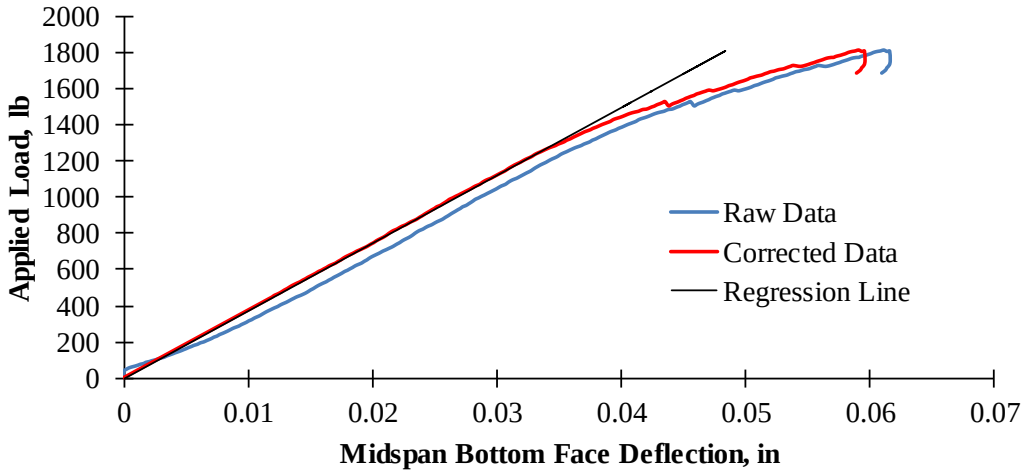		
Slope of the Regression Line	37,385	lb/in
Offset Correction in Bottrom Face Deflection	0.002	in
Coefficient of Determination	0.9999	
Number of Data Points	100	
Range of Corrected Deflection Used	0.012 - 0.034	in

Table C.5: Summary of Three Point Flexural Test for Specimen 2-1-S (Continued)

Regression Analysis for Correcting the Load vs. Crosshead Displacement			
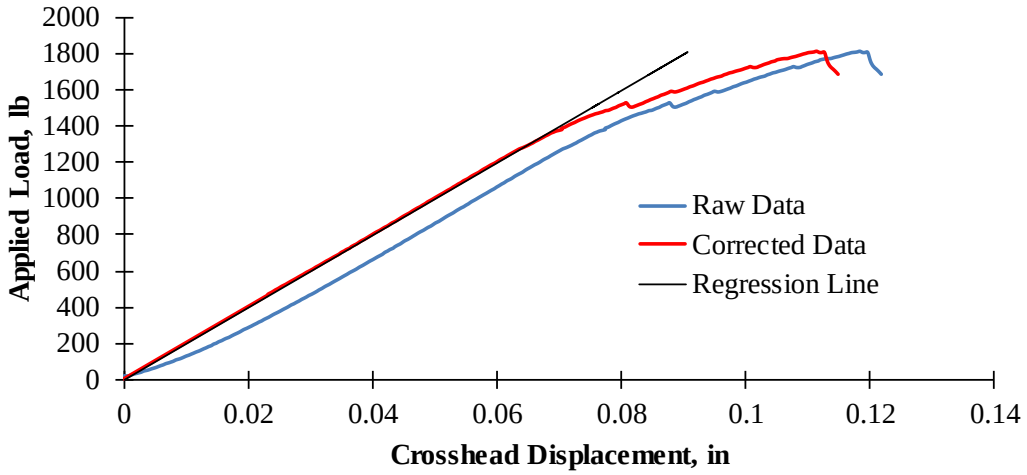			
Slope of the Regression Line	19,981		lb/in
Offset Correction in Crosshead Displacement	0.007		in
Coefficient of Determination	1.0000		
Number of Data Points	100		
Range of Corrected Displacement Used	0.023	- 0.064	in
Regression Analysis for Correcting the Load vs.Bottom Face Strain			
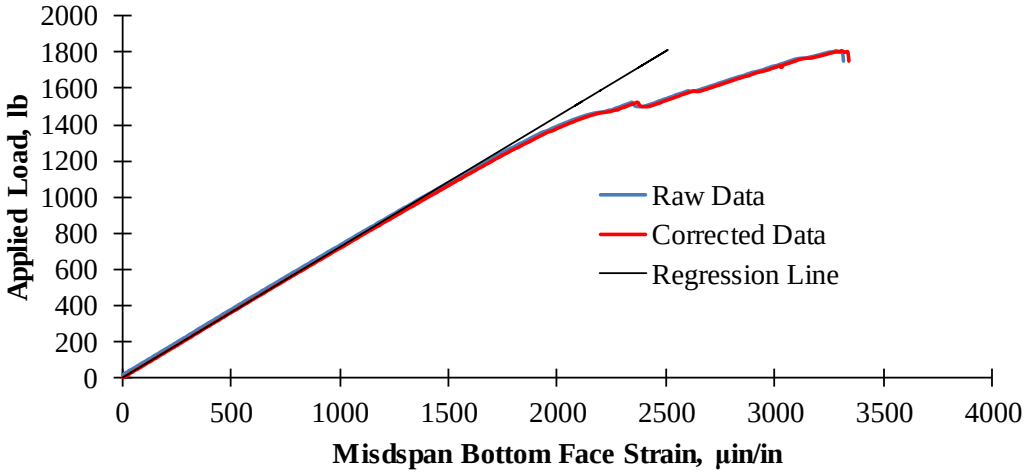			
Slope of the Regression Line	0.723		lb/µin/in
Offset Correction in Bottom Face Strain	-25		µin/in
Coefficient of Determination	1.0000		
Number of Data Points	100		
Range of Corrected Strain Used	25	- 914	µin/in

Table C.5: Summary of Three Point Flexural Test for Specimen 2-1-S (Continued)

Corrected Load vs.Bottom Face Deflection

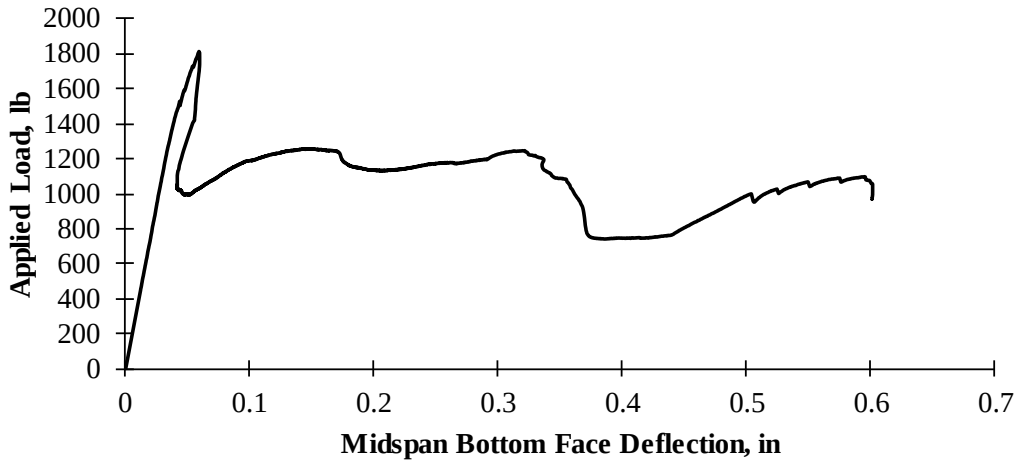

Corrected Load vs.Crosshead Displacement

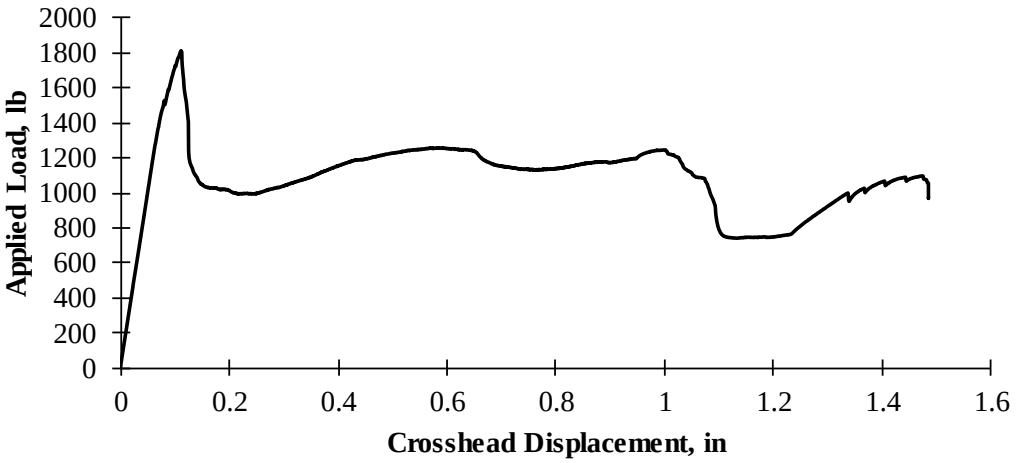

Corrected Load vs.Bottom Face Strain

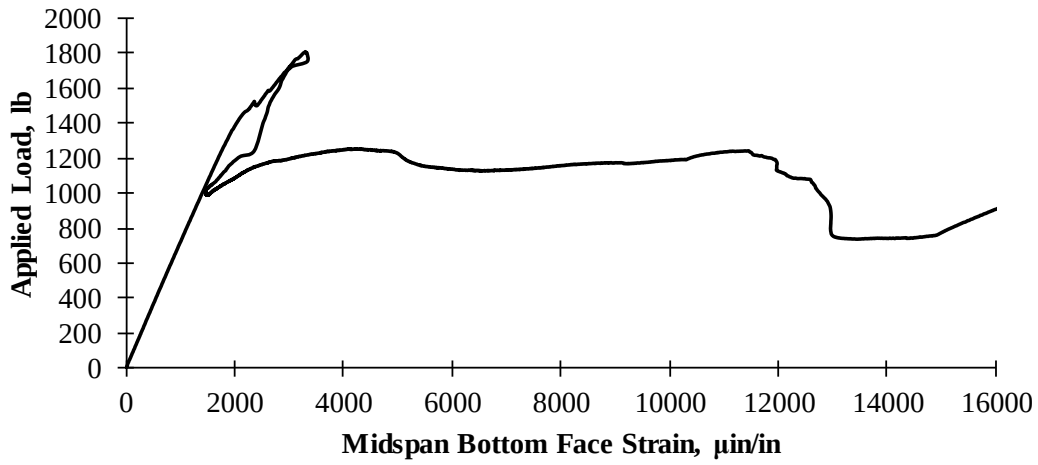

Table C.5: Summary of Three Point Flexural Test for Specimen 2-1-S (Continued)

Strength Analysis		
Initial Failure Mode	Localized Crushing of the Core Coupled with Wrinkling of the Top Facing Immediately Under the Load (Local Indentation)	
Estimation of the Intial Failure Load Using the Offset Method		
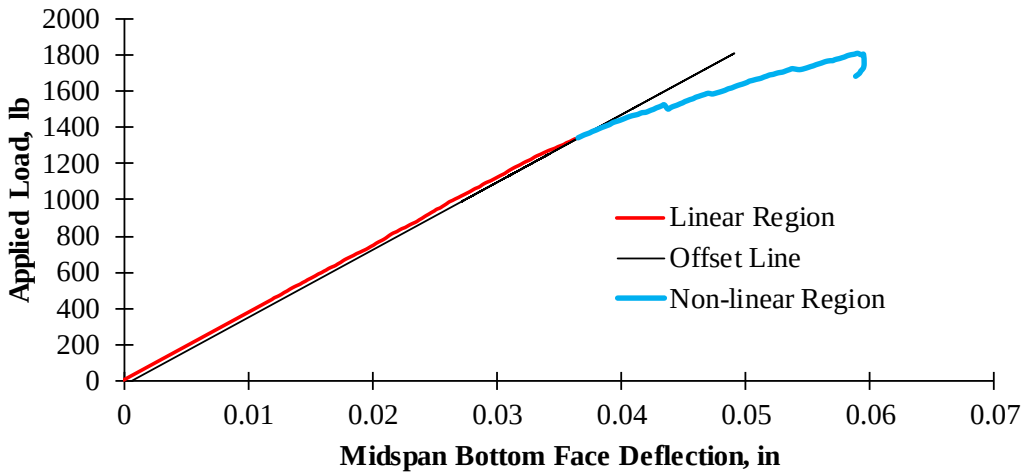		
Offset of Linear Region as a Pecent of Span Length	0.01%	
Load at Initial Failure	1344	lb
Max. Internal Bending Moment at Initial Failure	2015	lb*in
Max. Internal Shear Force at Initial Failure	672	lb
Average Pressure Under the Load at Initial Failure	450	psi
Max. Average Bending Stress in the Facings	3316	psi
Max. Average Shear Stress in the Core	105	psi
Ultimate Failure Mode	Excessive Crushing of the Core Coupled with Excessive Wrinkling of the Top Facing Immediately Under the Load (Local Indentation)	
Load at Ultimate Failure	1812	lb
Max. Internal Bending Moment at Ultimate Failure	2718	lb*in
Max. Internal Shear Force at Ultimate Failure	906	lb
Average Pressure Under Load at Ultimate Failure	606	psi
Max. Average Bending Stress in the Facing	4471	psi
Max. Average Shear Stress in the Core	141	psi
Serviceability Analysis		
Limiting Deflection (L/800)	0.0075	in
Load at Limiting Deflection	280	lb
Comparison of Serviceability to Strength		
Ratio of Initial Failure to Serviceability Load	4.79	
Ratio of Ultimate Failure to Serviceability Load	6.46	

Table C.6: Summary of Three Point Flexural Test for Specimen 2-2-S

General Information		
Specimen Label	2-2-S	
Displacement Controlled Loading Rate	0.05	in/min
Data Recording Rate for Load and Displacment	2	Hz
Total Time Elapsed During Testing	25	min
Specimen Dimensions		
Total Height of the Specimen, h	2.333	in
Thickness of the Facings, f	0.095	in
Thickness of the Core, c	2.143	in
Width of the Specimen, b	3.019	in
Ratio of the Core Thickness to Facing Thickness, c/f	22.63	
Moment Arm Between the Facings, d	2.238	in
Length of the Specimen, l	8.0	in
Moment of Inertia of the Facings, I_f	0.716	in^4
Area of the Longitudinal Stitches, A_s	6.472	in^2
Configuration and Dimension of the Flexural Setup		
Span Between the Supports, L	6.0	in
Width of the Load and Support Bars, l_{pad}	1.0	in
Loading Configuration	3-Point Midspan Loading	
Regression Analysis for Correcting the Load vs. Bottom Face Deflection		
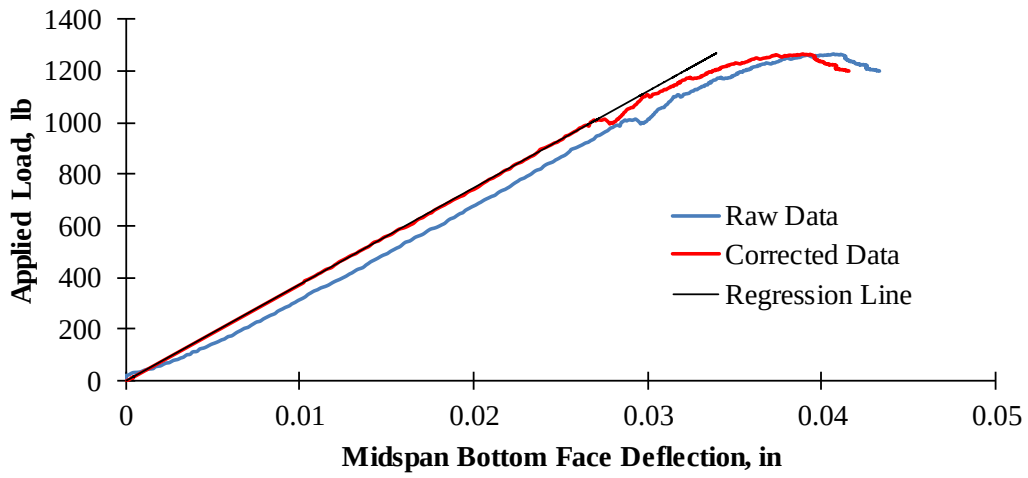		
Slope of the Regression Line	37,335	lb/in
Offset Correction in Bottrom Face Deflection	0.002	in
Coefficient of Determination	0.9998	
Number of Data Points	100	
Range of Corrected Deflection Used	0.010 - 0.027	in

Table C.6: Summary of Three Point Flexural Test for Specimen 2-2-S (Continued)

Regression Analysis for Correcting the Load vs. Crosshead Displacement			
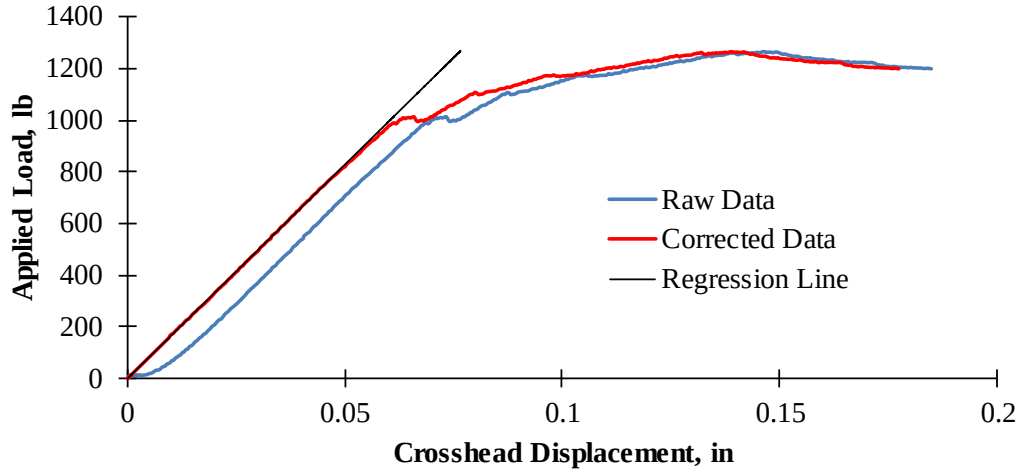			
Slope of the Regression Line	16,509		lb/in
Offset Correction in Crosshead Displacement	0.007		in
Coefficient of Determination	0.9999		
Number of Data Points	100		
Range of Corrected Displacement Used	0.010	- 0.050	in
Regression Analysis for Correcting the Load vs.Bottom Face Strain			
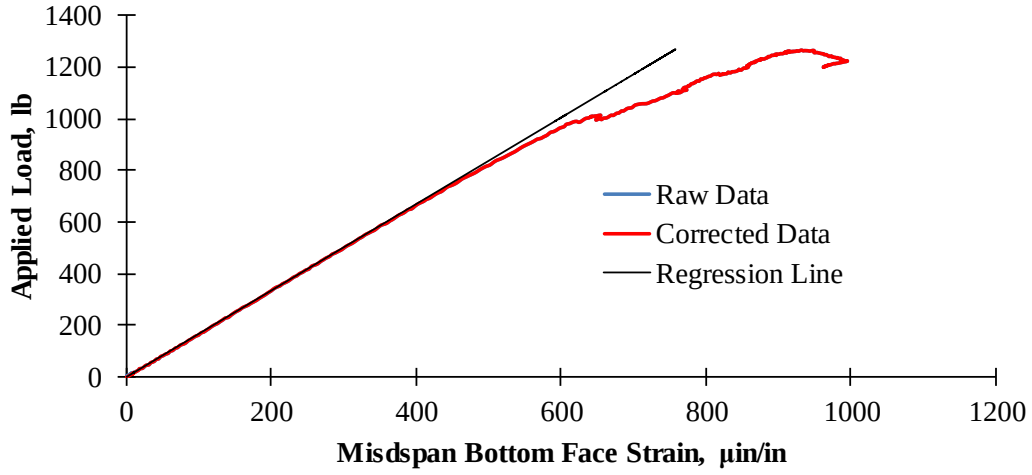			
Slope of the Regression Line	1.670		lb/µin/in
Offset Correction in Bottom Face Strain	0.338		µin/in
Coefficient of Determination	0.9999		
Number of Data Points	100		
Range of Corrected Strain Used	19	- 394	µin/in

Table C.6: Summary of Three Point Flexural Test for Specimen 2-2-S (Continued)

Corrected Load vs.Bottom Face Deflection

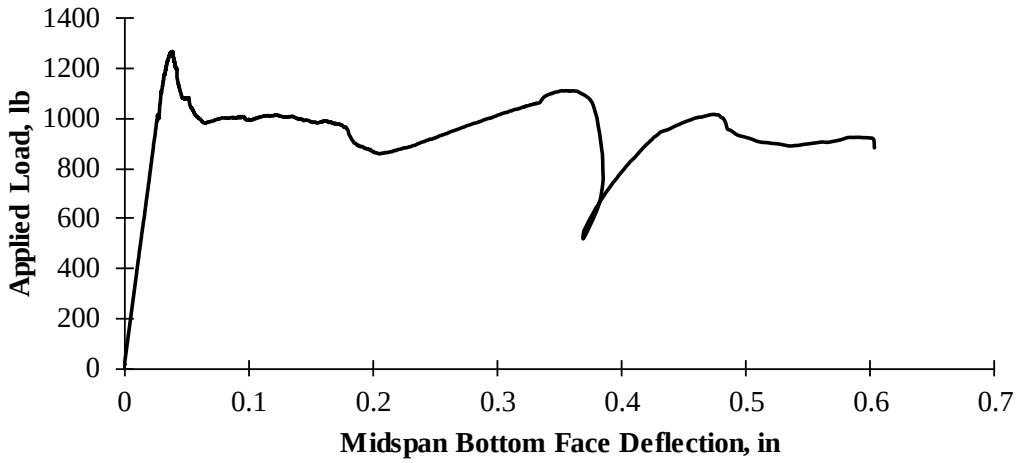

Corrected Load vs.Crosshead Displacement

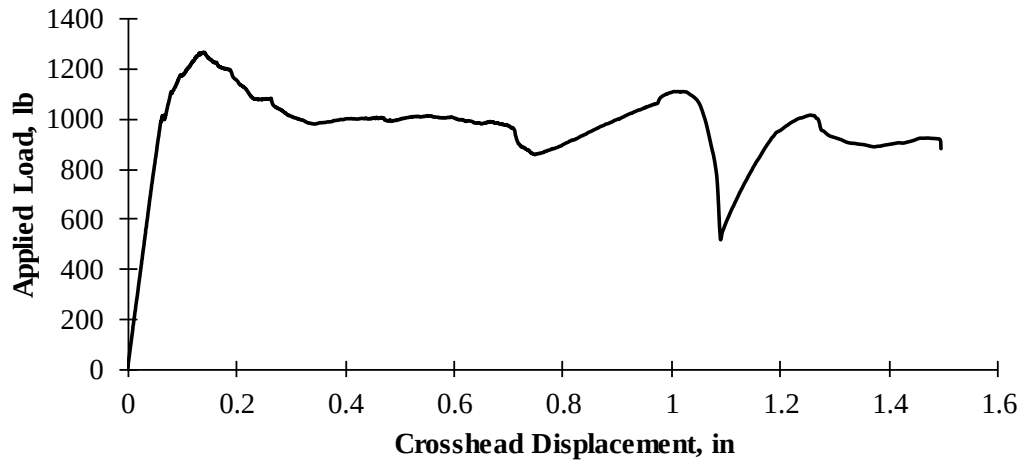

Corrected Load vs.Bottom Face Strain

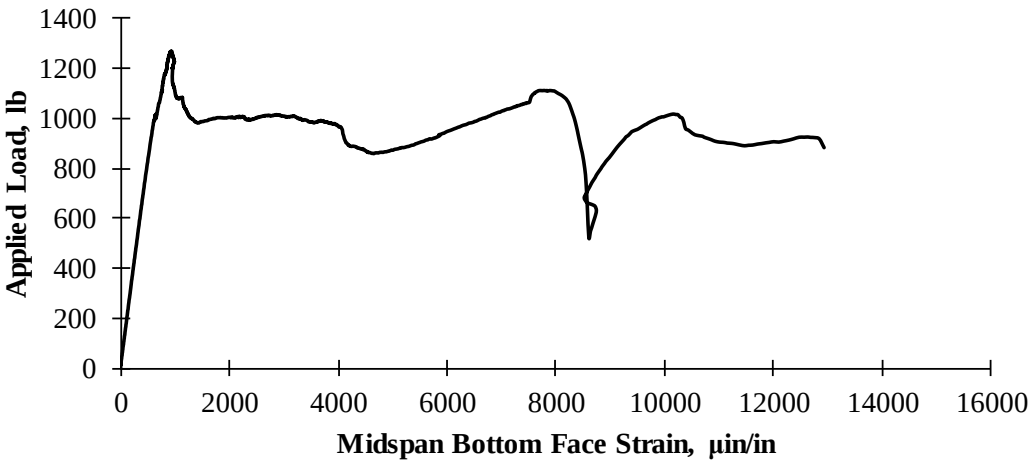

Table C.6: Summary of Three Point Flexural Test for Specimen 2-2-S (Continued)

Strength Analysis		
Initial Failure Mode	Localized Crushing of the Core Coupled with Wrinkling of the Top Facing Immediately Under the Load (Local Indentation)	
Estimation of the Intial Failure Load Using the Offset Method		
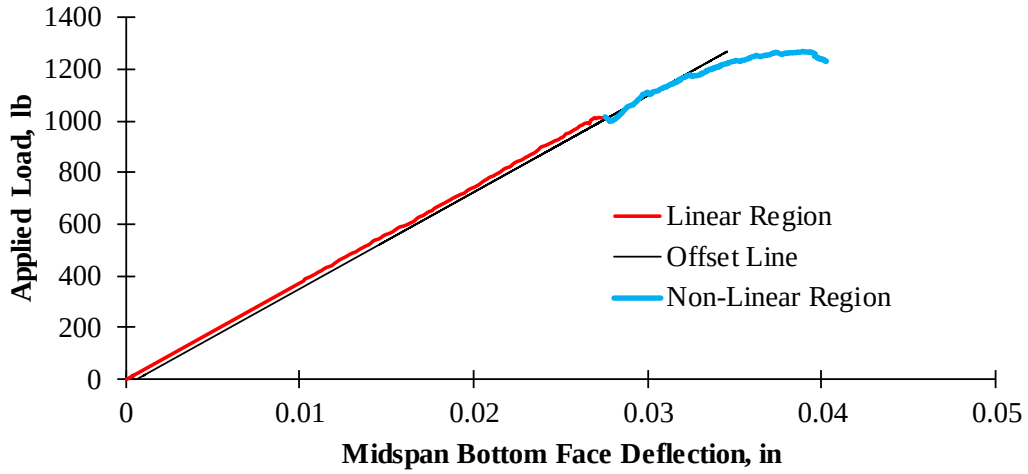		
Offset of Linear Region as a Pecent of Span Length	0.01%	
Load at Initial Failure	1015	lb
Max. Internal Bending Moment at Initial Failure	1522	lb*in
Max. Internal Shear Force at Initial Failure	507	lb
Average Pressure Under the Load at Initial Failure	336	psi
Max. Average Bending Stress in the Facings	2479	psi
Max. Average Shear Stress in the Core	78	psi
Ultimate Failure Mode	Excessive Crushing of the Core Coupled with Excessive Wrinkling of the Top Facing Immediately Under the Load (Local Indentation)	
Load at Ultimate Failure	1267	lb
Max. Internal Bending Moment at Ultimate Failure	1900	lb*in
Max. Internal Shear Force at Ultimate Failure	633	lb
Average Pressure Under Load at Ultimate Failure	420	psi
Max. Average Bending Stress in the Facing	3095	psi
Max. Average Shear Stress in the Core	98	psi
Serviceability Analysis		
Limiting Deflection (L/800)	0.0075	in
Load at Limiting Deflection	280	lb
Comparison of Serviceability to Strength		
Ratio of Initial Failure to Serviceability Load	3.62	
Ratio of Ultimate Failure to Serviceability Load	4.52	

Table C.7: Summary of Three Point Flexural Test for Specimen 2-3-S

General Information		
Specimen Label	2-3-S	
Displacement Controlled Loading Rate	0.05	in/min
Data Recording Rate for Load and Displacment	2	Hz
Total Time Elapsed During Testing	26	min
Specimen Dimensions		
Total Height of the Specimen, h	2.333	in
Thickness of the Facings, f	0.095	in
Thickness of the Core, c	2.143	in
Width of the Specimen, b	2.972	in
Ratio of the Core Thickness to Facing Thickness, c/f	22.63	
Moment Arm Between the Facings, d	2.238	in
Length of the Specimen, l	8.0	in
Moment of Inertia of the Facings, I_f	0.705	in^4
Area of the Longitudinal Stitches, A_s	6.371	in^2
Configuration and Dimension of the Flexural Setup		
Span Between the Supports, L	6.0	in
Width of the Load and Support Bars, l_{pad}	1.0	in
Loading Configuration	3-Point Midspan Loading	
Regression Analysis for Correcting the Load vs. Bottom Face Deflection		
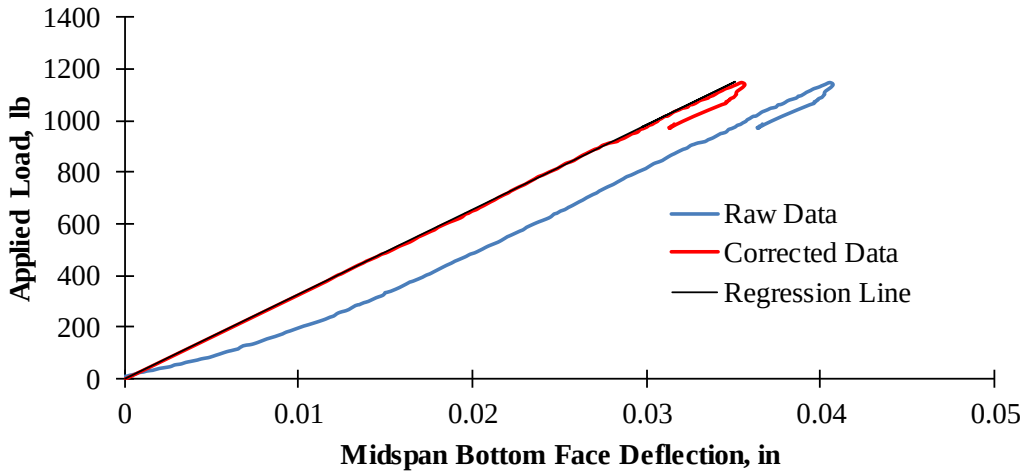		
Slope of the Regression Line	32,770	lb/in
Offset Correction in Bottrom Face Deflection	0.005	in
Coefficient of Determination	0.9996	
Number of Data Points	100	
Range of Corrected Deflection Used	0.012 - 0.031	in

Table C.7: Summary of Three Point Flexural Test for Specimen 2-3-S (Continued)

Regression Analysis for Correcting the Load vs. Crosshead Displacement			
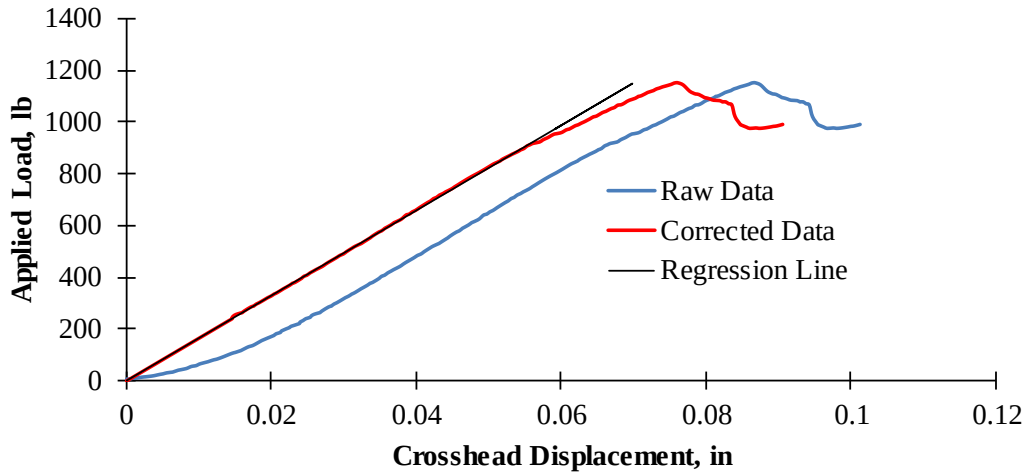			
Slope of the Regression Line	16,468		lb/in
Offset Correction in Crosshead Displacement	0.011		in
Coefficient of Determination	0.9998		
Number of Data Points	100		
Range of Corrected Displacement Used	0.010	- 0.050	in
Regression Analysis for Correcting the Load vs.Bottom Face Strain			
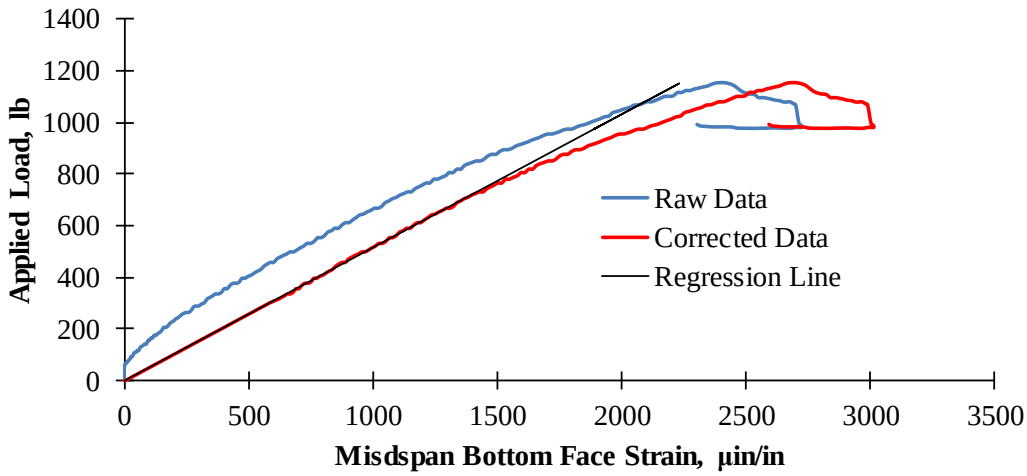			
Slope of the Regression Line	0.516		lb/µin/in
Offset Correction in Bottom Face Strain	-289		µin/in
Coefficient of Determination	0.9990		
Number of Data Points	60		
Range of Corrected Strain Used	622	- 1368	µin/in

Table C.7: Summary of Three Point Flexural Test for Specimen 2-3-S (Continued)

Corrected Load vs.Bottom Face Deflection

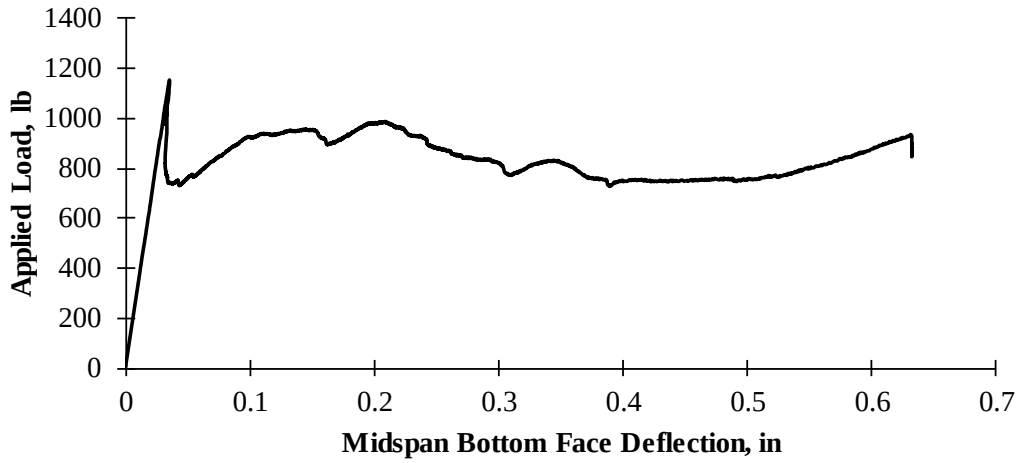

Corrected Load vs.Crosshead Displacement

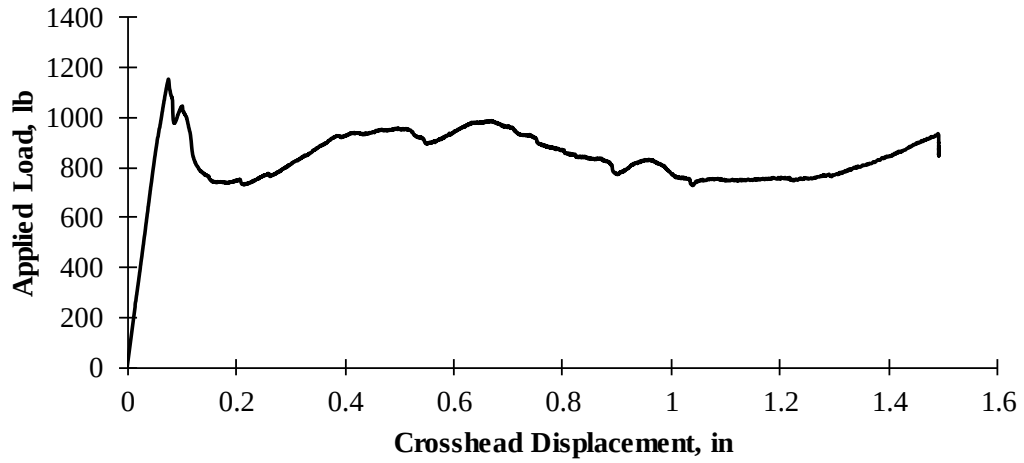

Corrected Load vs.Bottom Face Strain

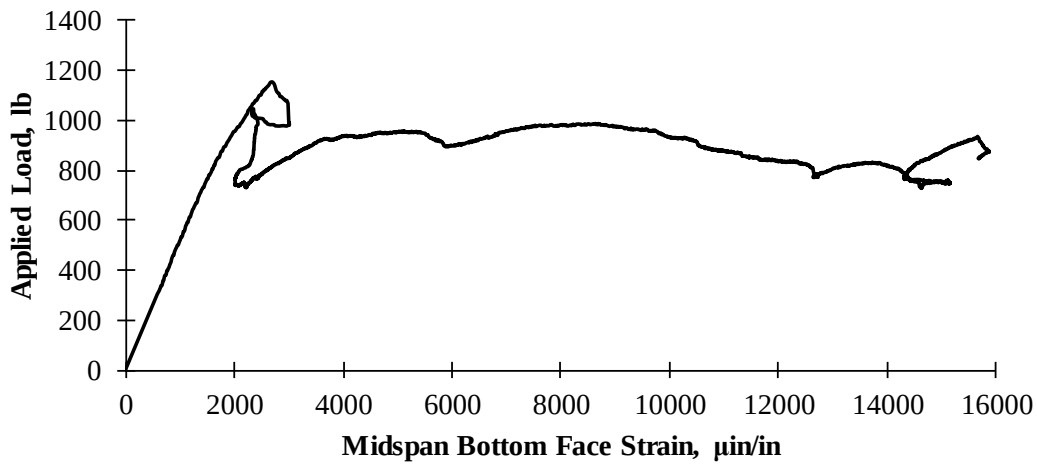

Table C.7: Summary of Three Point Flexural Test for Specimen 2-3-S (Continued)

Strength Analysis		
Initial Failure Mode	Localized Crushing of the Core Coupled with Wrinkling of the Top Facing Immediately Under the Load (Local Indentation)	
Estimation of the Intial Failure Load Using the Offset Method		
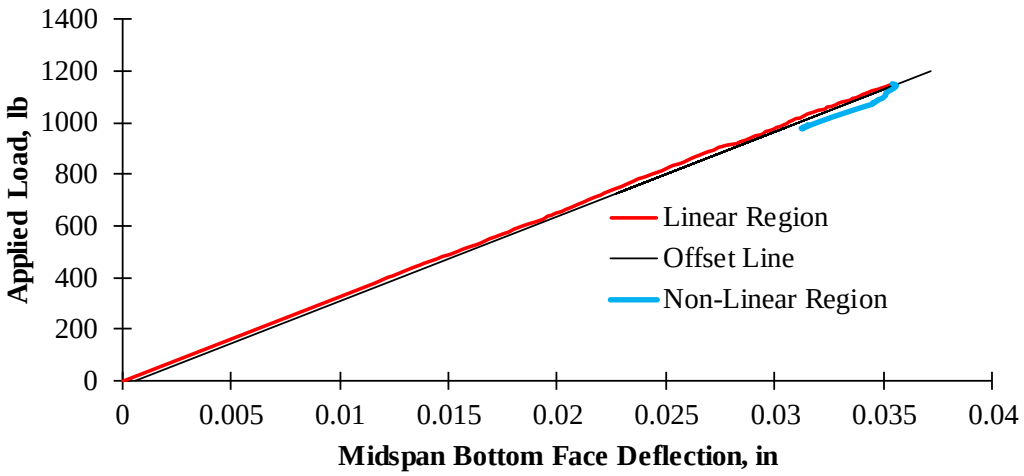		
Offset of Linear Region as a Pecent of Span Length	0.01%	
Load at Initial Failure	1150	lb
Max. Internal Bending Moment at Initial Failure	1725	lb*in
Max. Internal Shear Force at Initial Failure	575	lb
Average Pressure Under the Load at Initial Failure	387	psi
Max. Average Bending Stress in the Facings	2853	psi
Max. Average Shear Stress in the Core	90	psi
Ultimate Failure Mode	Excessive Crushing of the Core Coupled with Excessive Wrinkling of the Top Facing Immediately Under the Load (Local Indentation)	
Load at Ultimate Failure	1150	lb
Max. Internal Bending Moment at Ultimate Failure	1725	lb*in
Max. Internal Shear Force at Ultimate Failure	575	lb
Average Pressure Under Load at Ultimate Failure	387	psi
Max. Average Bending Stress in the Facing	2853	psi
Max. Average Shear Stress in the Core	90	psi
Serviceability Analysis		
Limiting Deflection (L/800)	0.0075	in
Load at Limiting Deflection	246	lb
Comparison of Serviceability to Strength		
Ratio of Initial Failure to Serviceability Load	4.68	
Ratio of Ultimate Failure to Serviceability Load	4.68	

Table C.8: Summary of Three Point Flexural Test for Specimen 3-1-S

General Information		
Specimen Label	3-1-S	
Displacement Controlled Loading Rate	0.1	in/min
Data Recording Rate for Load and Displacment	2	Hz
Total Time Elapsed During Testing	15	min
Specimen Dimensions		
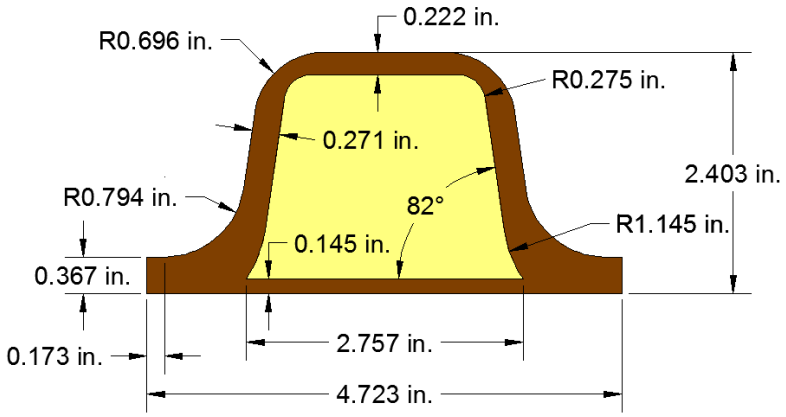		
Total Height, h	2.403	in
Width of the Loading Area, w_{pad}	1.206	in
Total Area of the Cross-section, A	7.288	in^2
Moment of Inertia of the FRP, I_{frp}	1.913	in^4
Area of the FRP, A_{frp}	2.747	in^2
Centriod of the FRP, $\bar{y}_{frp}$	0.906	in
Length of the Specimen, l	8.0	in
Configuration and Dimension of the Flexural Setup		
Span Between the Supports, L	6.0	in
Width of the Load and Support Bars, l_{pad}	1.0	in
Loading Configuration	3-Point Midspan Loading	
Regression Analysis for Correcting the Load vs. Bottom Face Deflection		
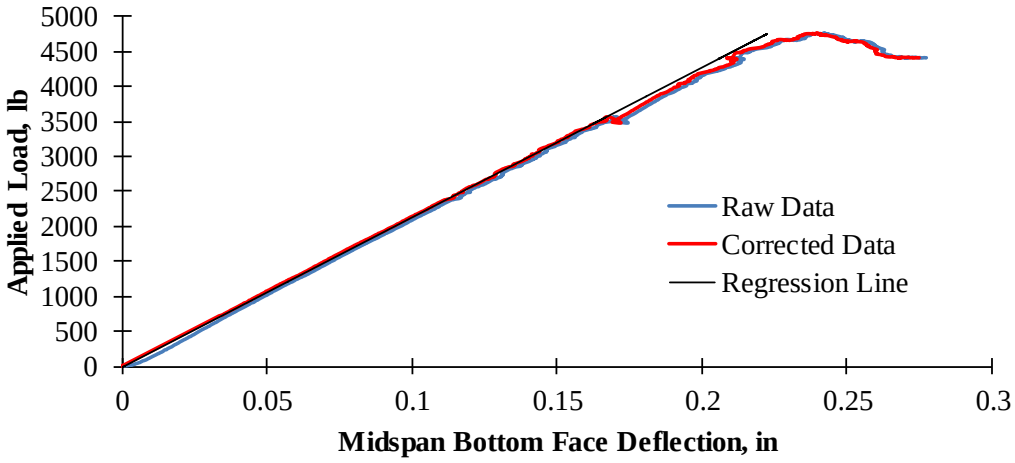		

Table C.8: Summary of Three Point Flexural Test for Specimen 3-1-S (Continued)

Slope of the Regression Line	21,396	lb/in
Offset Correction in Bottrom Face Deflection	0.002	in
Coefficient of Determination	0.9999	
Number of Data Points	300	
Range of Corrected Deflection Used	0.034 - 0.111	in
Regression Analysis for Correcting the Load vs. Crosshead Displacement		
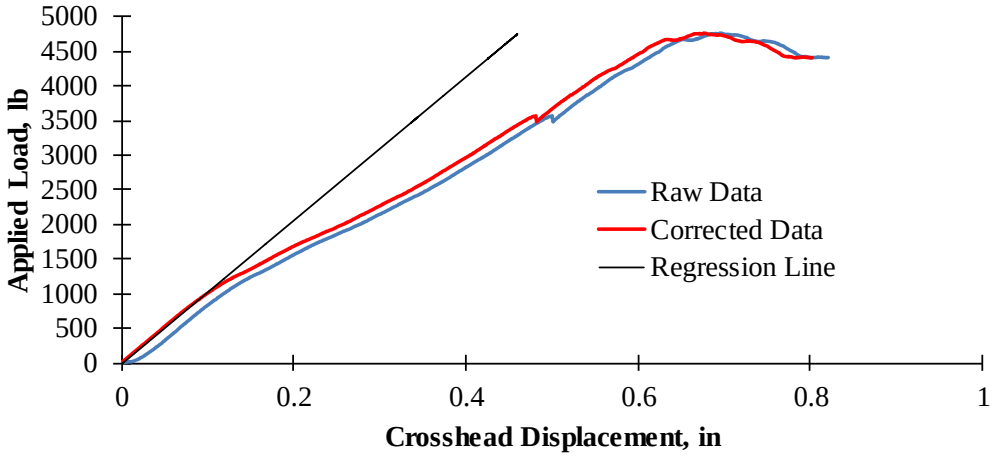		
Slope of the Regression Line	10,375	lb/in
Offset Correction in Displacement	0.020	in
Coefficient of Determination	0.9998	
Number of Data Points	70	
Range of Corrected Displacement Used	0.023 - 0.078	in
Regression Analysis for Correcting the Load vs.Bottom Face Strain		
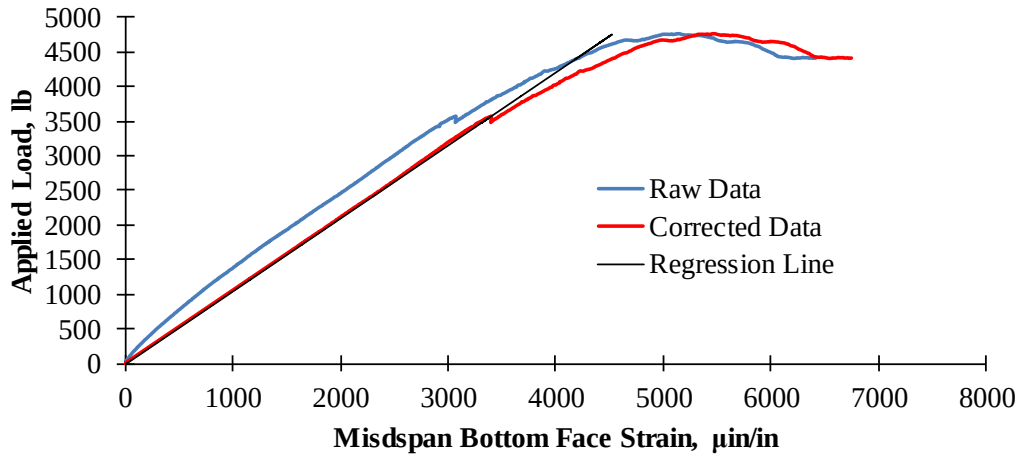		
Slope of the Regression Line	1.054	lb/µin/in
Offset Correction in Bottom Face Strain	-329.606	µin/in
Coefficient of Determination	0.9999	
Number of Data Points	200	
Range of Corrected Strain Used	1581 - 2538	µin/in

Table C.8: Summary of Three Point Flexural Test for Specimen 3-1-S (Continued)

Corrected Load vs.Bottom Face Deflection

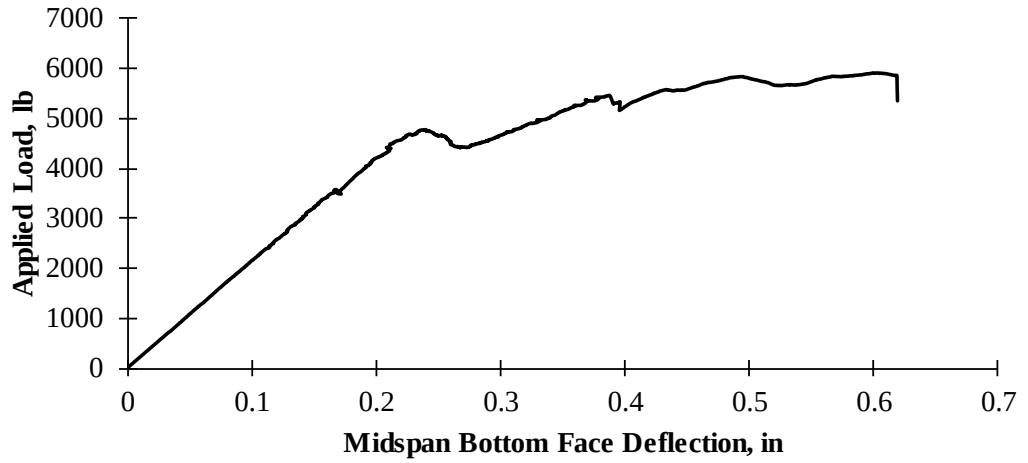

Corrected Load vs.Crosshead Displacement

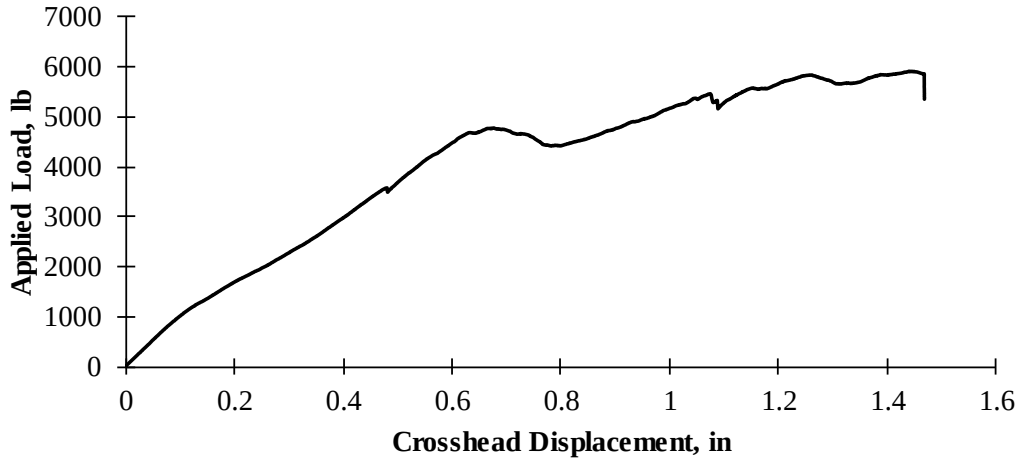

Corrected Load vs.Bottom Face Strain

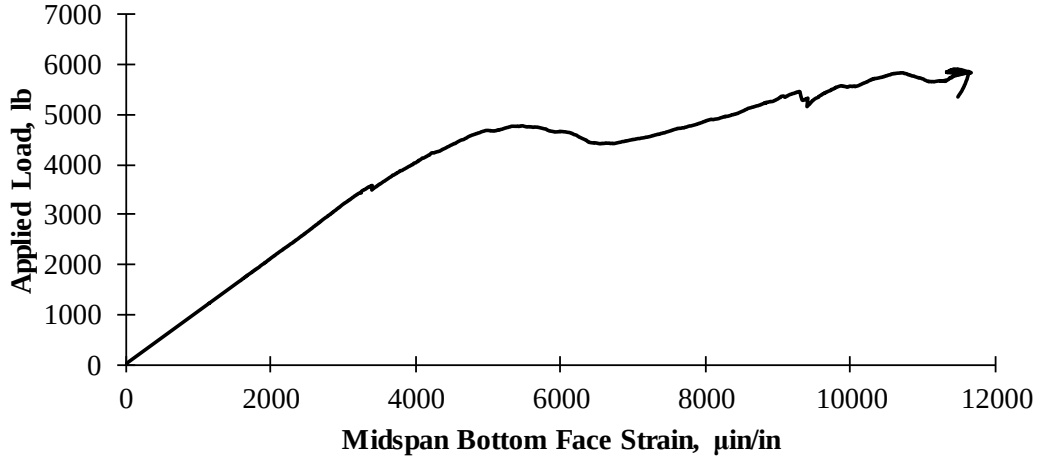

Table C.8: Summary of Three Point Flexural Test for Specimen 3-1-S (Continued)

Strength Analysis		
Initial Failure Mode	Delamination Between the Shear Layers Immediately Above the Support	
Estimation of the Intial Failure Load Using the Offset Method		
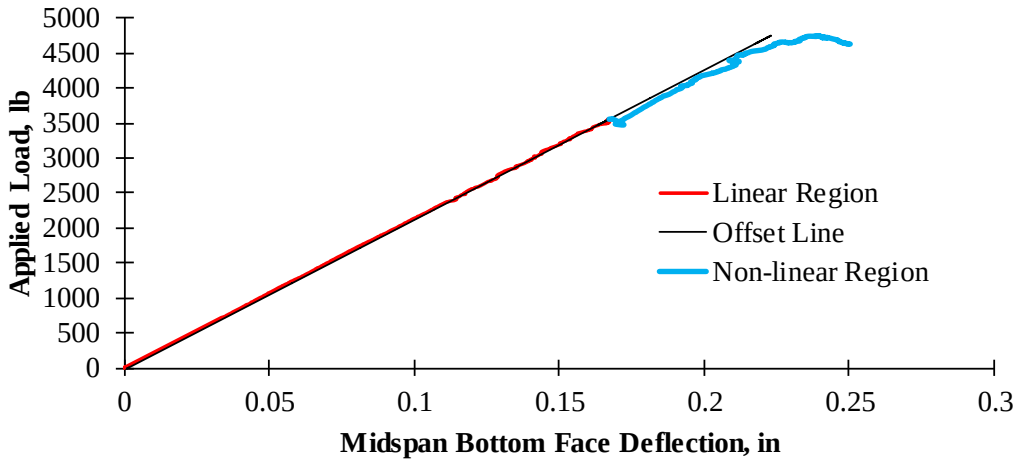		
Offset of Linear Region as a Pecent of Span Length	0.01%	
Load at Initial Failure	3479	lb
Max. Internal Bending Moment at Initial Failure	5218	lb*in
Max. Internal Shear Force at Initial Failure	1739	lb
Average Pressure Under the Load at Initial Failure	2885	psi
Max. Bending Stress in the Top Facing	4084	psi
Max. Bending Stress in the Bottom Facing	2471	psi
Max. Average Shear Stress in the Core	239	psi
Ultimate Failure Mode	Compression Failure in the Top Facing Immediately Under the Load Point	
Load at Ultimate Failure	5895	lb
Max. Internal Bending Moment at Ultimate Failure	8843	lb*in
Max. Internal Shear Force at Ultimate Failure	2948	lb
Average Pressure Under Load at Ultimate Failure	4888	psi
Max. Bending Stress in the Top Facing	6920	psi
Max. Bending Stress in the Bottom Facing	4187	psi
Max. Average Shear Stress in the Core	404	psi
Serviceability Analysis		
Limiting Deflection (L/800)	0.008	in
Load at Limiting Deflection	160	lb
Comparison of Serviceability to Strength		
Ratio of Initial Failure to Serviceability Load	21.68	
Ratio of Ultimate Failure to Serviceability Load	36.74	

APPENDIX D:

FOUR POINT FLEXURAL TESING RESULTS

Table D.1: Summary of Four Point Flexural Test for Specimen 1-1-L

General Information		
Specimen Label	1-1-L	
Displacement Controlled Loading Rate	0.05	in/min
Data Recording Rate for Load and Displacment	2	Hz
Total Time Elapsed During Testing	18	min
Specimen Dimensions		
Total Height of the Specimen, h	2.133	in
Thickness of the Facings, f	0.095	in
Thickness of the Core, c	1.944	in
Width of the Specimen, b	3.924	in
Ratio of the Core Thickness to Facing Thickness, c/f	20.56	
Moment Arm Between the Facings, d	2.039	in
Length of the Specimen, l	26.0	in
Moment of Inertia of the Facings, I_f	0.771	in^4
Area of the Core, A_c	7.628	in^2
Configuration and Dimension of the Flexural Setup		
Span Between the Supports, L	24.0	in
Span Between the Load Points, S	8.0	in
Width of the Load and Support Bars, l_{pad}	1.5	in
Loading Configuration	4-Point Third Point Loading	
Regression Analysis for Correcting the Load vs. Bottom Face Deflection		
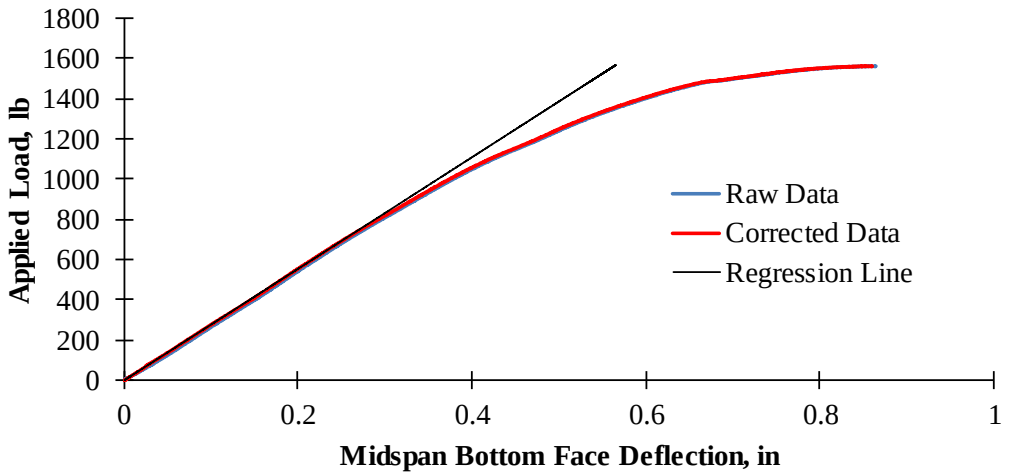		
Slope of the Regression Line	2,776	lb/in
Offset Correction in Bottrom Face Deflection	0.004	in
Coefficient of Determination	0.9999	
Number of Data Points	600	
Range of Corrected Deflection Used	0.025 - 0.273	in

Table D.1: Summary of Four Point Flexural Test for Specimen 1-1-L (Continued)

Regression Analysis for Correcting the Load vs. Crosshead Displacement		
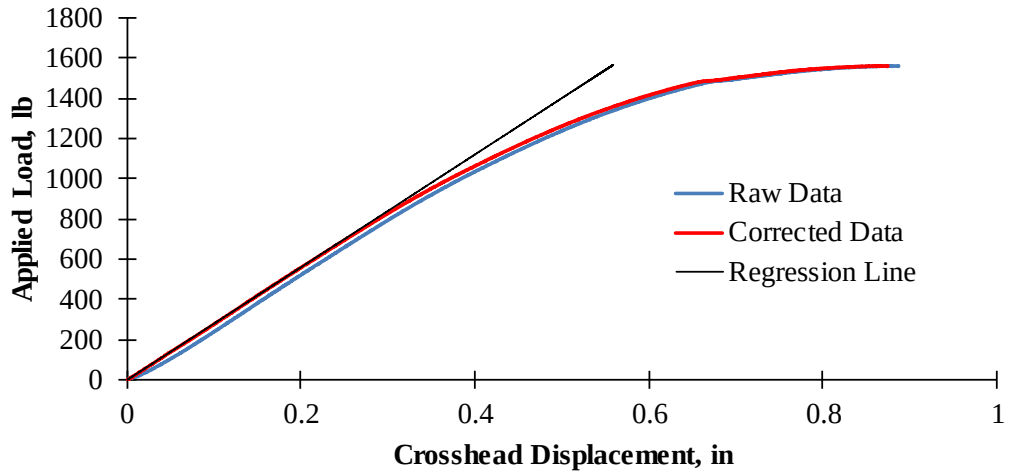		
Slope of the Regression Line	2,802	lb/in
Offset Correction in Crosshead Displacement	0.013	in
Coefficient of Determination	0.9999	
Number of Data Points	500	
Range of Corrected Displacement Used	0.044 - 0.251	in
Regression Analysis for Correcting the Load vs. Top Face Strain		
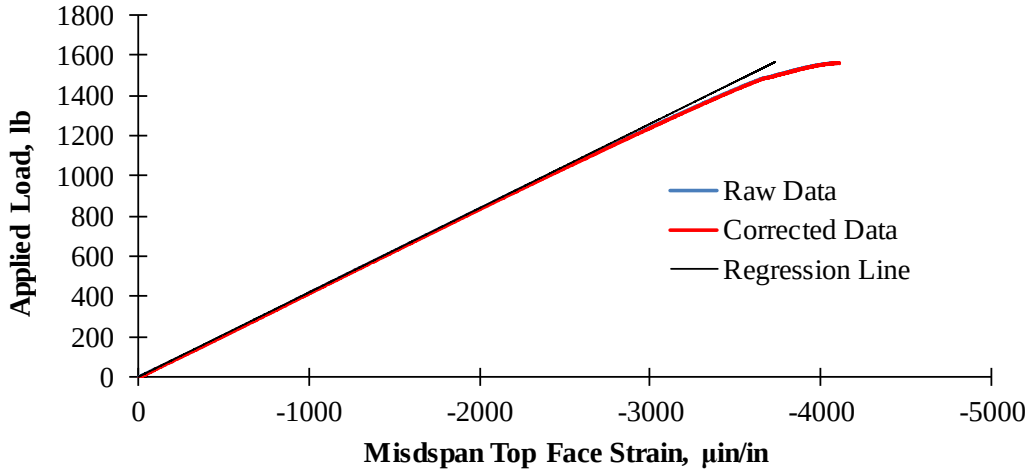		
Slope of the Regression Line	-0.419	lb/in
Offset Correction in Top Face Strain	3.90	µin/in
Coefficient of Determination	1.0000	
Number of Data Points	800	
Range of Corrected Strain Used	-85 - -2210	µin/in

Table D.1: Summary of Four Point Flexural Test for Specimen 1-1-L (Continued)

Regression Analysis for Correcting the Load vs.Bottom Face Strain

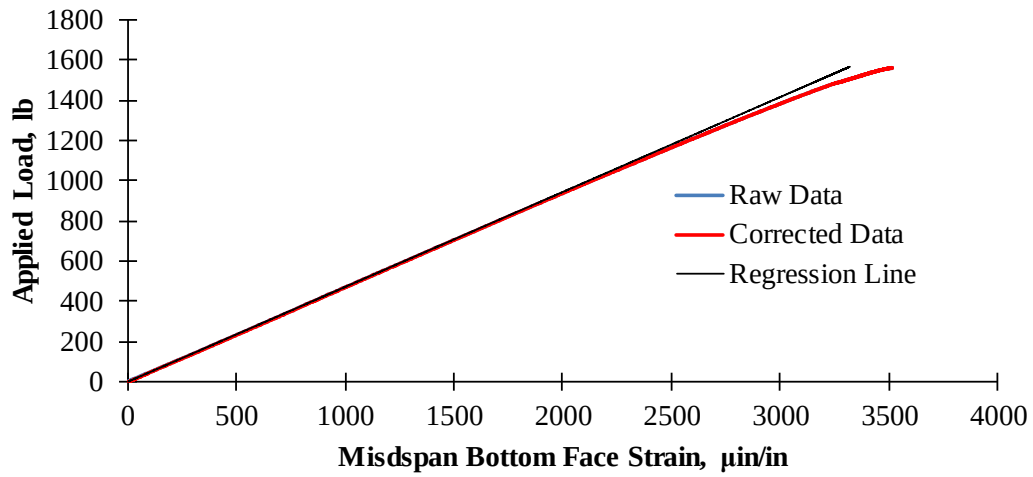

Slope of the Regression Line	0.471	lb/µin/in
Offset Correction in Bottom Face Strain	-4.22	µin/in
Coefficient of Determination	1.0000	
Number of Data Points	800	
Range of Corrected Strain Used	91 - 1985	µin/in

Corrected Load vs.Bottom Face Deflection

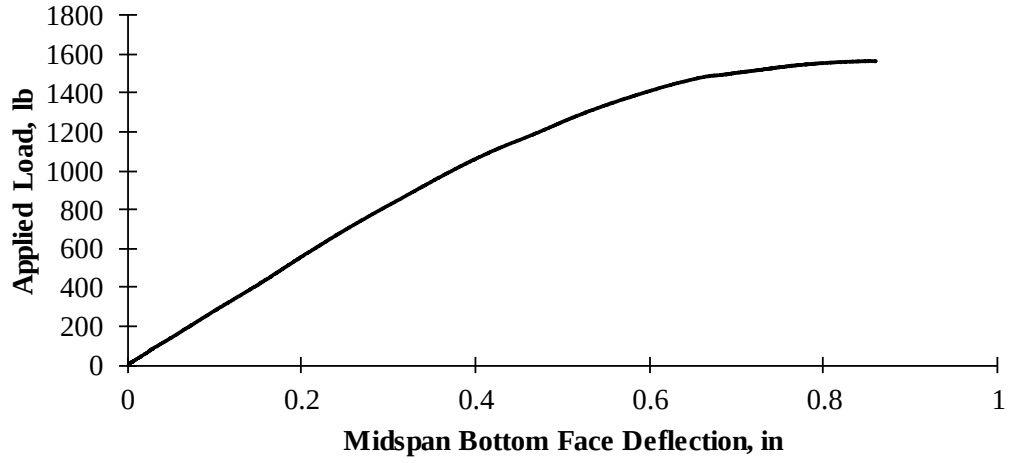

Table D.1: Summary of Four Point Flexural Test for Specimen 1-1-L (Continued)

Corrected Load vs.Crosshead Displacement

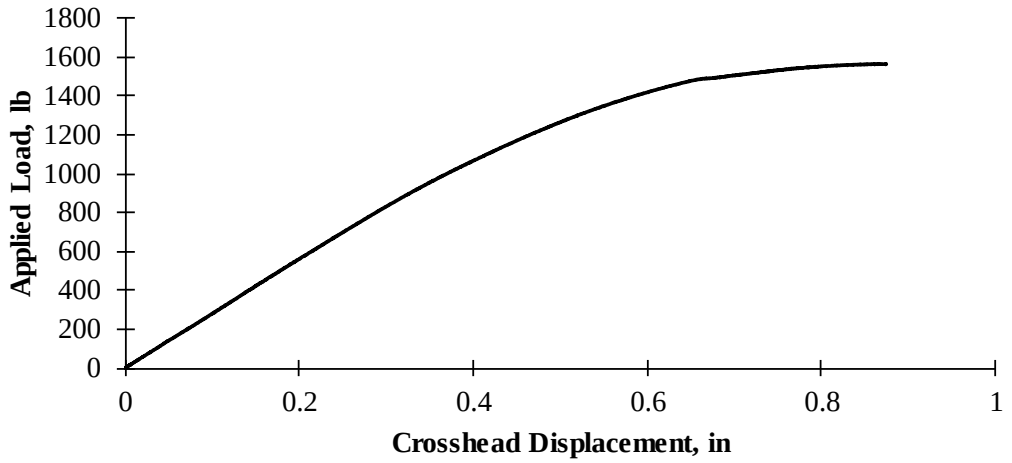

Corrected Load vs.Core Compression

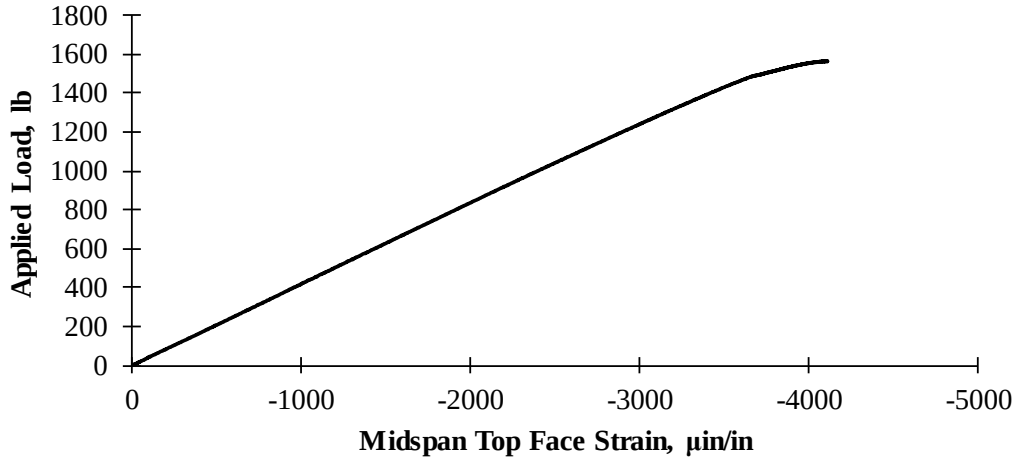

Corrected Load vs.Bottom Face Strain

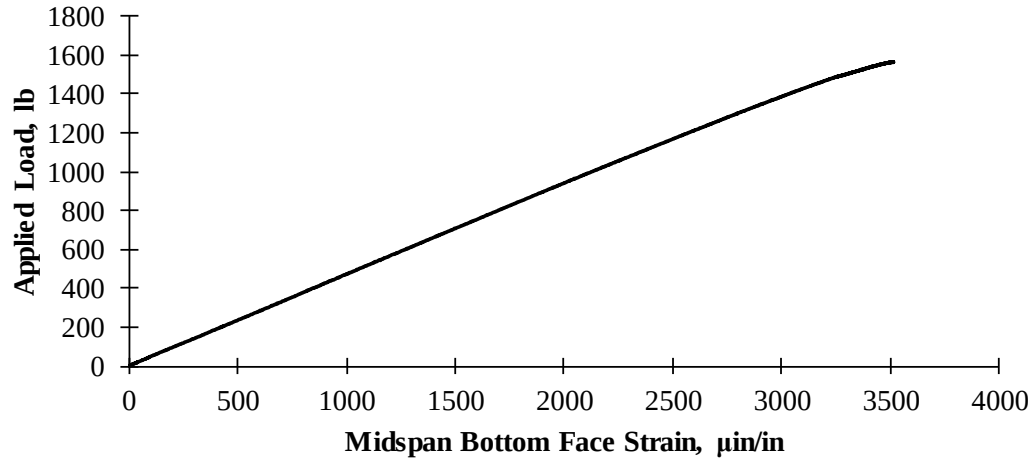

Table D.1: Summary of Four Point Flexural Test for Specimen 1-1-L (Continued)

Strength Analysis		
Initial Failure Mode	Localized Crushing of the Core Coupled with Wrinkling of the Top Facing Immediately Under the Load Points (Local Indentation)	
Estimation of the Intial Failure Load Using the Offset Method		
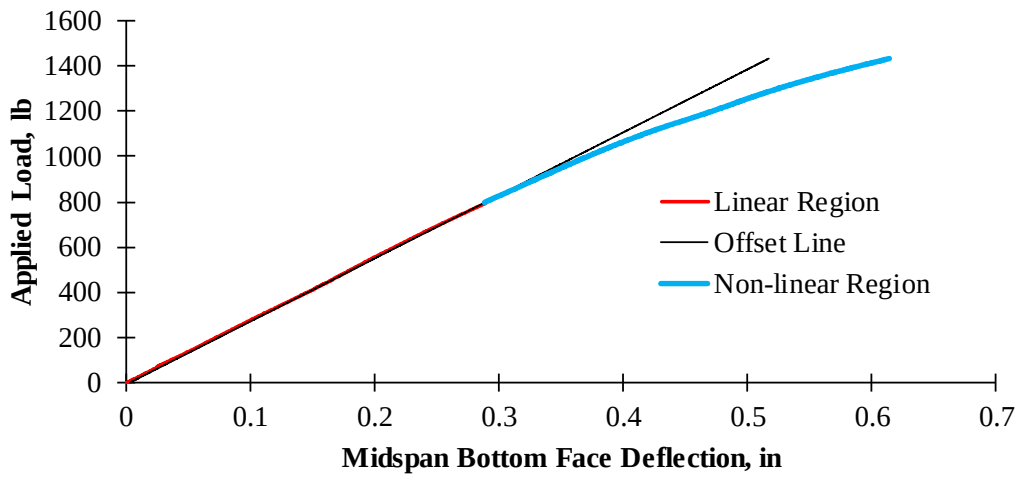		
Offset of Linear Region as a Pecent of Span Length	0.010%	
Load at Initial Failure	794	lb
Max. Internal Bending Moment at Initial Failure	3175	lb*in
Max. Internal Shear Force at Initial Failure	397	lb
Average Pressure Under the Load at Initial Failure	67	psi
Max. Average Bending Stress in the Facings	4392	psi
Max. Average Shear Stress in the Core	52	psi
Ultimate Failure Mode	Shear Failure in the Core Material Characterized by a Sudden Diagonal Fracture	
Load at Ultimate Failure	1566	lb
Max. Internal Bending Moment at Ultimate Failure	6266	lb*in
Max. Internal Shear Force at Ultimate Failure	783	lb
Average Pressure Under Load at Ultimate Failure	133	psi
Max. Average Bending Stress in the Facing	8668	psi
Max. Average Shear Stress in the Core	103	psi
Serviceability Analysis		
Limiting Deflection (L/800)	0.030	in
Load at Limiting Deflection	83	lb
Comparison of Serviceability to Strength		
Ratio of Initial Failure to Serviceability Load	9.53	
Ratio of Ultimate Failure to Serviceability Load	18.81	

Table D.2: Summary of Four Point Flexural Test for Specimen 1-2-L

General Information		
Specimen Label	1-2-L	
Displacement Controlled Loading Rate	0.05	in/min
Data Recording Rate for Load and Displacment	2	Hz
Total Time Elapsed During Testing	47	min
Specimen Dimensions		
Total Height of the Specimen, h	2.133	in
Thickness of the Facings, f	0.095	in
Thickness of the Core, c	1.944	in
Width of the Specimen, b	3.785	in
Ratio of the Core Thickness to Facing Thickness, c/f	20.56	
Moment Arm Between the Facings, d	2.039	in
Length of the Specimen, l	26.0	in
Moment of Inertia of the Facings, I_f	0.744	in^4
Area of the Core, A_c	7.359	in^2
Configuration and Dimension of the Flexural Setup		
Span Between the Supports, L	24.0	in
Span Between the Load Points, S	8.0	in
Width of the Load and Support Bars, l_{pad}	1.5	in
Loading Configuration	4-Point Third Point Loading	
Regression Analysis for Correcting the Load vs. Bottom Face Deflection		
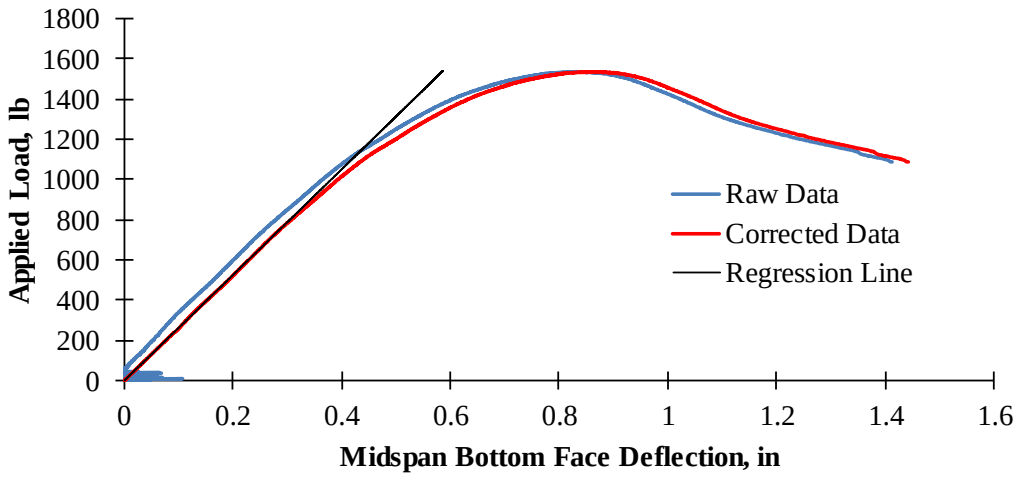		
Slope of the Regression Line	2,622	lb/in
Offset Correction in Bottrom Face Deflection	-0.030	in
Coefficient of Determination	0.9998	
Number of Data Points	500	
Range of Corrected Deflection Used	0.095 - 0.307	in

Table D.2: Summary of Four Point Flexural Test for Specimen 1-2-L (Continued)

Regression Analysis for Correcting the Load vs. Crosshead Displacement		
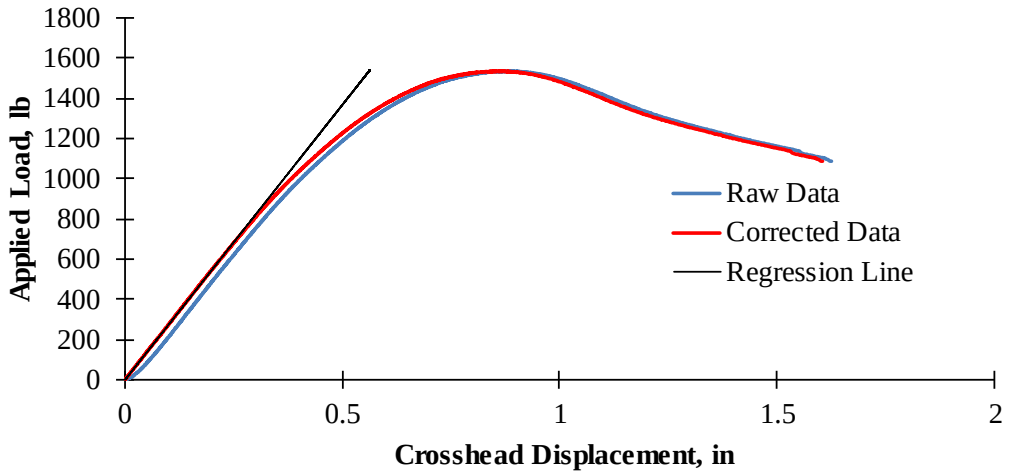		
Slope of the Regression Line	2,739	lb/in
Offset Correction in Crosshead Displacement	0.023	in
Coefficient of Determination	0.9999	
Number of Data Points	400	
Range of Corrected Displacement Used	0.052 - 0.217	in
Regression Analysis for Correcting the Load vs. Top Face Strain		
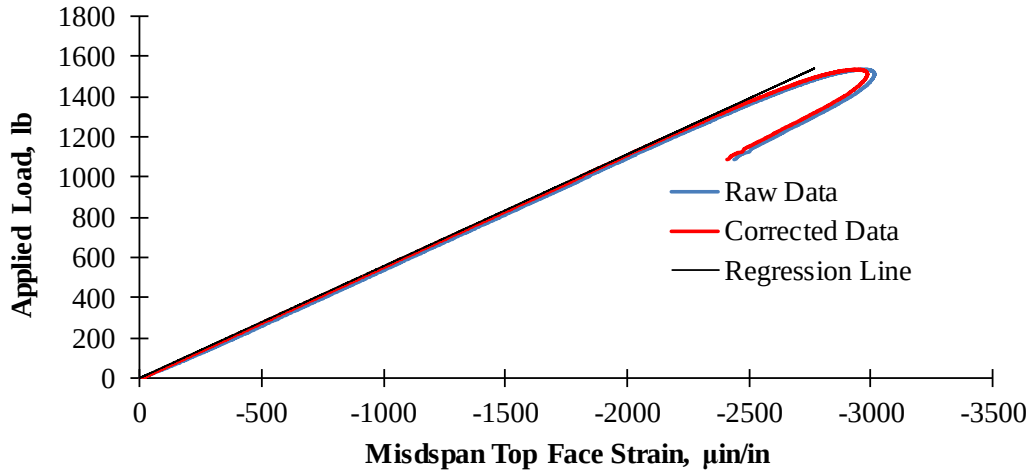		
Slope of the Regression Line	-0.556	lb/in
Offset Correction in Top Face Strain	-26	µin/in
Coefficient of Determination	1.0000	
Number of Data Points	1000	
Range of Corrected Strain Used	-366 - -2197	µin/in

Table D.2: Summary of Four Point Flexural Test for Specimen 1-2-L (Continued)

Regression Analysis for Correcting the Load vs.Bottom Face Strain

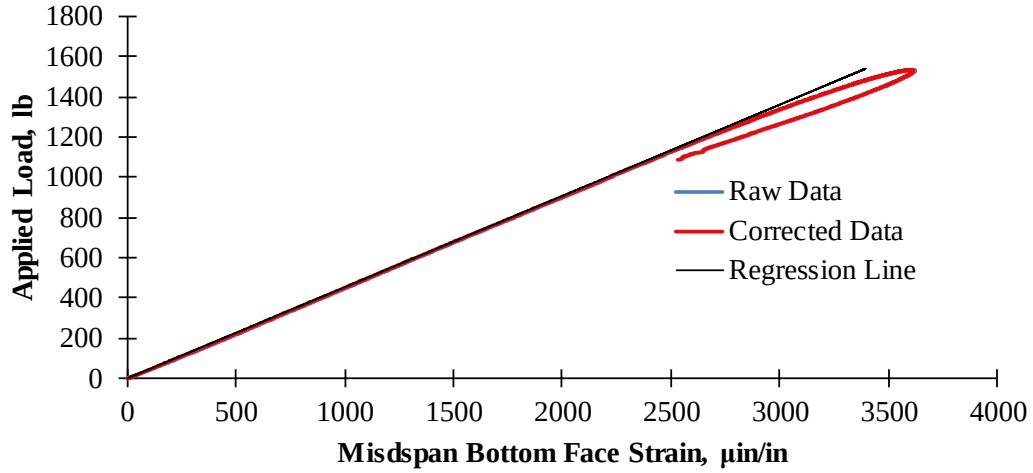

Slope of the Regression Line	0.453	lb/µin/in
Offset Correction in Bottom Face Strain	12	µin/in
Coefficient of Determination	1.0000	
Number of Data Points	1000	
Range of Corrected Strain Used	193 - 2507	µin/in

Corrected Load vs.Bottom Face Deflection

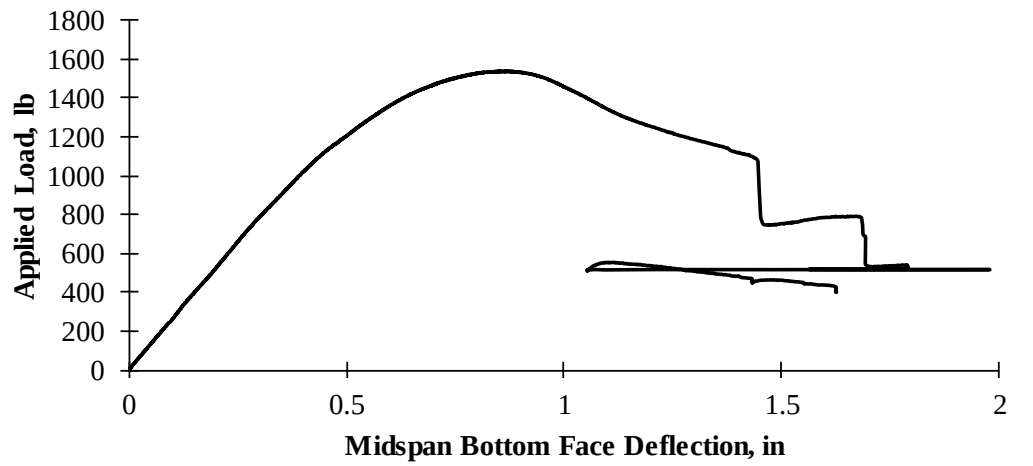

Table D.2: Summary of Four Point Flexural Test for Specimen 1-2-L (Continued)

Corrected Load vs.Crosshead Displacement

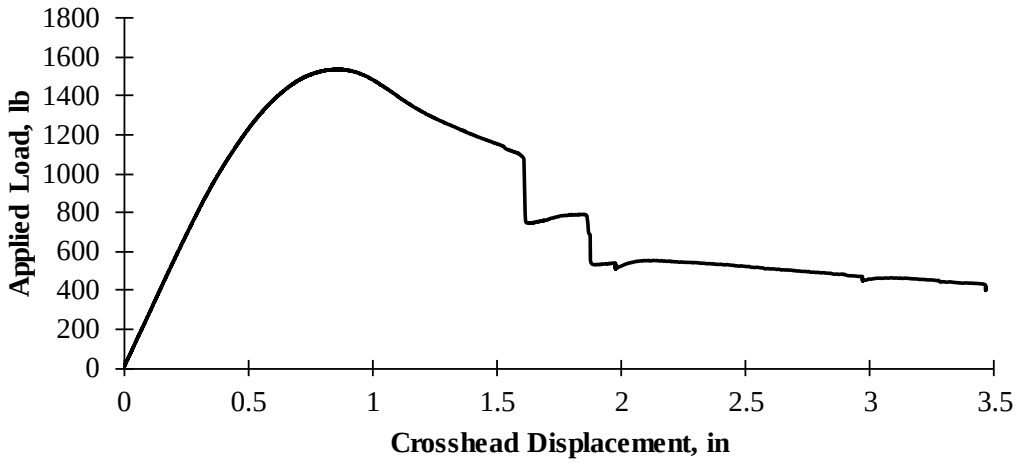

Corrected Load vs.Core Compression

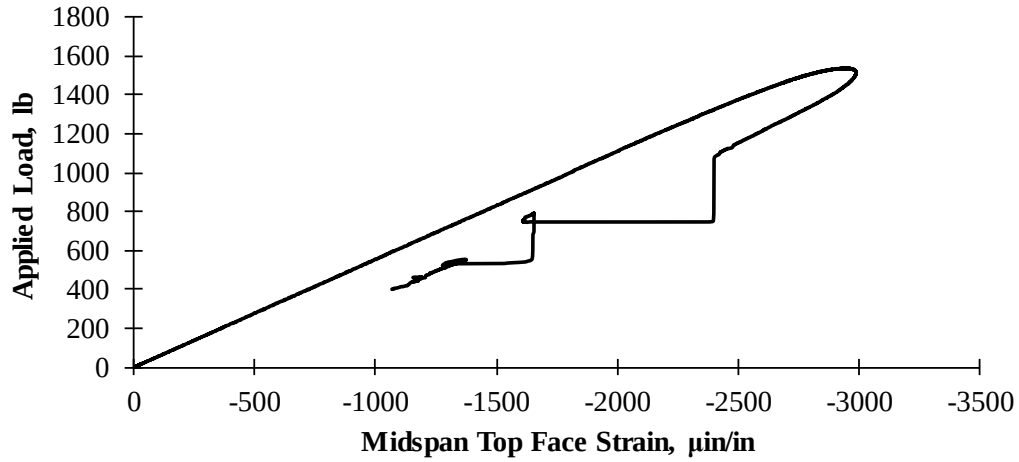

Corrected Load vs.Bottom Face Strain

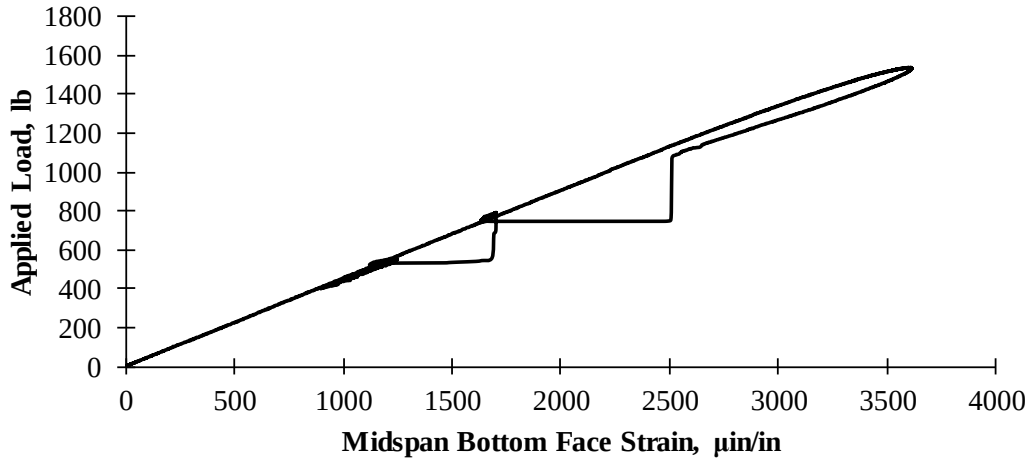

Table D.2: Summary of Four Point Flexural Test for Specimen 1-2-L (Continued)

Strength Analysis		
Initial Failure Mode	Localized Crushing of the Core Coupled with Wrinkling of the Top Facing Immediately Under the Load Points (Local Indentation)	
Estimation of the Intial Failure Load Using the Offset Method		
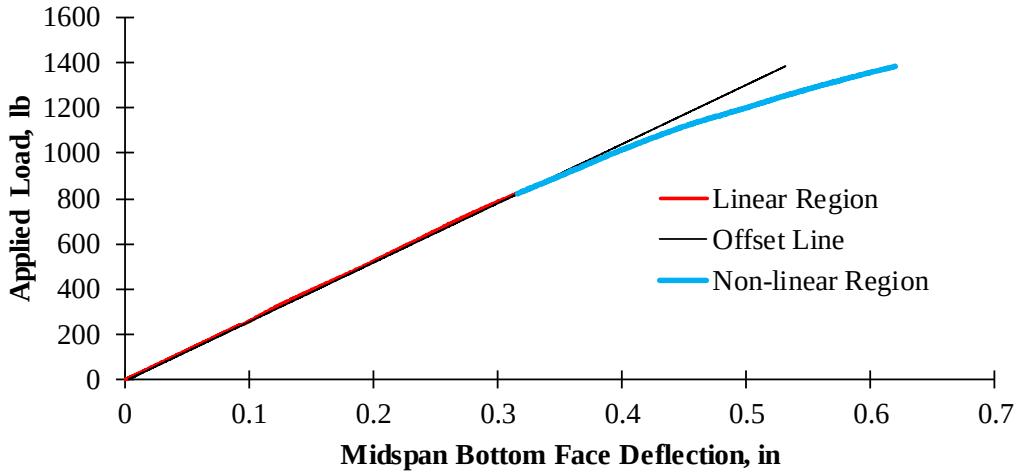		
Offset of Linear Region as a Pecent of Span Length	0.01%	
Load at Initial Failure	823	lb
Max. Internal Bending Moment at Initial Failure	3290	lb*in
Max. Internal Shear Force at Initial Failure	411	lb
Average Pressure Under the Load at Initial Failure	72	psi
Max. Average Bending Stress in the Facings	4718	psi
Max. Average Shear Stress in the Core	56	psi
Ultimate Failure Mode	Excessive Crushing of the Core Coupled with Excessive Wrinkling of the Facing Immediately Under the Load (Local Indentation)	
Load at Ultimate Failure	1539	lb
Max. Internal Bending Moment at Ultimate Failure	6156	lb*in
Max. Internal Shear Force at Ultimate Failure	769	lb
Average Pressure Under Load at Ultimate Failure	136	psi
Max. Average Bending Stress in the Facing	8827	psi
Max. Average Shear Stress in the Core	105	psi
Serviceability Analysis		
Limiting Deflection (L/800)	0.030	in
Load at Limiting Deflection	79	lb
Comparison of Serviceability to Strength		
Ratio of Initial Failure to Serviceability Load	10.46	
Ratio of Ultimate Failure to Serviceability Load	19.57	

Table D.3: Summary of Four Point Flexural Test for Specimen 1-3-L

General Information		
Specimen Label	1-3-L	
Displacement Controlled Loading Rate	0.1	in/min
Data Recording Rate for Load and Displacment	2	Hz
Total Time Elapsed During Testing	10	min
Specimen Dimensions		
Total Height of the Specimen, h	2.113	in
Thickness of the Facings, f	0.084	in
Thickness of the Core, c	1.945	in
Width of the Specimen, b	4.367	in
Ratio of the Core Thickness to Facing Thickness, c/f	23.22	
Moment Arm Between the Facings, d	2.029	in
Length of the Specimen, l	26.0	in
Moment of Inertia of the Facings, I_f	0.753	in^4
Area of the Core, A_c	8.494	in^2
Configuration and Dimension of the Flexural Setup		
Span Between the Supports, L	24.0	in
Span Between the Load Points, S	8.0	in
Width of the Load and Support Bars, l_{pad}	1.5	in
Loading Configuration	4-Point Third Point Loading	
Regression Analysis for Correcting the Load vs. Bottom Face Deflection		
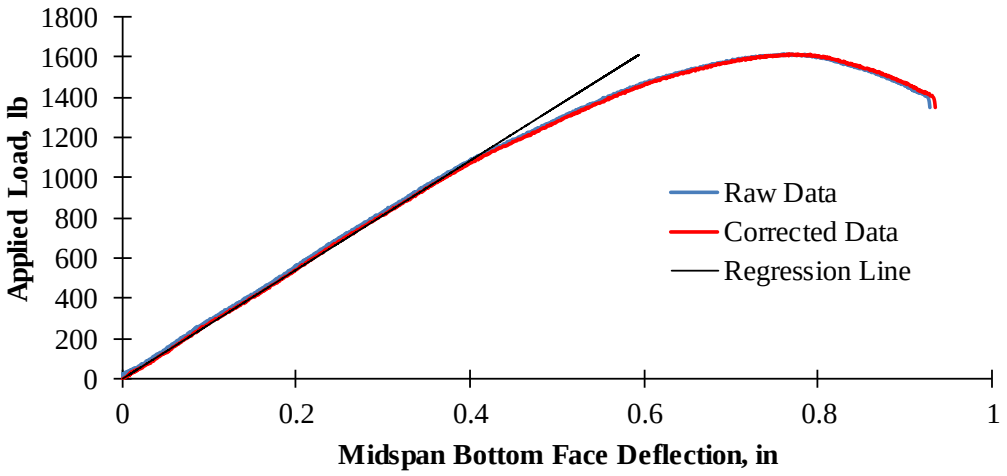		
Slope of the Regression Line	2,719	lb/in
Offset Correction in Bottrom Face Deflection	-0.007	in
Coefficient of Determination	0.9998	
Number of Data Points	400	
Range of Corrected Deflection Used	0.008 - 0.330	in

Table D.3: Summary of Four Point Flexural Test for Specimen 1-3-L (Continued)

Regression Analysis for Correcting the Load vs. Crosshead Displacement		
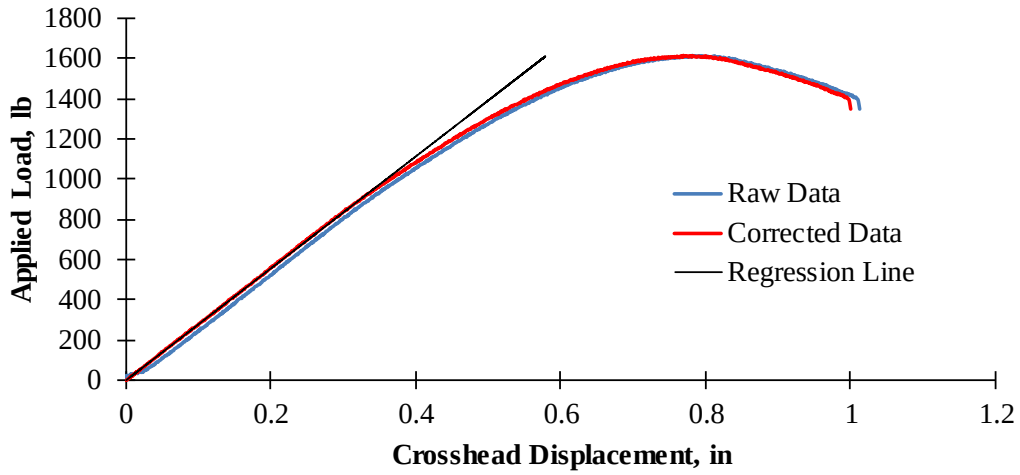		
Slope of the Regression Line	2,791	lb/in
Offset Correction in Crosshead Displacement	0.012	in
Coefficient of Determination	0.9999	
Number of Data Points	300	
Range of Corrected Displacement Used	0.046 - 0.292	in
Regression Analysis for Correcting the Load vs. Top Face Strain		
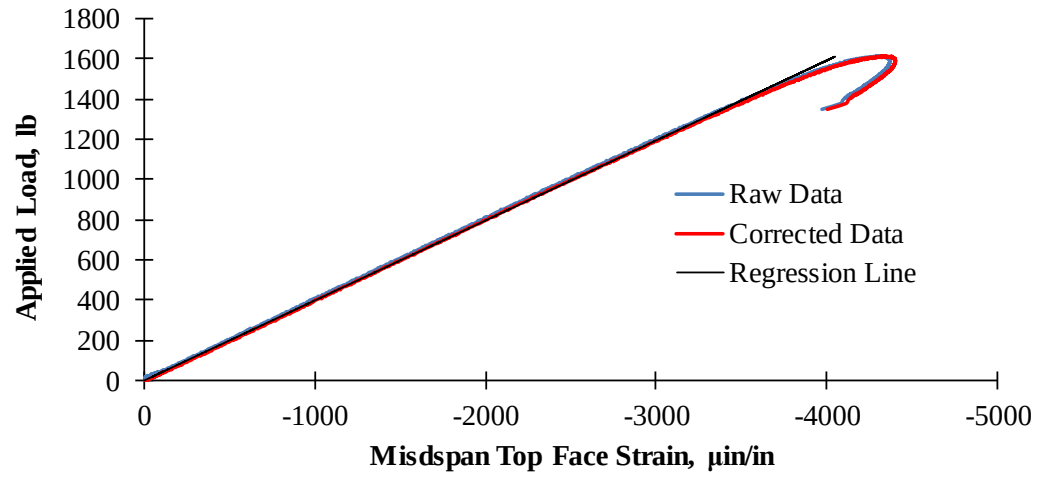		
Slope of the Regression Line	-0.399	lb/in
Offset Correction in Top Face Strain	30	µin/in
Coefficient of Determination	0.9999	
Number of Data Points	500	
Range of Corrected Strain Used	-91 - -2818	µin/in

Table D.3: Summary of Four Point Flexural Test for Specimen 1-3-L (Continued)

Regression Analysis for Correcting the Load vs.Bottom Face Strain

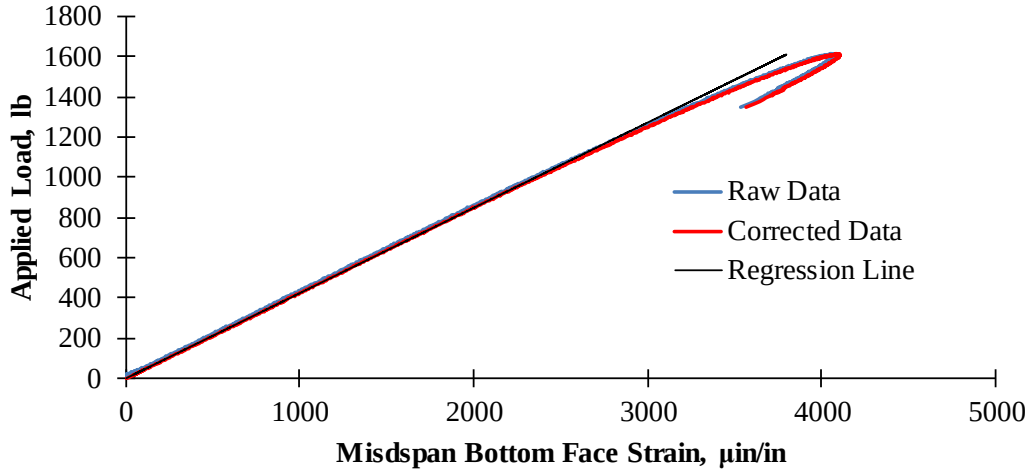

Slope of the Regression Line	0.425	lb/µin/in
Offset Correction in Bottom Face Strain	-30	µin/in
Coefficient of Determination	0.9999	
Number of Data Points	400	
Range of Corrected Strain Used	98 - 2197	µin/in

Corrected Load vs.Bottom Face Deflection

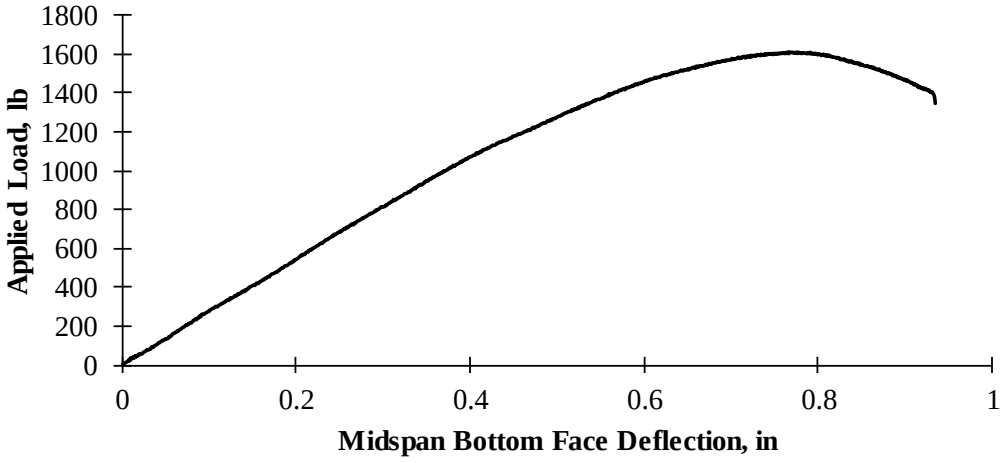

Table D.3: Summary of Four Point Flexural Test for Specimen 1-3-L (Continued)

Corrected Load vs.Crosshead Displacement

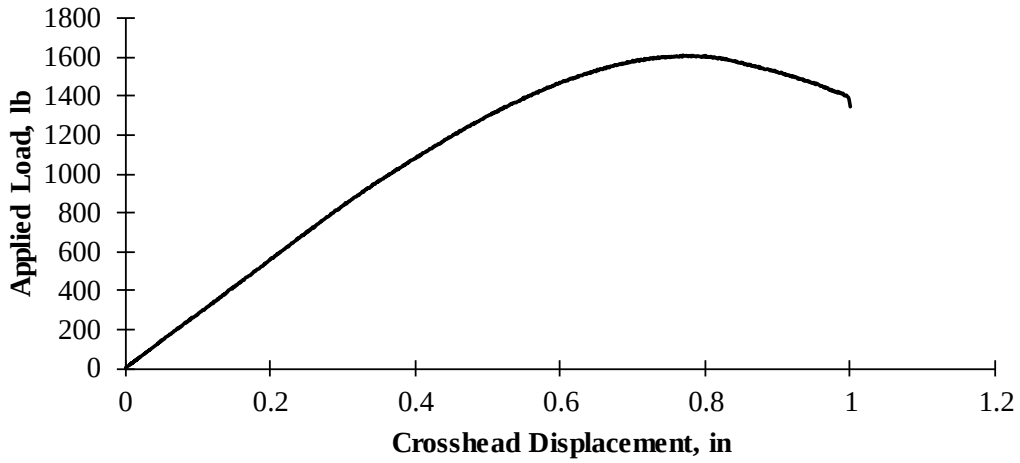

Corrected Load vs.Core Compression

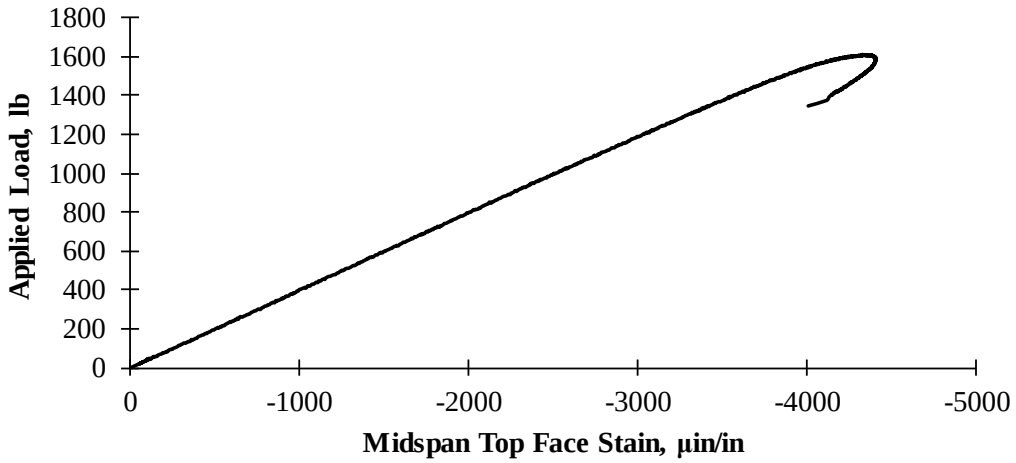

Corrected Load vs.Bottom Face Strain

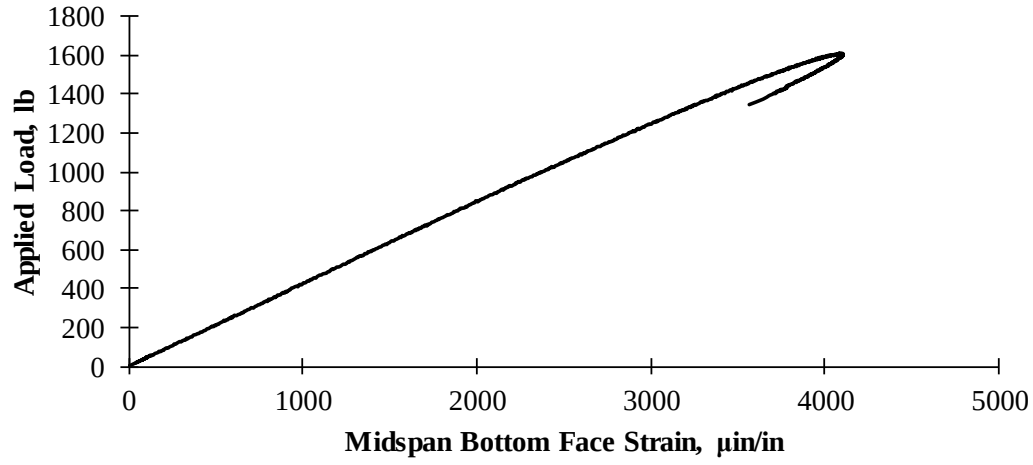

Table D.3: Summary of Four Point Flexural Test for Specimen 1-3-L (Continued)

Strength Analysis		
Initial Failure Mode	Localized Crushing of the Core Coupled with Wrinkling of the Top Facing Immediately Under the Load Points (Local Indentaion)	
Estimation of the Intial Failure Load Using the Offset Method		
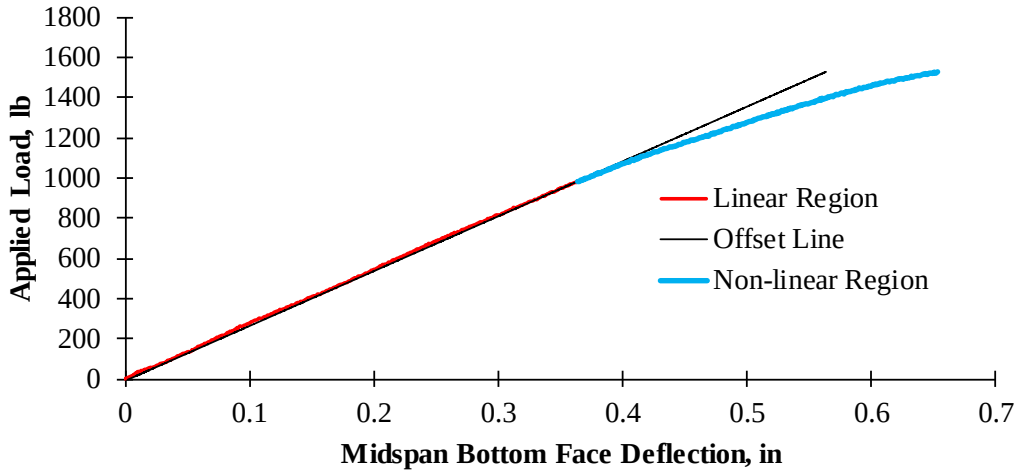		
Offset of Linear Region as a Pecent of Span Length	0.01%	
Load at Initial Failure	984	lb
Max. Internal Bending Moment at Initial Failure	3936	lb*in
Max. Internal Shear Force at Initial Failure	492	lb
Average Pressure Under the Load at Initial Failure	75	psi
Max. Average Bending Stress in the Facings	5524	psi
Max. Average Shear Stress in the Core	58	psi
Ultimate Failure Mode	Excessive Crushing of the Core Coupled with Excessive Wrinkling of the Facing Immediately Under the Load (Local Indentation)	
Load at Ultimate Failure	1613	lb
Max. Internal Bending Moment at Ultimate Failure	6452	lb*in
Max. Internal Shear Force at Ultimate Failure	806	lb
Average Pressure Under Load at Ultimate Failure	123	psi
Max. Average Bending Stress in the Facing	9054	psi
Max. Average Shear Stress in the Core	95	psi
Serviceability Analysis		
Limiting Deflection (L/800)	0.030	in
Load at Limiting Deflection	82	lb
Comparison of Serviceability to Strength		
Ratio of Initial Failure to Serviceability Load	12.06	
Ratio of Ultimate Failure to Serviceability Load	19.77	

Table D.5: Summary of Four Point Flexural Test for Specimen 2-1-L

General Information		
Specimen Label	2-1-L	
Displacement Controlled Loading Rate	0.05	in/min
Data Recording Rate for Load and Displacment	2	Hz
Total Time Elapsed During Testing	16	min
Specimen Dimensions		
Total Height of the Specimen, h	2.333	in
Thickness of the Facings, f	0.095	in
Thickness of the Core, c	2.143	in
Width of the Specimen, b	4.346	in
Ratio of the Core Thickness to Facing Thickness, c/f	22.63	
Moment Arm Between the Facings, d	2.238	in
Length of the Specimen, l	26.0	in
Moment of Inertia of the Facings, I_f	1.031	in^4
Area of the Core, A_c	9.316	in^2
Configuration and Dimension of the Flexural Setup		
Span Between the Supports, L	24.0	in
Span Between the Load Points, S	8.0	in
Width of the Load and Support Bars, l_{pad}	1.5	in
Loading Configuration	4-Point Third Point Loading	
Regression Analysis for Correcting the Load vs. Bottom Face Deflection		
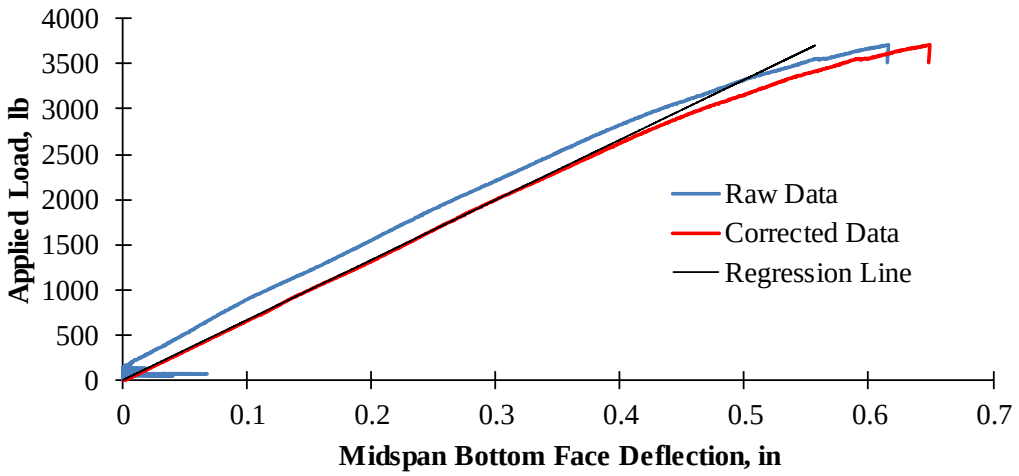		
Slope of the Regression Line	6,658	lb/in
Offset Correction in Bottrom Face Deflection	-0.034	in
Coefficient of Determination	0.9998	
Number of Data Points	500	
Range of Corrected Deflection Used	0.110 - 0.324	in

Table D.5: Summary of Four Point Flexural Test for Specimen 2-1-L (Continued)

Regression Analysis for Correcting the Load vs. Crosshead Displacement		
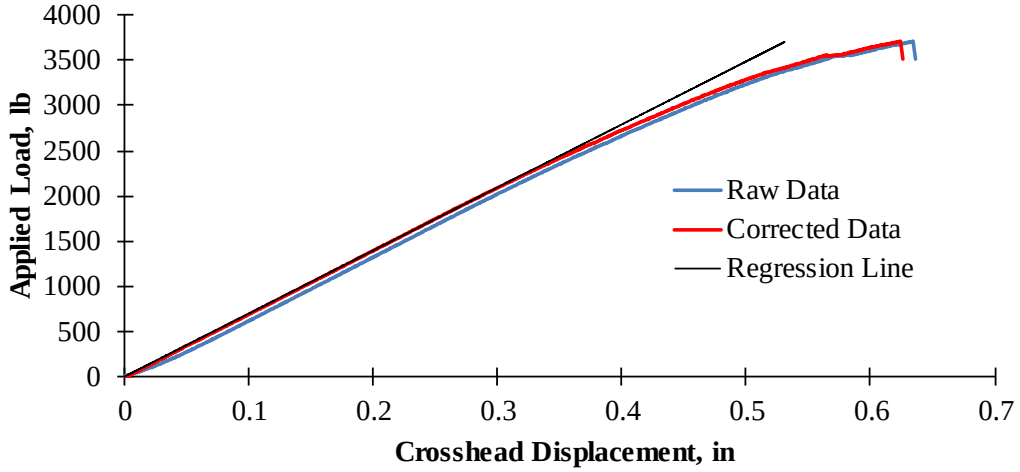		
Slope of the Regression Line	7,001	lb/in
Offset Correction in Crosshead Displacement	0.010	in
Coefficient of Determination	1.0000	
Number of Data Points	600	
Range of Corrected Displacement Used	0.045 - 0.292	in
Regression Analysis for Correcting the Load vs. Top Face Strain		
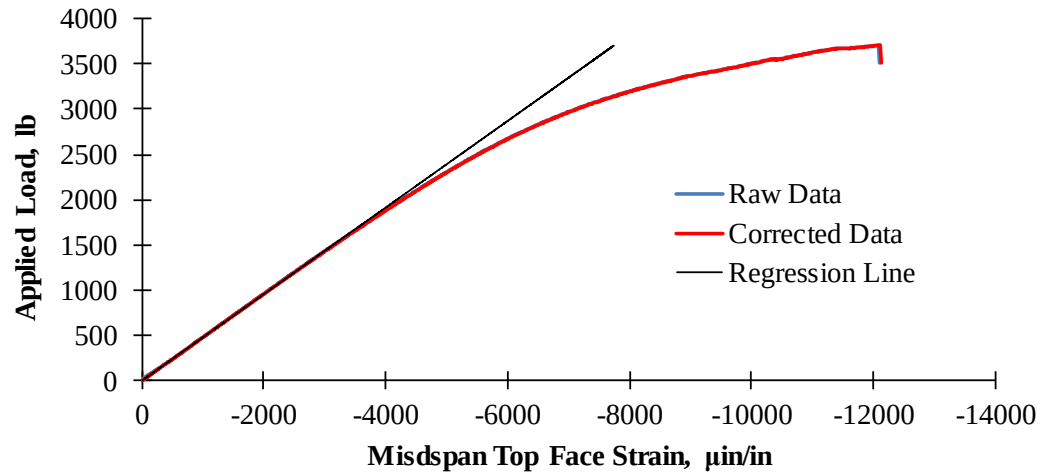		
Slope of the Regression Line	-0.480	lb/in
Offset Correction in Top Face Strain	5	µin/in
Coefficient of Determination	0.9999	
Number of Data Points	400	
Range of Corrected Strain Used	-294 - -2644	µin/in

Table D.5: Summary of Four Point Flexural Test for Specimen 2-1-L (Continued)

Regression Analysis for Correcting the Load vs.Bottom Face Strain

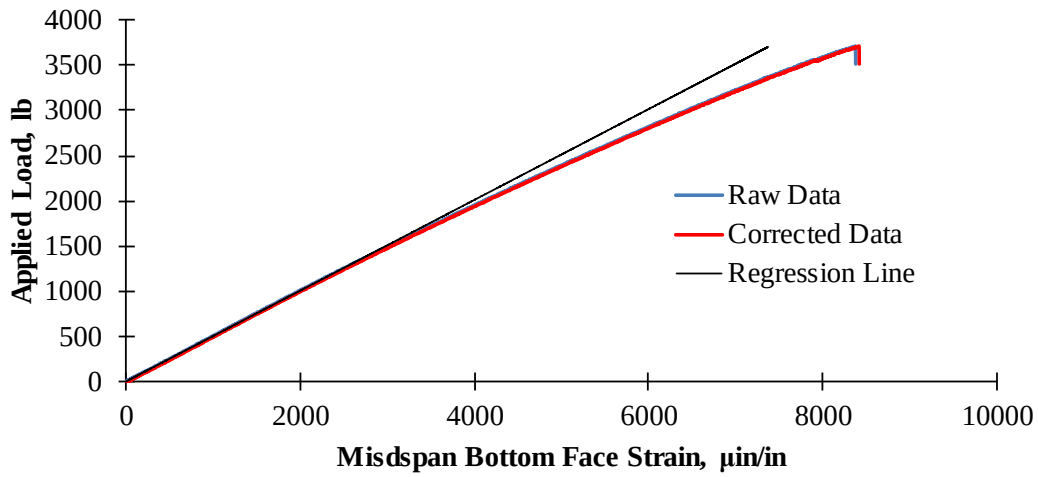

Slope of the Regression Line	0.503	lb/µin/in
Offset Correction in Bottom Face Strain	-28	µin/in
Coefficient of Determination	0.9999	
Number of Data Points	400	
Range of Corrected Strain Used	53 - 2181	µin/in

Corrected Load vs.Bottom Face Deflection

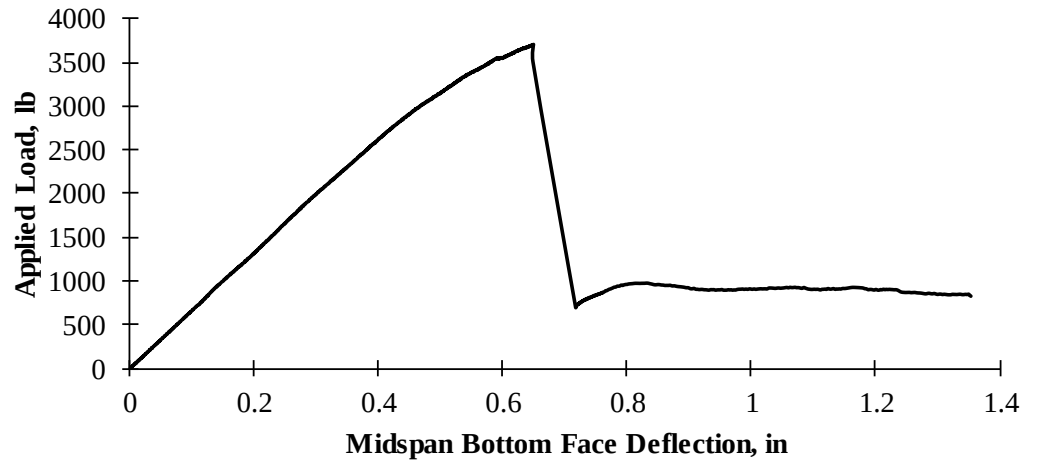

Table D.5: Summary of Four Point Flexural Test for Specimen 2-1-L (Continued)

Corrected Load vs.Crosshead Displacement

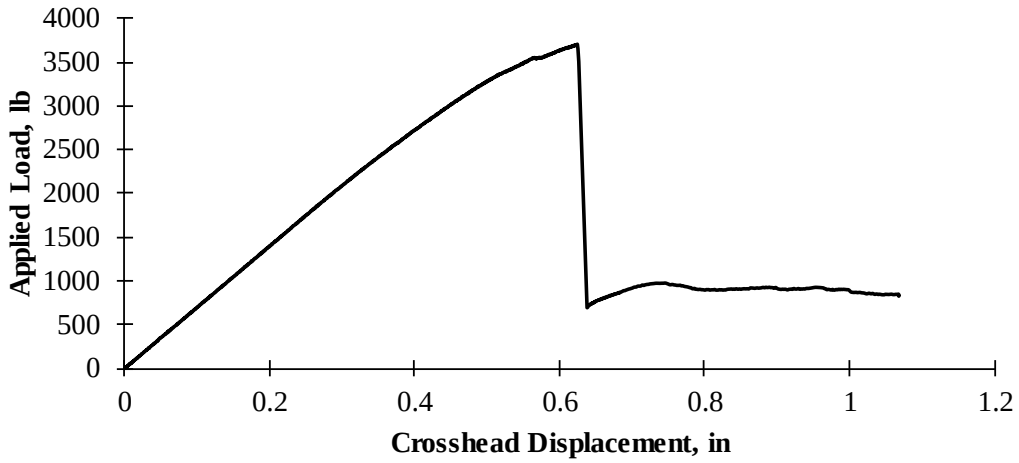

Corrected Load vs.Top Face Strain

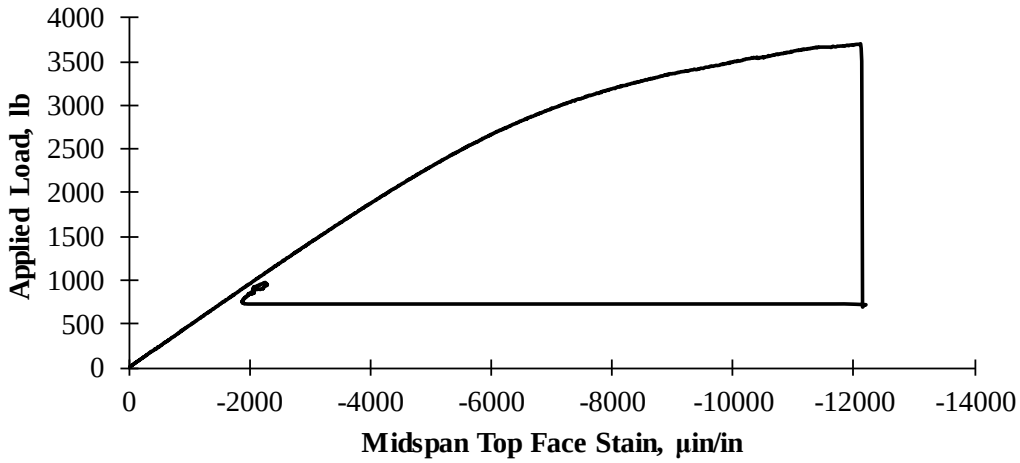

Corrected Load vs.Bottom Face Strain

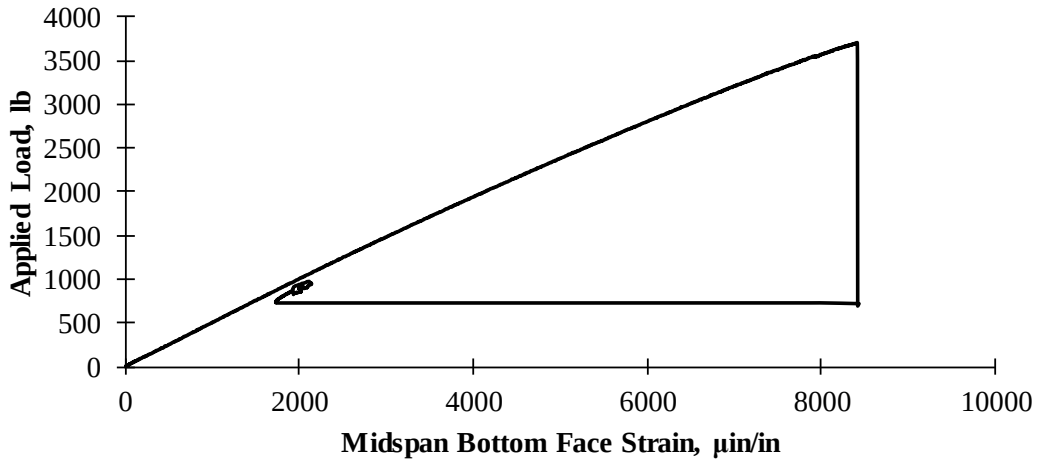

Table D.5: Summary of Four Point Flexural Test for Specimen 2-1-L (Continued)

Strength Analysis		
Initial Failure Mode	Wrinkling of the Top Facing Between Web Reinforcement (Intra-cellular Dimpling)	
Estimation of the Intial Failure Load Using the Offset Method		
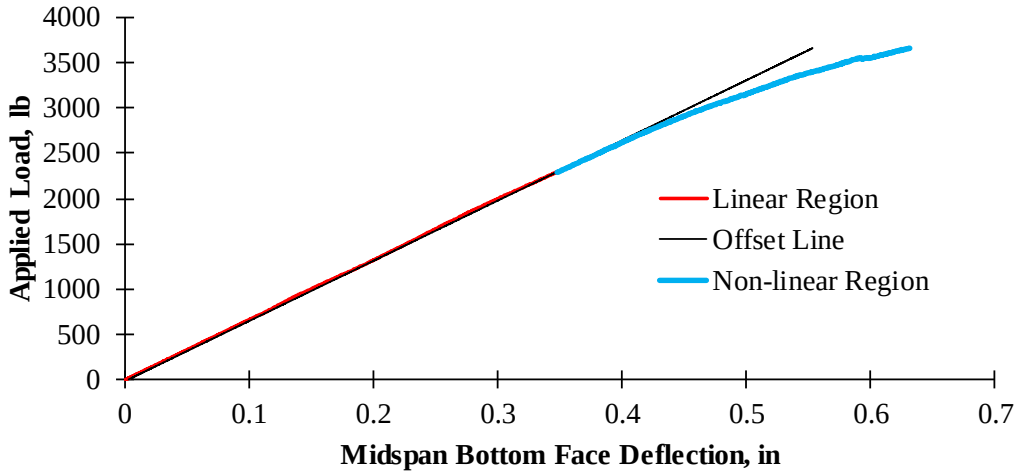		
Offset of Linear Region as a Pecent of Span Length	0.010%	
Load at Initial Failure	2299	lb
Max. Internal Bending Moment at Initial Failure	9196	lb*in
Max. Internal Shear Force at Initial Failure	1150	lb
Average Pressure Under the Load at Initial Failure	176	psi
Max. Average Bending Stress in the Facings	10405	psi
Max. Average Shear Stress in the Core	123	psi
Ultimate Failure Mode	Compression Failure of the Top Facing Characterized by a Sudden Fracture	
Load at Ultimate Failure	3712	lb
Max. Internal Bending Moment at Ultimate Failure	14850	lb*in
Max. Internal Shear Force at Ultimate Failure	1856	lb
Average Pressure Under Load at Ultimate Failure	285	psi
Max. Average Bending Stress in the Facing*	16802	psi
Max. Average Shear Stress in the Core	199	psi
Serviceability Analysis		
Limiting Deflection (L/800)	0.030	in
Load at Limiting Deflection	200	lb
Comparison of Serviceability to Strength		
Ratio of Initial Failure to Serviceability Load	11.51	
Ratio of Ultimate Failure to Serviceability Load	18.59	

Table D.6: Summary of Four Point Flexural Test for Specimen 2-2-L

General Information		
Specimen Label	2-2-L	
Displacement Controlled Loading Rate	0.05	in/min
Data Recording Rate for Load and Displacment	2	Hz
Total Time Elapsed During Testing	15	min
Specimen Dimensions		
Total Height of the Specimen, h	2.333	in
Thickness of the Facings, f	0.095	in
Thickness of the Core, c	2.143	in
Width of the Specimen, b	3.725	in
Ratio of the Core Thickness to Facing Thickness, c/f	22.63	
Moment Arm Between the Facings, d	2.238	in
Length of the Specimen, l	26.0	in
Moment of Inertia of the Facings, I_f	0.884	in^4
Area of the Longitudinal Stitches, A_s	7.984	in^2
Configuration and Dimension of the Flexural Setup		
Span Between the Supports, L	24.0	in
Span Between the Load Points, S	8.0	in
Width of the Load and Support Bars, l_{pad}	1.5	in
Loading Configuration	4-Point Third Point Loading	
Regression Analysis for Correcting the Load vs. Bottom Face Deflection		
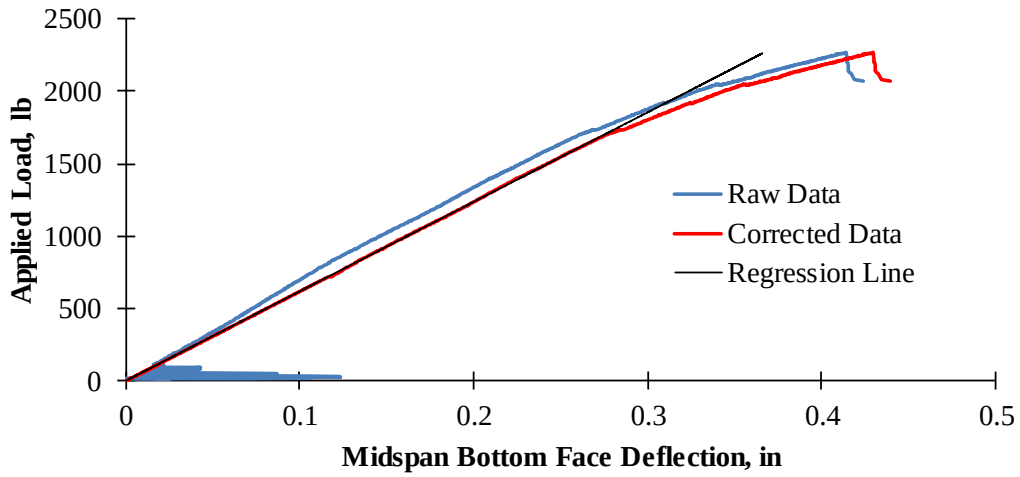		
Slope of the Regression Line	6,189	lb/in
Offset Correction in Bottrom Face Deflection	-0.015	in
Coefficient of Determination	0.9998	
Number of Data Points	400	
Range of Corrected Deflection Used	0.118 - 0.276	in

Table D.6: Summary of Four Point Flexural Test for Specimen 2-2-L (Continued)

Regression Analysis for Correcting the Load vs. Crosshead Displacement		
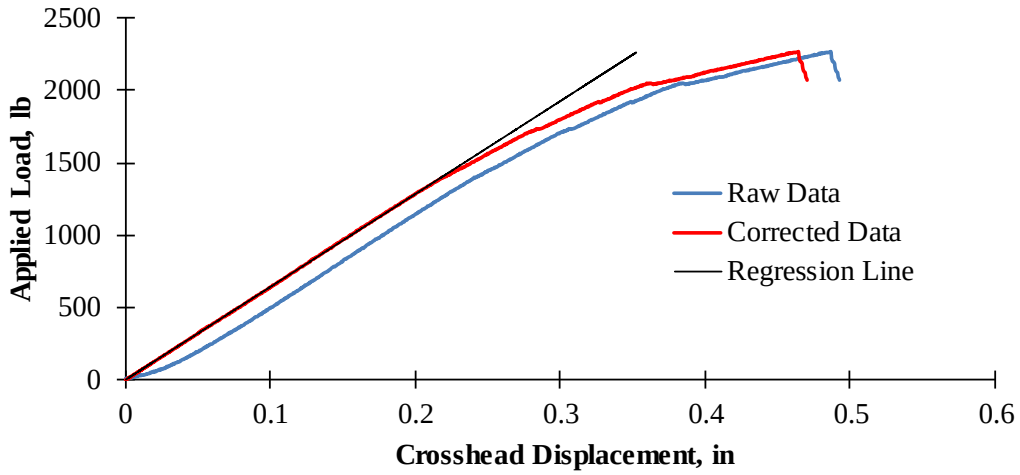		
Slope of the Regression Line	6,429	lb/in
Offset Correction in Crosshead Displacement	0.022	in
Coefficient of Determination	0.9999	
Number of Data Points	400	
Range of Corrected Displacement Used	0.051 - 0.214	in
Regression Analysis for Correcting the Load vs. Top Face Strain		
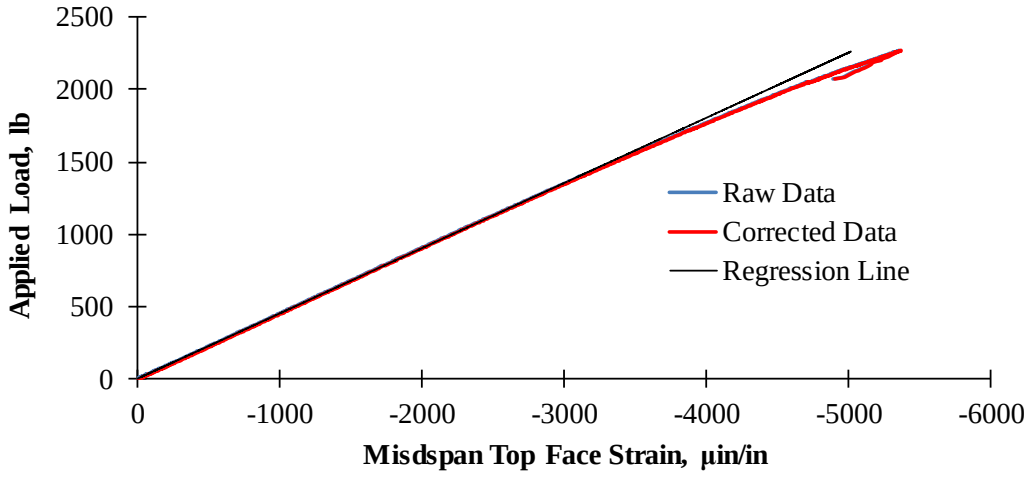		
Slope of the Regression Line	-0.451	lb/in
Offset Correction in Top Face Strain	18	µin/in
Coefficient of Determination	1.0000	
Number of Data Points	500	
Range of Corrected Strain Used	-27 - -2628	µin/in

Table D.6: Summary of Four Point Flexural Test for Specimen 2-2-L (Continued)

Regression Analysis for Correcting the Load vs.Bottom Face Strain

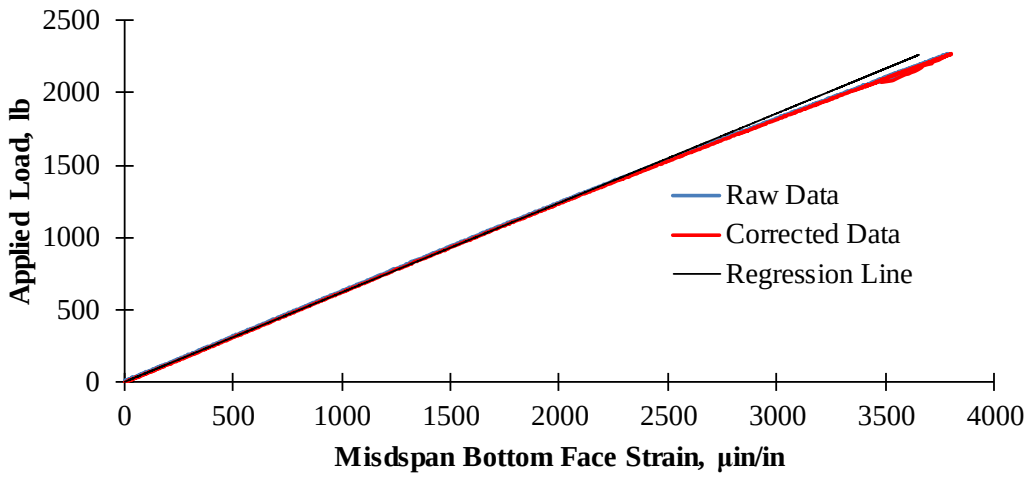

Slope of the Regression Line	0.620	lb/µin/in
Offset Correction in Bottom Face Strain	-16	µin/in
Coefficient of Determination	0.9999	
Number of Data Points	500	
Range of Corrected Strain Used	18 - 1908	µin/in

Corrected Load vs.Bottom Face Deflection

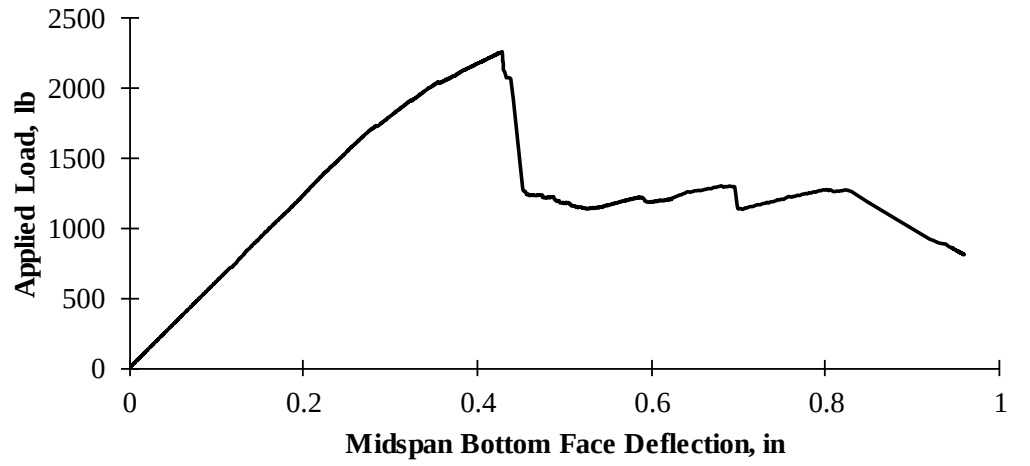

Table D.6: Summary of Four Point Flexural Test for Specimen 2-2-L (Continued)

Corrected Load vs.Crosshead Displacement

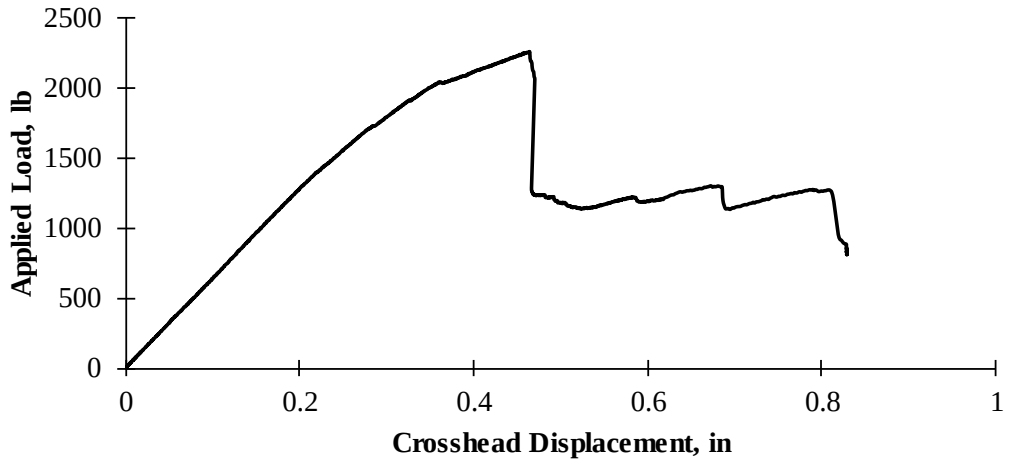

Corrected Load vs.Top Face Strain

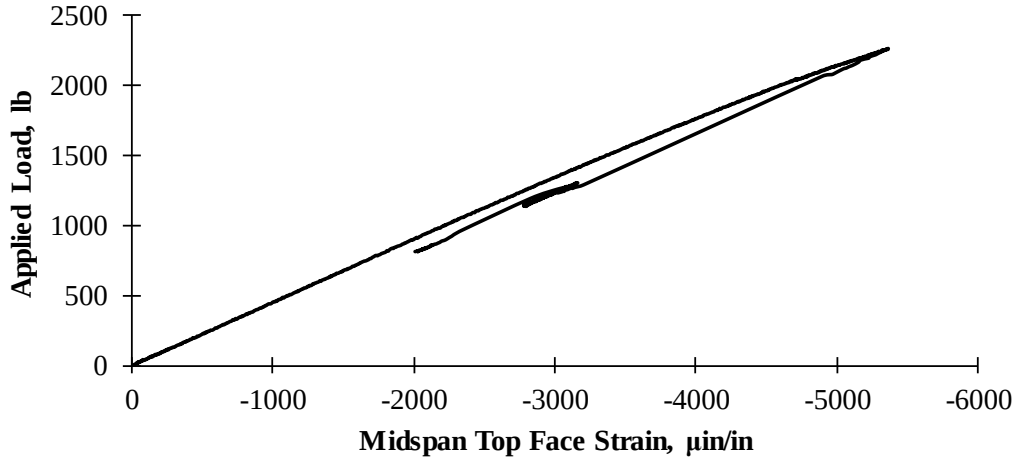

Corrected Load vs.Bottom Face Strain

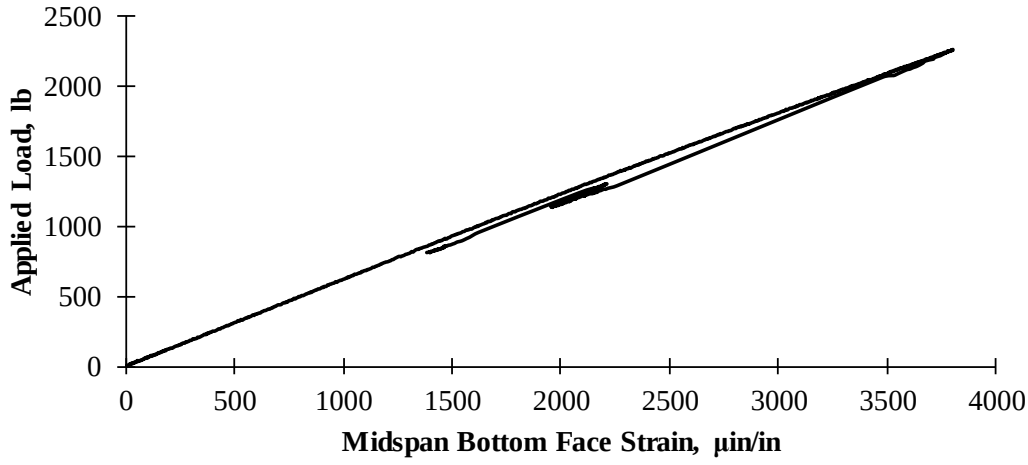

Table D.6: Summary of Four Point Flexural Test for Specimen 2-2-L (Continued)

Strength Analysis		
Initial Failure Mode	Wrinkling of the Top Facing Between Web Reinforcement (Intra-cellular Dimpling)	
Estimation of the Intial Failure Load Using the Offset Method		
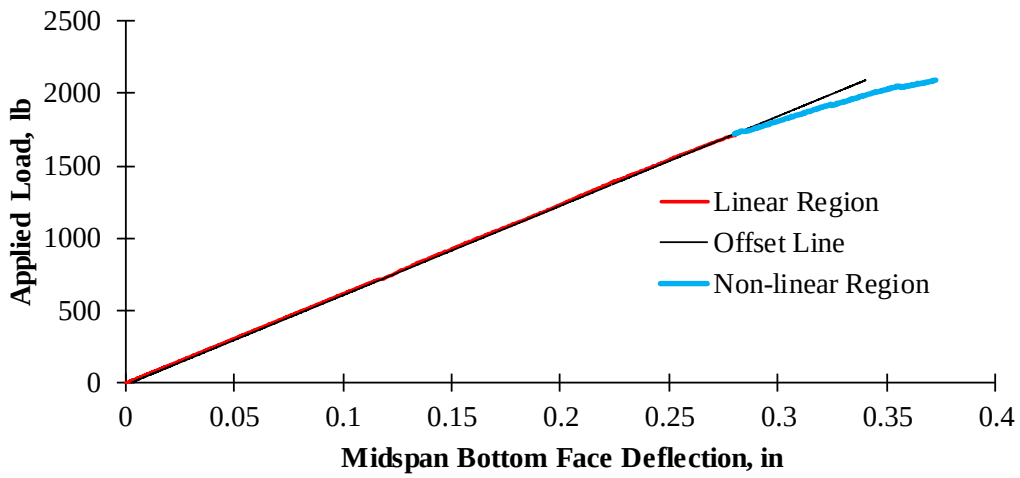		
Offset of Linear Region as a Pecent of Span Length	0.010%	
Load at Initial Failure	1713	lb
Max. Internal Bending Moment at Initial Failure	6853	lb*in
Max. Internal Shear Force at Initial Failure	857	lb
Average Pressure Under the Load at Initial Failure	153	psi
Max. Average Bending Stress in the Facings	9047	psi
Max. Average Shear Stress in the Core	107	psi
Ultimate Failure Mode	Shear Failure of the Core Material Characterized by a Sudden Diagonal Fracture	
Load at Ultimate Failure	2267	lb
Max. Internal Bending Moment at Ultimate Failure	9068	lb*in
Max. Internal Shear Force at Ultimate Failure	1134	lb
Average Pressure Under Load at Ultimate Failure	203	psi
Max. Average Bending Stress in the Facing	11972	psi
Max. Average Shear Stress in the Core	142	psi
Serviceability Analysis		
Limiting Deflection (L/800)	0.030	in
Load at Limiting Deflection	186	lb
Comparison of Serviceability to Strength		
Ratio of Initial Failure to Serviceability Load	9.23	
Ratio of Ultimate Failure to Serviceability Load	12.21	

Table D.7: Summary of Four Point Flexural Test for Specimen 2-3-L

General Information		
Specimen Label	2-3-L	
Displacement Controlled Loading Rate	0.05	in/min
Data Recording Rate for Load and Displacment	2	Hz
Total Time Elapsed During Testing	17	min
Specimen Dimensions		
Total Height of the Specimen, h	2.333	in
Thickness of the Facings, f	0.095	in
Thickness of the Core, c	2.143	in
Width of the Specimen, b	4.373	in
Ratio of the Core Thickness to Facing Thickness, c/f	22.63	
Moment Arm Between the Facings, d	2.238	in
Length of the Specimen, l	26.0	in
Moment of Inertia of the Facings, I_f	1.037	in^4
Area of the Longitudinal Stitches, A_s	9.373	in^2
Configuration and Dimension of the Flexural Setup		
Span Between the Supports, L	24.0	in
Span Between the Load Points, S	8.0	in
Width of the Load and Support Bars, l_{pad}	1.5	in
Loading Configuration	4-Point Third Point Loading	
Regression Analysis for Correcting the Load vs. Bottom Face Deflection		
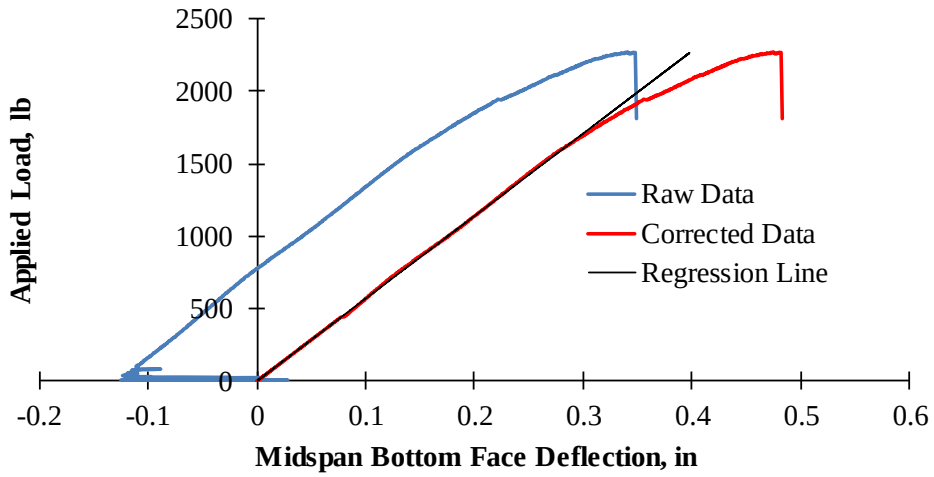		
Slope of the Regression Line	5,704	lb/in
Offset Correction in Bottrom Face Deflection	-0.135	in
Coefficient of Determination	0.9997	
Number of Data Points	500	
Range of Corrected Deflection Used	0.081 - 0.294	in

Table D.7: Summary of Four Point Flexural Test for Specimen 2-3-L (Continued)

Regression Analysis for Correcting the Load vs. Crosshead Displacement		
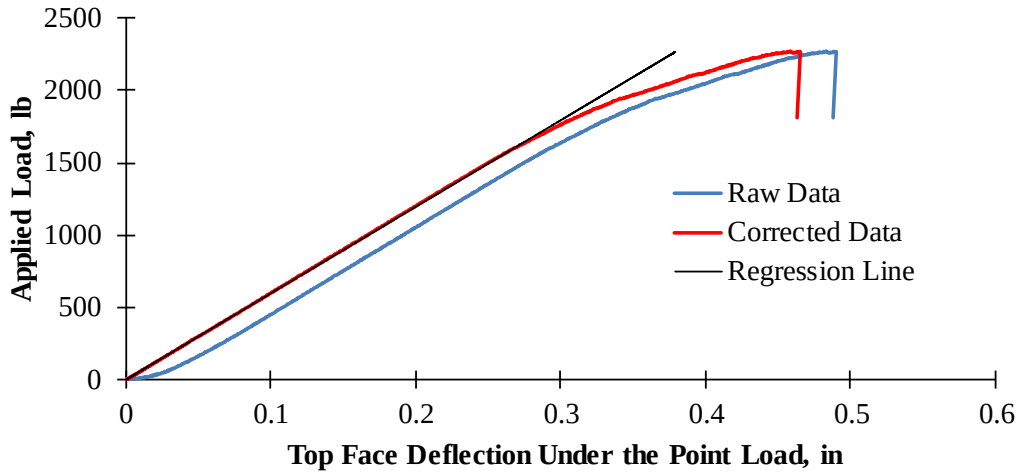		
Slope of the Regression Line	5,996	lb/in
Offset Correction in Crosshead Displacement	0.024	in
Coefficient of Determination	1.0000	
Number of Data Points	500	
Range of Corrected Displacement Used	0.043 - 0.250	in
Regression Analysis for Correcting the Load vs. Top Face Strain		
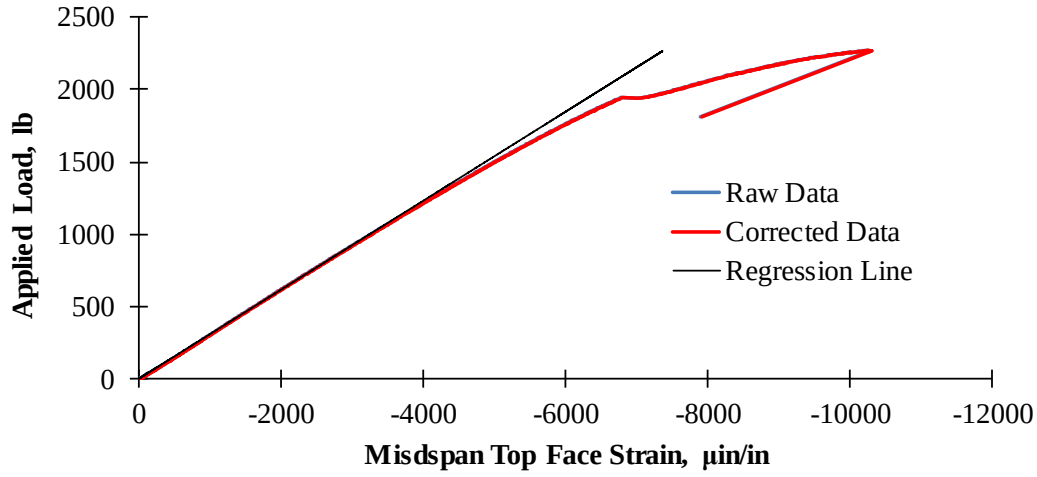		
Slope of the Regression Line	-0.308	lb/in
Offset Correction in Top Face Strain	14	µin/in
Coefficient of Determination	0.9999	
Number of Data Points	500	
Range of Corrected Strain Used	-14 - -3208	µin/in

Table D.7: Summary of Four Point Flexural Test for Specimen 2-3-L (Continued)

Regression Analysis for Correcting the Load vs.Bottom Face Strain

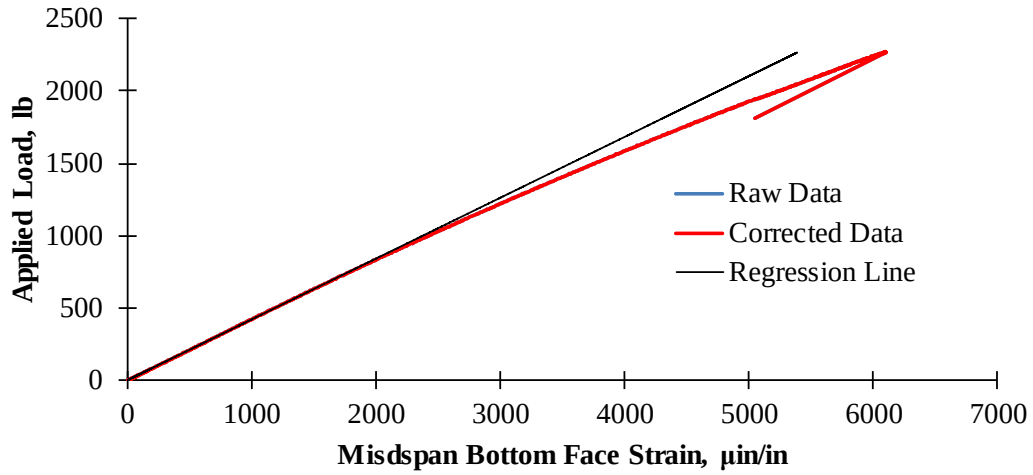

Slope of the Regression Line	0.421	lb/µin/in
Offset Correction in Bottom Face Strain	-8	µin/in
Coefficient of Determination	0.9999	
Number of Data Points	400	
Range of Corrected Strain Used	16 - 1804	µin/in

Corrected Load vs.Bottom Face Deflection

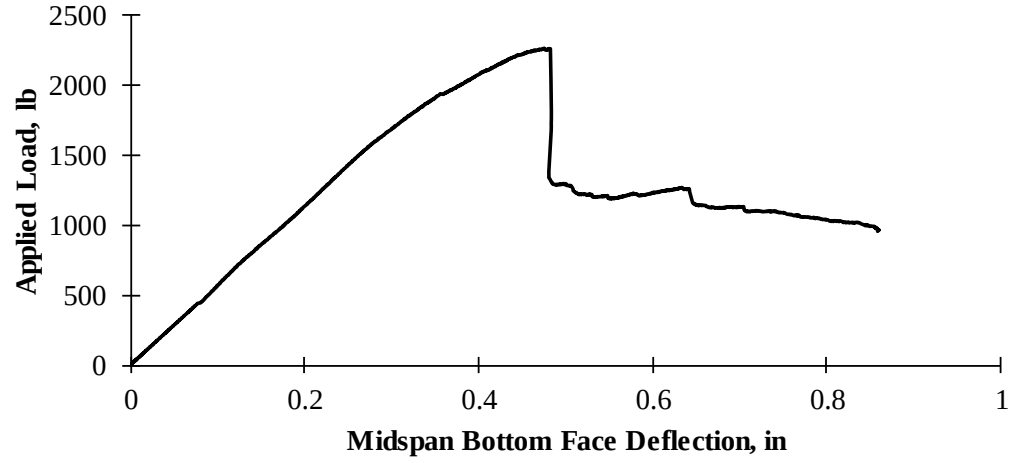

Table D.7: Summary of Four Point Flexural Test for Specimen 2-3-L (Continued)

Corrected Load vs.Crosshead Displacement

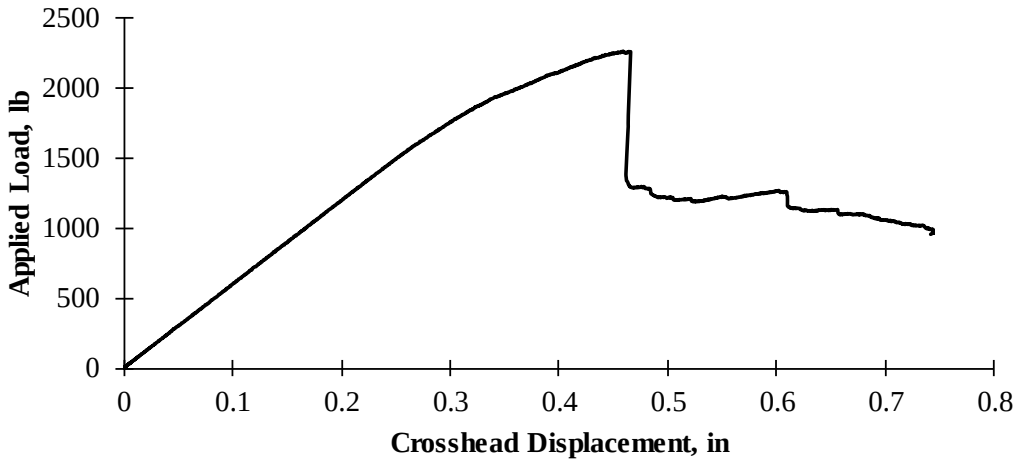

Corrected Load vs.Top Face Strain

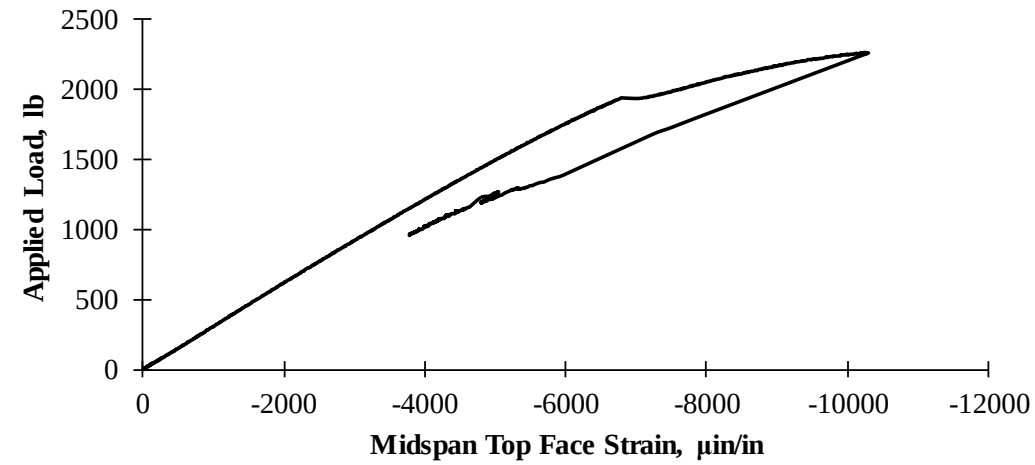

Corrected Load vs.Bottom Face Strain

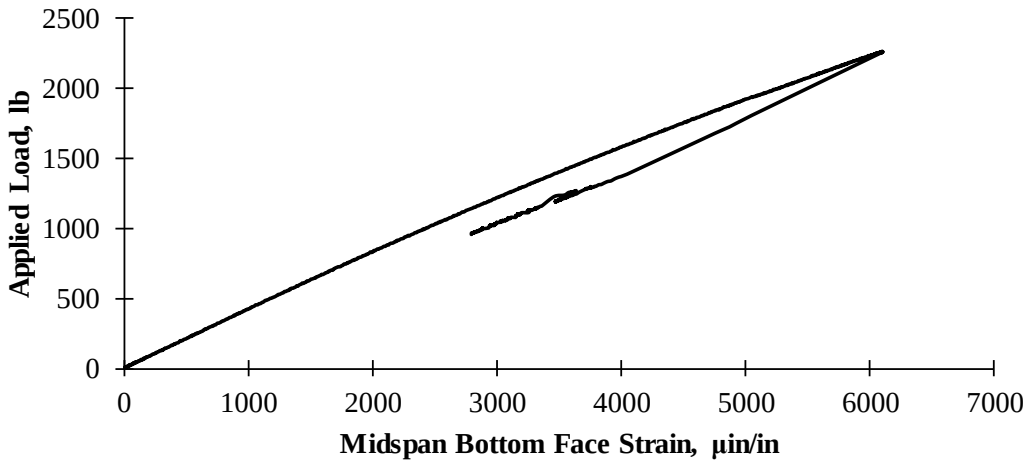

Table D.7: Summary of Four Point Flexural Test for Specimen 2-3-L (Continued)

Strength Analysis		
Initial Failure Mode	Wrinkling of the Top Facing Between Web Reinforcement (Intra-cellular Dimpling)	
Estimation of the Intial Failure Load Using the Offset Method		
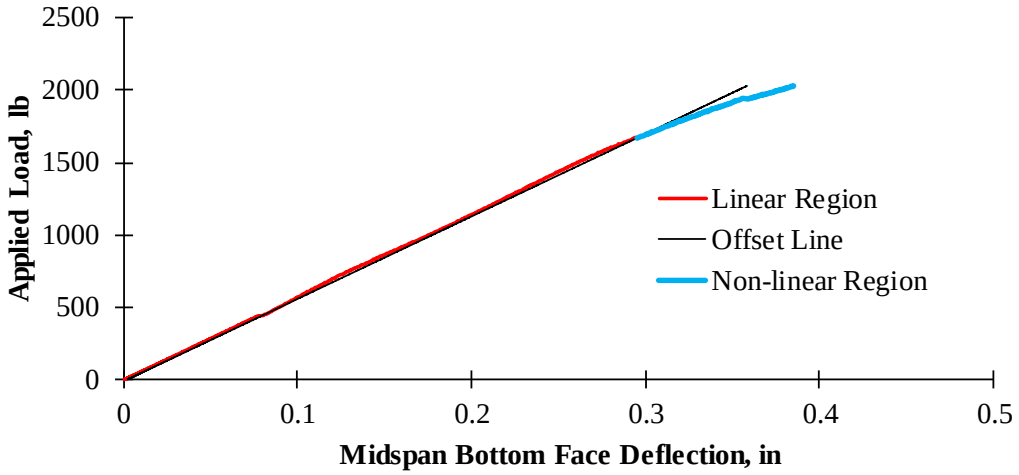		
Offset of Linear Region as a Pecent of Span Length	0.010%	
Load at Initial Failure	1666	lb
Max. Internal Bending Moment at Initial Failure	6664	lb*in
Max. Internal Shear Force at Initial Failure	833	lb
Average Pressure Under the Load at Initial Failure	127	psi
Max. Average Bending Stress in the Facings	7494	psi
Max. Average Shear Stress in the Core	89	psi
Ultimate Failure Mode	Shear Failure of the Core Material Characterized by a Sudden Diagonal Fracture	
Load at Ultimate Failure	2269	lb
Max. Internal Bending Moment at Ultimate Failure	9078	lb*in
Max. Internal Shear Force at Ultimate Failure	1135	lb
Average Pressure Under Load at Ultimate Failure	173	psi
Max. Average Bending Stress in the Facing	10209	psi
Max. Average Shear Stress in the Core	121	psi
Serviceability Analysis		
Limiting Deflection (L/800)	0.030	in
Load at Limiting Deflection	171	lb
Comparison of Serviceability to Strength		
Ratio of Initial Failure to Serviceability Load	9.73	
Ratio of Ultimate Failure to Serviceability Load	13.26	

Table D.8: Summary of Four Point Flexural Test for Specimen 3-1-L

General Information		
Specimen Label	3-1-L	
Displacement Controlled Loading Rate	0.1	in/min
Data Recording Rate for Load and Displacment	2	Hz
Total Time Elapsed During Testing	15	min
Specimen Dimensions		
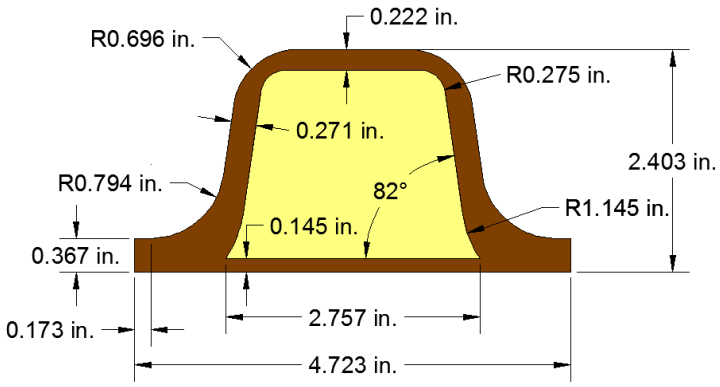		
Total Height, h	2.403	in
Width of the Loading Area, w_{pad}	1.206	in
Total Area of the Cross-section, A	7.288	in^2
Moment of Inertia of the FRP, I_{frp}	1.913	in^4
Area of the FRP, A_{frp}	2.747	in^2
Centriod of the FRP, $\bar{y}_{frp}$	0.906	in
Configuration and Dimension of the Flexural Setup		
Span Between the Supports, L	24.0	in
Span Between the Loading Points, s	8.0	in
Width of the Load and Support Bars, l_{pad}	1.5	in
Loading Configuration	4-Point Third Point Loading	
Regression Analysis		
Regression Analysis for Correcting the Load vs. Bottom Face Deflection		
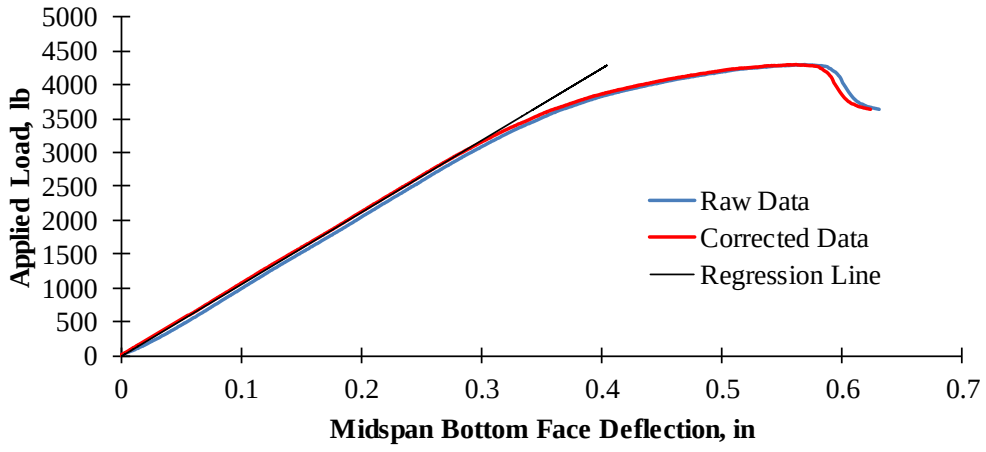		

Table D.8: Summary of Four Point Flexural Test for Specimen 3-1-L (Continued)

Slope of the Regression Line	10,587	lb/in
Offset Correction in Bottrom Face Deflection	0.008	in
Coefficient of Determination	1.0000	
Number of Data Points	300	
Range of Corrected Deflection Used	0.057 - 0.279	in
Regression Analysis for Correcting the Load vs. Top Face Deflection		

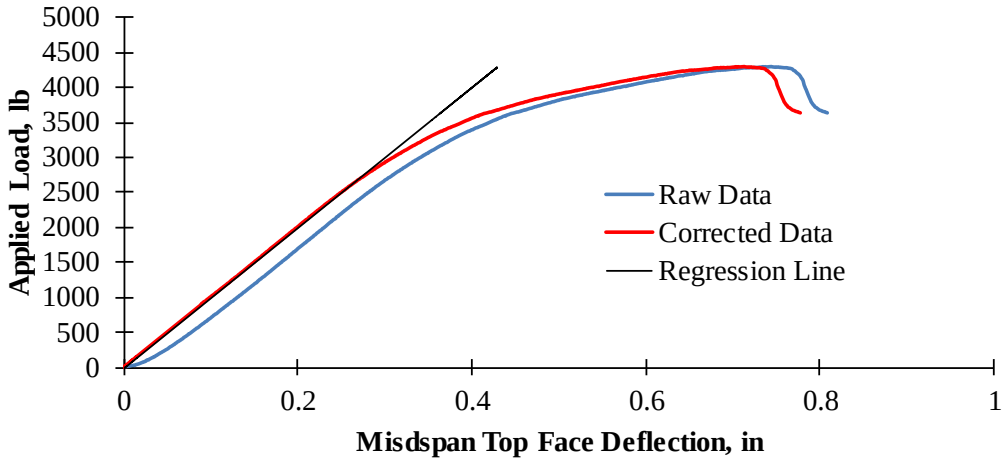

Slope of the Regression Line	10,019	lb/in
Offset Correction in Top Face Deflection	0.032	in
Coefficient of Determination	0.9998	
Number of Data Points	200	
Range of Corrected Deflection Used	0.089 - 0.252	in
Regression Analysis for Correcting the Load vs. Top Face Strain		

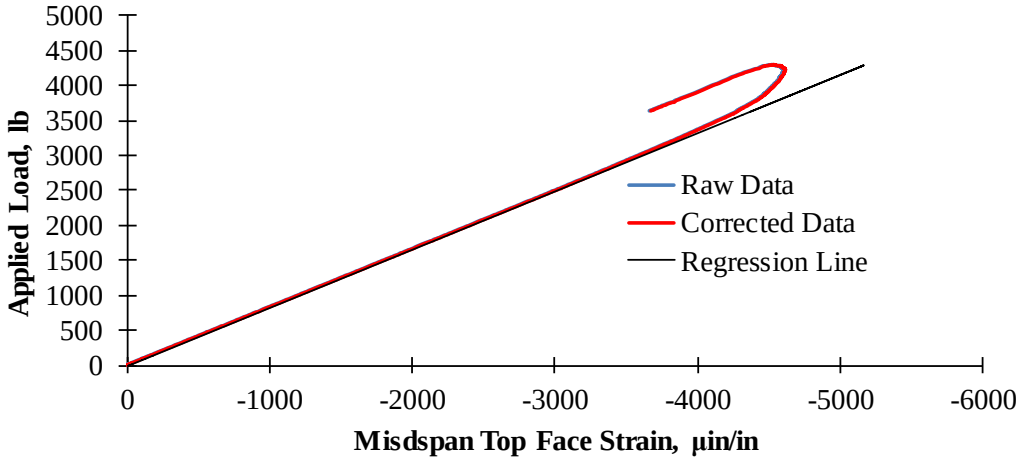

Table D.8: Summary of Four Point Flexural Test for Specimen 3-1-L (Continued)

Slope of the Regression Line	-0.830	lb/in
Offset Correction in Top Face Strain	8	µin/in
Coefficient of Determination	1.0000	
Number of Data Points	300	
Range of Corrected Strain Used	-173 - -2978	µin/in
Regression Analysis for Correcting the Load vs.Bottom Face Strain		

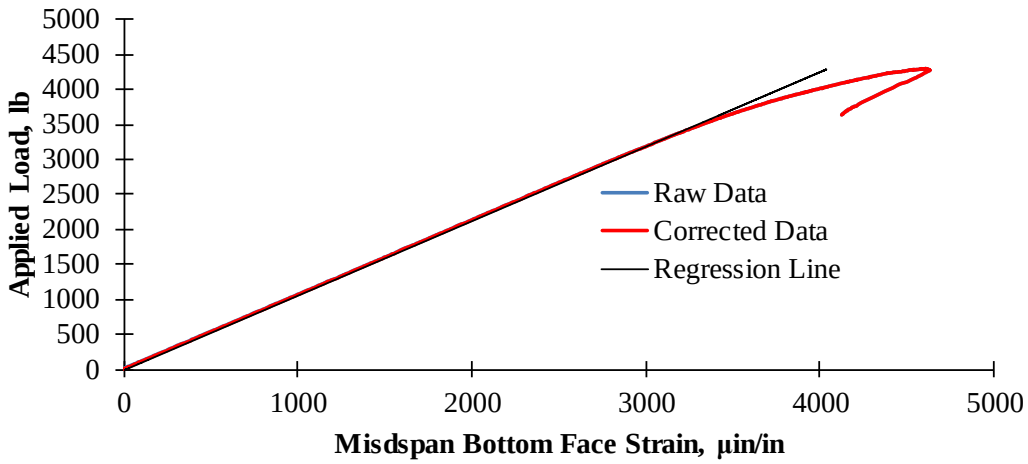

Slope of the Regression Line	1.062	lb/µin/in
Offset Correction in Bottom Face Strain	-6.787	µin/in
Coefficient of Determination	1.0000	
Number of Data Points	400	
Range of Corrected Strain Used	60 - 2875	µin/in
Corrected Data		
Corrected Load vs.Bottom Face Deflection		

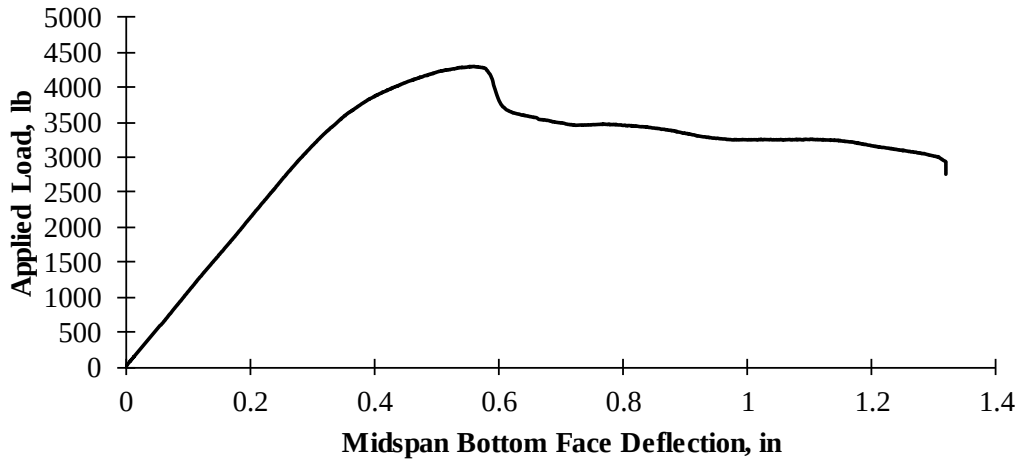

Table D.8: Summary of Four Point Flexural Test for Specimen 3-1-L (Continued)

Corrected Load vs.Top Face Deflection

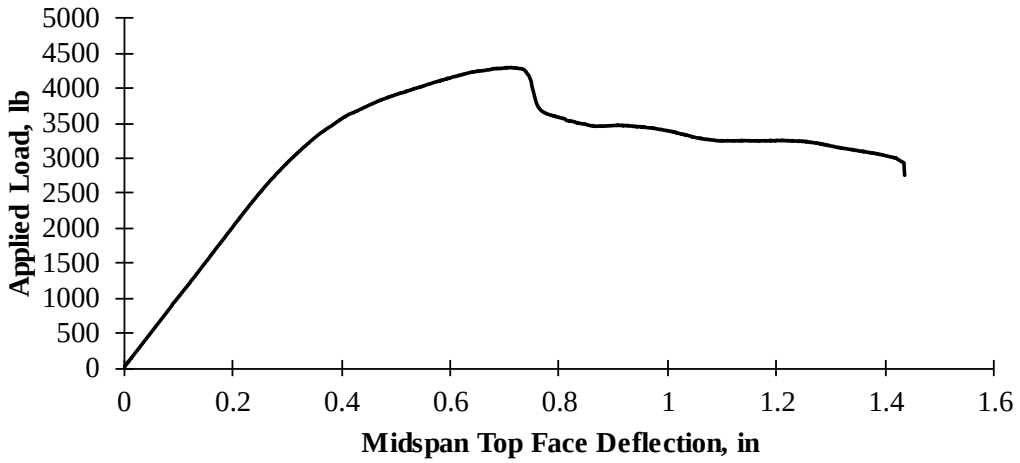

Corrected Load vs.Core Compression

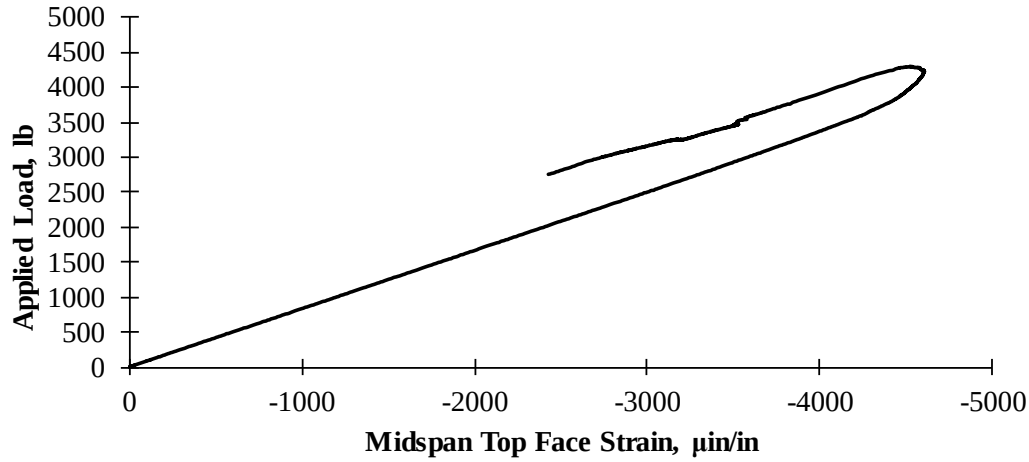

Corrected Load vs.Bottom Face Strain

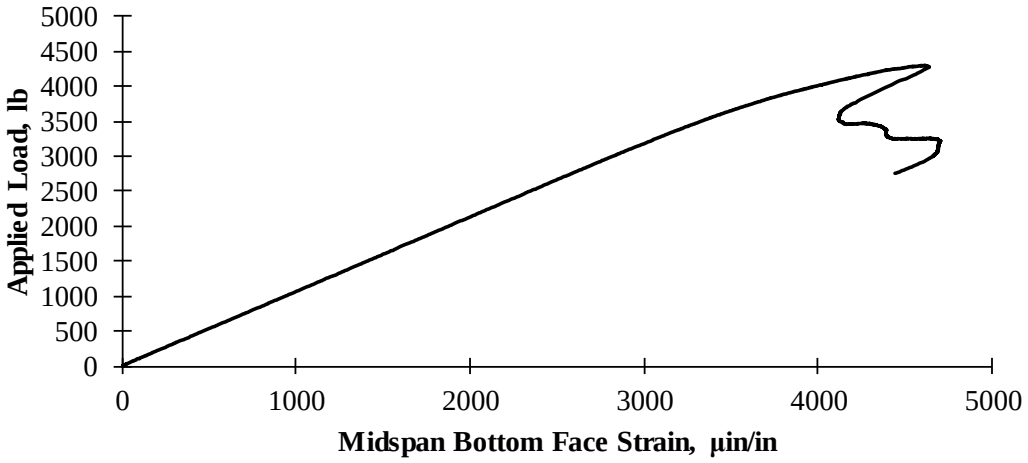

Table D.8: Summary of Four Point Flexural Test for Specimen 3-1-L (Continued)

Strength Analysis		
Initial Failure Mode	Compression Failure in the Top Facing Immediately Under the Load Point	
Estimation of the Intial Failure Load Using the Offset Method		
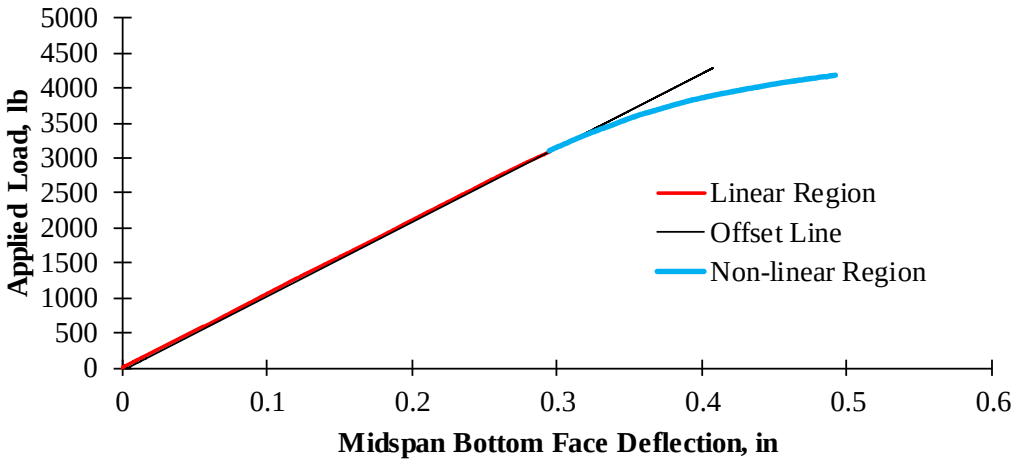		
Offset of Linear Region as a Pecent of Span Length	0.010%	
Load at Initial Failure	3097	lb
Max. Internal Bending Moment at Initial Failure	12386	lb*in
Max. Internal Shear Force at Initial Failure	1548	lb
Average Pressure Under the Load at Initial Failure	856	psi
Max. Bending Stress in the Top Facing	9693	psi
Max. Bending Stress in the Bottom Facing	5866	psi
Max. Average Shear Stress in the Core*	212	psi
Ultimate Failure Mode	Compression Failure in the Top Facing Immediately Under the Load Point	
Load at Ultimate Failure	4288	lb
Max. Internal Bending Moment at Ultimate Failure	17152	lb*in
Max. Internal Shear Force at Ultimate Failure	2144	lb
Average Pressure Under Load at Ultimate Failure	1185	psi
Max. Bending Stress in the Top Facing	13423	psi
Max. Bending Stress in the Bottom Facing	8122	psi
Max. Average Shear Stress in the Core	294	psi
Serviceability Analysis		
Limiting Deflection (L/800)	0.030	in
Load at Limiting Deflection	318	lb
Comparison of Serviceability to Strength		
Ratio of Initial Failure to Serviceability Load	9.75	
Ratio of Ultimate Failure to Serviceability Load	13.50	

APPENDIX E:

RESULTS OF THE FLEXURAL STIFFNESS ANALYSIS

Table E.1: Summary of the Flexural Stiffness Analysis for the Type 1 Specimens

Short Beam Specimens							
Label				1-1-S	1-2-S	1-3-S	1-4-S
Width of the Specimen, in				2.977	2.979	3.012	3.018
Ratio of Load to Midspan Bottom Face Deflection, lb/in				9,032	8,875	8,867	9,207
Length Between the Supports, in				6.0			
Loading Configuration				3-Point Midspan Loading			
Long Beam Specimens							
Label				1-1-L	1-2-L	1-3-L	
Width of the Specimen, in				3.924	3.785	4.367	
Ratio of Load to Midspan Bottom Face Deflection, lb/in				2,776	2,622	2,719	
Length Between the Supports, in				24.0			
Loading Configuration				4-Point Third Point Loading			
Flexural Properties Based on Timoshenko Beam Theory							
Bending Stiffness per Unit Width, lb*in				Shear Stiffness per Unit Width, lb/in			
436,512	449,988	459,489	432,520	4,697	4,606	4,547	4,706
413,260	425,319	433,796	409,680	4,706	4,614	4,555	4,734
320,953	328,180	328,180	333,204	4,752	4,659	4,659	4,599
Total Number of Iterations				12			
Average Bending Stiffness per Unit Width, lb*in				397,590			
Standard Deviation, lb*in				51,184			
Coefficient of Variation				0.129			
Average Shear Stiffness per Unit Width, lb/in				4,653			
Standard Deviation, lb/in				66			
Coefficient of Variation				0.014			

Table E.2: Summary of the Flexural Stiffness Analysis for the Type 2 Specimens

3-Point Flexural Test Specimens					
Label			2-1-S	2-2-S	2-3-S
Width of the Specimen, in			2.989	3.019	2.972
Ratio of Load to Midspan Bottom Face Deflection, lb/in			37,385	37,335	32,770
Length Between the Supports, in			6.0		
Loading Configuration			3-Point Midspan Loading		
4-Point Flexural Test Specimens					
Label			2-1-L	2-2-L	2-3-L
Width of the Specimen, in			4.346	3.725	4.373
Ratio of Load to Midspan Bottom Face Deflection, lb/in			6,658	6,189	5,704
Length Between the Supports, in			24.0		
Loading Configuration			4-Point Third Point Loading		
Flexural Properties Based on Timoshenko Beam Theory					
Bending Stiffness per Unit Width, lb*in			Shear Stiffness per Unit Width, lb/in		
530,746	533,720	567,774	20,987	20,707	18,121
600,266	604,072	648,065	20,702	20,430	17,908
421,624	423,498	423,498	21,652	21,354	21,354
Total Number of Iterations			9		
Average Bending Stiffness per Unit Width, lb*in			528,140		
Standard Deviation, lb*in			81,788		
Coefficient of Variation			0.155		
Average Shear Stiffness per Unit Width, lb/in			20,357		
Standard Deviation, lb/in			1304		
Coefficient of Variation			0.064		

Table E.3: Summary of the Flexural Stiffness Analysis for the Type 3 Specimens

3-Point Flexural Test Specimens	
Label	3-1-S
Ratio of Load to Midspan Bottom Face Deflection, lb/in	21,396
Length Between the Supports, in	6
Loading Configuration	3-Point Midspan Loading
4-Point Flexural Test Specimens	
Label	3-1-L
Ratio of Load to Midspan Bottom Face Deflection, lb/in	10,587
Length Between the Supports, in	24
Loading Configuration	4-Point Third Point Loading
Flexural Properties Based on Timoshenko Beam Theory	
Number of Iterations	1
Total Flexural Bending Stiffness, lb*in^2	~~7,731,702~~
Total Flexural Shear Stiffness, lb	~~31,699~~
Flexural Properties Based on Euler-Bernoulli Beam Theory Using 4-Point Results	
Number of Iterations	1
Total Flexural Bending Stiffness, lb*in^2	2,597,369

BIBLIOGRAPHY

Ahmad, S.H. and Plecnik, J. M. (1989), *Transfer of Composite Technology to Design and Construction of Bridges*, Federal Highway Administration, Washington, DC, and North Carolina State University, Raleigh, North Carolina.

Alampalli, S., O'Conner, J., and Yannotti, A.P. (2000), *Design, Fabrication, Construction, and Testing of an FRP Superstructure*, Federal Highway Administration, Washington, DC, New York State Department of Transportation, Albany, NY.

Allen, H.G. (1969), *Analysis and Design of Structural Sandwich Panels*, Pergamon Press, Oxford.

ASCE (2013), "Report Card for America's Infrastructure," *American Society of Civil Engineers*, <http://www.infrastructurereportcard.org>.

Ashby, M.F., Evans A., Fleck, N.J., Gibson, L.J., Hutchinson, J.W. and Wadley, H.N.G, (2000), *Metal Foams-A Design Guide*, Butterworth-Heinemann, Woburn.

ASTM C273 (2011), *Standard Test Method for Shear Properties of Sandwich Core Materials*, American Society of Testing and Materials, West Conshohocken, PA.

ASTM C297 (2010), *Standard Test Method for Flatwise Tensile Strength of Sandwich Constructions*, American Society of Testing and Materials, West Conshohocken, PA.

ASTM C365 (2011), *Standard Test Method for Flatwise Compressive Properties of Sandwich Cores*, American Society of Testing and Materials, West Conshohocken, PA.

ASTM C393 (2011), *Standard Test Method for Core Shear Properties of Sandwich Constructions by Beam Flexure*, American Society of Testing and Materials, West Conshohocken, PA.

ASTM D3039 (2014), *Standard Test Method for Tensile Properties of Polymer Matrix Composite Materials*, American Society of Testing and Materials, West Conshohocken, PA.

ASTM D3410 (2008), *Standard Test Method for Compressive Properties of Polymer Matrix Composite Materials with Unsupported Gage Section by Shear Loading*, American Society of Testing and Materials, West Conshohocken, PA.

ASTM D5379 (2012*), Standard Test Method for Shear Properties of Composite Materials by the V-Notched Beam Method*, American Society of Testing and Materials, West Conshohocken, PA.

ASTM D7249 (2012), *Standard Test Method for Facing Properties of Sandwich Constructions by Long Beam Flexure*, American Society of Testing and Materials, West Conshohocken, PA.

ASTM D7250 (2012), Standard Practice for Determining Sandwich Beam Flexural and Shear Stiffness

Bakeri, P.A. and Sunder, S.S. (1990). "Concepts for Hybrid FRP Bridge Deck System," Serviceability and Durability of Construction Materials, Proceedings of the First Materials Engineering Congress, American Society of Civil Engineers, Denver, Colorado.

Bakri, P.A. (1989), "Analysis and Design of Polymer Composite Bridge Decks," M.S. Thesis, Massachusetts Institute of Technology, Cambridge, MA.

Bank, L.C. (2006), "Application of FRP Composites to Bridges in the USA," Proceedings of the International Colloquium on Application of FRP to Bridges, Japan Society of Civil Engineers Tokyo, Japan.

Carlsson, L.A. and Kardomateas G.A. (2011), *Structural and Failure Mechanics of Sandwich Composites*, Springer, New York.

Chajes, M. J., Gillespie, J.W., Mertz, D.R., Shenton, H.W., and Eckel, D.A. (2000), *Delaware's First All-Composite Bridge*, Structures Congress, CD-Rom Proceedings, Philadelphia, PA.

Cousins, T.E. and Lesko, J.L. (2004), *Plate and Tube Bridge Deck Evaluation in the Deck Test Bed of the Troutville, Virginia, Weigh Station*, Virginia Transportation Research Council, Charlottesville, Virginia.

Frostig, Y., Baruch, M., Vilnay, O. and Sheinman I. (1992). "High-Order Theory for Sandwich-Beam Behavior with Transversely Flexible Core," *Journal of Engineering Mechanics*, 118(5), 1026–1043.

GangaRao, H. V. S. and Sotiropoulos, S. N. (1991). *Development of FRP Bridge Superstructural Systems*, United States Department of Transportation, Washington, DC, West Virginia Department of Transportation, Charleston, WV, and Mid-Atlantic Universities Transportation Center, Pennsylvania State University, University Park, PA.

GangaRao, H.V.S., Thippeswamy, H. K., Shekar, V., and Craigo, C. (1999). "Development of glass fiber reinforced polymer composite bridge deck," *SAMPE Journal*, 35(4), 12-24.

Gill, S. R. and Plunkett, J.D. (2000), *Testing, Evaluation, and Installation of Fiber-Reinforced Polymer Honeycomb Composite Panels in Bridge Deck Applications*, National Cooperative Highway Research Program.

Hassan, T.K. and Reis, M.E. (2003), *Innovative 3-D FRP Sandwich Panels for Bridge Decks, North Carolina State University*, Raleigh NC.

Hastak, M., Halpin, D.W., and Hong, T. (2004), *Constructability, Maintainability, and Operability of Fiber-Reinforced Polymer (FRP) Bridge Deck Panels*, Federal Highway Administration, Washington, DC, Indiana Department of Transportation, Indianapolis, IN, Purdue University, West Lafayette, IN.

Henderson, M. (2000), *Evaluation of Salem Avenue Bridge Deck Replacement: Issues Regarding the Composite Materials Systems Used*, Ohio Department of Transportation, Columbus, OH.

Henry, J.A. (1985), "Deck Girders System for Highway Bridges Using Fiber Reinforced Plastics," M.S. Thesis, North Carolina State University, Raleigh, North Carolina.

McGhee, K.K., Barton, F. W. and Mckeel, W.T. (1991), "Optimum Design of Composite Bridge Deck Panels," Advanced Composite Materials in Civil Engineering Structures, Proceedings of the Specialty Conference, American Society of Civil Engineers, Las Vegas, Nevada.

Mongi, A.N.K. (1991), "Theoretical and Experimental Behavior of FRP Floor System," M.S. Thesis, West Virginia University, Morgantown, WV.

Nystrom, H., Watkins, S., Nanni, A., and Stone D.K. (2002), *Laboratory and Field Testing of FRP Composite Bridge Decks and FRP-Reinforced Concrete Bridge for the City of St. James, Phelps County, MO*, Missouri Department of Transportation, Jefferson City, MO, University of Missouri-Rolla, Rolla, MO.

Plantema, F.J. (1966), *Sandwich Construction: The Bending and Buckling of Sandwich Beams, Plates, and Shells*, Wiley Publishing, New York.

Plecnik, J.M. and Azar, W.A. (1991), "Structural Components in Highway Bridge Deck Applications," *International Encyclopedia of Composites*, 6, 430-445.

Reising, R., Shahrooz, B., Hunt, V., Lenett, M., Christopher, S., Neumann, A., Helmicki, A., Miller, R., Kondury, S. and Morton, S. (2001), *Performance of a Five-Span Steel Bridge with Fiber Reinforced Polymer Composite Deck Panels*, Transportation Research Board Annual Meeting, CD-Rom Proceedings, Washington, D.C.

Shekar, V., 2000, "Advancement in FRP Composites Using 3D Stitched Fabrics and Enhancement in FRP Bridge Deck Component Properties," M.S. Thesis, West Virginia University, Morgantown, WV.

Shekar, V., Petro S., and GangaRao H.V.S. (2002), *Construction of FRP Modular Decks for Highway Bridges*, Transportation Research Board Annual Meeting, CD-Rom Proceedings, Washington, D.C.

Steeves, C.A. and Feck, N. (2004), "Collapse Mechanism of Sandwich Beams with Composite Faces and Foam Core, Loaded in Three-Point Bending," *International Journal of Mechanical Sciences*, 46, 561-608.

Temeles, A. B. (2001), "Field and Laboratory Tests of a Proposed Bridge Deck Panel Fabricated from Pultruded Fiber-reinforced polymer Components," M.S. Thesis, Virginia Polytechnic Institute and State University, Blacksburg, Virginia.

Thomsen, O.T. (1977), "Localized Loads," in D. Zenkert (Ed.), *An Introduction to Sandwich Construction*, Chapter 12, EMAS, London.

Wagh, V. P. (2001), "FRP Bridge Deck Design and Construction," *Structural Engineer*, May, 46-50.

Zhou, A., Coleman, J.T., Lesko, J.L., and Cousins, T.E. (2001), "Structural Analysis of FRP Bridge Deck Systems from Adhesively Bonded Pultrusions," *FRP Composites in Civil Engineering*, 2, 1413-1420.

Zoghi, M., Fahrey, D.N., and Foster, D.C. (2002), *Construction and Performance Evaluation of a Fiber-reinforced Polymer Composite Bridge*, Transportation Research Board Annual Meeting, CD-Rom Proceedings, Washington, D.C.

Zureick, A., Engindeniz, M., Arnette, J., and Schneider, C. (2003), *Acceptance Test Specifications and Guidelines for Fiber-Reinforced Polymeric Bridge Decks*, Federal Highway Administration, Washington, DC, and Georgia Institute of Technology, Atlanta, GA.

VITA

Matthew Scott Hopkins grew up in Burfordville, MO. He attended Jackson Senior High School in Jackson, MO where he graduated with honors in 2007. He then attended the Missouri University of Science and Technology in Rolla, MO. Where he graduated with academic honors and earned his B.S. degree in Civil Engineering in 2011. After receiving the Chancellor's Fellowship, he pursued graduate studies at the Missouri S&T. He completed his M.S. degree in Civil Engineering in 2014, and upon completion he will pursue his PhD in the field of Civil Engineering.